Transient Study of Hybrid Concentrating Photovoltaic-Thermoelectric Systems and Solar Thermoelectric Generators

Nezhad, Sajjad Mahmoudi

Publication date:
2018

Document Version
Publisher's PDF, also known as Version of record

TRANSIENT STUDY OF HYBRID CONCENTRATING PHOTOVOLTAIC-THERMOELECTRIC SYSTEMS AND SOLAR THERMOELECTRIC GENERATORS

BY
SAJJAD MAHMOUDI NEZHAD

DISSERTATION SUBMITTED 2018

AALBORG UNIVERSITY
DENMARK

TRANSIENT STUDY OF HYBRID CONCENTRATING PHOTOVOLTAIC-THERMOELECTRIC SYSTEMS AND SOLAR THERMOELECTRIC GENERATORS

PH.D. DISSERTATION

Sajjad Mahmoudi Nezhad

AALBORG UNIVERSITY
DENMARK

Department of Energy Technology
Aalborg University, Denmark

Dissertation submitted December 2018

Dissertation submitted:	December, 2018
PhD supervisor:	Prof. Lasse Rosendahl, Aalborg University
Assistant PhD supervisor:	Associate Prof. Alireza Rezaniakolaei, Aalborg University
PhD committee:	Associate Professor Kim Sørensen (chairman) Aalborg University
	Professor Dario Narducci University of Milano Bicocca
	Professor Gao Min Cardiff University
PhD Series:	Faculty of Engineering and Science, Aalborg University
Department:	Department of Energy Technology

ISSN (online): 2446-1636
ISBN (online): 978-87-7210-365-5

Published by:
Aalborg University Press
Langagervej 2
DK – 9220 Aalborg Ø
Phone: +45 99407140
aauf@forlag.aau.dk
forlag.aau.dk

Printed in Denmark by Rosendahls, 2018

CV

Sajjad Mahmoudi Nezhad received the B.Sc. degree in Mechanical Engineering from Persian Gulf University, Bushehr, Iran, in 2007, and the M.Sc. degree in Mechanical Engineering from Razi University, Kermanshah, Iran, in 2009.

He is currently working towards the Ph.D. degree in the Department of Energy Technology, Aalborg University, Denmark. His research interests include photovoltaic- thermoelectric hybrid systems, Solar thermoelectric generators, thermoelectric waste heat recovery systems, numerical simulation and computational fluid dynamics, convective and conductive heat transfer, renewable energy and optical interferometry.

ENGLISH SUMMARY

Fossil resources are in huge supply but they are expensive, difficult to access and have substantial impact on the climate. In order to avoid the climate chaos, it is necessary to make a significant change within the next years. Therefore, additional renewable, sustainable and clean energy sources are required to be added to the current energy sources. Furthermore, harvesting the heat loss in different applications and converting a fraction the waste heat into usable energy is another approach to deliver a part of the energy demand. In this Ph.D. thesis, both strategies are addressed using photovoltaic (PV) cells and thermoelectric generators (TEGs).

Sun is an inexhaustible source of energy, and solar energy is clean and sustainable and decreases the costs of mitigating global warming. These special features make solar energy one of the best alternatives for fossil fuels. Solar energy can be directly converted to electricity using solar thermoelectric generators (STEGs) and photovoltaics (PVs). In the regions with partly cloudy climates, the instabilities of the weather conditions and consequently daily solar radiation have a substantial influence on the conversion efficiency and performance of PVs and TEGs. These fluctuations in the output power can be a critical concern to stabilize the electrical response of the systems.

A TEG is a circuit comprising two dissimilar thermoelectric (TE) materials that directly converts heat into electricity. A voltage potential will be created when there is a temperature gradient across the TEG. The efficiency of the TEG is restricted to the Carnot Efficiency. In this Ph.D. thesis, the main goal is to investigate transient behavior of the TEGs in the hybrid concentrated photovoltaic-thermoelectric generator (CPV-TEG) systems and STEGs. In order to achieve this target, firstly the transient behavior of the TEGs in a waste heat recovery system is examined under variable thermal boundary conditions. The significance of the impact of different parameters and operating conditions on the performance and transient response of the TEGs is investigated. Furthermore, two types of the STEG systems with different materials are experimentally examined under concentrated solar radiations. A solar simulator is used to deliver the concentrated light to the STEG system in the experiments. In parallel, a thermally coupled numerical model is developed and solved by using the finite volume method (FVM). The model includes detailed phenomena of thermoelectricity such as temperature dependent material properties, Peltier coefficient, Thomson coefficient and the Seebeck coefficient. The numerical model is established to determine the significance of the role of the absorber in the

energy harvester systems and to predict the performance of the systems at the high temperatures.

PV cells are the most common devices to harvest the solar energy and convert it to usable electrical energy. Multi-junction (MJ) solar cells are getting more of interest due to having higher conversion efficiency than the conventional PV cells. However, even in the MJ cells, more than half of the input solar energy is converted to heat and must be dissipated form the system properly. The TEG devices are appropriate candidate to harvest this waste heat. In this thesis, moreover, the studied TEG is integrated with a concentrated triple-junction (CTJ) cell to maximize utilizing the solar energy. Time-dependent and steady-state conditions are considered to study performance of the hybrid system. Power generation and conversion efficiency of the system are acquired experimentally and numerically. The role of the CTJ cell and TEG device in the overall power generation by the system is evaluated. In addition, the impact of some of the key design parameters on the performance of the hybrid system is examined.

The results of the study on the STEG systems indicate that the use of absorber is an appropriate and advantageous technique for low solar concentration applications to compensate the low rate of the input heat flux. In the CTJ-TEG hybrid systems, the results show that in the transient condition, the conversion efficiencies of the TEG and CTJ have a reverse variation with the fluctuation of the solar radiation and it helps to stabilize the power generated by the system. Output power by the CTJ has a stepwise variation similar to the solar radiation, but the variation of the output power by the TEG generally follows the variation of the temperatures of the hot and cold sides of the TEG. Furthermore, the TEG plays a more significant role in the overall power generation by the system at higher solar concentrations. It is also found that thermal contact resistance has a critical impact on the system performance, and cannot be ignored in real applications.

Keywords: Hybrid Energy Harvester, Thermoelectric Generator (TEG); Photovoltaic (PV) Cells; Transient Behavior; Concentrated Triple-Junction (CTJ) Cells; Solar Thermoelectric Generators (STEG); Seebeck Coefficient; Finite Volume Method (FVM).

DANSK RESUME

Fossile ressourcer er i stor udbud, men de er dyre, vanskelige at få adgang til og har stor indflydelse på klimaet. For at undgå et klimakaos er det nødvendigt at foretage et betydeligt skifte inden for de kommende år. Derfor er der behov for yderligere vedvarende, bæredygtige og rene energikilder, som skal tilføjes til og på længere sigt erstatte de nuværende energikilder. Desuden er der et stort potentiale til at levere en del af energibehovet ved at høste varmetabet fra forskellige applikationer og omdanne en brøkdel af denne til brugbar energi. Begge strategier bliver adresseret i denne Ph.D. afhandling ved hjælp af fotovoltaiske (PV) celler og termoelektriske generatorer (TEG'er).

Solen er en uudtømmelig energikilde, og solenergi er ren og bæredygtig og reducerer omkostningerne til afbøde virkningen af den globale opvarmning. Disse særlige træk gør solenergi til et af de bedste alternativer til fossile brændstoffer. Solenergi kan omdannes direkte til elektricitet ved hjælp af soltermoelektriske generatorer (STEG'er) og solceller (PV). I regioner med delvis uklare klimaer har ustabiliteten af vejrforholdene og dermed den daglige variation i solstråling en betydelig indflydelse på konverteringseffektiviteten og ydeevnen af PV'er og TEG'er. Disse udsving i udgangseffekten kan medføre kritiske stabilitetsproblemer for systemet.

En TEG er et kredsløb bestående af to forskellige termoelektriske (TE) materialer, som direkte konverterer varme til elektricitet. Et spændingspotentiale opstår, når der er en temperaturgradient over TEG'en. Virkningsgraden af en TEG er begrænset af Carnot virkningsgraden. I denne Ph.D. afhandling, er hovedmålet at undersøge transient adfærd af TEG'erne i en hybrid-koncentreret solcelle-termoelektriske generator (CPV-TEG) systemer og STEG'er. For at nå dette mål, undersøges først den transiente adfærd af TEG'erne i et spildvarmegenvindingssystem under variable termiske betingelser. Betydningen af virkningen af forskellige parametre og driftsbetingelser på TEGs præstation og forbigående respons undersøges. Derudover undersøges to typer af STEG-systemer med forskellige materialer eksperimentelt under koncentrerede solstråler. En solsimulator bruges til at levere det koncentrerede lys til STEG-systemet i forsøgene. Parallelt udvikles og løses en termisk koblet numerisk model ved anvendelse af den endelige volumenmetode (FVM). Modellen indeholder detaljerede fænomener termoelektricitet, såsom temperaturafhængige materialegenskaber, Peltier-koefficient, Thomson-koefficient og Seebeck-koefficienten. Den numeriske model er etableret for at bestemme betydningen af

absorberens rolle i energisystemerne og at forudsige systemets ydeevne ved de høje temperaturer.

PV-celler er de mest almindelige enheder til at høste solenergien og konvertere den til brugbar elektrisk energi. Multi-junction (MJ) solceller bliver mere interesserante på grund af deres højere konverteringseffektivitet end de konventionelle PV-celler. Men selv i MJ-cellerne bliver mere end halvdelen af den indstrålede solenergi omdannet til varme som skal dissiperes væk. TEG-enhederne er passende kandidater til at høste og udnytte denne spildvarme. I denne afhandling er den undersøgte TEG desuden integreret med en koncentreret tredobbelt (CTJ) celle for at maksimere udnyttelsen af solenergien. Tidsafhængige og steady state betingelser analyseres for at studere ydeevne af hybridsystemet. Systemets energiproduktion og konverteringseffektivitet undersøges eksperimentelt og numerisk. CTJ-celle- og TEG-enhedens rolle i systemets samlede elproduktion vurderes. Derudover undersøges virkningen af nogle af de vigtigste designparametre på præstationen af hybridsystemet.

Resultaterne af undersøgelsen på STEG-systemerne viser, at brugen af absorber er en hensigtsmæssig og fordelagtig teknik til applikationer med lav solkoncentration for at kompensere den lave indstråling. I CTJ-TEG-hybridsystemerne viser resultaterne, at konverteringseffektiviteten af TEG og CTJ i dynamisk tilstand har en omvendt variation med udsvinget i solstrålingen, og det hjælper med at stabilisere den strøm, der genereres af systemet. Udgangseffekten ved CTJ har en trinvis variation svarende til solstrålingen, men variationen i udgangseffekten fra TEG følger generelt variationen i temperaturerne på de varme og kolde sider af TEG. Desuden spiller TEG en mere væsentlig rolle i systemets samlede elproduktion ved højere solkoncentrationer. Det konstateres også, at termisk kontaktmodstand har en kritisk indvirkning på systemets ydeevne og derfor ikke kan ignoreres i reelle applikationer.

Nøgleord: Hybrid Energy Harvester, Thermoelectric Generator (TEG); Photovoltaic (PV) Celler; Transient Behavior; Koncentrerede Triple-Junction (CTJ) celler; Solar termoelektriske generatorer (STEG); Seebeck koefficient; Finite Volume Method (FVM).

PREFACE

This dissertation, which is a collection of papers, is submitted to the Doctoral School of Engineering and Science at Aalborg University in partial fulfilment of the requirements for the Danish Ph.D. degree. It covers research work in the Department of Energy Technology at Aalborg University from the period January 2016 to December 2018. The work has been conducted under supervision of Prof. Lasse Rosendahl and Assoc. Prof. Alireza Rezaniakolaei at the Department of Energy Technology, Aalborg University.

ACKNOWLEDGEMENTS

I would like to express my sincere gratitude to my supervisors from Aalborg University, Department of Energy Technology, Prof. Lasse Rosendahl and Assoc. Prof. Alireza Rezaniakolaei for their support and friendship during the course of this work.

I would also like to thank Prof. Daniel Tudor Cotfas and Prof. Petru Adrian Cotfas for their kindly supports. I had the pleasure to stay for 3 months in the Transilvania University of Brasov during my study and work with them in a very friendly environment.

A big thank you is also extended to my colleagues in Department of Energy Technology with special thanks to my group mates Seyed Mojtaba Mir Hosseini, Shaowei Qing, Seyed Mohammad Mortazavinatanzi, and Majid Khazaee.

Finally, I greatly dedicate this thesis to my parents, my brothers and my sister, for their love and endless supports through all my life from the day that I born to the day that you read this; also to all my teachers for their encouragement at all the time; and also to all my friends who be with me all through my life and sharing all my tears and joys and bring me up to this level by their shoulders.

Sajjad Mahmoudi Nezhad

Aalborg, Denmark, December 2018

THESIS DETAIL AND PUBLICATIONS

Thesis Title: Transient Study of Hybrid Concentrating Photovoltaic-Thermoelectric Systems and Solar Thermoelectric Generators.

Ph.D. Student: Sajjad Mahmoudi Nezhad

Supervisor: Prof. Lasse Rosendahl, Aalborg University

Co-supervisor: Assoc. Prof. Alireza Rezaniakolaei, Aalborg University

The main body of this thesis is based on the following selected papers, which have been completed during the PhD period. The papers are found in Part Appendix of this dissertation.

Publications:

[A] S. Mahmoudinezhad, A. Rezaniakolaei, L.A. Rosendahl, Experimental Study on Effect of Operating Conditions on Thermoelectric Power Generation, *Energy Procedia 142 (2017) 558-563.*

[B] S. Mahmoudinezhad, A. Rezania, A. A. Ranjbar, L. A. Rosendahl, Transient Behavior of the Thermoelectric Generators to the Load Change; An Experimental investigation, *Energy Procedia 147 (2018) 537-543.*

[C] S. Mahmoudinezhad, P. A. Cotfas, D. T. Cotfas, A. Rezania, L. A. Rosendahl, Performance evaluation of a high-temperature thermoelectric generator under different solar concentrations, *Energy Procedia 147 (2018) 624-630.*

[D] S. Mahmoudinezhad, A. Rezania, P.A. Cotfas, D.T. Cotfas, L.A. Rosendahl, Transient Behavior of Concentrated Solar Oxide Thermoelectric Generator, *Energy, Vol. 168, 2018, p. 823-832.*

[E] S. Mahmoudinezhad, D.T. Cotfas, A. Rezania, P.A. Cotfas, L.A. Rosendahl, Transient Response of Bi_2Te_3 Based Thermoelectric Generator to Variant Solar radiation; An Experimental and Numerical study (*Submitted to the journal of Renewable Energy).*

[F] S. Mahmoudinezhad, S. Qing, A. Rezaniakolaei, L.A. Rosendahl, Transient Model of Hybrid Concentrated Photovoltaic with Thermoelectric Generator, *Energy Procedia 142 (2017) 564-569.*

[G] S. Mahmoudinezhad, A. Rezania, L.A. Rosendahl, Behavior of hybrid concentrated photovoltaic-thermoelectric generator under variable solar radiation, *Energy Conversion and Management 164 (2018) 443–452.*

[H] S Mahmoudinezhad, S. Ahmadi Atouei, P.A. Cotfas, A. Rezania, D.T. Cotfas, L.A. Rosendahl, Transient Response of Concentrating Triple Junction Solar Cell-Thermoelectric Generator Hybrid System to the Fluctuating Solar Irradiance; Experimental and Numerical Study, *(Submitted to the journal of Energy Conversion and Management).*

[I] S. Mahmoudinezhad, A. Rezania, D.T. Cotfas, P.A. Cotfas, L.A. Rosendahl, Experimental and Numerical Investigation of Hybrid Concentrated Photovoltaic–Thermoelectric Module under Low Solar Concentration, *Energy 159 (2018) 1123-1131.*

[J] S. Mahmoudinezhad, A. Rezania, L.A. Rosendahl, Numerical parametric study on the performance of CPV-TEG hybrid system, *10^{th} International Conference on Applied Energy (ICAE2018), 22-25 August 2018, Hong Kong, China.*

In addition the included publication, the following paper was completed during the PhD period.

- S. Mahmoudinezhad, A. Rezania, T. Yousefi, M.S. Shadloo, L. A. Rosendahl, Adiabatic partition effect on natural convection heat transfer inside a square cavity: experimental and numerical studies, *Heat and Mass Transfer 54 (2), 291-304.*

TABLE OF CONTENTS

CHAPTER 1. INTRODUCTION

The introduction firstly establishes an overview of thermoelectricity, associated effects, and applications. This section is followed by an introduction to the solar thermoelectric generators (STEG) and efficiency and applications of the STEG systems. Furthermore, photovoltaics (PV) are introduced, and their strengths and weaknesses are discussed. The chapter is concluded with a definition of project objectives and an outline of the dissertation.

1.1 INTRODUCTION TO THE THERMOELECTRIC DEVICES

Due to quick increment in the world population and developments in industry and technology, additional energy sources are needed to be replaced to the existing energy reserves. Currently, fossil fuels (oil, coal and natural gas, etc.) are known as the main sources of energy consumption. Using these fossil fuels has produced destructive environmental effects consisting of global warming and air pollution.

The accessibility of highly reliable generators with long lifetime and low maintenance cost, capable of converting temperature differences directly into the electricity are attractive in many practical applications. Thus thermoelectric generator (TEG) has the potential to play an important role in future energy devices. A TEG operates as a thermal engine; it works between a heat source and a heat sink and transforms a portion of the heat into electricity. By matching the TEG's thermal impedance with the thermal impedances of the heat exchangers, used to transmit the heat from the heat source to the heat sink, the output power by the TEG can be maximized. Similar to other heat engines working based on Carnot cycle, by enhancing the temperature difference across the device, the performance of a TEG increases. The temperature gradient through the TEG and the material properties of the semiconductors are two key parameters in the efficiency of a thermoelectric generator. The low conversion efficiency of the TEGs restricts the use of these to niche applications. In the last years, remarkable ongoing efforts on material analysis have delivered both new materials for TEG energy conversion along with innovative ideas to reach higher efficiencies. Promising potentials to enhance the efficiencies can be observed with current progress in the nanotechnology and low dimensional schemes.

1.2 FUNDAMENTALS OF THERMOELECTRIC DEVICES

A thermoelectric device is a circuit comprising two dissimilar thermoelectric materials, an n-type (negatively charged); and a p-type (positively charged) semiconductors, that are connected thermally in parallel and electrically in series, as shown in Figure 1.1. Metal interconnectors are used to connect the semiconductors. The semiconductor materials are recognized as thermoelectric (TE) materials. They are the main part, and are known as the core of the TEG. Semiconductors are sandwiched between two ceramic layers. When there is a temperature gradient across the two junctions of the TE materials, a direct electric current that normally has a proportionate relationship with the temperature gradient will flow through the circuit.

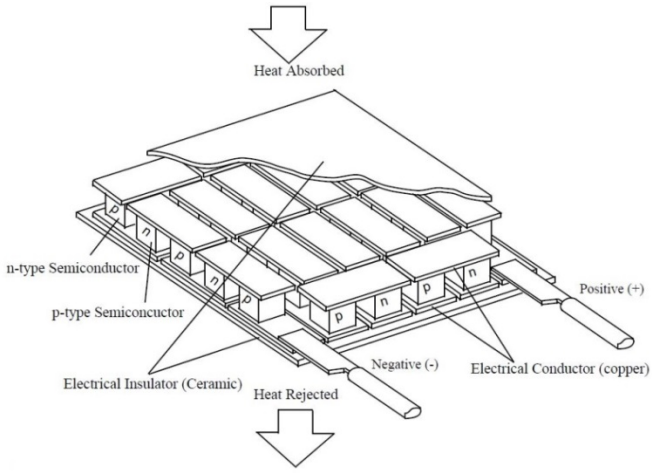

Fig. 1.1: Cutaway of a thermoelectric generator module [1].

Seebeck, Peltier and Thomson effects are the elementary effects of every working TEG. In the following sections, these effects will be explained in the order of their finding.

1.2.1 SEEBECK EFFECT

In 1821-3 Thomas Johann Seebeck found that an electromotive force (EMF) or potential difference could be generated by a circuit made from two different metals, shown in Figure 1.2, when there is a temperature gradient between two junctions of dissimilar metals [2]. An electric current is driven in the closed circuit by the produced electric potential. This is

recognized as the Seebeck effect. Figure 1.2 illustrates a circuit made from two unalike semiconductors a and b. The semiconductors are connected thermally in parallel and electrically in series. When there is a temperature difference between junctions A and B, an open circuit EMF is developed between C and D, which can be given by:

$$V = \alpha(T_h - T_c) \qquad (1-1)$$

where α is the Seebeck coefficient with the unit V/K or more frequently used as $\mu V/K$. The Seebeck coefficient is the voltage per unit temperature difference that can be produced by the TE material [3].

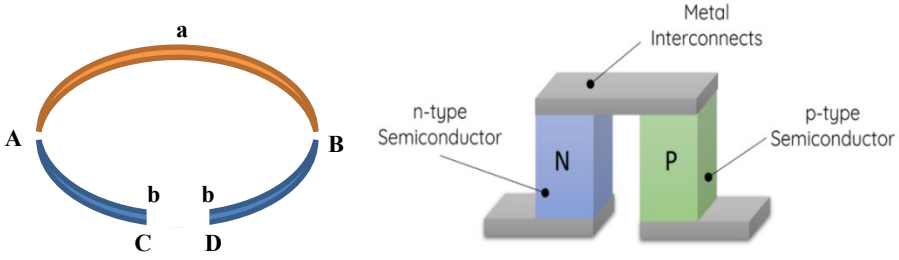

(a) *(b)*

Fig. 1.2: (a) Schematic of the basic thermocouple, (b) Schematic of a uni-couple TEG.

1.2.2 PELTIER EFFECT

Thirteen years later, in 1834, Jean Charles Athanase Peltier illustrated that if an external EMF source applied through C and D and an electrical current flow in the circuit, a temperature change will occur at the junctions [4]. This phenomenon is known as the Peltier effect. Somewhat, the Peltier effect defines the phenomenologically inverse effect of the Seebeck effect. The rate of heat generation (q) is produced at junction A or B, and the cooling rate ($-q$) is generated at another junction. In this system, shown in Figure 1.2, the ratio between q and I is known as the Peltier coefficient (π) and its unit is W/A or V [4].

$$\pi = \frac{q}{I} \qquad (1-2)$$

1.2.3 THOMSON EFFECT

In 1851 William Thomson (and later Lord Kelvin) [5] presented an inclusive description of the Seebeck and Peltier effects and defined their interrelationship (recognized as the Kelvin relations). Thermodynamics is connecting the Peltier and Seebeck coefficients. Based on this thermodynamic relationship, Thomson introduced the third thermoelectric effect, called Thomson effect. Compare to the Peltier and Seebeck effects, Thomson effect has less impact in TEGs but still should not be ignored in the detailed computations. Thomson effect illustrates the amount of the produced reversible heat (q) inside a semiconductor when it is exposed to a temperature gradient (ΔT) while flowing an electrical current (I) through it [3].

$$q = \beta I \Delta T \qquad (1-3)$$

In equation (1-3), β is the Thomson coefficient that has the same unit with Seebeck coefficient, V/K.

1.2.4 THE KELVIN RELATIONSHIPS

Kelvin relations were obtained by combining the three equations mentioned above for different TE effects. Therefore, for two different joined materials "a" and "b" [3]:

$$\alpha_{ab} = \frac{\pi_{ab}}{T} \qquad (1-4)$$

$$\frac{d\alpha_{ab}}{dT} = \frac{\beta_a - \beta_b}{T} \qquad (1-5)$$

1.2.5 FIGURE OF MERIT

For a particular material the capability of generating TE power is depended to its dimensionless figure of merit (zT) defined as [3]:

$$zT = \frac{\alpha^2}{\rho\kappa} T = \frac{\alpha^2 \sigma}{\kappa} T \qquad (1-6)$$

Equation (1-6) illustrates that zT is a function of the thermal conductivity κ, Seebeck coefficient α, temperature T and electrical conductivity σ.

1.2.6 THERMOELECTRIC GENERATOR APPLICATIONS

Long lifetime, high reliability, silent operation and simplicity of TEG enable this solid-state technology to be used in different applications. TE effects are consequences of the interfering of heat flow and electrical current in different materials. Heat can be directly converted to electricity [6–9] using this interaction. Different types of TEGs with different materials can be used in various applications and over a wide range of the temperature from room temperature up to 1000 °C. TEGs along with thermal generators have been used in the space industry from the commencement of the conquest of space [10-17]. TEGs can generate electricity with high reliability and low maintenance cost for the remote applications [18-19]. Converting the recovered waste heat to electricity is one of the main challenges for the scientists and industry. TEGs can harvest a fraction of the waste heat in different devices like automobile applications [20-26], aircraft and helicopters [27-29], ships [30-32], locomotive industries [33] and other devices [34-37]. About 17% of the world populations, who live in the developing countries, do not have access to the electricity grid [38]. TEGs can be used in domestic applications like cookers and stoves in the both developing [39-45] and developed countries [46-50]. Smart sensors need just a few hundred microwatts to operate. TEGs as solid-state devices can provide this amount of power [51-61]. Solar radiation, as an infinite source of energy, can be used as the heat source for the solar TEG systems [62-64]. TEGs also can be integrated with other devices like photovoltaic cells to harvest the waste heat and convert a fraction of that to the electricity [65-67]. Several studies have considered the various applications of the TEGs in different industries [68–77].

Alongside the currently known niches, by increasing the power density and efficiency and, also, ongoing improvement of energy costs, TEGs can be used in further applications competitively with the conventional sources of energy.

1.3 SOLAR THERMOELECTRIC GENERATORS

Solar thermoelectric generators (STEGs) are interesting devices to convert solar energy into electricity. STEGs are capable of tolerating high incident solar radiations. They are highly reliable with a simple structure and without any moving parts.

The fundamental idea in the STEG systems is to utilize the solar radiation as a heat source for the TEG [67]. The simplest STEG system comprises of a TEG that is located between a solar absorber and a heat sink. Typically and in general terms, an inclusive STEG system is composed of five main components [78], see Figure 1.3:

1. **Optical collector**, that collects and concentrates the photons receiving from the Sun. Commonly, flat plate, parabolic troughs, Fresnel lenses, and parabolic dishes are using as the solar collector in the STEG systems.
2. **An opto-thermal converter**, which transforms photons into heat. That is normally an appropriate solar selective absorber, which is deposited on a metallic layer. This thermal absorber should maximize the absorbed heat and minimize the radiative heat losses.
3. **A thermoelectric converter**, which is the most important component of the STEG system that converts the thermal input into electricity.
4. **A cooling system,** which ejects heat at the cold side of the TEG. Selecting a high-performance heat sink is very vital for the STEG system in order to maximize the temperature difference between the hot and cold side of the TEG.
5. **A thermal collector**, which directs the heat to the TEG. In order to reduce the heat losses, high thermal conductivity and low emittance material are needed for this element of the STEG system. Furthermore, an evacuated encapsulation is required to diminish thermal convective losses.

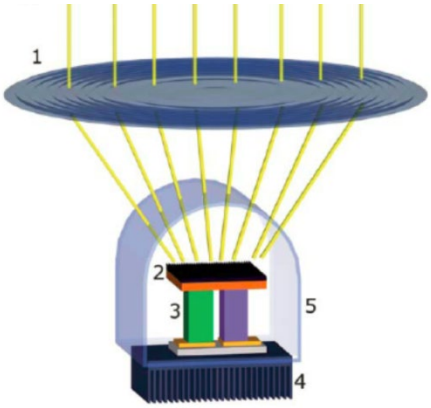

Fig. 1.3: Schematic of a typical STEG system (1) Optical concentration. (2) Thermal absorber. (3) TEG. (4) Heat sink. (5) Vacuum encapsulation [79].

1.3.1 EFFICIENCY OF STEGS

Figure 1.3 illustrates that the components of the STEG system are thermally in series, and consequently the efficiency of the STEGs can be defined as the product of the efficiencies of all the components [78]:

$$\eta_{STEG} = \eta_{opt}\eta_{ot}\eta_{TEG}\eta_{HS} \qquad (1-7)$$

In equation (1-7), η_{opt} is the efficiency of the optical collector that is not dependent on the temperature. η_{ot} is the efficiency of the opto-thermal converter that along with the efficiency of the TEG, η_{TEG}, are the main parameters that are affecting the efficiency of the STEG system. The efficiency of the heat sink is defined as η_{HS}, which is changing case by case and depends on the selected heat sink [78].

1.4 INTRODUCTION TO PHOTOVOLTAICS, OPPORTUNITIES AND CHALLENGES

Photovoltaics (PVs) are the best known and most efficient devices to convert solar energy into the useful electric power. Each solar panel includes some solar cells that convert radiative energy into electricity using semiconducting materials that display the photovoltaic effect. Similar to any other device, solar cells have some pros and cons as well. They are pollution-free, have no moving parts and long lifetime [80] with a very low maintenance fee. The efficiency of the PV cells is quickly increasing while mass-production charges are dropping very fast [81]. One of the biggest disadvantages of the PV system is that almost 10-25 % of the input solar energy will be lost if a tracking system is not used. Another drawback of the PV system is that clouds, dust, and other obstructions in the atmosphere are also affecting the output power and efficiency of the PV systems [83].

1.4.1 SOLAR CELL I-V CHARACTERISTIC CURVE

Figure 1.4 illustrates the current-voltage (I-V) characteristics for typical PV cell working under standard conditions. The output power of a solar cell can be obtained by multiplication of voltage and current ($V \times I$).

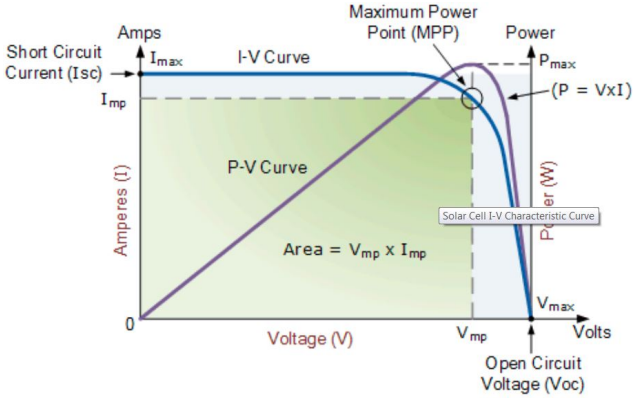

Fig. 1.4: I-V-P characteristics for typical PV cell [84].

When the PV cell is not connected to an electrical load, the current will be zero, and the voltage through the PV cell has its maximum value, recognized as the PV cells open circuit voltage, V_{oc}. On the other hand, when the negative and positive leads are directly connected, the PV cell will be short circuited. In this situation, the output current of the PV cell reaches to the short circuit current, I_{sc}, that is the maximum value of the current in the PV system while the voltage across the cell will be zero.

Figure 1.5 displays the electrically equivalent circuit for a solar cell. In the ideal condition, a PV cell can be demonstrated by a current source in parallel with a diode, but in the real condition, there is no ideal solar cell. Therefore, a series and a shunt resistance element are added to the model [85].

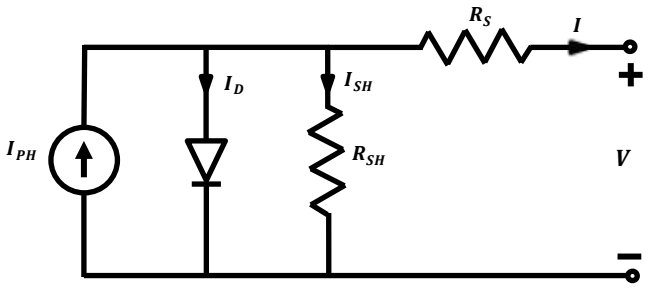

Fig. 1.5: The equivalent circuit of the CPV module with a single-diode system.

Using this model, the current of the PV cell can be defined as a function of the voltage of the PV cell. Therefore, the I-V relationship is given as [86-87]:

$$I = I_{PH} - \frac{V + IR_S}{R_{SH}} - I_0\left[\exp\left(\frac{V + IR_S}{nV_T}\right) - 1\right] \quad (1-8)$$

where, I_{PH} is the photogenerated current, R_{SH} is the shunt resistance, R_S is the series resistance, I_0 is the reverse saturation current , the thermal voltage $V_T = kT/q$ and n is the diode ideality factor which for the ideal diode is 1. Power generation by the PV cell can be obtained by the product of the voltage and current of the cell, then:

$$P = VI \quad (1-9)$$

In Figure 1.4, the maximum power by the PV cell is:

$$P_{max} = V_{mp} I_{mp} \quad (1-10)$$

The efficiency of a PV cell can be defined based on this maximum power:

$$\eta_{STEG} = \frac{P_{max}}{P_{in}} \quad (1-11)$$

In equation (1-11), P_{in} is the total input power to the PV cell per area for a certain photon spectrum $\Phi^0(\lambda)$ and can be calculated as [78]:

$$P_{in} = \int_{\lambda} \frac{hc}{\lambda} \Phi_0(\lambda) d\lambda \quad (1-12)$$

where c is the speed of light and h is the Planck constant.

1.4.2 SOLAR CELL APPLICATIONS

The total solar radiation received to the earth is approximately ten thousand times more than the present world electrical power consumption. PV cells are promising devices to harvest solar radiation. A solar PV system is a power system intended to produce useful solar power using photovoltaics. PV systems transform solar radiation directly to electrical energy and can play an important role encounter with the world's energy demand. PV cells are being used in a diversity of both terrestrial and space energy generation applications.

Solar PV systems can be used in a rooftop and building integrated systems [88-89]. Normally, residential rooftop PV panels have low capacities of about 5–10 kW, but

commercial rooftop PV panels mostly amount to some hundreds of kW [90]. PV cells are used in photovoltaic thermal (PVT) hybrid solar systems that change solar radiation into thermal and electrical energy [91-92]. PV systems are using for electrification of the rural areas. In the developing countries, where the distances of the villages from the grid power are mostly more than 5 km, PV systems are getting more of interest [93-96]. Recently, PV systems have been used in standalone applications including water pumps [97], trash compactors [98], parking meters [99-100], solar lamps, emergency telephones, charging stations [101-102], temporary traffic signs, and remote guard posts and signals. PV systems are mostly used in boats, cars, and airplanes to produce auxiliary power and not motive power [103-104]. Solar arrays can be used in telecommunication and signaling systems [105] and spacecraft applications to activate the cooling and heating systems, run the sensors, and communications [106].

1.4.3 A PRIMER ON MULTI-JUNCTION (MJ) SOLAR CELLS

Solar cells are in different types and classifications based on the materials and form of the applications. Single-junction solar cells are made of only one single layer of light absorbing material. In order to take advantage of different absorption and charge separation mechanisms, MJ cells can be used. They were produced for space application with massive investments, but the expense is now reasonable for domestic uses. The price of a $5mm \times 5mm$ triple-junction solar cell is 9.9 USD [107]. MJ cells have multiple p-n junctions made of different semiconductor materials to match the solar spectrum.

The main advantage of the MJ cells is that for various wavelengths of light, the p-n junction of each semiconductor material generates electric current. With using different materials in the MJ cells, a wider range of wavelengths can be absorbed, see Figures 1.6 and 1.7. With increasing the number of the junctions, the efficiency of the cell is also enhanced. In theory, using a MJ solar cell with an infinite number of junctions leads to having a maximum efficiency of 86.8% under highly concentrated light while the common single-junction cells have a limiting theoretical efficiency of 34% [108].

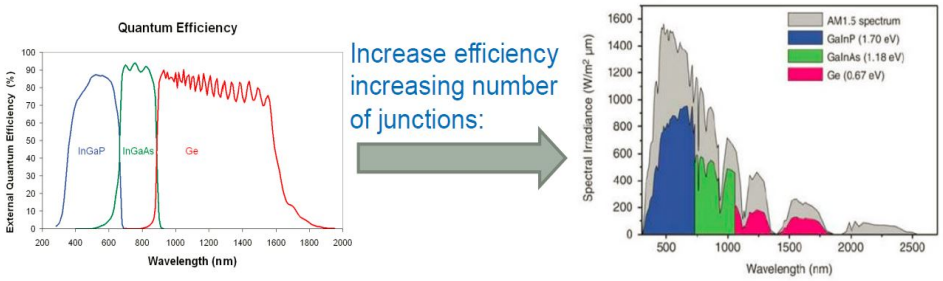

Fig. 1.6: Variation of the external quantum efficiency and spectral irradiance for different materials versus the wavelength [109].

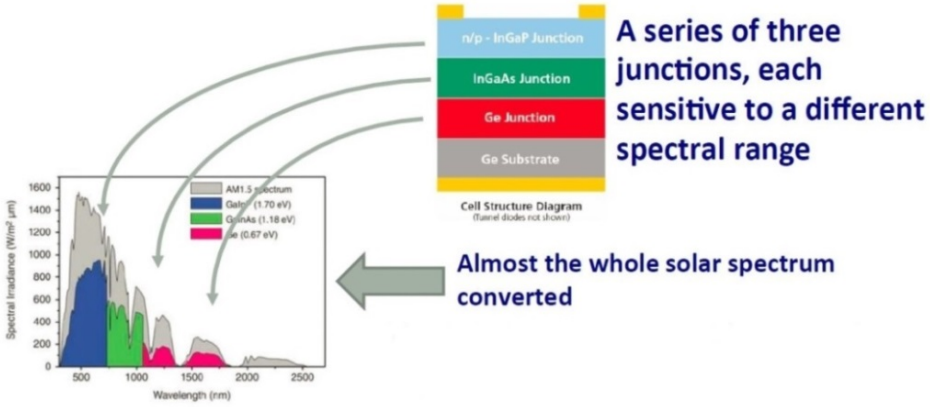

Fig. 1.7: AMI1.5 Spectrum published by the American Society for different materials [109].

1.4.4 CONCENTRATED PV CELL

In contradiction of traditional PV systems, concentrating photovoltaic (CPV) system employs different optical systems to concentrate a big area of light onto small, but more efficient, MJ solar cells for maximum efficiency. CPV technology entered the market as a utility-scale choice to generate electricity from solar energy. Generally, according to the concentration factor, there are two classifications for the CPV systems. Low concentration PV (LCPV) that is related to the concentration ratios less than 100 suns. In the LCPV systems, one or two axis tracking system can be used, and the type of the converter is mostly c-Si cells however other cells can also be used. The second class of the CPV cells is

high concentrating photovoltaic (HCPV) systems associated with solar concentrations varying between 300 to 1000 suns. III-V multi-junction solar cells are used for the HCPV systems. In HCPV systems, two-axis sun tracking system should be used [110]. Particularly, the HCPV systems have the maximum efficiency, 46% [111], of all current PV technologies and have the capability to compete with the other technologies in the close future. The main reason for large-scale power plants using HCPV is the substantial enhancement in the efficiency of individual modules, which diminish the area-related system expenses as well. Furthermore, in the HCPV systems smaller photovoltaic array also decreases the balance of system expenses.

The crucial point about using the CPV is employing the cost-efficient concentrating optics which dramatically decreases the cell area. Consequently, a more expensive cell with higher efficiency can be used that is capable of reducing the cost of electricity and competing with the traditional flat-plate PV technology and concentrated solar power in sunny regions with high direct normal irradiance (DNI) [111]. CPVs are more appropriate for the areas with the DNI more than 2000 $kWh/(m^2a)$.

Similar to any other technologies, CPVs also have some strengths and weaknesses. Having high efficiencies, low temperature coefficient, stable energy generation during the day owing to the tracking system, very small energy payback time and low environmental effect are the main advantages of the CPV systems. They also have lower sensitivity to the variation of the semiconductor prices and have higher competence for enhancing the efficiency in the future in comparison with single-junction flat plate systems.

CPV systems also have some drawbacks. HCPV systems cannot harvest the diffuse radiation, and LCPV can utilize a part of it. CPVs also need highly accurate and reliable tracking systems. They need regular cleaning to diminish soiling losses. CPVs have restricted market because they can just be employed in areas with high DNI and also they cannot be simply mounted on rooftops. They also have extra optical losses, and there is a lack of technology standardization for the CPVs. [110]

1.5 THESIS OBJECTIVES

The general objective of this Ph.D. project is to progress the state-of-the-art in the fields of TEGs, STEGs and hybrid CPV-TEG systems. To this end, the following specific objectives are elaborated:

1. TEG systems:
    a. Study the impact of different operating conditions on the power generation of the TEG.
    b. Considering the effect of employing force convection heat transfer instead of natural convection heat transfer on the output power of the TEG.
    c. Investigation of the transient response of the TEG system to the electrical load variation.
    d. Determination of the impact of the volumetric flow rate in the heat exchangers on the performance of the TEG system.
2. STEG systems:
    a. Evaluation of the performance of the oxide-based STEG system under various solar concentrations.
    b. Determination of the influence of using graphite sheet as an absorber on the performance of the Bi-Te and oxide-based STEG systems under the steady state condition.
    c. Investigating the transient response of the Bi-Te and oxide-based STEG systems under variant solar concentrations.
    d. Establishment of a numerical transient model to validate the experimental results and to optimize the STEG systems.
3. Hybrid CPV-TEG system:
    a. Development of a comprehensive numerical model to evaluate the performance of the CPV and TEG in a hybrid CPV-TEG system under both transient and steady state conditions.
    b. Determination of the role of each energy harvesting device in the hybrid CPV-TEG system in the power generation by the system and evaluate the effect of the TEG on stabilizing the output power by the hybrid system under the transient condition.
    c. Simulation of detailed transient response of the hybrid CPV-TEG system under variant solar concentrations by development of COMSOL Multiphysics Modeling Software.
    d. Study the impact of critical parameters on the performance of the hybrid CPV-TEG system.

1.6 THESIS OUTLINES

The dissertation includes two main sections. In the first part, a summary report based on the published and submitted papers is presented. The second part of the thesis comprises of the Papers A-J that are already published or submitted for publication. The outcomes of this investigation are presented in six chapters. A summary of the content of each chapter in the first part of the thesis is given as follows:

Chapter 1: Briefly describes the thermoelectricity phenomenon, different TE effects, and applications of the TEGs. Furthermore, the STEG systems are introduced, and application and efficiency of the STEG systems are discussed concisely. An introduction to the PV cells and their application is presented. MJ cells and the CPV systems along with their weaknesses and strengths are also considered in this chapter. The chapter is accomplished with the objectives and outlines of the thesis.

Chapter 2: Starts with a literature review in the field of waste heat recovery and the effect of different operating conditions on the performance of the TEG systems. In the next part, an overview of the literature in the fields of STEG systems and hybrid CPV-TEG systems are presented. For each section, after presenting the literature review, the state of the art of the current investigations is summarized.

Chapter 3: Describes the experiments conducted to investigate the effect of the different boundary conditions on the performance of the TEG system. Effect of using force convection heat transfer instead of the natural heat transfer on the power generation by the TEG system is also examined. Furthermore, the transient thermal response of the TEG system to a load change is tested under different operating conditions. This chapter contains results described in Papers A and B.

Chapter 4: Describes the experimental procedure to evaluate the performance of the Bi-Te and oxide-based STEG systems in the steady state and transient conditions. In addition, a numerical simulation using the finite volume method is presented in this chapter to validate the experimental results and optimize the STEG systems to maximize the utilization of solar energy. Moreover, the impact of using a self-adhesive graphite sheet is examined experimentally and numerically. This chapter is a summary of Papers C, D, and E.

Chapter 5: Presents a comprehensive overview of the CPV-TEG hybrid system. In the first section of this chapter, both experimental and numerical approaches are used to investigate the transient response of the hybrid system under variant solar concentrations. Furthermore, COMSOL Multiphysics Modeling Software is employed to support the experimental

results. In the next part of this chapter, a steady-state study for the CPV-TEG hybrid system, under low concentration ratios, is presented using both numerical and experimental procedures. The contribution of each device in the output power by the system is obtained and discussed. In the last part of this chapter, a parametric study is carried out to evaluate the significance of the impact of different parameters in the hybrid system. This chapter covers outcomes described in Papers F, G, H, I and J.

Chapter 6: Summarizes the main conclusions from the whole study and suggestions and perspectives for future work.

CHAPTER 2. LITERATURE REVIEW AND STATE OF THE ART

A description of previous and on-going experimental and numerical studies in the field of waste heat recovery and the impact of various operating conditions on the performance of the TEG systems is firstly presented. It is followed by the literature review in the field of STEG systems and different hybrid PV-TEG systems. The states of the art of the current studies in different fields are briefly explained after the literature review of each section.

2.1 WASTE HEAT RECOVERY BY THERMOELECTRIC GENERATORS

TEGs are highly reliable devices with long lifetime and silent operation with no moving parts. All these specifications make TEG systems environmentally friendly and proper alternative energy technology to reduce reliance on traditional fuel sources. TEGs have low maintenance costs and do not require any fuel sources, therefore, they can be an appropriate option to harvest energy by the direct waste heat recovery and transform it into useful electricity. TEGs have been used in different applications like automobiles, power plants and other industries to harness the waste heat [112-115].

Ding et al. [116] investigated the performance and reliability of a Bi_2Te_3 TEG under different operating conditions. TEGs were exposed to continuous operation and thermal cycling to evaluate the performance of the system. They found that the commercially available Bi_2Te_3 TEGs used in the experiments are reliable for at least 500 cycles under thermally cycled hot side temperature < 90 ℃ and cooled at ambient temperature. Different operating conditions were applied [117] to a TEG system to evaluate the performance of the TEG system. The impact of different parameters such as the number of modules, the temperature of the hot side and flow rate of the water were studied experimentally. It was found that the effect of the heating temperature in the performance of the TEG system is more significant than other parameters.

Yu et al. [118] established a numerical model to consider the influence of the complex vehicle driving circumstances on the power generation by the TEG system. It is illustrated

that with faster deceleration or acceleration, the difference in the power generation by the TEGs becomes more significant. In addition, the transient thermal and electrical response of the TEG is more substantial in deceleration than acceleration. An analytic model is established by Hsiao et al. [119] to determine the characteristics of the TEG system. The impact of the coolant temperature of the radiator and the speed of the engine on the performance of the TEG were investigated, and the thermal efficiency and output power by the TEG system were obtained and discussed.

24 TEGs were used by Hsu et al. [120] to harvest heat from the exhaust pipe of an automobile and convert it to the useful electrical energy. Both numerical and experimental approaches were used to obtain the open circuit voltage and output power by the system under variant temperature differences. In order to recover the waste heat from a combustion chamber an experimental and numerical study was carried out by Aranguren et al. [121]. They considered the energy consumption of the cooling system of the TEG and investigated different cold heat exchangers and concluded that their sample has the capability to generate 100 W/m^2.

The purpose of the experimental investigation that would be presented in the chapter 3 of this thesis and paper A is to determine TEGs electrical performance to under different thermal boundary conditions. The influence of different parameters like the temperature and volumetric flow rate of the exhaust gas, and the impact of different volumetric flow rate in the heat sink of the TEGs are examined. In addition, in the cold side, the impact of using force convection heat transfer instead of natural convection heat transfer is studied.

2.2 TRANSIENT RESPONSE OF THE THERMOELECTRIC GENERATORS TO THE LOAD CHANGE

Owing to the reduction of conventional energy sources, finding clean and renewable energy sources are getting essential. As mentioned before, TEGs are small, solid-state and compact devices. These special aspects of the TEGs make them a suitable choice for various uses. In the real applications, we mostly face transient situations; therefore, the behavior of the TEGs under the transient condition is very vital to study. There are several of investigations which evaluated the performance of the TEGs under unsteady state conditions.

Finite element method was used by Jia et al. [122] to develop a numerical model to predict the transient behavior of the linear-shaped TEGs. It was found that decreasing the required time to reach the steady-state condition enhances the overall power generation and

efficiency of the TEG system. Transient behavior of a TEG subjected to the non-uniform heating was examined by Blandino and Lawrence [123] using both numerical and experimental approaches. The results showed that extremely efficient heat sink has to be used in this application to reach higher temperature differences through the TEG and then higher efficiencies.

A mathematical model was developed by Alata and Naji [124-125] to study the unsteady performance of a thermoelectric cooler (TEC). Normally, a complicated treatment is required to model the transient conduction heat transfer problems mathematically. There are different thermoelectric effects in a TEG system that makes the mathematical modeling more difficult. In order to model the time-dependent response of a TEG exposed to a transient heat source, the finite-difference scheme was used by Nguyen and Pochiraju [126]. The results showed the significant impact of the Thompson effect on the performance of the TEG. Fisac et al. [127] established a new TEG structure to increase the working frequency by reducing the response time of the TEG. The numerical results for the power generation by the new TEG were validated by an experimental examination.

The response of a Bi-Te based TEG in the unstable state of a silicon production plant is investigated by Savani et al. [128]. It was found that by enhancing the cooling efficiency, in order to maximize the performance TEG should be located as close as possible to the silicon melt and should have higher fractional area. Crane et al. [129-130] developed a numerical model to study a gas/liquid cylindrical TEG under both transient and steady-state conditions. Their model has the capability to simulate a broad range of operating conditions.

Most of the previous investigations in the field of waste heat recovery by the TEGs are focused on the steady-state conditions. While due to the importance of the transient conditions in the real applications, predicting the performance of the TEGs in the unsteady state condition is very crucial. In the experimental examination that would be considered in chapter 3 and paper B, the thermal response of a TEG system to a load change will be investigated. The impact of different parameters on the behavior of the system will be discussed.

2.3 SOLAR THERMOELECTRIC GENERATOR SYSTEMS

Due to the fast growth in energy demand, the consumption of energy has become a crucial concern. Fossil fuels are depleting very fast, and the demand for clean and renewable

energy is increasing rapidly. Sun is an infinite source of energy, and solar energy is clean, free and inexhaustible. Therefore, it can be a promising alternative for conventional energy sources. Various devises can be used to convert solar energy into useful electrical energy. Reducing the cost of the STEG systems in recent years makes the application of these devices interesting to harvest solar energy. Several investigations have been carried out to evaluate the performance of the STEG systems over a broad range of the temperature.

One of the primary investigations with significant results was presented by Telkes [131]. The efficiency of the STEG system in this study reaches to 3.35% for the optical concentration of 50. This remarkable result made lots of attractions among the scientists to employ TEGs for harvesting solar energy [132-135]. Chen [136] theoretically studied the efficiency of STEGs in the low-temperature range ($150 - 250\ ^{\circ}C$). The results showed that Bi-Te based materials are suitable in this range of the temperature and, in addition, in small or even no solar concentration, STEGs can reach the higher efficiencies in an evacuated environment.

An experimental analysis of a novel flat-plate STEG system was presented by Kraemer et al. [137]. The efficiency of the STEG system reached 4.6% with no solar concentration. In the next study, Kraemer et al. [138] developed a model and an optimization method for the earth-based STEG systems. The model with Bi-Te based material predicts 5 % efficiency for the TEG. In 2016, Kraemer et al. [139] presented another STEG system. The efficiency of the STEG was increased to 9.6 % for the solar concentration of 211 suns.

Madkhali et al. [140] developed a model to simulate and maximize the efficiency of a STEG system. They found that employing two radiation shields and cover glasses cause to enhance the efficiency until 7 %. A STEG system under concentrating light was investigated by McEnaney et al. [141]. The results showed that for the solar concentration 45 suns and with the existing bismuth telluride and skutterudite materials, the STEG system could reach to the efficiencies higher than 10 %. Liu et al. [142] numerically studied a flat-plate STEG system. Impact of using different geometries for the TEG and also the thermal concentration ratio were considered. The results indicated that the thermal concentration ratio and the length of the TEG legs are the most effective parameters in the performance of the STEG system.

A Bi-Te based STEG system is investigated by Candadai et al. [143] using both experimental and numerical approaches. The output power and the efficiency of the STEG system in the real temperature range of the TEG and for different solar concentrations were presented in their study. A useful correlation for the critical solar concentrations of STEGs was found by Rehman and Siddiqui [144]. It was found that the maximum temperature that

a TE module can withstand has the most considerable impact on the critical solar concentration.

Both experimental and numerical methods were used by Sun et al. [145] to study a flat-panel STEG system. They established an approach to optimize the STEG system. The results indicated that to maximize the performance of the STEG system, it is necessary to match the impedance of the generator and electrical load. The performance of a thermal-concentrated STEG system is investigated by Chen et al. [146] using both experimental and numerical methods. The study was carried out for three different geometry of the TEG. It was found that the best performance is related to the smallest TEG with the efficiency of 4.15 %. Kossyvakis et al. [147] employed ANSYS Workbench to simulate and optimize a STEG system. The results showed using low power TE modules are more efficient for the STEG systems that are using thermal concentration.

Many references have been focused on the application of the low-temperature TEGs in the STEG systems. However, there are fewer investigations on the use of the TEGs with medium and high-temperature ranges in the STEG systems. Progresses in the high-temperature TEGs have been developed a new class of the STEG systems that are capable of working under higher solar concentrations [148].

Pereira et al. [149] investigated a $Si_{80}Ge_{20}$ TE material based STEG system that was working under a high-temperature condition (> 450 ℃) and high concentration ratios (> 100). The results showed that the highest conversion efficiency of the STEG system is 1.8 %. In order to evaluate the efficiency of a STEG system, a numerical model is established by Baranowski et al. [150]. The STEG system was modeled as two separate subsystems including the solar absorber and the TEG. Thermally insulating cavities and solar selective absorber were two applied methods to reach 85 % efficiency for the absorber. The results indicated that for the concentration ratios between 250 to 300 suns, the efficiency of the STEG system could reach 15 %.

Tomeš et al. [151-152] examined a STEG system for direct conversion of the concentrated solar irradiance to the useful electrical energy. The consequence of the coated graphite sheet on the TEG on the performance and efficiency of the STEG system is evaluated as well. It is found that the STEG system with the coated graphite layer has higher temperature difference and the output power and efficiency of the system increases significantly. The optimum number of the TEGs that should be employed in a concentrated STEG system is specified by Kutt et al. [153]. A novel high-performance STEG system was examined by Rowe [154]. Si-Ge based TEG is used in this study, and it is found that the conversion efficiency of the STEG system can reach to 12 % in the operating

temperature of 1000 K. This remarkable result shows the advantage of operation at the high temperatures.

Three different bulk materials including silver antimony lead telluride alloys; skutterudite and Bi_2Te_3 were used by Li et al. [155] to examine the performance of a SCTEG system. A theoretical model was developed, and it is found that for the stated materials, the maximum possible efficiency can reach 14.1 %, 13.5 %, and 9.8 %, respectively. High-performance TE materials were used in the three-dimensional finite-element model of a STEG system established by Yang et al. [156]. The results showed that the contact resistance and heat losses are two key parameters that have the most significant effect on the overall efficiency of the STEG system. The efficiency of the STEG system for the working temperature between 300 K and 700 K reached 9.95 %.

The performance and conversion efficiency of different STEG systems in both steady state and transient condition will be presented in chapter 4 and papers C, D and E. Oxide-based and Bi-Te based STEG system are firstly examined experimentally. Furthermore, the finite volume method is used to develop a time-dependent numerical model for the STEG system. The numerical model is used to validate the experimental results and also to predict the performance of the STEG systems under different operating conditions.

2.4 HYBRID SYSTEMS

Despite the enormous progress in the PV technologies, in order to maximize the use of this energy source, the efficiency of the PV cells require to be more ameliorated. Currently, even the PV cells with the highest efficiencies can only convert less than half of the solar energy into the electricity. Therefore, more than half of the input energy is dissipated to the ambient via heat. TEGs can be used to harvest this waste heat and convert a part of it to the useful electrical energy.

Different references evaluated the feasibility of using TEGs to harvest the waste heat from the PV cells and enhance the overall efficiency of the hybrid system. These studies can be categorized as follows:

2.4.1 PHOTOVOLTAIC-THERMOELECTRIC (PV-TEG) HYBRID SYSTEMS UNDER THE STANDARD ILLUMINATION CONDITION

PV-TEG systems under natural sunlight condition have been studied in many of investigations in the field of hybrid systems. A numerical model to predict the performance of a PV-TEG hybrid system under different weather conditions was established by Rezania et al. [157]. The results showed that with existing TE materials, the role of the TEG in the overall power generation by the hybrid system is insignificant compare to the output power by the PV cell. Dallan et al. [158] studied a hybrid PV-TEG system under a non-concentrated light. A PV cell and a TE module were located thermally in series. The results indicated that under identical thermal input situations the output power by the PV cell in the hybrid system enhances up to 39 % compared to the operation of the PV cell when it works alone. The impact of temperature and different illumination levels, as two crucial factors, on the performance of a PV-TEG hybrid system was studied by Cotfas et al. [159]. It was found that, using the TEG in the hybrid system cause a reduction in the temperature of the PV cell and subsequently the power generation by the PV cell increases.

A theoretical study on the performance of a PV-TEG hybrid system using for space application was presented by Kwan and Wu [160]. Optimization on the design of the TEG was carried out. The results indicated that for the space applications, TEG plays an important role in power generation by the hybrid system. An optimization approach for the PV-TEG hybrid systems is offered by Kraemer et al. [161]. PV-TEG hybrid system was modeled by Sark [162] in order to evaluate the performance and efficiency of the hybrid system. It is found that, depends on the integrated PV and TEG, the efficiency of the hybrid system can be improved 8-23 %. Dye-sensitized and poly-Si solar cells were used in the theoretical and experimental investigation by Kossyvakis et al. [163] to consider the performance of the PV-TEG hybrid system. The study was carried out for different geometries of the thermoelement of the TEG, and it is found that the performance of the PV-TEG hybrid system enhances by reducing the length of the thermoelements. Different PV-TEG hybrid systems were examined under non-concentrated and concentrated solar radiations [164]. It is found that some of the PV-TEG hybrid systems require higher efficient materials to be applicable in the future.

2.4.2 PHOTOVOLTAIC-THERMOELECTRIC HYBRID SYSTEMS UNDER CONCENTRATED SOLAR RADIATION

Several investigations have been studied PV-TEG hybrid systems under solar concentration. The last advances in TE materials, STEG systems, and CPV-TEG hybrid systems were reviewed by Sundarraj et al. [165]. It is predicted that CPV-TEG hybrid systems have the potential to make remarkable progress in renewable technologies. In order to enhance the efficiency and optimize the design of the CPV-TEG system, a thermal resistance analysis was proposed by Yin et al. [166]. The results showed that the polymer PV cells and amorphous silicon are the best options under the concentrating light. A CPV-TEG hybrid system composed of a commercial TEG and GaAs-based PV module was studied by Kil et al. [167] under solar concentrations less than 50 suns. It is found that the efficiency of the CPV-TEG hybrid system is 3 % more than the efficiency of the PV-only system at concentration ratio 50. In order to present various approaches to design a CPV-TEG system, Zhang and Xuan [168] proposed a three-dimensional model of the CPV-TEG hybrid system. The impact of the thermal resistance on the performance of the hybrid system is evaluated, and it was found that the thermal resistance between TEG and environment has a more significant effect on the output power compared to the thermal contact resistance between TEG and PV cell.
In order to evaluate the performance of CPV-TEG hybrid system, a thermodynamic model was established by Lamba and Kaushik [169]. All the TE effects including Seebeck, Thomson, Joule and Fourier heat conduction effects were considered in their model, and it was found that in the optimal condition, the efficiency of the CPV-TEG hybrid system is 13.37 % higher than the PV-only system. A three-dimensional model of a CPV-TEG system was developed by Xu et al. [170] using COMSOL Multiphysics Software. The results illustrated that with using an identical cooling condition, the PV cell has a higher temperature in the CPV-TEG system than the PV-only system and consequently the power generation by the PV cell in the PV-only system is higher. Although in the CPV-TEG system the temperature and generated power have more stable distributions. COMSOL Multiphysics Software is also employed by Kiflemariam et al. [171] to simulate the behavior of a CPV-TEG system under different solar concentrations. The results showed that decreasing the thermal resistance can have a significant impact on the temperature and consequently the output power by the PV cell.

A theoretical model for both glazed and unglazed PV-TEG system was developed by Wu et al. [172]. The performance of the glazed system and unglazed were compared in their study. The impact of different parameters like the flow rate of the nanofluid and the wind velocity on the behavior of the system are also examined. The results showed that for an identical TE module, with increasing the figure of merit, Z, the overall efficiency of the

system will not be enhanced necessarily. Zhang et al. [173] established a theoretical model to investigate the effect of different parameters on the performance and efficiency of the CPV-TEG system under concentrated light. The results indicated that when the temperature of the polymer PV cell enhances, the efficiency of the cell primarily boosts and then decreases. A CPV-TEG hybrid system is investigated by Liao et al. [174]. Energy conservation law is used to establish a theoretical model for low solar concentrations. The results indicated that despite producing more power, CPV-TEG system is more efficient than CPV-only systems.
The role of different parameters in power generation and efficiency of a CPV-TEG hybrid system is examined by Zhang et al. [175]. The results showed that temperature is the most important factor in the efficiency of the hybrid systems. Furthermore, higher convection heat transfer coefficient enhances the temperature gradient and output power by the TEG. In order to evaluate the performance of the CPV-TEG hybrid systems, Li et al. [176] used energy and exergy analysis approach. The exergy losses and the exergy and energy efficiencies were obtained. It is found that the overall efficiency of the system can increase significantly by using a proper PV cell in higher solar concentrations. A numerical model for a spectrum splitting hybrid PV-TEG system was developed by Ju et al. [177]. It is found that the efficiency and performance of the spectrum splitting hybrid systems are higher than the PV-only system under high solar concentrations, and consequently, hybrid systems are more proper options in this working condition.

2.4.3 MULTI-JUNCTION PHOTOVOLTAIC-THERMOELECTRIC HYBRID SYSTEMS UNDER CONCENTRATED SOLAR RADIATION

Multi-junction (MJ) solar cells have higher efficiency in a smaller area, and it makes them interesting to study. The third category of the hybrid systems that have been examined less than two others are Concentrated MJ solar cells-Thermoelectric (CMJ-TEG) hybrid systems.

Sweet et al. [178-179] investigated the electro-thermal behavior of a novel concentrated CTJ-TEG hybrid system using both experimental and numerical approaches. The lifetime and output power by the hybrid system can be improved using the results of this study. Furthermore, the energy cost decreases. Cotfas et al. [180] experimentally investigated a hybrid system composed of a flat plate solar collector, MJ PV cells and TEGs. The impact of different illumination levels on the performance of the hybrid system was examined. It is found that when the hybrid system works under load resistance, the maximum generated power by the TEG drops considerably.

A CTJ-TEG hybrid system was experimentally investigated by Tamaki et al. [181]. The results showed that at high operating temperatures, the Bi-Te based TEG used in the hybrid system can harness a part of the waste heat from the CTJ and convert it to the useful electrical energy.

Beeri et al. [182] examined another CTJ-TEG hybrid system using both experimental and theoretical methods. The results illustrated that with increasing the concentration ratio, the share of the output power by the TEG in overall power generation enhances significantly. This contribution can reach 40 % for the concentration ratio of 200 suns. Moreover, the hybrid system has the potential to reach the efficiency of 50 % with using more efficient TE materials and CPV cells. The significant role of the TEG in the higher sun concentration levels was also examined and confirmed in a numerical investigation carried out by Rezania and Rosendahl [183].

In this thesis, a comprehensive study on the performance of the CTJ-TEG hybrid system will be presented in chapter 5 and papers F, G, H, I and J. Steady-state and transient conditions will be considered in the investigations. Both experimental and numerical approaches will be used to evaluate the contribution of each device in the overall power generation and conversion efficiency of the hybrid system. The significance of the impact of different parameters on the performance of the CTJ-TEG hybrid system will also be investigated.

CHAPTER 3. WASTE HEAT RECOVERY USING TEGS

In this chapter, an experimental study is carried out to evaluate the performance of a TEG system under different operating conditions. Impact of different parameters such as the temperature and volumetric flow rate in the heat sink and heat source over a broad range of electrical load is examined. The significance of employing force convection heat transfer instead of natural convective heat transfer is investigated as well. Moreover, the transient response of the TEG system to the load change is studied. This chapter summarizes work documented in Papers A [185] and B [184].

3.1 EXPERIMENTAL SETUP

The experiments were carried out in the Department of Energy Technology in Aalborg University (AAU). Figure 3.1 displays a view of the experimental setup. Four Bi-Te based commercial TEGs with the dimension of 30mm × 30mm × 4.2mm are employed in the experiments. TEGs are electrically connected in series and are located among finned plates with identical areas (100mm × 100mm), see Figure 3.2.

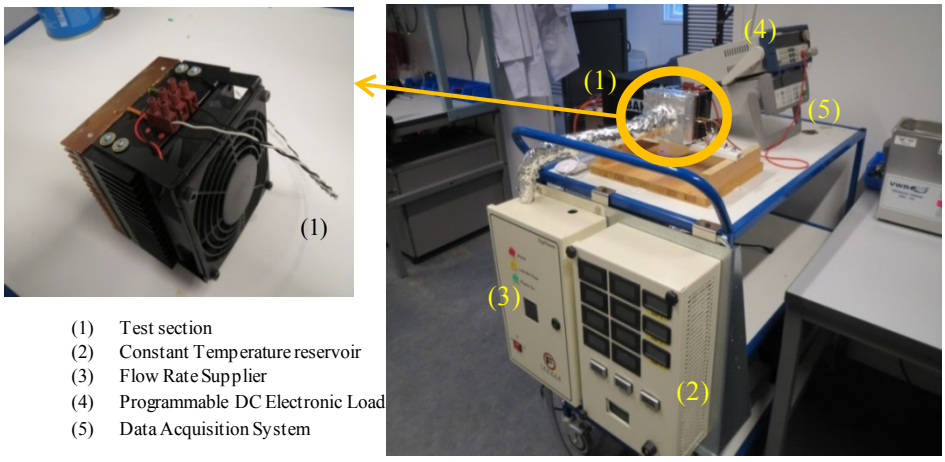

(1) Test section
(2) Constant Temperature reservoir
(3) Flow Rate Supplier
(4) Programmable DC Electronic Load
(5) Data Acquisition System

Fig. 3.1: A view of the TEG experimental setup [184].

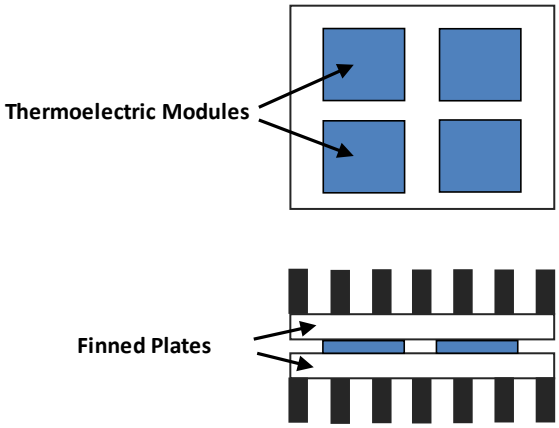

Fig. 3.2: Schematic diagram of the test section [185].

In order to deliver force convection heat transfer, an axial fan with an adjustable power source is employed in the experiments. As shown in Figure 1.1, a constant temperature reservoir and a hot gas supplier are used in the heat sink to provide different operating conditions. In order to measure the temperatures of the ambient and cold and hot sides of the TEGs, T-type thermocouples are used. In order to deliver different values of the electrical load to the TEGs, a programmable DC electronic load device is employed. The value of the volumetric flow rate in the heat sink is manageable using a DC power supply and with changing the fan power. The temperature and the volumetric flow rate in the heat sink are controlled by a constant temperature reservoir and a hot gas supplier, respectively. Values of the volumetric flow rate of the heat sink and heat source, output power and voltage by the TEGs and the temperatures of different places are measured and recorded through the experiments. All the obtained data are collected using an LXI (34972A) data acquisition system and can be observed continuously on a PC.

3.1.1 UNCERTAINTY ANALYSIS

The approaches offered by Kline [186] and Coleman and Steele [187] are used for uncertainty analysis of the measurements. All the experimental apparatuses are calibrated before the tests to ascertain the precision of them. The resolutions of different devices over the measuring range are illustrated in Table 3.1. The relative uncertainty of the equipment can be obtained by [187]:

$$\text{Relative uncertainty} = \frac{0.5 \times \text{resolution}}{\text{measuring value}} \tag{3.1}$$

Based on the values in table 3.1, programmable DC electronic load has the highest relative uncertainty equal to 2%.

Table 3.1: List of equipment relative uncertainties [184].

Equipment	Measuring range	Resolution	Relative uncertainty
Hot gas supplier	30 L/min-90 L/min	0.1 L/min	0.17%
Constant temperature reservoir	100° C-400° C	0.1° C	0.05%
DC power supply (for voltage)	3 V-13 V	0.00125	0.02%
Programmable DC electronic load (for electric current)	0.025 A-1.2 A	0.001 A	2%

Study of the errors in the experiment is also accomplished. The values of the temperature of different parts of the system together with the generated current and voltage by the TEG system are presented in table 3.2. The mean value ($\overline{X}$) is given by [187]:

$$\overline{X} = \frac{1}{n}\sum_{i=1}^{n} X_i \tag{3.2}$$

And the standard deviation (S_X) are obtained as [187]:

$$S_X = \left[\frac{1}{n-1}\sum_{i=1}^{n}(X_i - \overline{X})^2\right]^{1/2} \tag{3.3}$$

Then the uncertainty (S_J) can be defined as:

$$S_J = \frac{S_X}{\overline{X}} \times 100 \tag{3.4}$$

In Table 3.2, it can be observed that the maximum uncertainty is related to the cold side temperature and is equal to 1.98% that is lower than 6%. Therefore, it can be concluded that the experimental results are reliable.

As it can be seen in Table 3.2, the maximum uncertainty is 1.98% which is less than 6%. It shows that the experiments are reliable.

Table 3.2: List of experiment uncertainties [184].

Variable	1st	2nd	3rd	Mean value	Sample standard deviation	Uncertainty
T_{HA} (°C)	215.1°C	216.39°C	217.84°C	216.44°C	1.37°C	0.63%
T_H (°C)	165.37°C	166.52°C	163.91°C	165.26°C	1.31°C	0.79%
T_C (°C)	65.86°C	63.3°C	64.46°C	64.54°C	1.28°C	1.98%
V_{OC} (V)	11.874 V	11.919 V	11.932 V	11.908 V	0.0303 V	0.25%
V (V) (@P_{max})	5.763 V	5.697 V	5.724 V	5.728 V	0.0330 V	0.58%
I (A) (@P_{max})	0.451 A	0.450 A	0.448 A	0.450 A	0.0012 A	0.27%

3.2 EFFECT OF OPERATING CONDITIONS ON TEG POWER GENERATION

The electrical response of the TEGs to the different thermal boundary conditions is investigated in this experimental investigation. The significance of the impact of the temperature and volumetric flow rate on the performance of the TEGs are evaluated. Additionally, a comparison between natural and forced convection cooling in the heat sink is also presented. Figure 3.3 (a) displays the variation of the voltage against the current for various temperature differences. Based on equation 3.5, the internal resistance of the TEGs is indicated by the slope of the V-I curves.

$$V = RI \tag{3.5}$$

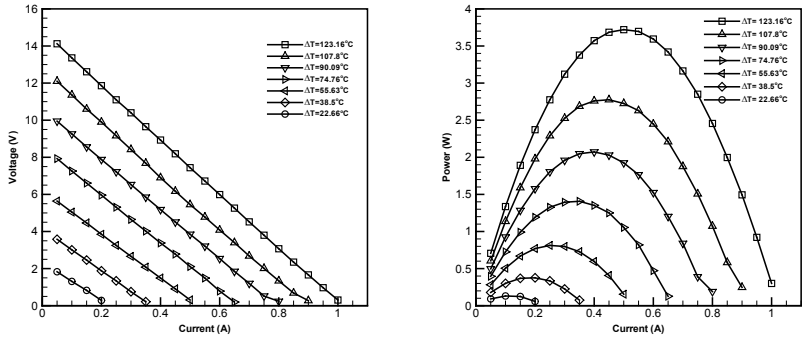

(a) *(b)*

Fig. 3.3: (a) V-I curves; (b) P-I curves for different temperature differences and with $Q_h = 90\ Lit/min$ and $Q_c = 406.3\ Lit/min$ [185].

Due to changing the slope of the V-I curves for various temperature differences, the thermal resistance also in varying between 10.29 Ω to 14.54 Ω. Consequently, the electrical load resistance should be about 12.41 Ω to achieve the maximum power. As it mentioned before, the slope of the V-I curves is slightly enhanced by increasing the temperature difference. The reason is that the operating temperature of the TEG affects the conductance of the materials [188-189]. Therefore, by enhancing the average temperature, the electrical resistance should also be increased.

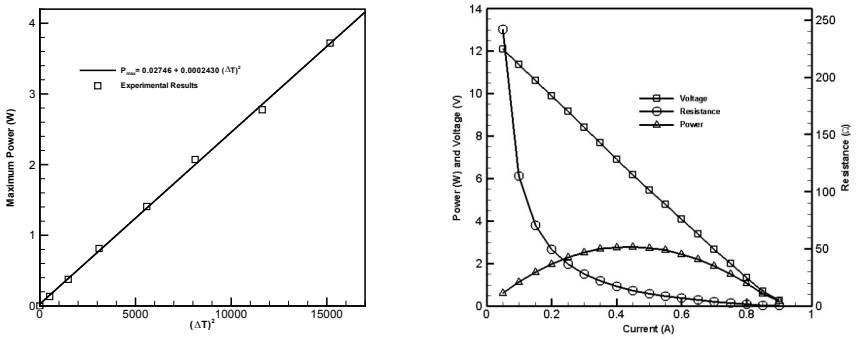

(a) *(b)*

Fig. 3.4: (a) Maximum power versus ΔT^2; (b) V-I, R-I and P-I curves for $\Delta T = 107.8°C$, $Q_h = 90\ Lit/min$ and $Q_c = 406.3\ Lit/min$ [185].

Figure 3.3 (b) shows the variation of the power generated by the TEGs versus the current for variant temperature differences. It can be observed that each curve has a maximum value. Figure 3.4 (a) illustrates the variation of these maximum power values against ΔT^2. The maximum output power by the TEGs for a given ΔT can be obtained as:

$$P_{max} = \frac{V_{OC}\, I_{SC}}{4} = \frac{(\alpha \Delta T)^2}{4R} \tag{3.6}$$

In equation 3.6, V_{OC} is the open circuit voltage and I_{SC} is the short circuit current. Equation 3.6 illustrates that the slope of the line in Figure 3.4 (a) represents the value of $\alpha^2/4R$. For the current TEG system, the slope is equal to 0.0002430. Using the internal resistance 12.41 Ω, the Seebeck coefficient will be obtained 0.1098 V/K. The variation of the voltage, resistance, and power versus current for the temperature difference ($\Delta T =$ 107.8°C) and with a volumetric flow rate $Q_c = 406.3$ Lit/min are shown in Figure 3.4 (b).

3.2.1 IMPACT OF USING FORCED CONVECTION HEAT TRANSFER INSTEAD OF NATURAL CONVECTION HEAT TRANSFER

The variations of the voltage and output power by the TEGs versus the current for different volumetric flow rates in the heat sink are shown in Figures 3.5 (a) and 3.5 (b), respectively. The significant impact of using forced convective heat transfer instead of natural convective heat transfer can be observed by comparing Figures 3.5 (a) and 3.5 (b) with Figures 3.6 (a) and 3.6 (b). The V-I and P-I curves for the TEG system when the natural convection is used are displayed in Figures 3.6 (a) and 3.6 (b).

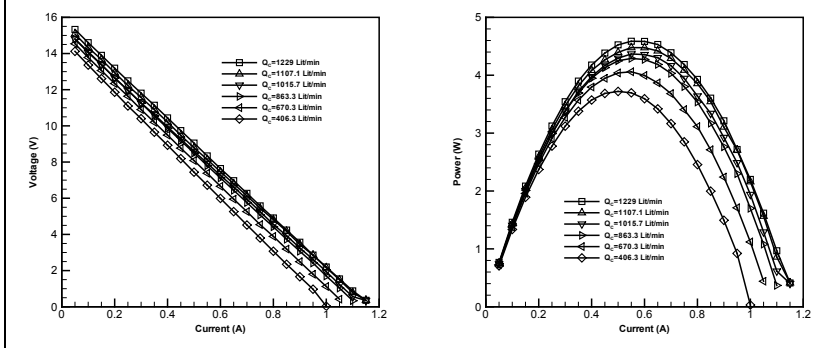

(a) *(b)*

Fig. 3.5: (a) V-I; (b) P-I curves, both for different volumetric flow rates of the fan in the cold side [185].

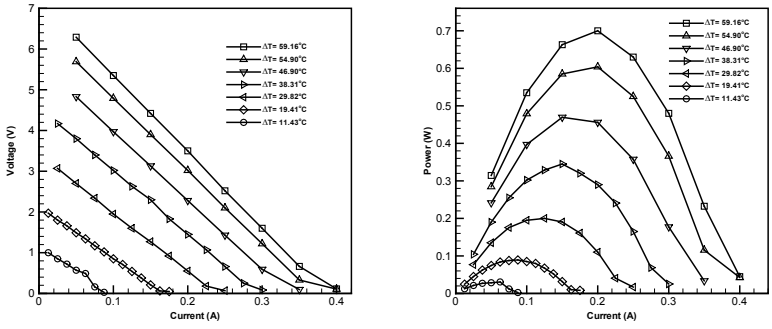

(a) *(b)*

Fig. 3.6: (a) V-I; (b) P-I curves, both for different temperature differences and $Q_h = 90\ Lit/min$ (natural convection cooling) [185].

Figure 3.6 illustrates that using natural cooling in the heat sink caused to have very less amount of voltage and power. Figure 3.5 shows that even using low volumetric flow rates in the heat sink, make a huge difference in output power and voltage. Figure 3.5 indicates that with increasing the volumetric flow rate, the output power in enhancing but this increment is not very significant. Therefore, in order to save energy used by the fan to produce higher volumetric flow rates, less volumetric flow rates are proposed to use in the heat sink.

The temperatures of the hot side T_H, the cold side T_C, the temperature differences ΔT, open circuit voltages V_{OC} and the maximum powers P_{max} for different operating conditions are presented in Table 3.3. The value of the both hot and cold sides temperatures are decreased with increasing the volumetric flow rate. However, the increasing of the temperature differences lead to have higher output power and voltage.

Table 3.3: The value of different parameters for various operating conditions [185].

	T_H (^oC)	T_C (^oC)	ΔT (^oC)	V_{OC} (V)	P_{max} (W)
Natural convection	236.9	177.74	59.16	7.2	0.7
Q_c=406.3 Lit/min	211.6	88.44	123.16	14.96	3.72
Q_c=670.3 Lit/min	202.14	74.33	127.81	15.35	4.06
Q_c=863.3 Lit/min	198.97	68.66	130.31	15.55	4.29
Q_c=1015.7 Lit/min	197.61	66.17	131.44	15.61	4.37
Q_c=1107.1 Lit/min	196.47	63.65	132.82	15.86	4.48
Q_c=1229 Lit/min	195.31	61.53	133.78	16.10	4.59

3.2.2 IMPACT OF VOLUMETRIC FLOW RATE IN THE HEAT SINK

Figure 3.7 illustrates the variation of the voltage and power against the current for the constant temperature of the reservoir ($T_{STR} = 200$°C) and various volumetric flow rates. Enhancing the volumetric flow rate and consequently having higher convective heat transfer in the heat sink cause to increment in the hot side temperature. However, the cold side temperature is also increases but, the temperature difference and consequently voltage and power are also enhanced. Figure 3.7 indicates the substantial impact of the volumetric flow rate on the temperature difference, voltage and power generation by the TEG system.

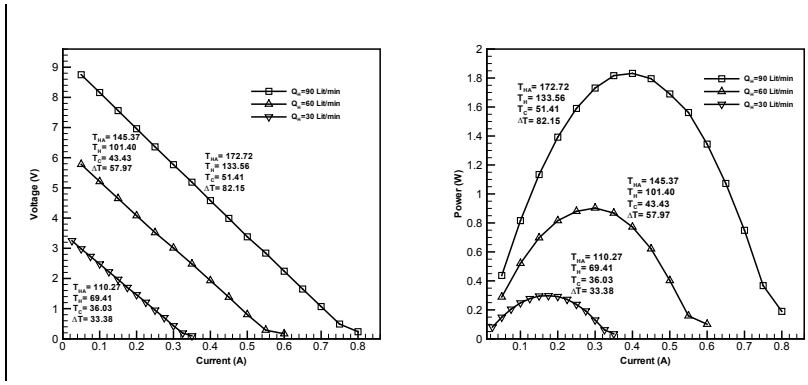

(a) *(b)*

Fig. 3.7: (a) V-I; (b) P-I curves, both for different volumetric flow in the hot side and $Q_c = 1015.7\ Lit/min$ *[185].*

3.3 TRANSIENT BEHAVIOR OF THE TEGS TO THE VARIANT LOAD

Most of the studies in the field of waste heat recovery application have been considered the steady-state condition. Though, in the practical applications, we mostly face transient conditions. The unsteady condition makes a significant deviation in the performance of the TEGs. In this section, the time-dependent thermal response of the TEG system to the electrical load change is examined experimentally. In the last section, the I-V-P curves in the steady state condition are achieved for different operating conditions. The maximum power and the equivalent current and voltage for various operating conditions are obtained. In order to examine the transient response of the TEG system, the voltage drops promptly from the open circuit value to the equivalent voltage for the maximum power that is acquired earlier.

3.3.1 EFFECT OF THE VOLUMETRIC FLOW RATE ON THE TRANSIENT RESPONSE OF THE TEG SYSTEM

Figures 3.8 and 3.9 display the temperature variations of the hot and cold sides of the TEG for the same temperature of constant temperature reservoir, T_{STR}, and different volumetric flow rates. In Figure 3.8, the voltage quickly changes from open circuit voltage, $V_{oc} =$

3.45 V, to the correspondent voltage of the maximum power, $V_{@P_{max}} = 1.66$ V. This variation for Figure 3.9 is from $V_{oc} = 8.67$ V to $V_{@P_{max}} = 3.98$ V. It can be observed that for both conditions, the hot side temperatures have a sensible variation. The hot side temperature variations in Figures 3.8 and 3.9 are 2.5°C and 5°C, respectively. Due to the lower applied volumetric flow rate in Figure 3.8, the variation of the cold side temperature is negligible while this value for Figure 3.9 is about 1°C.

This behavior can be described using the Peltier effect. Peltier effect acts against the power generation by the TEG and deviates the highest operational point from the commonly known maximum power point (MPP). The generated current by the TEG as a result of the Peltier effect changes the heat transfer passing through the TEG from the hot side to the cold side.

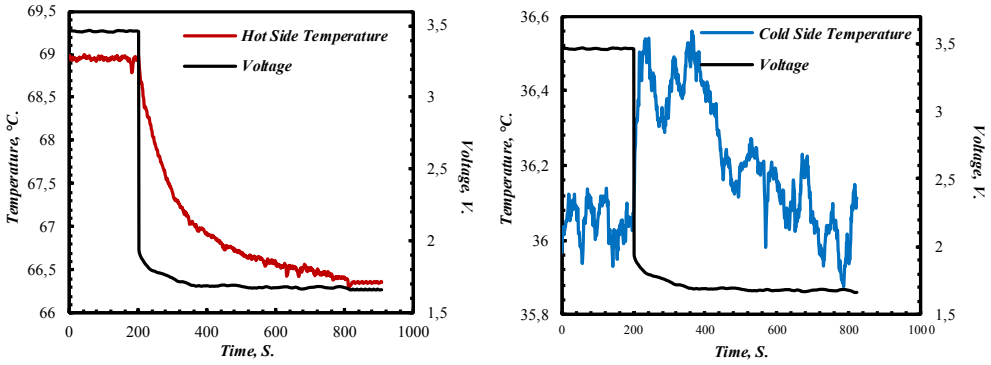

(a) (b)

Fig. 3.8: Variation of the hot and cold side temperatures and voltage versus time for $Q_h = 30\ Lit/min$ and $Q_c = 406.3\ Lit/min$ and $T_{STR} = 250°C$ [184].

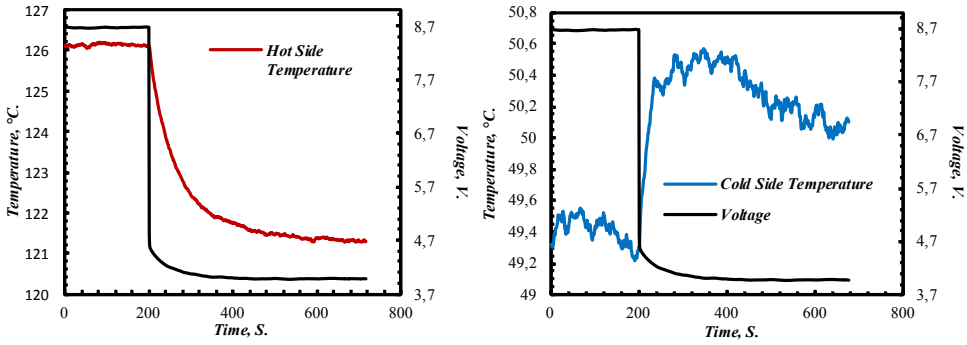

(a) *(b)*

Fig. 3.9: Variation of hot and cold side temperatures and voltage versus time for $Q_h = 90\ Lit/min$ *and* $Q_c = 1015.7\ Lit/min$ *and* $T_{STR} = 250°C$ *[184].*

3.3.2 EFFECT OF THE TEMPERATURE ON THE TRANSIENT RESPONSE OF THE TEG SYSTEM

Figure 3.10 displays the variation of the temperatures of hot and cold sides of the TEGs versus time for the same volumetric flow rate in the heat sink and the heat source and different temperatures of the reservoir, $T_{STR} = 400°C$. The voltage is changing promptly form open circuit voltage, $V_{oc} = 15.05$, to the correspondent voltage to reach the maximum power, $V_{@P_{max}} = 7.42$ V. As it can be observed, in comparison with Figure 3.9 in Figure 3.10 the reduction in the hot side temperature and the increment in the cold side temperature are higher. These values are 7.5°C and 2.5°C, respectively.

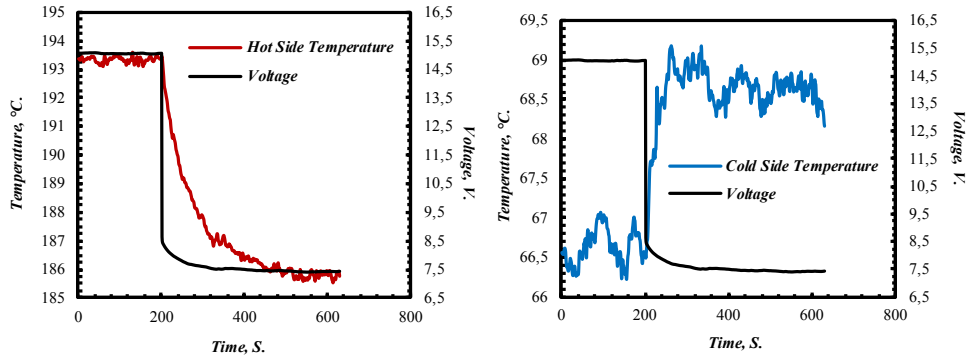

(a) *(b)*

Fig. 3.10: Variation of hot and cold side temperatures and voltage versus time for $Q_h = 90\ Lit/min$ *and* $Q_c = 1015.7\ Lit/min$ *and* $T_{STR} = 400°C$ *[184].*

CHAPTER 4. SOLAR THERMOELECTRIC GENERATOR SYSTEMS

The experimental method to investigate the performance of an oxide-based STEG system and a Bi-Te based STEG system is described in this chapter. A numerical model based on finite volume method is developed. This model can be used for every material with different properties. The model is applied to validate the experimental work, optimize the STEG system and predict the performance of the STEG system in the higher temperatures. In addition, the effect of attaching graphite sheet on the surface of the TEGs on the performance of the STEG system is investigated. This chapter covers outcomes described in Papers C [195], D [196] and E [204].

4.1 HIGH-TEMPERATURE OXIDE-BASED SOLAR THERMOELECTRIC GENERATORS

In this section, the behavior of an oxide-based STEG system under constant and transient solar concentrations is investigated using both experimental and numerical approaches. All of the experimental works presented in this chapter are carried out in Solar Technology Laboratory of Paul Scherrer Institute (PSI), Villigen, Switzerland. Furthermore, the established numerical model will be presented as well.

4.1.1 EXPERIMENTAL SETUP

In general, in the practical applications, TEG, solar collector and heat sink are three main components of a STEG system. Fresnel lenses, flat plate, parabolic dishes, and parabolic troughs are the most common collectors that are using in the real STEG systems. In this framework, in order to have more uniform solar concentrations with higher precision, a solar simulator is used. The high-flux solar simulator, shown in Figure 4.1, composed of 10 xenon arc lamps. The solar simulator is cooled by High-pressure water. The solar simulator is capable of generating extremely concentrated light up to 11000 suns ($11000\ kW/m^2$) on the focal point [190-191].

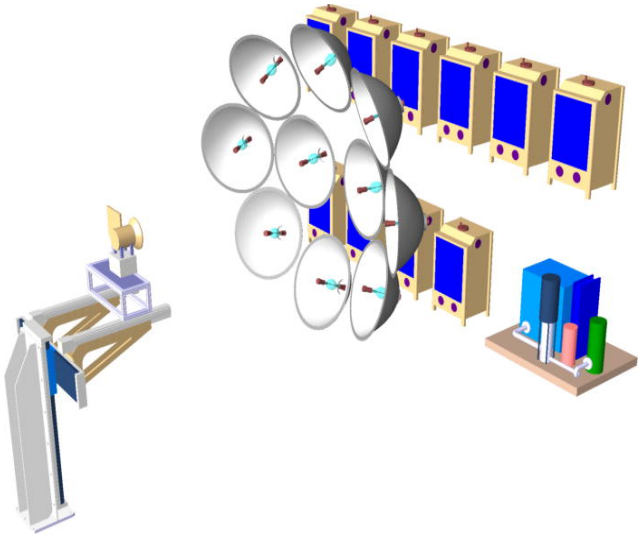

Fig. 4.1: solar simulator used in this study [192].

In the study of oxide-based STEG system, just six lamps are used to simulate up to 338 suns. An optical mixer is placed horizontally in front of the STEG system to make the concentrated light more uniform.

In order to find the solar intensity map, the distribution of radiative heat flux is measured and calibrated in advance using a thermogage sensor located on the exit plane of the optical mixer. Finding the area, $(42mm \times 42mm)$, with the most homogenous heat flux is very crucial to maximize the performance of the STEG system and the accuracy of the measurements.

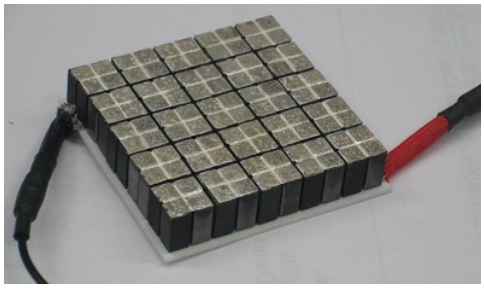

Fig. 4.2: Oxide TEGs used in experiments [193].

The TEG used in the experiments is a commercial oxide TEG model $CMO-25-42S$, see Figure 4.2. The high-temperature TEG has 50 uni-couples with the size of 42mm × 42mm. The P-Type and N-Type materials are $Ca_3Co_4O_3(Co-349)$ and $CaMnO_3(Mn-113)$, respectively [193]. A self-adhesive graphite sheet is used in the experiments [194] to increase the absorption of the input solar energy.

Figure 4.3 illustrates the schematic of the experimental setup. In order to remove the heat from the cold side of STEG system, a heat exchanger with constant mass flow rate 5 Lit/min of water, as the working fluid, is used. All the parameters like temperatures, power, voltage and current are measured with a data acquisition and control systems based on National Instruments cRIO. Two and three thermocouples are used to measure the temperature of the hot and cold sides of the TEG, respectively. The ambient temperature is also measured with another thermocouple.

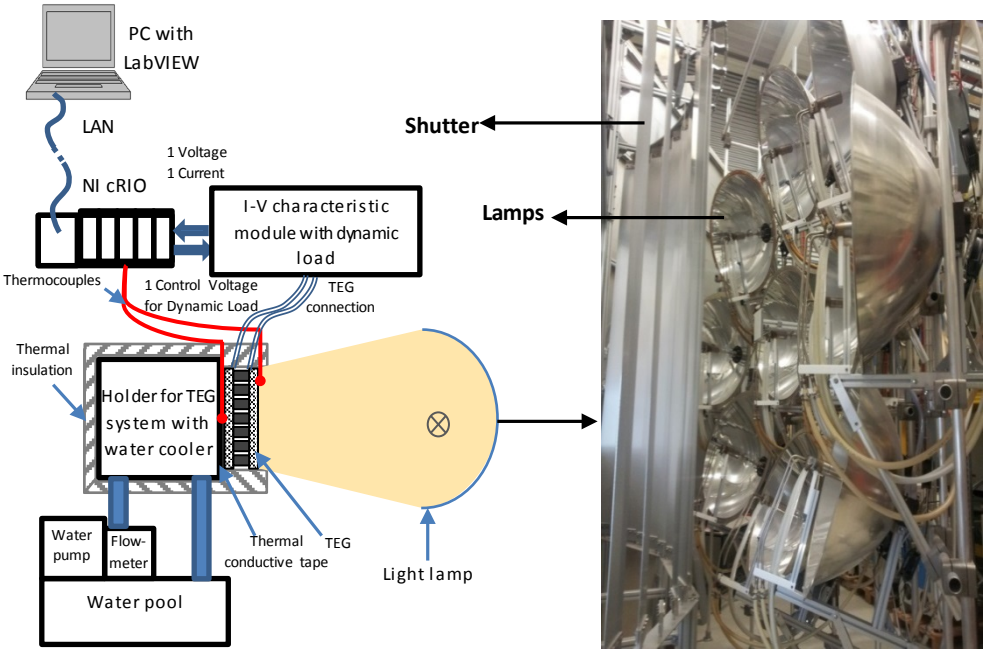

Fig. 4.3: Schematic of the experimental setup [195].

Dynamic impedance of a capacitor in the charging process (see Figure 4.4) is used to impose the dynamic electrical load to the STEG system. TEG works as a voltage source

when capacitor C is connected to it. To avoid the connection circuit resistance, the capacitor is pre-charged with the voltage source, V, when the switch K is in position 2. When the pre-charging process is completed, and with closing the switch K (position 1 in Figure 4.4), the capacitor will be discharged through TEG and then it will start changing until the value of the capacitor's voltage reaches to V_{OC}. In this way, it would be assured that the whole I-V characterization procedure is considered from $V_{TEG} = 0$ to $V_{TEG} = V_{OC}$.

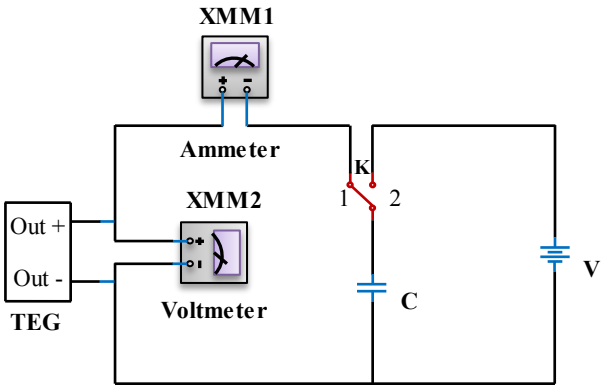

Fig. 4.4: Simplified schematic of the dynamic electrical load [196].

4.1.2 HIGH-TEMPERATURE STEGS UNDER CONSTANT SOLAR CONCENTRATIONS

In this section, the significance of the effect of attaching a graphite sheet on the top surface of the TEG in the STEG system will be discussed. When there is no graphite sheet, a high amount of the heat will be reflected from the surface, and consequently, the amount of the absorbed heat is less. With attaching the graphite sheet to the TEG, more energy will be absorbed. It can be concluded that for the same solar concentrations, the temperature of the STEG system with graphite sheet is higher than the STEG system without graphite sheet. The self-adhesive graphite sheet that is applied in the experiments has a temperature limit equal to 400°C. Therefore, the solar concentration should be managed in a way that the temperature does not exceed this temperature limit. Table 4.1 illustrates the applied solar concentrations to the both STEG systems with and without graphite sheet along with the open-rate percentage of the shutter. It is stated before that six lamps are used in this experiments to generate up to 338 suns. These lamps are permanently on during the

experiments, and the amount of solar concentrations is regulated with a shutter situated in front of the lamps.

Table 4.1: Solar radiation on the TEGs versus open- rate percentage of the shutter [195].

Shutter percentage (%)	5	20	30	40	50	60	70
Solar radiation (kW/m^2) for STEG without Gr	30	107	155	205	252	292	338
Solar radiation (kW/m^2) for STEG with Gr	30	107	-	-	-	-	-

The temperatures of the hot and cold sides of the TEG in both STEG systems are displayed in Figure 4.5. Due to the temperature limitation of the self-adhesive graphite sheet, the maximum solar concentration applied to the system with graphite is 128 suns. Both hot and cold side temperatures are enhanced with increasing the solar radiation. Due to the higher rate of absorbance in the STEG system with graphite sheet, the rate of increment of the hot side temperature is higher than the STEG system without graphite sheet. Consequently, the temperature of the system with graphite sheet enhances in the lower solar concentrations. It can be observed that the hot side temperature for both systems reaches to around 400℃ while the solar concentration for the systems with and without graphite sheet is 128 and 292 suns, respectively.

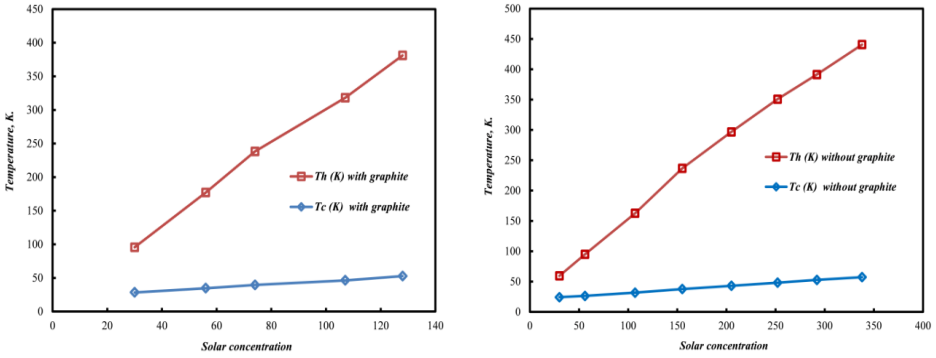

(a) *(b)*

Fig. 4.5: Hot and cold side temperatures of the STEG (a) with graphite sheet; (b) without graphite sheet, versus solar concentration [195].

Since the enhancement of the hot side temperature is higher than the cold side temperature, then, the temperature difference also rises. Figure 4.6 illustrates the variation of the open circuit voltage and short circuit current versus solar concentration. With increasing the solar concentration, both quantities are enhancing in a mostly linear trend. For the same values of solar concentrations, owing to having higher absorbance rate, the STEG system with

graphite sheet has higher open circuit voltage and short circuit current. It can be concluded that the same open circuit voltage and short circuit current can be acquired by the system with the graphite sheet using lower solar concentrations. For instance, the value of these parameters for the system with graphite sheet is 1.56 V and 1.21 A for solar concentration 107 suns While these values are 1.5 V and 1.18 A for the system without graphite sheet and solar concentration 252 suns.

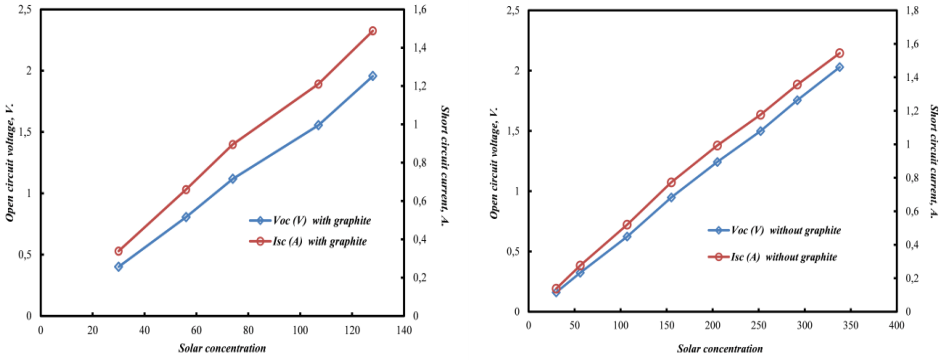

(a) (b)

Fig. 4.6: Open circuit voltage and short circuit current versus solar concentration for STEG (a) with graphite sheet; (b) without graphite sheet [195].

The significant impact of using a graphite sheet on the surface of the TEG in the STEG system can be observed in Figure 4.7. The variations of the current and power against voltage for different solar concentrations for both STEG systems are illustrated in Figure 4.7. For an identical value of the solar concentration, the output power by the STEG system with graphite sheet is considerably more than the system without graphite sheet. In order to compensate for the small level of input energy for the low concentration applications, this technique is appropriate and useful.

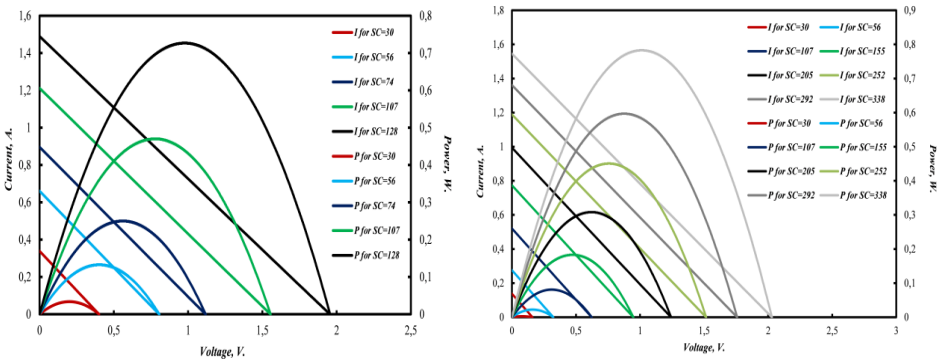

(a) *(b)*

Fig. 4.7: I-V-P curves for the STEG system (a) with graphite sheet; (b) without graphite sheet, and different solar concentrations [195].

Figure 4.7 showed the substantial effect of attaching a graphite sheet on the surface of the TEG in the STEG system in the steady state condition. This considerable difference between generated powers can be represented by the ratio of the output power by the system with graphite sheet to the output power by the system without graphite sheet. Figure 4.8 displays the variation of this fraction versus the solar concentration. It indicates that with increasing the solar concentration, the ratio of the output powers decreases slightly, but this ratio still has a high value. For the solar concentration 107, this ratio is 5.8 that show the huge impact of using the graphite sheet in the STEG system.

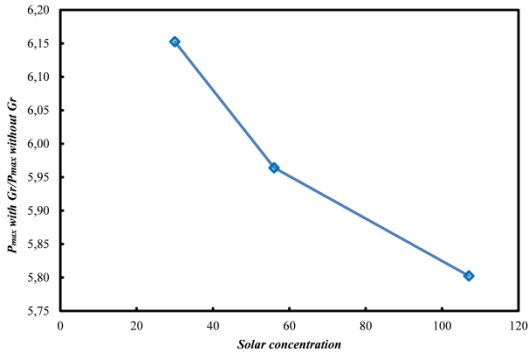

Fig. 4.8: The ratio of the maximum power for the STEG with graphite sheet to the STEG without graphite sheet versus solar concentration [195].

4.1.3 SOLAR OXIDE THERMOELECTRIC GENERATOR UNDER TRANSIENT CONCENTRATED LIGHT

In the next step, the transient response of the oxide-based STEG system to the variant solar concentrations is investigated. The experimental study and numerical validation and optimization in this part can be applicable and useful in places with cloudy weather condition. The transient concentrated solar radiation is applied to the STEG system based on the values shown in Table 4.1 and with using six xenon lamps and different percentage of the shutter.

4.1.3.1 STEG without graphite absorber

First, the STEG system without graphite sheet is studied under variable concentrated solar radiation. Figure 4.9 shows the arbitrary pattern for the concentrated solar radiation applied to the STEG system. To consider the transient behavior of the STEG system, the time interval was considered 1 minute. The STEG system was run before, and after it reaches the steady state condition, the transient condition is started after the first minute. The variation of the temperatures of the cold and hot sides of the TEG is shown in Figure 4.9 (a). Both hot and cold side temperatures are changing with the same manner and follow the solar radiation's variation. Due to some material properties of the TEG like density, thermal conductivity and heat capacity, the variation of the cold side temperature has a delay than the hot side temperature.

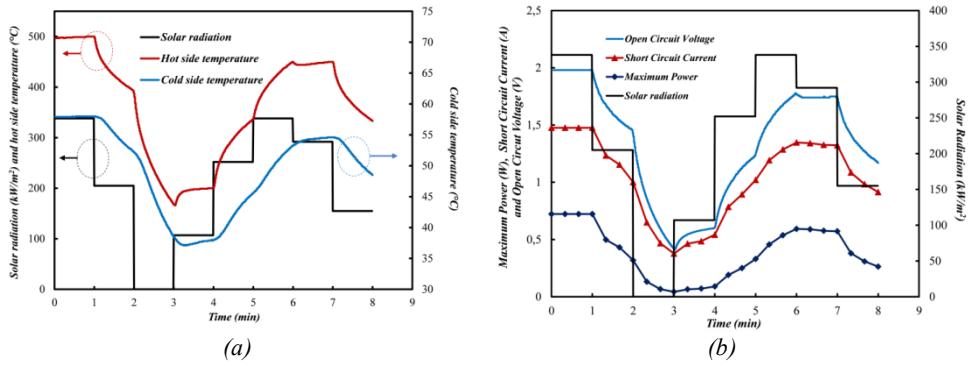

Fig. 4.9: (a) Solar radiation and hot and cold side temperatures variation, (b) Solar radiation, Open circuit voltage, short circuit current, and maximum power for the STEG without graphite layer [196].

The variation of the maximum power, short circuit current and open circuit voltage versus time are illustrated in Figure 4.9 (b). The maximum power and short-circuit current are

measured every 20 seconds, and the open circuit voltage is recorded every 200 milliseconds. All of these parameters have the same trend with the temperatures. Since 1 minute is not enough for the TEG to reach the steady state condition, even for the identical solar radiation values (for example 338 suns), the short circuit current and open circuit voltage cannot acquire the maximum value in the next cycle.

4.1.3.2 STEG with graphite absorber

The material properties of the TEG and also the temperature gradient through the module are two key parameters in power generation by the STEG system. For a STEG system with the constant material, in order to improve the conversion efficiency, it is crucial to maximizing the temperature gradient. It can be achieved by increasing the absorbed energy from the solar simulator and reduce the heat loss from the system. In addition, a highly efficient heat sink should be employed to dissipate more heat from the cold side of the TEG. Using a self-adhesive graphite sheet increases the heat flux by absorbing a higher amount of solar radiation.

In order to evaluate the transient behavior of the STEG system with attached graphite sheet, an identical pattern with dissimilar values of the concentrated solar radiations is applied to the system. As mentioned before, the maximum temperature that the self-adhesive graphite sheet can tolerate is 400°C. Therefore, the delivered solar radiations have to be regulated in a way that the hot side temperature does not go above 400°C, See Figure 4.10 (a). For that reason, the solar radiation for each time step is considered 1/3 of the value used for the STEG without the graphite sheet. As can be observed in Figure 4.10, the maximum considered solar radiation is 117.3 suns.

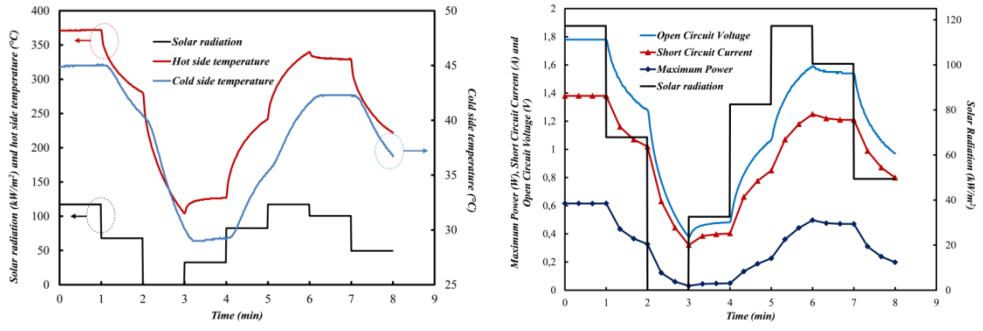

Fig. 4.10: (a) Solar radiation and hot and cold side temperatures variation, (b) Solar radiation, Open circuit voltage, short circuit current and maximum power for the STEG with graphite layer [196].

The variation of the temperatures, maximum power, open circuit voltage, and short circuit current against time is displayed in Figure 4.10. Comparing the obtained values for different parameters in Figure 4.10 with Figure 4.9 indicates the significant effect of the graphite sheet on the power generation. It can be observed that with considerably lower values of the concentrated solar radiations, the STEG system with graphite sheet can generate almost the same power with the STEG system without graphite sheet. The self-adhesive graphite sheet increases the absorbance coefficient, while the ceramic layer reflects a high amount of the received solar radiation and has low absorbance coefficient.

4.1.3.3 Modeling and simulation

The performance and conversion efficiency of the oxide-based TEGs improves with increasing the temperature [197-198]. These materials have a higher figure of merit in the higher temperatures. In this section, firstly the experimental results will be validated using the numerical model, and then the behavior of the STEG system in higher temperatures will be predicted. As mentioned before, there is a limitation for the temperature of the self-adhesive graphite sheet, and then the temperature of the system cannot exceed 400°C. Since the oxide-based STEG system has better performance in the higher temperatures, it is essential to consider higher temperatures in the simulation.

To realize the transient response of the STEG system under variable concentrated solar radiations, a one-dimensional unsteady-state heat transfer model is established. A set of partial differential equations are obtained using energy conservation law, and finite volume method [199] is used to solve these coupled equations. All the effects of the TEG comprising Seebeck effect, Thomson effect, Joule effect, Peltier effect, and Fourier effect are considered in the obtained equations. All the material properties of the P-Type and N-Type semiconductors are considered temperature dependent [200-201]. The TEG is presumed thermally insulated, and the radiative and convective heat transfers between the legs are neglected. Figure 4.11 illustrates the physical model of the STEG system.

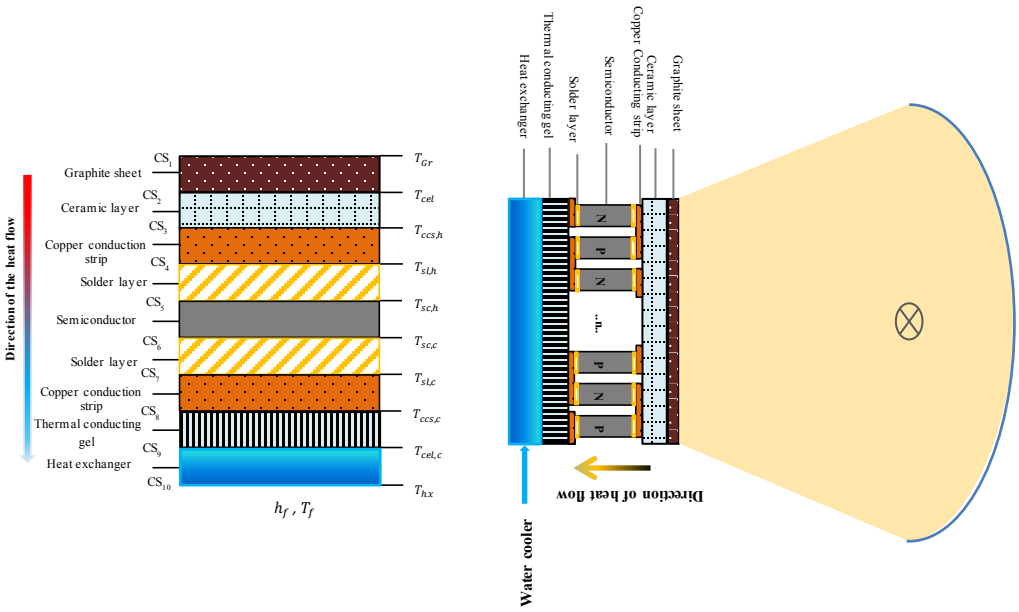

Fig. 4.11: One-dimensional heat transfer physical model of the STEG system [196].

Figure 4.11 displays different layers of the STEG system used in the modeling. With using energy conservation law for different layers, a set of non-linear equations are achieved. Considering all the TEG effects leads to having the below-mentioned equations for each contact surface.

On the upper surface of the graphite sheet, (CS_1):

$$\rho_{Gr} c_{Gr} V_{Gr} \frac{\partial T_{Gr}}{\partial t} = \alpha \times SC \times G \times A_{Gr} - Q_{rad} + KA\left(\frac{\partial T}{\partial x}\right)\Big|_{x=CS_1^b} \qquad (4-1)$$

Where, Q_{rad} is the radiative heat loss from the top surface of the STEG system and given as:

$$Q_{rad} = \varepsilon \sigma A_{Gr}\left({T_{Gr}}^4 - {T_{sky}}^4\right) \qquad (4-2)$$

Where Stefan-Boltzmann constant $\sigma = 5.67 \times 10^{-8} W/m^2K^4$ and the sky temperature T_{sky} is a function of the ambient temperature [202].

Equation (4-3) is used for the contact surfaces 2 to 5. The value of constants C_1 to C_6 are

presented in Table 4-2.

$$\rho_i c_i V_i \frac{\partial T_i}{\partial t} = C_1 k_{(i-1)} n_{(i-1)} A_{(i-1)} \left(\frac{\partial T}{\partial x}\right)\Big|_{x=CS_i^t} - C_2 \frac{n_{(i-1)} I^2 r_{(i-1)}}{2} - C_3 k_i n_i A_i \left(\frac{\partial T}{\partial x}\right)\Big|_{x=CS_i^b} + C_4 n_i S_{i,h} I T_{i,h} - C_5 \frac{n_i I^2 r_{i,l}}{2} - C_6 \frac{n_i \tau_l I\left(T_{i,h} - T_{i,2}\right)}{2} \quad (4-3)$$

Table 4.2: Corresponding constants for different layers in the equation (4-3) [196].

i	C_1	C_2	C_3	C_4	C_5	C_6
2	1	0	1	0	0	0
3	1	0	1	0	1	0
4	1	1	1	0	1	0
5	1	1	1	1	1	1

Equation (4-4) is applied for the contact layers 6 to 9. For each layer, the corresponding equation can be obtained using the constants presented in Table 4.3.

$$\rho_i c_i V_i \frac{\partial T_i}{\partial t} = C_7 k_i n_i A_i \left(\frac{\partial T}{\partial x}\right)\Big|_{x=CS_i^b} - C_8 n_i S_{i,h} I T_{i,h} - C_9 \frac{n_i I^2 r_{i,m}}{2} - C_{10} \frac{n_i \tau_m I\left(T_{i,m} - T_{i,c}\right)}{2} - C_{11} k_{(i+1)} n_{(i+1)} A_{(i+1)} \left(\frac{\partial T}{\partial x}\right)\Big|_{x=CS_i^t} + C_{12} \frac{n_{(i+1)} I^2 r_{(i+1)}}{2} \quad (4-4)$$

Table 4-3: Corresponding constants for different layers in the equation (4-4) [196].

i	C_7	C_8	C_9	C_{10}	C_{11}	C_{12}
6	1	1	1	1	1	1
7	1	0	1	0	1	-1
8	1	0	1	0	1	0
9	1	0	0	0	1	0

For the contact surface between the working fluid and the heat exchanger base, (CS_{10}):

$$\rho_{hx} c_{hx} V_{hx} \frac{\partial T_{hx}}{\partial t} = k_{hx} A_{hx} \left(\frac{\partial T}{\partial x}\right)\Big|_{x=CS_{10}^t} + h_f A_f \left(T_{hx,2} - T_f\right) \quad (4-5)$$

The time-dependent temperatures of different layers of the STEG system can be achieved by solving the equations above.
Thus, the electromotive force (EMF) of the TEG can be obtained considering the impact of the Thomson effect:

$$E = n_{sc}\left[S_{sc,h}T_{sc,h} - S_{sc,c}T_{sc,c} - \sum_{i=1}^{m-1}\tau_i(T_i - T_{i+1})\right] \quad (4-6)$$

The internal electrical resistance of the TEG module including the electrical resistance of the solder layer, copper conduction strip, and semiconductors can be determined as:

$$R_i = \left(n_{ccs}r_{ccs} + n_{sl}r_{sl} + n_{sc}\sum_{i=1}^{m} r_{sc,i}\right) \quad (4-7)$$

Then the power generation by the TEG is given by:

$$P_{TEG} = \left(\frac{E}{R_i + R_L}\right)^2 R_L$$
$$= \left[n_{sc}\left[S_{sc,h}T_{sc,h} - S_{sc,c}T_{sc,c} - \sum_{i=1}^{m-1}\tau_i(T_i - T_{i+1})\right]\right]^2 R_L \Big/ \left[\left(n_{ccs}r_{ccs} + n_{sl}r_{sl} + n_{sc}\sum_{i=1}^{m} r_{sc,i}\right) + R_L\right]^2 \quad (4-8)$$

And the instantaneous efficiency of the TEG will be defined as [183]:

$$\eta_{TEG} = P_{TEG}/(SC \times G \times A - Q_{rad}) \quad (4-9)$$

It is worthy to note that the solar simulator used in the experiments delivers concentrated solar radiation with high accuracy. Therefore, these values of solar radiations can be used in the numerical model. In addition, the numerical model that is presented in this section is capable of considering every time-dependent pattern for solar radiation.

4.1.3.4 Numerical results of the feasibility study

The main purpose of developing the numerical model is to predict the performance of the oxide-based STEG system in higher temperatures. Primarily, it is required to validate the current experimental results with the numerical model. The presented model has the potential to trace the temperature variation for every fluctuation of the solar radiations. The solar radiation pattern presented in Figure 4-10 is used as an input to validate the numerical results. Experimental and numerical results along with the applied solar radiation pattern

are illustrated in Figure 4.12. Close agreement between the experimental results and numerical simulation can be observed in this figure. The average obtained error between the experimental results and numerical ones is 7 %.

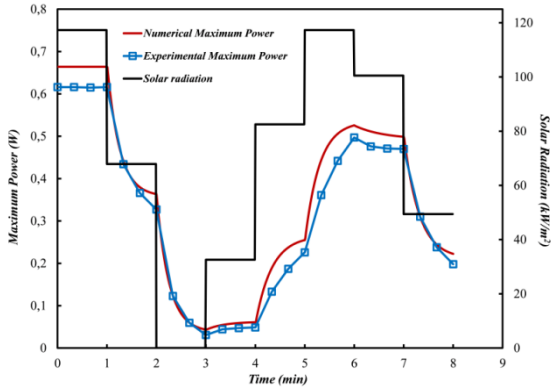

Fig. 4.12: Numerical and experimental results of the maximum power versus time for the STEG with the graphite layer [196].

To achieve higher temperatures and then higher performance and conversion efficiency by the oxide-based STEG system, the solar radiation and consequently the input heat flux should be increased. The maximum temperature that is considered in this study is 950 ℃, though the numerical model is capable of evaluating the performance of the STEG system for even higher temperatures. To reach this target, the same pattern with higher values is applied to the STEG system. The newly imposed solar radiation pattern and the numerically obtained output power by the STEG system are shown in black in Figure 4.13. The solar radiation pattern and generated power presented in Figure 4.12 is also displayed in blue in Figure 4.13. Using the black pattern leads to having a substantial enhancement in the generated power by the STEG system. Due to incensement in the heat flux and the temperature, the figure of merit of the oxide-based TEG is also enhanced, and consequently, the generated power increases considerably.

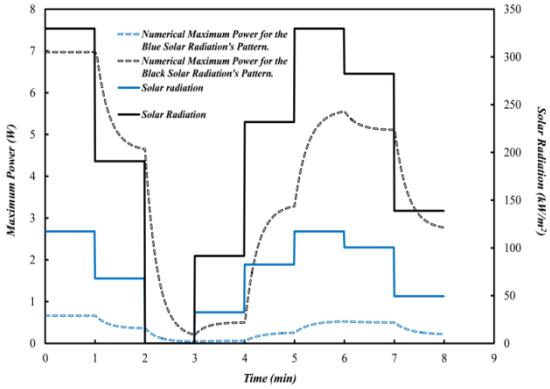

Fig. 4.13: Numerical power generation by the STEG with graphite layer for different solar radiation patterns versus time [196].

Although the major target of this investigation is to study the transient response of the oxide-based STEG system but to predict the conversion efficiency and performance of the STEG system a steady-state study is, additionally, carried out over a broad range of solar concentrations. The variation of the efficiency and maximum power of the STEG system with the graphite sheet versus solar radiation is illustrated in Figure 4.14. Conversion efficiency and output power corresponding to solar radiation of 117 kW/m^2 are 0.3 % and 0.62 W, respectively, while these values are 1.2% and 6.97 W, respectively at solar radiation of 329 kW/m^2. It indicates that both conversion efficiency and power generation of the system are enhanced with increasing the solar radiation.

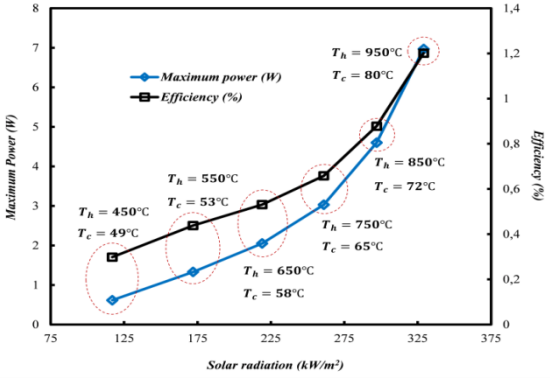

Fig. 4.14: Numerical results of maximum power and efficiency of the STEG system versus solar radiation [196].

4.2 BI-TE BASED SOLAR THERMOELECTRIC GENERATORS

Bi-Te based TEGs are one of the most common types of TEG that can be used in many low-temperature applications (up to around 450 K). They also have been used in the STEG systems to harvest the solar energy and convert it to the useful electrical energy.

In this section, the same experimental setup and procedure are used to evaluate the performance of a Bi-Te based TEG under variant solar radiations. The TEG used in the experiments is a Bi-Te based TEG model TEG2-07025HT-SS with 199 uni-couples and size 40mm × 40mm [203], see Figure 4.15.

Fig. 4.15: Bi-Te based TEG used in experiments [203].

To evaluate the performance of the STEG system, an arbitrary pattern for solar radiation is applied to the system, see Figure 4.16. To impose this pattern to the STEG system, six radiative lamps are used, and the shutter adjusts the radiation density. Using six lamps with 5% and 10% open-rate of the shutter leads to having solar radiations equal to 30 suns and 56 suns, respectively.

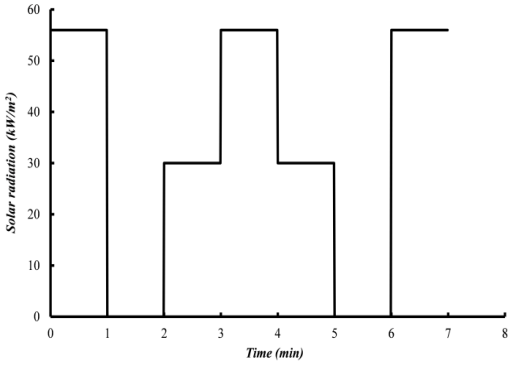

Fig. 4.16: Applied solar radiation patterns to the STEG [204].

The numerical procedure which used before for the oxide-based STEG system can be applied for the Bi-Te based STEG system using material properties of the Bi-Te based TEG. The solar radiation pattern shown in Figure 4.16 is used in the numerical simulation as well. For different layers of the STEG system, time-dependent temperatures are achieved. The temperature difference through the TEG is one of the most crucial factors in the power generation by the TEG. The numerical and experimental transient fluctuations of the temperatures of the cold and hot sides of the TEG under the variant solar radiation are illustrated in Figure 4.17. It is worthy to note that the system was reached to the steady state condition before and the variation is started after the first minute. Both hot and cold side temperatures are influenced by the sharp instabilities of solar radiation. The numerical simulation and the experimental results are in a reasonable agreement.

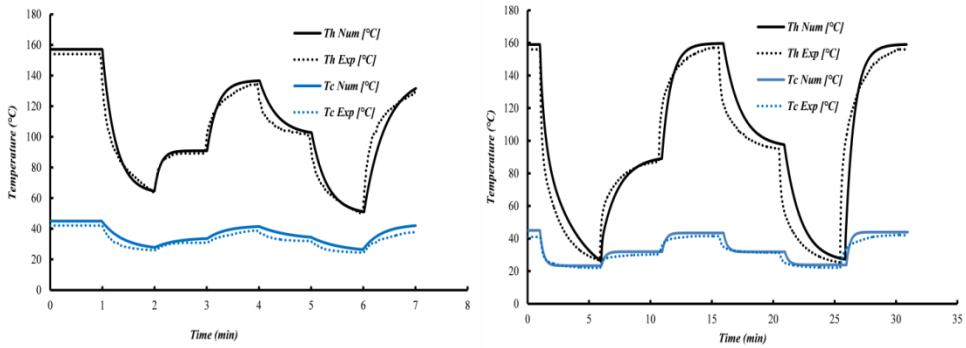

Fig. 4.17: Hot and cold side temperatures of the STEG for (a) 1-minute time interval, (b) 5 minutes time interval [204].

Experimental results for the fluctuations of the short circuit current and open circuit voltage for both 1 minute and 5 minutes time intervals are illustrated in Figure 4.18. For all the experiments, open circuit voltages are measured and recorded every 200 milliseconds. The short circuit current values are measured every 1 minute and 20 seconds when the time intervals are 5 minutes and 1 minute, respectively. Both parameters have the same trend and follow the temperature fluctuations for both time intervals. One minute is not sufficient for the STEG system to reach the thermally steady state condition, but as it can be observed after 5 minutes, open circuit voltage and short circuit current can almost reach to the steady state condition. For instance, for the identical solar radiation value (56 suns), both parameters reach the highest value that is almost equal to the value at steady state condition.

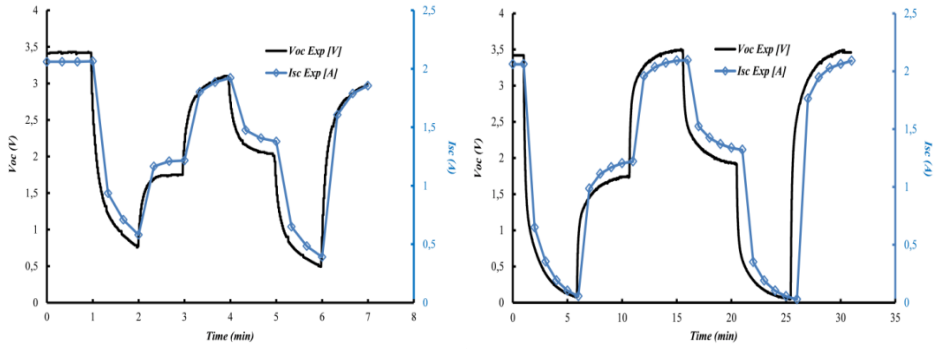

Fig. 4.18: Open circuit voltage and short circuit current of the TEG for (a) 1-minute time interval, (b) 5 minutes time interval [204].

Figure 4.19 displays the experimental and numerical variation of the output power against time. Due to the small temperature variation, the figure of merit as one of the most effective parameters in power generation by the TEG does not change considerably [205]. Consequently, the temperature gradient across the TEG is the most dominant parameter. In order to increase the output power and the conversion efficiency by the STEG system, the temperature difference should be maximized. Figure 4.19 indicates that enhancing solar radiation and consequently the heat flux leads to having higher temperature gradient and output power, and vice versa. Good agreement between numerical and experimental results can be observed.

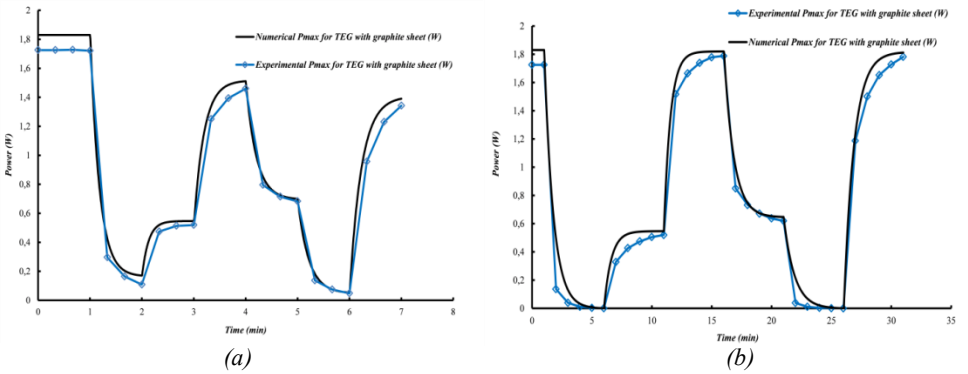

Fig. 4.19: Maximum power versus time for the STEG with graphite layer for (a) 1min time interval (b) 5mins time interval [204].

The Bi-Te based TEG used in the experimental study and numerical simulation is covered by a graphite layer. This graphite layer is acting as an absorber and has a significant impact on the power generation by the STEG system by absorbing more energy derived by the solar simulator. The significance of using this graphite layer is also evaluated numerically. In the established numerical model, the first layer that is the graphite sheet, see Figure 4.11, is removed. The ceramic layer has higher reflectance and absorbs less amount of received energy.

The maximum power generation by both systems and for time intervals 1 minute and 5 minutes are shown in Figure 4.20. It indicates the substantial impact of using graphite sheet. In the steady state condition, the maximum generated power by the STEG system with the graphite layer is approximately 2.5 times higher than the system without the graphite layer. It is due to the higher amount of the absorbed energy by the graphite sheet. Accordingly, the conversion efficiency, which is described as the ratio of the generated power to the solar radiation, of the STEG system with graphite layer (3.3%) is around 2.5 times more than the STEG system without graphite layer (1.3%).

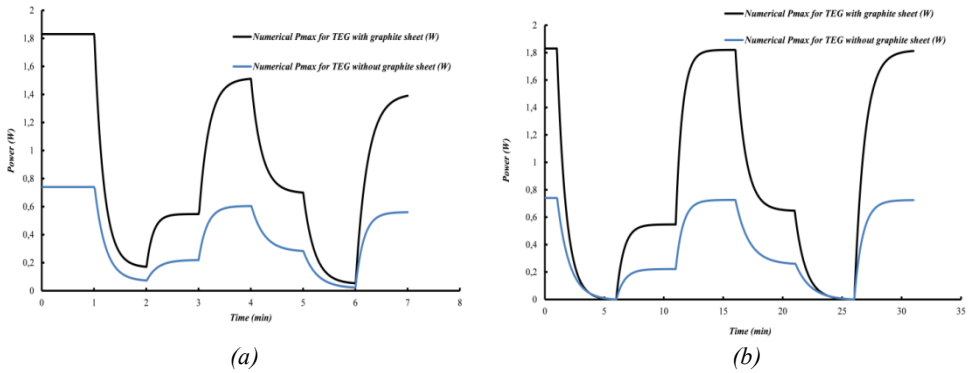

Fig. 4.20: Maximum power versus time for the STEG with and without graphite layer for (a) 1min time interval (b) 5mins time interval [204].

It can be concluded that for the low solar concentration applications it would be much beneficial to use the TEGs covered with graphite sheet. This technique is advantageous to compensate for the small amount of the input energy to acquire more power. Figures 4.19 and 4.20 are shown the electrical effect of the time intervals on the maximum power. By increasing the time interval between the solar radiation steps, the range of the variations of maximum power, open circuit voltage, and short circuit current are larger. For example, when the time interval is 5 minutes, the minimum generated power which occurs at minutes

6 and 26 are almost zero and the maximum generated power that takes place at minutes 16 and 31 are almost equal to the steady state condition.

CHAPTER 5. INTEGRATION OF THE CTJ CELLS AND TEGS

In this chapter, an inclusive study on the performance and conversion efficiency of the CTJ-TEG hybrid system is presented. Firstly, both numerical and experimental methods are employed to consider the behavior of the hybrid system in the transient condition. In addition, to validate the experiments, COMSOL Multiphysics Modeling Software is used as well. In the next section, the performance of the hybrid system in the steady state condition for the low solar concentrations are obtained and discussed. The role of TEG and CTJ in the power generation by the hybrid system is determined. In the last section, the significance of the impact of different parameters on the conversion efficiency and performance of the CTJ-TEG hybrid system is evaluated. This chapter contains results described in Papers F [206], G [207], H [218], I [225] and J [232].

5.1 TRANSIENT BEHAVIOR OF THE CTJ-TEG HYBRID SYSTEM UNDER VARIANT SOLAR CONCENTRATIONS

This section includes three main parts. First of all, a numerical one-dimensional transient model is developed for the hybrid CTJ-TEG system. All the TEG effects are considered in the developed model. Time-dependent variations of the temperatures, power, and efficiency of each component are determined and discussed. In the next section, an experimental study is carried out to consider the time-dependent response of the hybrid system. The last section is dedicated to the simulation of the hybrid system, using COMSOL Multiphysics Modeling Software.

5.1.1 THE TRANSIENT MODEL OF THE CTJ-TEG HYBRID SYSTEM

In the areas with partly cloudy climates, the instabilities of the weather conditions have a direct impact on the performance and conversion efficiency of different components in a hybrid CTJ-TEG system. In fact, due to the time-dependent variation of the daily solar radiation, the temperature of the CTJ and TEG in the hybrid system and subsequently the

efficiency and output power by the system become unsteady. These fluctuations in power generation by the hybrid system can be a critical concern to stabilize the electrical response of the hybrid system.

5.1.1.1 Conceptual model

Figure 5.1 shows the one and three dimensional physical model of the CTJ-TEG hybrid system. The hybrid system comprises of the CTJ cell and the TEG module. All the layers in the hybrid system are shown and named in the figures. Different types of the concentrators can be used to concentrate the solar irradiance. In order to dissipate heat from the cold side of the TEG and enhance the temperature difference between cold and hot sides of the TEG, a heat sink is used. Using the heat sink with higher efficiency decreases the temperature of the CTJ cell, and it causes to enhance in power generation by the CTJ. Both CTJ and TEG that are used in the numerical study have the same area 1 cm × 1 cm. The cross-sectional area of the 256 thermoelectric elements composed the TEG is 0.44 mm × 0.44 mm. The material properties and geometries of different components of the hybrid system are presented in Table 5.1.

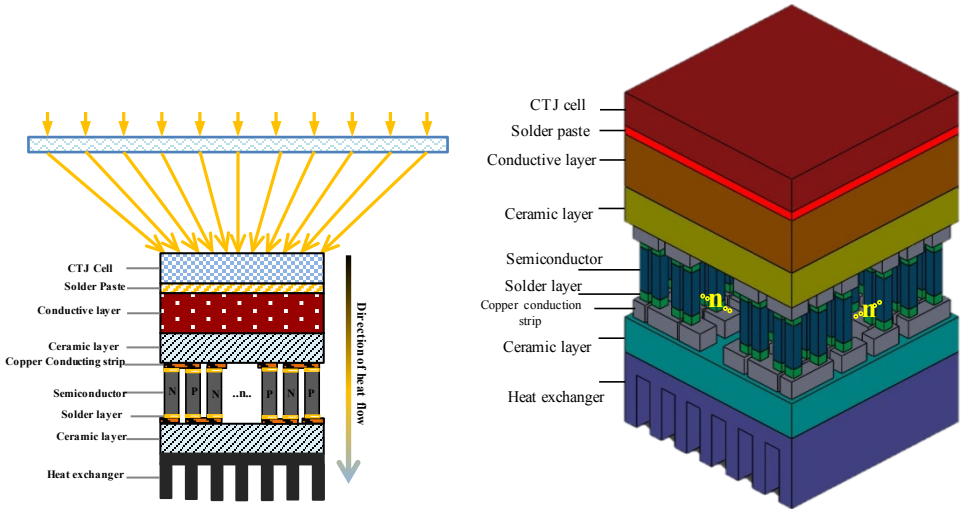

Fig. 5.1: (a) One-dimensional [206] and (b) Three-dimensional [207] physical model of the CTJ-TEG hybrid system.

Table 5.1: Geometry and material properties of different layers in the hybrid system [207].

Layer	Material	Thickness (mm)	Thermal conductivity(W/m.K)	Density (Kg/m^3)
CTJ cell	GaInP/GaInAs/Ge [208]	0.19 [209]	60	5350
Solder paste	$Sn_{95}Ag_5$ [210]	0.05	37.8	7390
Conductive layer	Cu [210]	0.3	385	8900
Ceramic layer	99.5%Al_2O_3 [210]	0.2	25	3700
Copper conducting strip	Cu	0.1	385	8900
Semiconductor	Bi_2Te_3 [211]	1.00	*	7300

$* K(T) = 5.32 - 0.0187T + 2.44 \times 10^{-5}T^2 - 3.24 \times 10^{-10}T^3$ $(W/(m.K))$ [211].

Due to variation in the temperature, all the material properties of the thermoelectric elements including thermal conductivity, electrical conductivity, and the Seebeck coefficient are considered temperature dependent.

5.1.1.2 Numerical model

Heat transfer numerical model is established to study the performance of the CTJ-TEG hybrid system under fluctuating concentrated solar radiations. The model is one-dimensional and unsteady-state. Energy conservation law is used to derive the equations for each layer, and finite volume method [199] is used to represent the obtained partial differential equations in the algebraic form. There are many components and special effects in a TEG module as a non-linear system. Below mentioned simplifying assumptions are considered in the established numerical model:

1. The CTJ-TEG hybrid system is well thermally insulated; therefore, heat transfer to the ambient is neglected excluding the radiative loss from the surface of the CTJ cell and heat transfer from the bottom of the CTJ that is acts as a heat source for the TEG.
2. Both convective and radiative losses among the TE elements are assumed to be zero.
3. The same materials are used for the P- and N-type semiconductors in the TEG.
4. All the layers in the CTJ-TEG hybrid system are well connected; thus the thermal and electrical contact resistances are considered negligible.

The time-dependent one-dimensional heat transfer model can be developed as:

$$\rho c \frac{\partial T}{\partial t} = \frac{\partial}{\partial x}\left(k \frac{\partial T}{\partial x}\right) + q \qquad (5-1)$$

Seebeck, Peltier and Thomson effects are the elementary TE effects, and Joule and Fourier's effects are the accessorial effects of the TEG. The Seebeck effect generates the electromotive force (EMF). Peltier, Thomson, and Joule heat are generated by Peltier, Thomson, and Joule effects, correspondingly. The Peltier heat is created just on the end sides of the thermoelements while the Peltier effect is not an interface effect. The Thomson and Joule heat are volumetric effects that are supposed to be equally relocated to the cold and hot junctions of the thermoelements [212-213]. One-dimensional heat transfer physical model of the CTJ-TEG is illustrated in Figure 5.2.

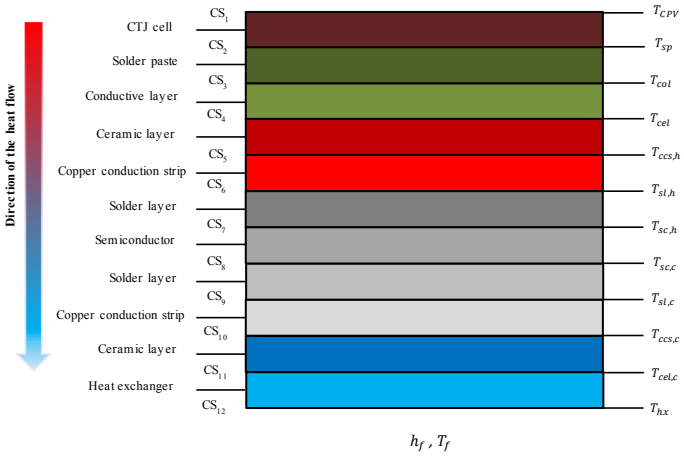

Fig. 5.2: One-dimensional heat transfer physical model of the CTJ-TEG module [207].

Water is used as the working fluid in the heat sink. The energy conversion law is used to obtain the governing equation for each contact surface. The temperature of each layer can be achieved using these set of nonlinear equations, and consequently, the output power and conversion efficiency of the CTJ and TEG can be obtained. The derived equations for various contact surfaces are listed as follow:

For the surface of the CTJ cell (CS_1):

$$\rho_{CTJ} c_{CTJ} V_{CTJ} \frac{\partial T_{CTJ}}{\partial t} = SC \times G \times A_{CTJ} - Q_{rad} + KA \left(\frac{\partial T}{\partial x}\right)\Big|_{x=CS_1^b} - P_{CTJ} \qquad (5-2)$$

Q_{rad} is the radiative heat loss. Owing to the small area of the CTJ cell, the value of the radiative loss is not significant, but it is still considered in the equations and can be achieved as follows:

$$Q_{rad} = \varepsilon\sigma A_{CTJ}\left({T_{CTJ}}^4 - {T_{sky}}^4\right) \quad (5-3)$$

In this equation, the Stefan-Boltzmann constant is $\sigma = 5.67 \times 10^{-8} W/m^2K^4$. The temperature of the sky depends on the temperature of the ambient as stated by an investigation by Nowak [202]. P_{CTJ} is the generated power by the CTJ cell and given as:

$$P_{CTJ} = SC \times G \times A_{CTJ} \times \eta_{CTJ} \quad (5-4)$$

η_{CTJ} is the efficiency of the CTJ that can be obtained as [214]:

$$\eta_{CTJ} = \eta_{T_{ref}}\left[1 - \beta_{ref}\left(T_{CTJ} - T_{ref}\right)\right] \quad (5-5)$$

In the Equation (5-5), $\eta_{T_{ref}}$ is the conversion efficiency of the CTJ cell for the reference solar radiation ($G_{ref} = 1000\ W/m^2$) and reference temperature ($T_{ref} = 25\ °C$) [215]. β_{ref} is the temperature coefficient of the CTJ cell at the reference temperature and it is considered $-0.1\ \%/K$ [208] in this investigation. The manufacturer generally offers this coefficient.

For the contact surface (CS_2):

$$\rho_{sp} c_{sp} V_{sp} \frac{\partial T_{sp}}{\partial t} = k_{CTJ} A_{CTJ} \left(\frac{\partial T}{\partial x}\right)\Big|_{x=CS_2^t} - k_{sp} A_{sp} \left(\frac{\partial T}{\partial x}\right)\Big|_{x=CS_2^b} \quad (5-6)$$

For the contact surface (CS_3):

$$\rho_{col} c_{col} V_{col} \frac{\partial T_{col}}{\partial t} = k_{sp} A_{sp} \left(\frac{\partial T}{\partial x}\right)\Big|_{x=CS_3^t} - k_{col} A_{col} \left(\frac{\partial T}{\partial x}\right)\Big|_{x=CS_3^b} \quad (5-7)$$

For the contact surface (CS_4):

$$\rho_{cel} c_{cel} V_{cel} \frac{\partial T_{cel}}{\partial t} = k_{col} A_{col} \left(\frac{\partial T}{\partial x}\right)\Big|_{x=CS_4^t} - k_{cel} A_{cel} \left(\frac{\partial T}{\partial x}\right)\Big|_{x=CS_4^b} \quad (5-8)$$

In the TEG considered in this investigation, there are n pairs of P–N junction. The semiconductors are divided to m control volumes. Considering all the TE effects, the obtained equations for different contact surfaces are given as:

For the contact surface (CS_5):

$$\rho_{ccs}c_{ccs}V_{ccs}\frac{\partial T_{ccs,h}}{\partial t}=k_{cel}n_{cel}A_{cel}\left(\frac{\partial T}{\partial x}\right)\Big|_{x=CS_5^t}-k_{ccs}n_{ccs}A_{ccs}\left(\frac{\partial T}{\partial x}\right)\Big|_{x=CS_5^b}-\frac{n_{ccs}I^2r_{ccs}}{2} \quad (5-9)$$

For the contact surface (CS_6):

$$\rho_{sl}c_{sl}V_{sl}\frac{\partial T_{sl,h}}{\partial t}=k_{ccs}n_{ccs}A_{ccs}\left(\frac{\partial T}{\partial x}\right)\Big|_{x=CS_6^t}-\frac{n_{ccs}I^2r_{ccs}}{2}-k_{sl}n_{sl}A_{sl}\left(\frac{\partial T}{\partial x}\right)\Big|_{x=CS_6^b}-\frac{n_{sl}I^2r_{sl}}{2} \quad (5-10)$$

For the contact surface (CS_7):

$$\rho_{sc}c_{sc}V_{sc}\frac{\partial T_{sc,h}}{\partial t}=k_{sl}n_{sl}A_{sl}\left(\frac{\partial T}{\partial x}\right)\Big|_{x=CS_7^t}-\frac{n_{sl}I^2r_{sl}}{2}-k_{sc}n_{sc}A_{sc}\left(\frac{\partial T}{\partial x}\right)\Big|_{x=CS_7^b}+n_{sc}\alpha_{sc,h}IT_{sc,h}-\frac{n_{sc}I^2r_{sc,l}}{2}-\frac{n_{sc}\tau_l I\left(T_{sc,h}-T_{sc,2}\right)}{2} \quad (5-11)$$

For the contact surface (CS_8):

$$\rho_{sc}c_{sc}V_{sc}\frac{\partial T_{sc,c}}{\partial t}=k_{sc}n_{sc}A_{sc}\left(\frac{\partial T}{\partial x}\right)\Big|_{x=CS_8^b}-n_{sc}\alpha_{sc,h}IT_{sc,h}-\frac{n_{sc}I^2r_{sc,m}}{2}-\frac{n_{sc}\tau_m I\left(T_{sc,m}-T_{sc,c}\right)}{2}-k_{sl}n_{sl}A_{sl}\left(\frac{\partial T}{\partial x}\right)\Big|_{x=CS_8^t}+\frac{n_{sl}I^2r_{sl}}{2} \quad (5-12)$$

For the contact surface (CS_9):

$$\rho_{sl}c_{sl}V_{sl}\frac{\partial T_{sl,c}}{\partial t}=k_{sl}n_{sl}A_{sl}\left(\frac{\partial T}{\partial x}\right)\Big|_{x=CS_9^t}-\frac{n_{sl}I^2r_{sl}}{2}-k_{ccs}n_{ccs}A_{ccs}\left(\frac{\partial T}{\partial x}\right)\Big|_{x=CS_9^b}-\frac{n_{ccs}I^2r_{ccs}}{2} \quad (5-13)$$

For the contact surface (CS_{10}):

$$\rho_{ccs}c_{ccs}V_{ccs}\frac{\partial T_{ccs,c}}{\partial t}=k_{ccs}n_{ccs}A_{ccs}\left(\frac{\partial T}{\partial x}\right)\Big|_{x=CS_{10}^t}-\frac{n_{ccs}I^2r_{ccs}}{2}-k_{cel}n_{cel}A_{cel}\left(\frac{\partial T}{\partial x}\right)\Big|_{x=CS_{10}^b} \quad (5-14)$$

For the contact surface (CS_{11}):

$$\rho_{cel} c_{cel} V_{cel} \frac{\partial T_{cel,c}}{\partial t} = k_{cel} n_{cel} A_{cel} \left(\frac{\partial T}{\partial x}\right)\Big|_{x=CS_{11}^{t}} - k_{hx} A_{hx} \left(\frac{\partial T}{\partial x}\right)\Big|_{x=CS_{11}^{b}} \quad (5-15)$$

For the contact surface (CS_{12}):

$$\rho_{hx} c_{hx} V_{hx} \frac{\partial T_{hx}}{\partial t} = k_{hx} A_{hx} \left(\frac{\partial T}{\partial x}\right)\Big|_{x=CS_{12}^{t}} + h_f A_f \left(T_{hx,2} - T_f\right) \quad (5-16)$$

The time-dependent temperatures for each point of the hybrid system are determined by solving the above equations.

After obtaining the temperature of the CTJ cell, the output power and efficiency of the CTJ cell can be achieved using Equations (5-4) and (5-5). Owing to the fluctuation in the temperature of the CTJ cell, both output power and efficiency of the CTJ cell are also varying with the time.

The generated power and efficiency of the TEG can be calculated using the obtained temperatures for each layer. Considering the influence of the Thomson effect, the EMF generated by the TEG can be acquired as:

$$E = n_{sc} \left[\alpha_{sc,h} T_{sc,h} - \alpha_{sc,c} T_{sc,c} - \sum_{i=1}^{m-1} \tau_i (T_i - T_{i+1}) \right] \quad (5-17)$$

And the internal electrical resistance of the TEG can be given as:

$$R_i = \left(n_{ccs} r_{ccs} + n_{sl} r_{sl} + n_{sc} \sum_{i=1}^{m} r_{sc,i} \right) \quad (5-18)$$

Then, the output power can be achieved as follows:

$$P_{TEG} = \left(\frac{E}{R_i + R_L}\right)^2 R_L$$
$$= \left[n_{sc} \left[\alpha_{sc,h} T_{sc,h} - \alpha_{sc,c} T_{sc,c} - \sum_{i=1}^{m-1} \tau_i (T_i - T_{i+1}) \right] \right]^2 R_L \Big/ \left[\left(n_{ccs} r_{ccs} + n_{sl} r_{sl} + n_{sc} \sum_{i=1}^{m} r_{sc,i} \right) + R_L \right]^2 \quad (5-19)$$

And the instantaneous conversion efficiency of the TEG is given as:

$$\eta_{TEG} = P_{TEG}/\left(SC \times G \times A - Q_{rad} - P_{CTJ}\right) \qquad (5-20)$$

5.1.1.3 Numerical results for the transient model of the CTJ-TEG hybrid system

The developed numerical model has the potential to follow the fluctuations of the temperature owing to the variation of solar radiation. The fluctuation of solar radiation for a cloudy day in Kunming, China [216] and for 15 minutes is displayed in Figure 5.2.

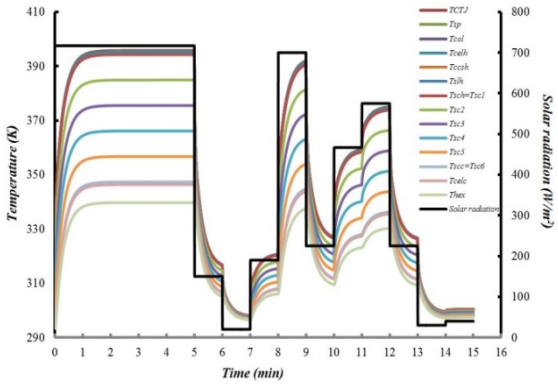

Fig. 5.3: Variation of solar radiation and the temperatures of hybrid module components versus time [207].

The variations of the temperatures for different layers of the CTJ-TEG hybrid system are shown in Figure 5.2. In this study, the solar concentration and the heat transfer coefficient of the heat sink are considered $SC = 400$ and $h_f = 2000\ W/m^2K$, respectively. The initial temperature for all the layers is considered 293 K, and consequently, there is a two minutes startup transient section beginning from $t = 0$. In Figure 5.2, the temperatures of all components are affected by the quick variation of the solar radiation. Owing to the high thermal conductivity of the CTJ cell, the value of the temperatures of the CTJ surface and hot side of the TEG is very close. On the other hand, the semiconductors have comparatively low thermal conductivity thus they are divided into 5 sections in the numerical simulation. The obtained temperatures for different segments of the semiconductors are illustrated as T_{sc1} to T_{sc6} in Figure 5.2. Lower thermal conductivity of the semiconductors compare to the other components cause to have higher temperature difference.

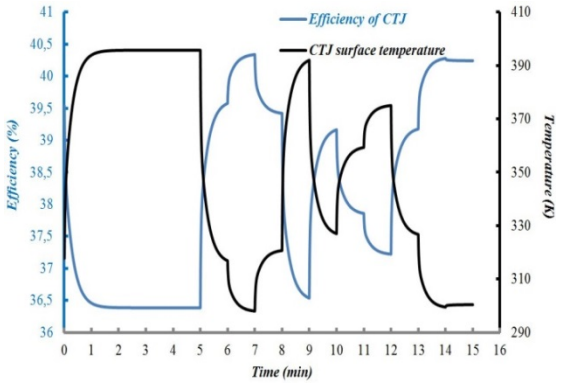

Fig. 5.4: Variation of efficiency and temperature of the CTJ cell versus time [207].

Temperature has a significant impact on the generated power by the TEG module and CTJ cell. It has an opposite influence on the performance of the TEG and CTJ. Enhancement in the temperature of the CTJ cell cause to decrease in the efficiency of the CTJ cell. On the other hand, to increase the conversion efficiency and output power by the TEG, the temperature difference should be enhanced. The variation of the surface temperature and conversion efficiency of the CTJ cell versus time is displayed in Figure 5.4. Equation (5-5) shows that there is an inversely proportional relationship between the conversion efficiency and the surface temperature of the CTJ cell. It can be observed that the efficiency of the CTJ drops around 4% with increasing solar radiation and surface temperature.

Figure 5.5 illustrates the variation of the generated power by the CTJ cell versus time. The solar radiation has the most crucial impact on the generated power by the CTJ cell. The insignificant impact of the temperature of the cell on the output power can also be observed in the transient part of Figure 5.5.

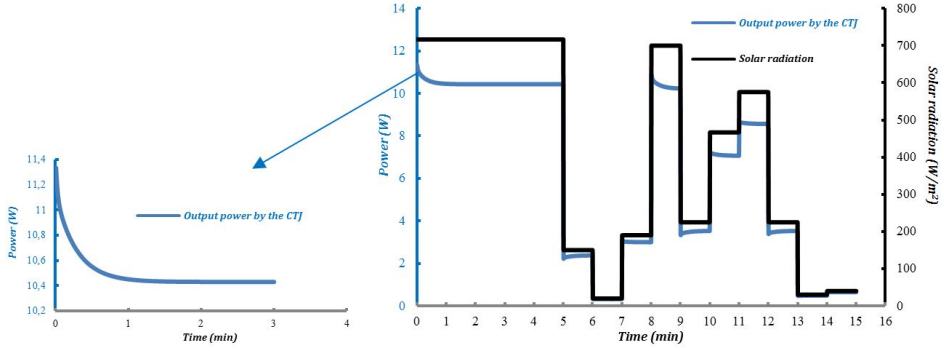

Fig. 5.5: Power generation by the CTJ cell [207].

The temperature gradient across the TEG and figure of merit are two main parameters in power produced by the TEG. The variation of the figure of merit within the considered range of the temperature is not significant in this study. Consequently, the temperature gradient across the TEG plays the most crucial role in the power generation by the TEG. The variation of the generated power and the temperature difference between the hot and cold sides of the TEG are illustrated in Figure 5.6. The significance of the impact of the temperature gradient on the power generation by the TEG can be seen in this figure. The time-dependent power is following the variation of the temperature gradient with an almost identical trend.

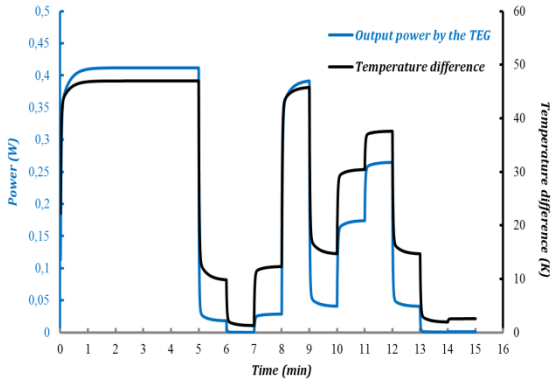

Fig. 5.6: Power generation by the TEG and temperature difference [207].

Figure 5.7 displays the transient fluctuation of the temperature difference across the TEG and the conversion efficiency of the TEG. Equation (5-20) indicates that the generated power by the TEG and the conversion efficiency of the TEG have a directly proportional relationship, see Figure 5.7.

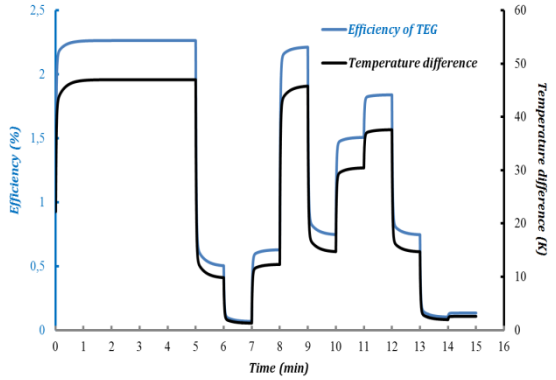

Fig. 5.7: Variation of the efficiency of the TEG and temperature difference versus time [207].

Figure 5.8 shows the variation of the conversion efficiency of both CTJ cell and TEG module versus time. It can be observed that they have opposite manner in response to the fluctuations of the solar irradiation. This reverse response of the TEG to the variation of the solar radiation can be advantageous in the hybrid system to compensate a part of the lost generated power by the CTJ cell.

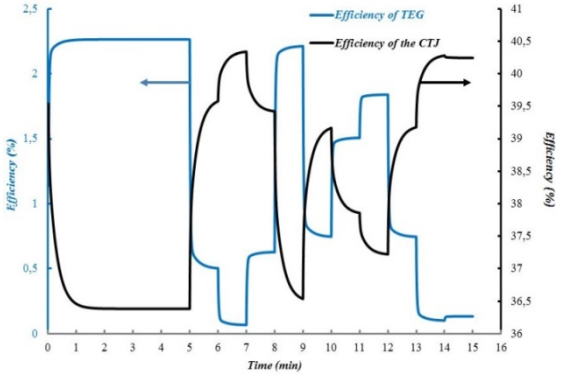

Fig. 5.8: Variation of the efficiency of the CTJ cell and the TEG versus time [207].

One of the simplifying assumptions for the first part of the simulation was perfect contact at the interfaces of the TEG and heat sink and the CTJ cell and the TEG module. Consequently, there is no thermal contact resistance and temperature drop at the interfaces. But in the real applications, the thermal contact resistance has a considerable impact on the performance of different systems. Thermal contact resistance can be given as:

$$R_c = \frac{\Delta T_{interface}}{\dot{Q}/A} \quad (m^2.°C/W) \qquad (5-21)$$

In the Equation (5-21), $\Delta T_{interface}$ is effective temperature drop at the interface and $\dot{Q}/A$ is the average heat flow across the interface. In order to evaluate the impact of the thermal contact resistance between the CTJ-TEG and TEG-heat sink on the performance of the hybrid system, the heat transfer equation should be added to the equations (5-8) and (5-15), respectively.

$$\dot{Q} = h_c A\, \Delta T_{interface} \qquad (5-22)$$

where h_c is the thermal contact conductance that is defined as the inverse of the thermal contact resistance.

Material properties, surface roughness, the kind of fluid trapped at the interface and the pressure and temperature at the interface are the main parameters affecting the amount of the thermal contact resistance. The value of the thermal contact resistance changes over a broad range in the experiments. In this study, this value is considered between 0.000005 to 0.0005 $m^2.℃/W$ [217]. For this range of the thermal contact resistance, the variation of the conversion efficiency and the temperature gradient across the TEG versus time are illustrated in Figure 5.9.

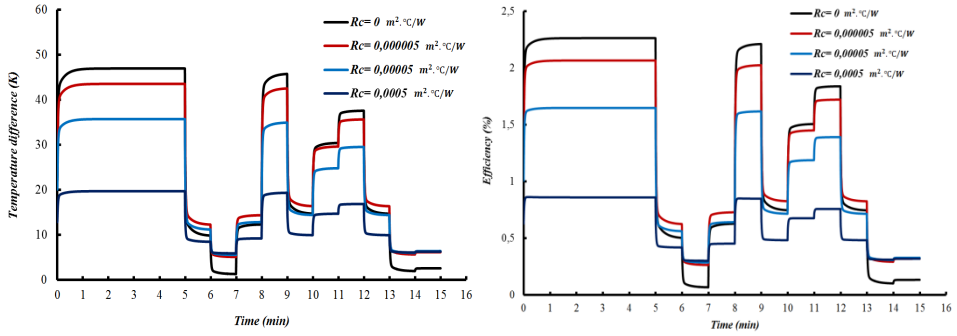

(a) *(b)*

Fig. 5.9: Variation of the (a) temperature difference and (b) Efficiency of the TEG versus time for different thermal contact resistance [207].

Figure 5.9 indicates that when the thermal contact resistance enhances, the temperature difference between the hot and cold sides of the TEG reduces and accordingly the conversion efficiency of the TEG decreases. The maximum conversion efficiency is around 2.25% that is for the perfect contact or when the thermal contact resistance is zero.

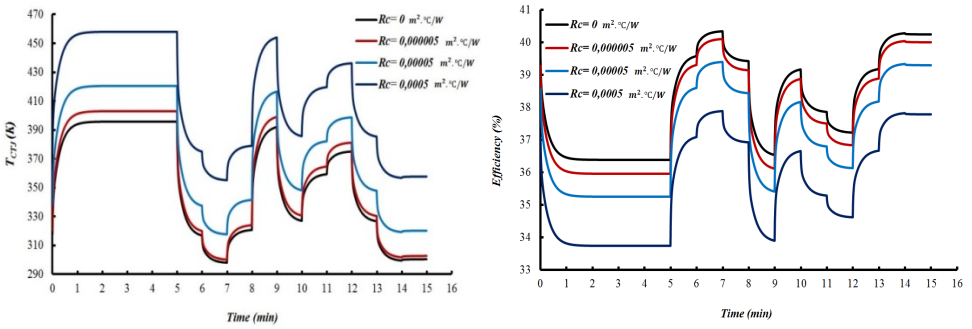

(a) *(b)*

Fig. 5.10: Variation of the (a) temperature and (b) Efficiency of the CTJ versus time for different thermal contact resistance [207].

Figure 5.10 displays the variation of the surface temperature and the conversion efficiency of the CTJ cell versus time. The cooling efficiency of the heat sink drops when the thermal contact resistance enhances. Therefore, the surface temperature of the CTJ cell increases with the enhancement of the thermal contact resistance and subsequently the efficiency of the CTJ cell decreases.

5.1.2 EXPERIMENTAL INVESTIGATION OF THE TRANSIENT RESPONSE OF THE CTJ-TEG HYBRID SYSTEM

The same solar simulator that was described before in section 4.1.1, is used to provide the concentrated light for the CTJ-TEG hybrid system. Owing the temperature restriction of the CTJ cell, the maximum concentrated solar radiation that can be applied to the system in this experimental study is 39 suns. Two lamps are enough to deliver this amount of concentrated light on the hybrid system. The schematic of the experimental rigs is displayed in Figure 5.11. In order to provide a uniform concentrated light, an optical mixer is located in front of the CTJ-TEG hybrid system.

The schematic of the CTJ-TEG hybrid system is shown in Figure 5.12 (a). The CTJ cell used in the experiments is a commercial CTJ [219] with the size $10.075\ \text{mm} \times 10.68\ \text{mm}$. The TEG used in the experiments is Bi-Te based [220] with the size of $8.7\ \text{mm} \times 8.7\ \text{mm}$ and 194 thermoelements. The CTJ and TEG are integrated to make the hybrid system, see Figure 5.12 (b) and (c). The same heat exchanger with the one used before for the STEG systems is used here with the same mass flow rate $5\ \text{Lit/min}$. Two thermocouples for each are used to measure the temperatures of the hot and cold sides of the TEG and the surface of the CTJ. The ambient temperature is obtained using another thermocouple.

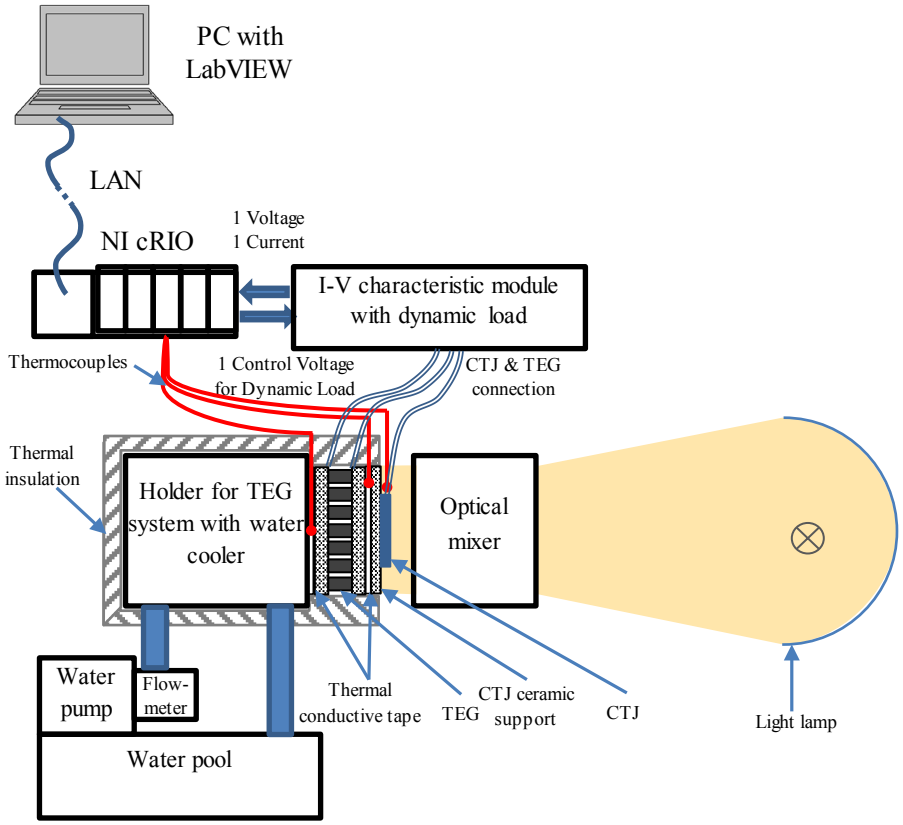

Fig. 5.11: Schematic of experimental setup [218].

Data logger and controllers based on National Instrument cRIO-9074 are used to obtain the I-V characteristics of the TEG and CTJ and measure the temperatures. This platform is on the basis of an FPGA Spartan-3 chip and a 400 MHz processor. The NI cRIO I/O modules used in these experiments are:

1. NI 9215: To measure the voltage of the TEG, an analog input module with 16bits resolution and $\pm 10\ V$ input range is used.
2. NI 9225: The current of the TEG is measured using a module with 24 bits resolution and 5 ARMS input range.
3. NI 9211 and NI 9213: In order to measure the temperatures, two modules with 24 bits resolution and $\pm 80\ mV$ input range and 24bits resolution and $\pm 78{:}125\ mV$ input range are employed. K type thermocouples are used in the measurements.

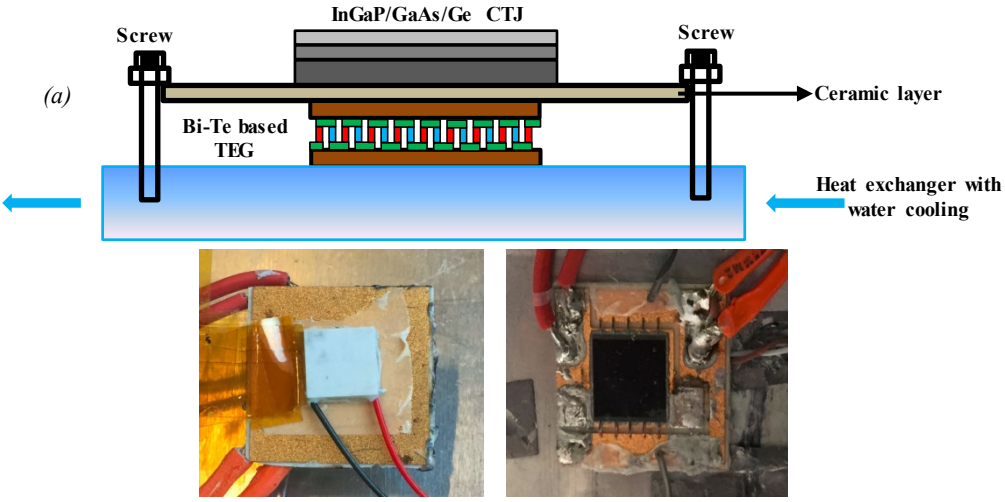

Fig. 5.12: (a) Schematic of the CTJ-TEG hybrid system, (b) Hybrid CTJ-TEG system, rear view, (c) Hybrid CTJ-TEG system, front view [218].

5.1.2.1 Experimental results for the transient CTJ-TEG hybrid system under the transient condition

An arbitrary time-dependent pattern for the solar radiation, see Figure 5.13, is applied to the CTJ-TEG hybrid system to evaluate the performance and transient response of the hybrid system. Figure 5.13 displays the fluctuations of the temperatures of the cold and hot sides of the TEG and the surface of the CTJ. All the temperatures are measured and recorded every 20 seconds. The hybrid system was run before until it reaches to steady state condition and the fluctuations are begun after the first minute. Figure 5.13 indicates that the variation of all the temperatures has an identical trend. As can be seen, the maximum solar radiation applied to the system is adjusted in a way that the maximum temperature of the CTJ cell does not exceed the allowed temperature [221].

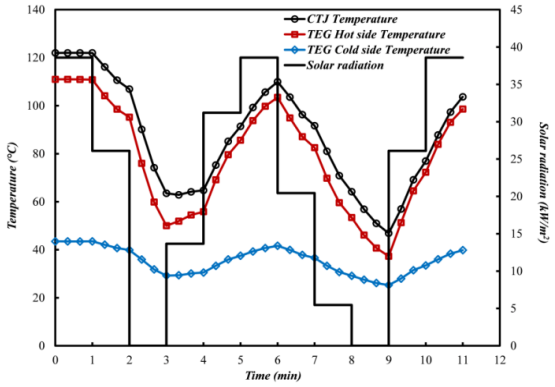

Fig. 5.13: Variation of the solar radiation and the temperatures of the CTJ and hot and cold sides of the TEG [218].

The variation of the maximum power, short circuit current and open circuit voltage versus the time can be observed in Figure 5.14. The value of the open circuit voltage for different solar radiations, excluding when it is zero, has an insignificant variation. These fluctuations are considerable for the maximum power and short circuit current. The variations of these parameters are stepwise, and both of them follow the solar radiation pattern shown in Figure 5.13. It takes a very short time for the short circuit current of the CTJ cell to reach the constant value and steady-state condition. When the solar radiation and subsequently the temperature of the CTJ cell drops, the open circuit voltage enhances slightly, see Area 1 in Figure 5.14. Therefore, a small increment occurs in the maximum power by the CTJ, shown in Area 2. The reverse manner can be observed in Areas 3 and 4 in Figure 5.14.

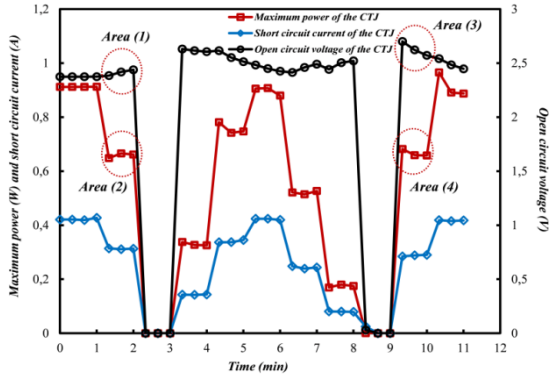

Fig. 5.14: Open circuit voltage, short circuit current and maximum power of the CTJ versus time [218].

Figure 5.15 shows the variations of the maximum power, short circuit current and open circuit voltage of the TEG versus the time. TEG has higher thermal resistance and thermal capacity than CTJ, and then the variation of the maximum power, short circuit current, and open circuit voltage are not stepwise like CTJ. These parameters for the TEG are mostly tracking the fluctuations of the hot and cold side temperatures shown before in Figure 5.13. The maximum generated power by the TEG for the solar concentration 39 suns is less than 0.02 W that is almost 2.1% of generated power by the CTJ at the same solar concentration value. This ratio can be enhanced using a geometrically optimized TEG with more efficient materials.

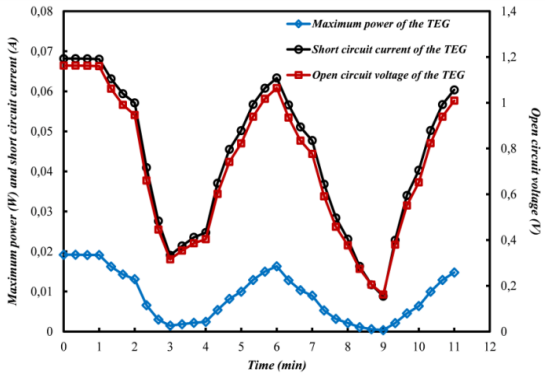

Fig. 5.15: Open circuit voltage, short circuit current and maximum power of the TEG versus time [218].

5.1.3 COMSOL MODELING AND SIMULATION APPROACH

In order to validate the experimental results and optimize the hybrid system, COMSOL Multiphysics 5.2 software is used. COMSOL is the finite element based software uses to analyze, solve and simulate different engineering and physics applications, mainly Multiphysics or coupled phenomena. In this section, a three-dimensional finite element model is developed to simulate the transient behavior of the CTJ-TEG hybrid system. In the first step, the 3D geometric model of the hybrid system is generated. Then, COMSOL pre-defined "fine" mesh is used to mesh the created geometry. The meshed geometry is displayed in Figure 5.16.

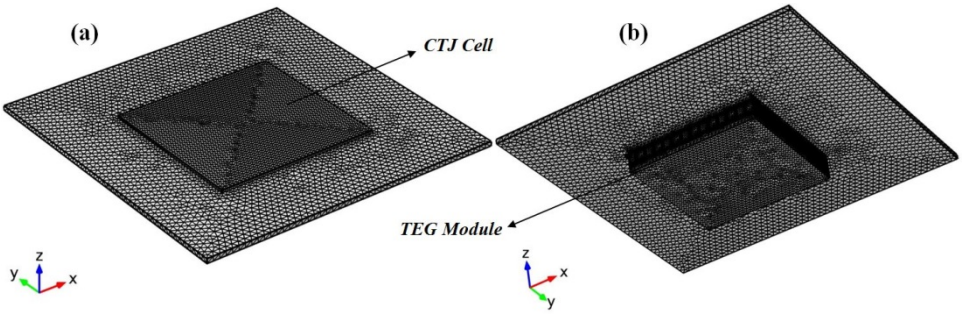

Fig. 5.16: Pre-defined fine mesh for the CTJ-TEG hybrid system, (a) Front view, (b) Rear view [218].

The material properties of different components of the CTJ and TEG are defined. The boundary conditions and initial values are also specified in the software. The material properties and geometry of the different materials used in the hybrid system are presented in table 5.2. The area of the TEG and CTJ considered in the numerical study are the same with the experimental work.

Table 5.2: Geometry and material properties of different layers in the hybrid system [218].

Layer	Material	Thickness, mm	Thermal conductivity, W/m K	Density, Kg/m^3
CTJ cell	GaInP/GaInAs/Ge [208]	0.185 [209]	60	5350
Solder paste	$Sn_{95}Ag_5$ [210]	0.05	37.8	7390
Conductive layer	Cu [210]	0.3	385	8900
Ceramic layer	99.5%Al_2O_3 [210]	0.4	25	3700
Copper conducting strip	Cu	0.1	385	8900
Semiconductor	Bi_2Te_3 [211]	0.7	*	7300

$* K(T) = 5.265 - 0.0283T + 6 \times 10^{-5}T^2 - 4 \times 10^{-8}T^3 \ (W/m.K)$[211]

5.1.3.1 Numerical results obtained from COMSOL modeling

The time-dependent thermal profile of the hybrid system is acquired using the solver. The variation of the temperature profiles across the CTJ-TEG hybrid system during the 6^{th} minute is illustrated in Figure 5.17. The propagation of the temperature through the CTJ-TEG hybrid system can be observed. For all the temperature profiles, the maximum and minimum temperatures are related to CTJ cell and the cold side of the TEG, respectively. For the applied pattern of the solar radiation shown in Figure 5.13 and for $t = 300\ s$, the maximum and minimum temperatures are 88.9 ℃ and 32.6 ℃, respectively. This values for the $t = 360\ s$ are 107 ℃ and 36.2 ℃.

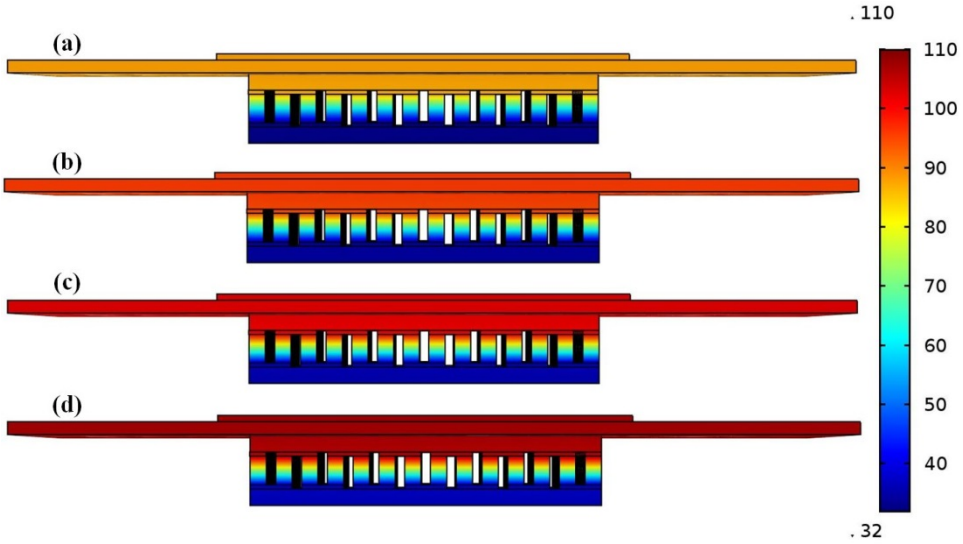

Fig. 5.17: Temperature contours for (a) t=300 s (b) t=320 s (c) t=340 s (d) t=360 s [218].

The electric potential and temperature fields are coupled in thermoelements. Figure 5.18 displays the three-dimensional distribution of the electric potential in the TEG module. The temperature gradient through the TEG and the current flowing across the thermoelements are two key factors in creating electric potential in the thermoelements [222]. When the temperature difference between the cold and hot sides of the TEG enhances, the generated electric potential increases as well. For $t = 300\ s$ and $t = 360\ s$, the maximum produced electric potential of the TEG are $0.96\ V$ and $1.23\ V$ respectively.

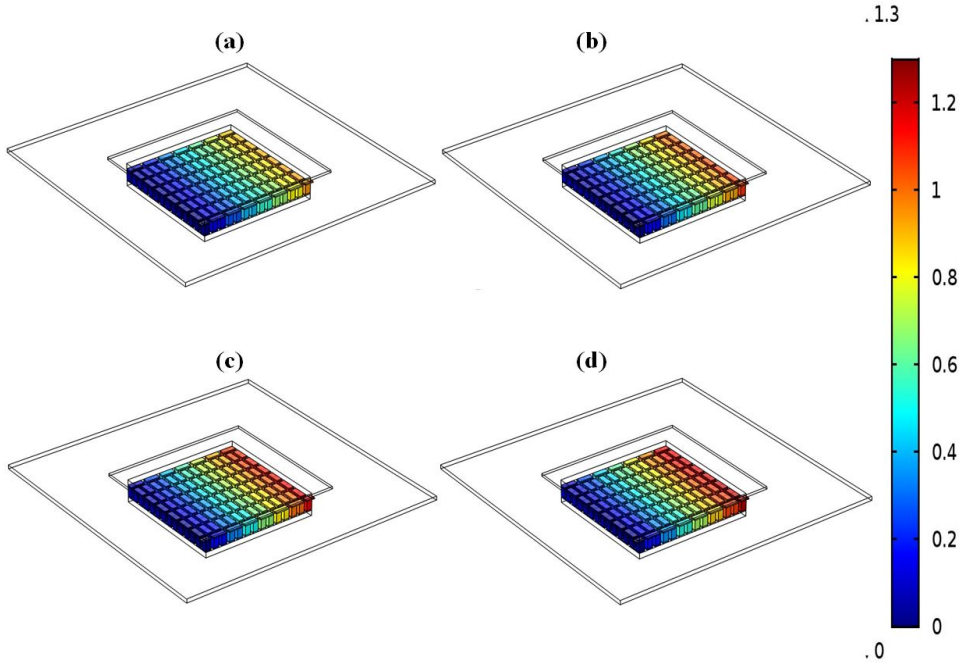

Fig. 5.18: Electric potential of the TEG for (a) t=300 s (b) t=320 s (c) t=340 s (d) t=360 s [218].

5.1.3.2 Validation of the experiments using COMSOL Modeling results

Figure 5.19 shows the variation of the generated maximum power by the CTJ cell, obtained from both numerical and experimental approaches, versus the time. Due to the variation of the concentrated solar radiations and consequently the input heat flux to the hybrid system, the output power by the CTJ cell also changes stepwise. Therefore there is a significant change in the generated power due to the variation of the input heat flux. In addition, the temperature of the CTJ cell also has a small impact on the output power. When the concentrated solar radiation and subsequently the temperature of the CTJ cell drops, an insignificant enhancement in the generated power by the CTG cell occurs, see Area (1) in Figure 5.19. The reverse variation of the generated power by the CTJ cell happens in Area (2). It shows that when the concentrated solar radiation and then the temperature of the CTJ cell enhances, a small drop in power generation takes place.

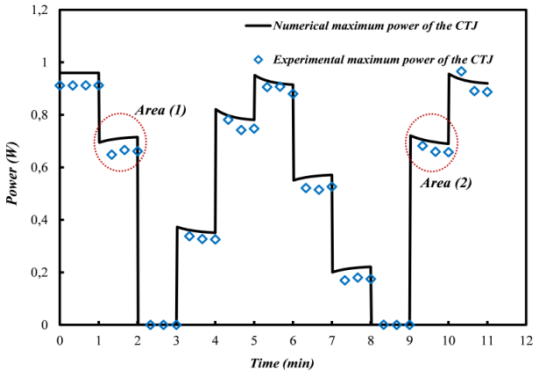

Fig. 5.19: Experimental and numerical maximum power generated by the CTJ versus time [218].

The generated power by the TEG obtained from the simulation and experiments are shown in Figure 5.20. The material properties of the TEG are not changed significantly over the temperature range displayed in Figure 5.13. Therefore, the figure of merit as one of the key parameters in power generation by the TEG is not changing considerably in the transient condition. Subsequently, the temperature gradient across the TEG module is the most important parameter in the generating power by the TEG in the transient condition. This point can be observed in Figure 5.20. It shows that the variation of the generated power by the TEG has the same trend with the variation of the temperatures shown in Figure 5.13. Make a comparison between areas (1) and (2) in Figures 5.19 and 5.20 indicates that the variation of the generated power by the CTJ and TEG have an opposite trend. This contradiction in power generation by two devices can help to stabilize the overall generated power by the hybrid system. To reach this target, geometrically optimized TEG with more efficient materials should be used in the hybrid systems.

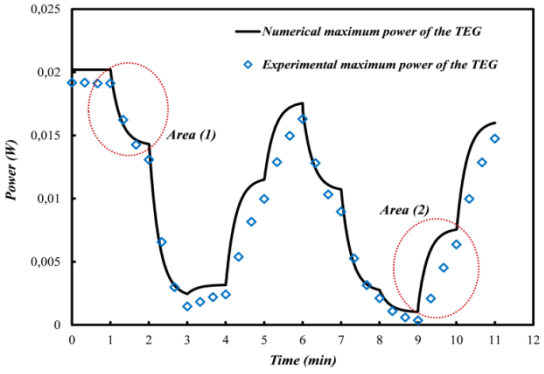

Fig. 5.20: Experimental and numerical maximum power generated by the TEG versus time [218].

Figure 5.19 and 5.20 show close agreement between the experimental and numerical results. There is an overestimation for the numerical results compare to the experimentally obtained output power. For the CTJ cell, the value of the numerically obtained temperature is less than the experimental ones. Therefore, the numerical results for the power generation by the CTJ are higher than the experimental values. For the TEG, however, the obtained values for the temperatures of the hot and cold sides of the TEG in the numerical simulation are less than the experimental results, but the temperature gradient across the TEG is higher. Accordingly, the power generation by the TEG obtained from the numerical study is higher than the experimental results.

5.2 STEADY-STATE STUDY OF THE CTJ-TEG HYBRID SYSTEM

In this section, the prototype used before for the transient study is employed to investigate the performance and conversion efficiency of the CTJ-TEG hybrid system under low concentrated solar radiations (less than 40 suns [223-224]). Both Experimental and numerical approaches are used for this steady-state examination. The experimental study is carried out in Paul Scherrer Institute (PSI), Villigen, Switzerland and finite volume method is used for the numerical investigation.

5.2.1 EXPERIMENTAL STUDY ON THE PERFORMANCE OF THE CTJ-TEG HYBRID SYSTEM

The same setup introduced in section 5.1.2 is used to study the steady-state performance of the CTJ-TEG hybrid system. As it mentioned before, two lamps that are always on throughout the experiments are used to deliver concentrated solar radiations up to 37 suns. A shutter located in front of the lamps, shown in Figure 4.3, is used to adjust the value of the concentrated light. Table 5.3 indicates the values of the correspondent concentrated light for the different open-rate percentage of the shutter.

Table 5.3: Solar radiation on the CTJ versus open-rate percentage of the shutter [225].

Shutter percentage (%)	3	6	9	12	15	18
Solar radiation (kW/m^2)	8	17	22	27	32	37

5.2.2 NUMERICAL MODELING OF THE CTJ-TEG HYBRID SYSTEM IN THE STEADY-STATE CONDITION

In order to achieve the temperature profile of the CTJ-TEG hybrid system in the steady-state condition, the same method used in section 5.1.1 is applied. All the equations obtained using energy conservation law for different layers. In the steady-state condition, the variation of the temperature with the time is zero, $\frac{\partial T}{\partial t} = 0$. Therefore, for the steady state condition, all the equations $(5-1)$ to $(5-16)$ can be applied if $\frac{\partial T}{\partial t}$ is considered zero in all the equations. The power generation and conversion efficiency of the TEG also can be obtained using equations $(5-19)$ and $(5-20)$.

In order to obtain power generation and conversion efficiency of the CTJ cell in the steady-state condition, a single diode model [226] is assumed for the CTJ cell. In the single diode model, shown in Figure 5.21, The CTJ cell current is stated as a function of the CTJ cell voltage as:

$$I = I_{PH} - \frac{V + IR_S}{R_{SH}} - I_0\left[\exp\left(\frac{V + IR_S}{nV_T}\right) - 1\right] \qquad (5-23)$$

In this equation, $V_T = kT/q$ is the thermal voltage, I_0 is defined as the reverse saturation current and n is the diode ideality factor. For the ideal diode, the value of n is equal to 1.

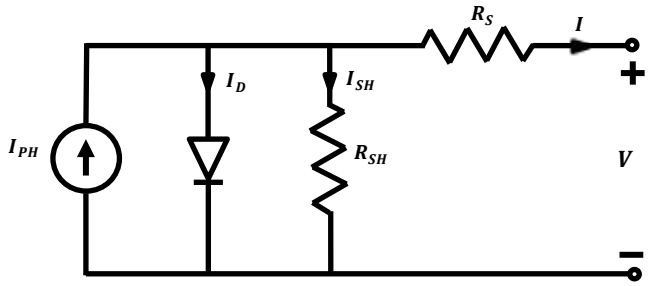

Fig. 5.21: The equivalent circuit of the CTJ module with a single-diode system [227].

In the Equation$(5-23)$, when the R_S is not zero, It is not possible to obtain the current directly from this equation. In this condition, Lambert W function [227-229] can be used to solve the equation and acquire the current. Thus, the equation $(5-23)$ can be represented as follows:

$$I = \frac{(I_{PH} + I_0) - \frac{V}{R_{SH}}}{1 + \frac{R_S}{R_{SH}}} - \frac{nV_T}{R_S} W\left(\frac{I_0 R_S}{nV_T\left(1 + \frac{R_S}{R_{SH}}\right)} \exp\left(\frac{V}{nV_T}\left(1 - \frac{R_S}{R_S + R_{SH}}\right) + \frac{(I_{PH} + I_0)R_S}{nV_T\left(1 + \frac{R_S}{R_{SH}}\right)}\right)\right) \quad (5-24)$$

The voltage of the CTJ cell is given as:

$$V = (I_{PH} + I_0)R_{SH} - I(R_S + R_{SH}) - nV_T W\left(\frac{I_0 R_{SH}}{nV_T} \exp\left(\frac{(I_{PH} + I_0 - I)R_{SH}}{nV_T}\right)\right) \quad (5-25)$$

Therefore, the power generation by the CTJ cell is defined as:

$$P_{CTJ} = VI \quad (5-26)$$

And the conversion efficiency of the CTJ cell can be obtained by:

$$\eta_{CTJ} = \frac{P_{CTJ}}{SC \times G \times A_{CTJ}} \quad (5-27)$$

5.2.3 EXPERIMENTAL AND NUMERICAL RESULTS FOR THE CTJ-TEG HYBRID SYSTEM IN THE STEADY-STATE CONDITION

Temperature plays the most significant role in the performance of the CTJ cell and TEG module. The variation of the temperatures of the cold and hot sides of the TEG and the CTJ cell versus time are displayed in Figure 5.22. The experiments are carried out for 10 minutes for each concentrated solar radiation varying between 8 to 37 suns. Figures 5.22 and 5.23 indicate that for each concentrated solar radiation, 10 minutes is enough to reach to the steady-state condition.

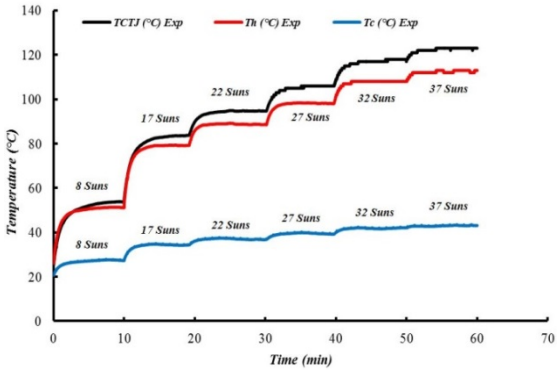

Fig. 5.22: Temperature variation of the CTJ and hot and cold side of the TEG [225].

Figure 5.23 shows the variation of the short circuit current and open circuit voltage for the TEG and CTJ versus time. The short circuit current is achieved and recorded every minute while the open circuit voltage is measured every second. When the solar concentration ratio and consequently the temperature of the CTJ cell increases, the short circuit current of the CTJ cell enhances but the open circuit voltage drops. For the TEG, there is the same manner for the short-circuit current and an inverse trend for the open circuit voltage rather than CTJ cell. In other words, for the TEG, both short circuit current and open circuit voltage are enhanced by increasing the solar concentration.

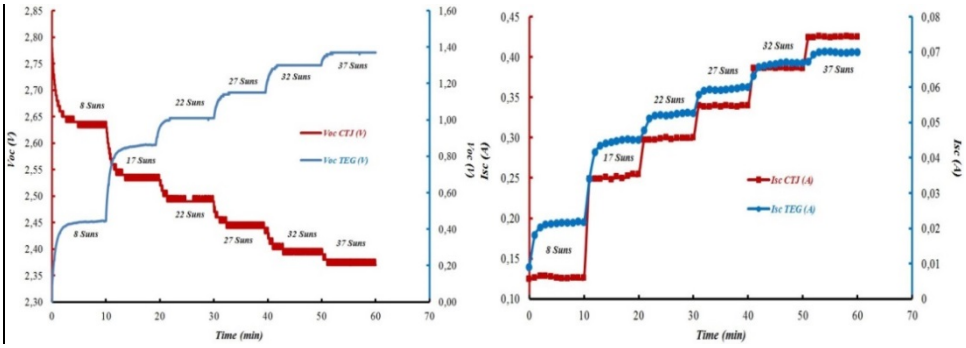

(a) *(b)*

Fig. 5.23: (a) Open circuit voltage and (b) short circuit current of the CTJ and TEG [225].

Experimental results and numerically obtained P-V and I-V curves for various concentrated solar radiations are illustrated in Figure 5.24. In order to find the best-fitted curve for the experimental results, the Newton–Raphson algorithm [230] is used. Lambert W function is

also applied in the numerical simulation to achieve the I-V characteristics of the CTJ cell. The temperature of the CTJ cell and the amount of the concentrated light are two main parameters in the performance of the CTJ cell. When the temperature enhances, due to an increment in the number of thermally generated carriers in the CTJ cell, the photogenerated current I_{PH}, in Equation $(5-23)$, also increases. Since the value of the short circuit current I_{SC} and photogenerated current I_{PH} are almost the same, the concentration ratio is the most dominant parameter in the variation of the short circuit current of the CTJ cell. Thus, the temperature has a smaller impact on the short-circuit current of the CTJ cell, but the influence of the temperature on the open circuit voltage of the CTJ cell is more noticeable. The results of the numerical simulation and experiments are in a good agreement. The numerically obtained values for the maximum power by the CTJ cell for 8 suns and 37 suns are 0.314 W and 0.902 W, respectively. These values for the experimental work are 0.283 W and 0.852 W, respectively.

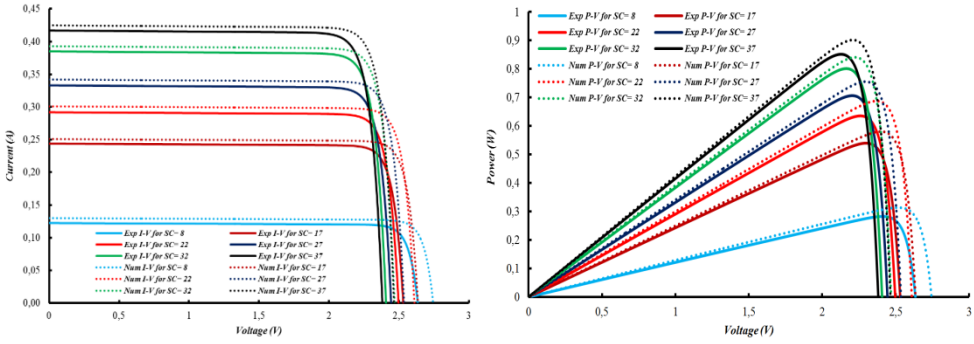

(a) *(b)*

Fig. 5.24: (a) I-V curve (b) P-V curve for the CTJ in hybrid CTJ-TEG system [225].

The P-V and I-V curves for the TEG in the CTJ-TEG hybrid system and various concentrated lights are shown in Figure 5.25. The temperature gradient across the TEG and the figure of merit of the TEG module are two main parameters in the performance of the TEG module. The variation of the figure of merit of the TEG within the studied range of temperature is insignificant [220]; therefore, the temperature difference between cold and hot sides of the TEG is the most effective parameter on the performance of the TEG. When the concentration ratio increases, the temperature gradient across the TEG and consequently the maximum generated power by the TEG are enhanced as well. The experimentally obtained maximum generated power by the TEG for the concentration ratios 8 suns and 37 suns are 2.43 mW and 24.1 mW, respectively. These values for the numerical simulation are 2.89 mW and 25.6 mW, correspondingly.

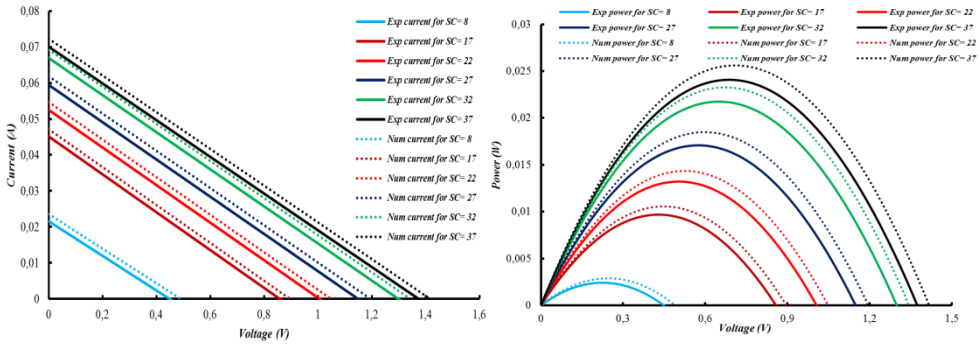

(a) *(b)*

Fig. 5.25: (a) I-V curve (b) P-V curve for the TEG in hybrid CTJ-TEG system [225].

Figure 5.26 displays the ratio of the maximum generated power by the TEG module to the maximum output power by the CTJ cell. The contribution of the TEG in the overall output power by the CTJ-TEG hybrid system increases by enhancement of the concentration ratio. This ration for the solar concentration 8 suns is 0.86 %, while this value for the concentration ratio 37 suns is equal to 2.83 %.

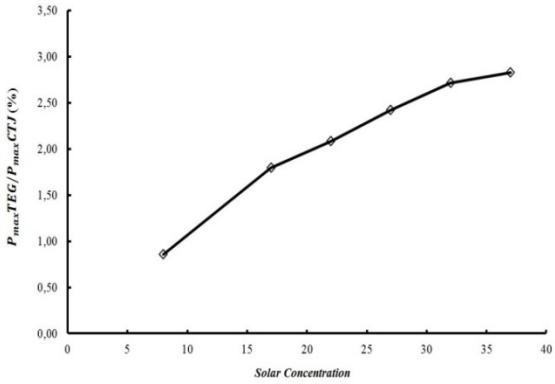

Fig. 5.26: Ratio of the maximum power of the TEG to CTJ versus solar concentration [225].

Experimental and numerical results for the efficiency of the CTJ and TEG in the CTJ-TEG hybrid system versus the concentration ratio are displayed in Figure 5.27. For the CTJ cell, the temperature of the cell has the most significant impact on the efficiency [231]. In all the

experiments the same heat sink with constant efficiency is used, therefore with enhancing the concentration ratio, the temperature of the CTJ cell increases and consequently the conversion efficiency of the CTJ cell drops. The numerically obtained minimum and maximum efficiencies of the CTJ cell are 24.38 % and 39.21 % that are related to concentration ratios 37 suns and 8 suns, respectively. These values are 23.02 % and 35.33 % for the experimental work. There is an overestimation for the numerical results rather than experimental ones. The reason is that the numerical model is one-dimensional with some simplifying assumptions, so the numerically obtained temperatures of the CTJ cell are less than the experimental values and consequently the numerical efficiencies are higher.

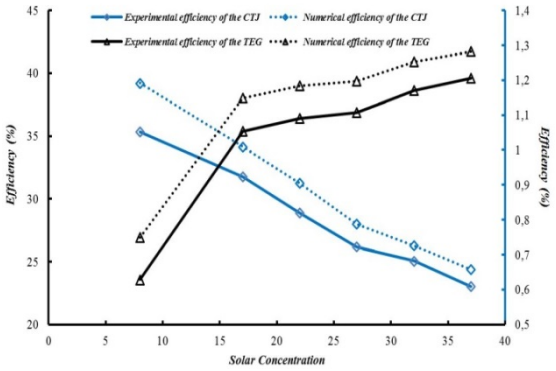

Fig. 5.27: Variation of the efficiencies of the CTJ and the TEG in hybrid CTJ-TEG system versus solar concentration [225].

For the TEG, as mentioned before, the variation of the figure of merit is small in the temperature range considered in this study. Therefore, the temperature gradient across the TEG is the major factor in the efficiency of the TEG. The temperature difference between the cold and hot sides of the TEG enhances when the concentration ratio increases, see Figure 5.22. Subsequently, the efficiency of the TEG enhances, see Figure 5.27. The maximum and minimum efficiencies of the TEG obtained from the numerical study are 1.28% and 0.75% that are related to the concentration ratios 37 suns and 8 suns, respectively. These values are 1.20% and 0.63% for the experimental investigation. Although the cold and hot side temperatures obtained from the numerical simulation are less than the experimental results, the temperature gradients across the TEG are higher, and consequently, the numerical efficiencies are higher than experimental ones.

5.3 PARAMETRIC STUDY ON THE PERFORMANCE OF CTJ-TEG HYBRID SYSTEM

The established numerical model is capable of considering the influence of different factors. The impact of different geometrical parameters and material properties on the power generation and conversion efficiency of the system can be achieved. In this section the variation of the output power and conversion efficiency of the CTJ-TEG hybrid system for different values of convective heat transfer coefficients in the heat sink, various solar concentrations, and thermal contact resistances are determined. Convective heat transfer is varied between $500 \text{ to } 5000\ \mathrm{W/m^2K}$ and Solar concentration and thermal contact resistance are altered among 100 to 900 suns ($1 \text{ sun} = 1000\ \mathrm{W/m^2}$) and 5×10^{-6} and $5 \times 10^{-4}\ \mathrm{m^2.°C/W}$, respectively.

The efficiency of the heat sink has a significant impact on the performance of the CTJ and TEG in the CTJ-TEG hybrid system. Conversion efficiency and output power by the CTJ and TEG for the constant concentration ratio $\mathrm{SC} = 300$ suns and semiconductor length of $\mathrm{L} = 1.5$ mm versus convective heat transfer coefficient are displayed in Figures 5.28 and 5.29. The graphs are presented for different values of the thermal contact resistances varying between 5×10^{-6} and $5 \times 10^{-4}\ \mathrm{m^2.°C/W}$. Thermal contact resistance has a significant effect on both conversion efficiency and output power by the CTJ and TEG. For the CTJ, this effect is more visible for the higher convective heat transfer coefficients. Figures 5.28 and 5.29 illustrate that thermal contact resistance has a more significant impact on the conversion efficiency and generated power by the TEG than the CTJ.

When the convective heat transfer coefficient enhances and consequently the temperature of the CTJ cell drops, both conversion efficiency and generated power by the CTJ increase. For the TEG, by enhancement of the convective heat transfer coefficient, the temperatures of both hot and cold sides of the TEG are decreased, but the rate of decrement of the cold side temperature is higher. Consequently, the temperature gradient across the TEG, conversion efficiency and generated power by the TEG are enhanced.

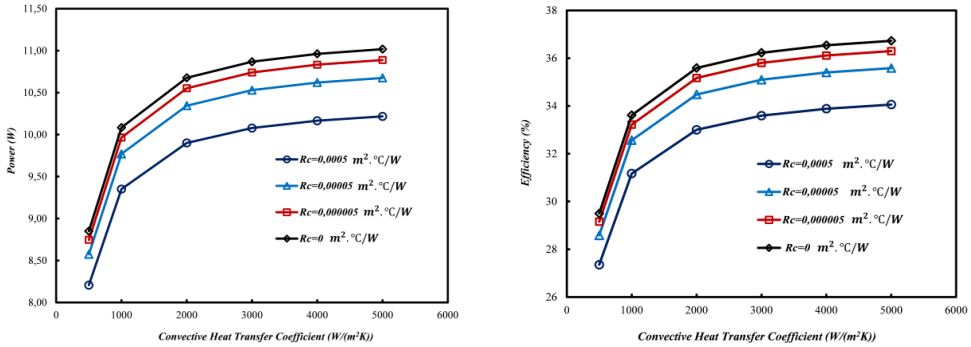

Fig. 5.28: Power generation and efficiency of the CPV versus convective heat transfer coefficient for different thermal contact resistance [232].

Figures 5.28 and 5.29 indicate that with increasing the convective heat transfer coefficient both conversion efficiency and generated power are enhanced. The rate of this enhancement drops for the higher convective heat transfer coefficients. Thus, an optimum value for the convective heat transfer coefficient can be acquired to decrease the cost of the cooling system. This optimum value depends on the considered material properties and geometry in the numerical model.

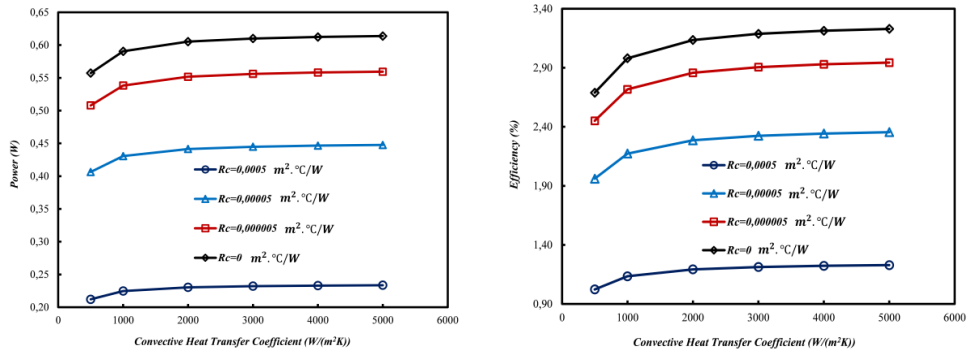

Fig. 5.29: Power generation and efficiency of the TEG versus convective heat transfer coefficient for different thermal contact resistance [232].

Figures 5.30 and 5.31 are displayed the conversion efficiency and output power by the TEG and CTJ versus concentration ratio for different thermal contact resistances. The length of

the thermoelements and convective heat transfer coefficient are considered $L = 1$ mm and $h = 2000\ W/(m^2K)$, respectively. When the concentration ratio and consequently the input heat flux is increased, the generated power by the CTJ and TEG are enhanced as well. The enhancement of the temperature of the CTJ cell due to the increment of the concentration ratio leads to a considerable drop in the efficiency of the CTJ cell. The opposite trend for the conversion efficiency of the TEG can be observed in Figure 5.31. With increasing the concentration ratio and consequently the heat flux and temperature gradient across the TEG, the conversion efficiency of the TEG is also increased.

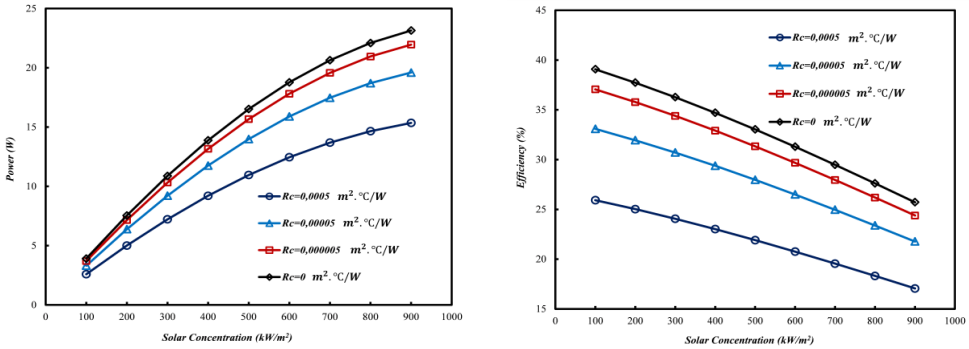

Fig. 5.30: Power generation and efficiency of the CPV versus solar concentration for different thermal contact resistance [232].

The significance of the destructive influence of the thermal contact resistance on the generated power and conversion efficiency of the TEG and CTJ cell can be observed in Figures 5.30 and 5.31. This negative impact on the power generation is more observable for the higher concentration ratios for both TEG and CTJ cell.

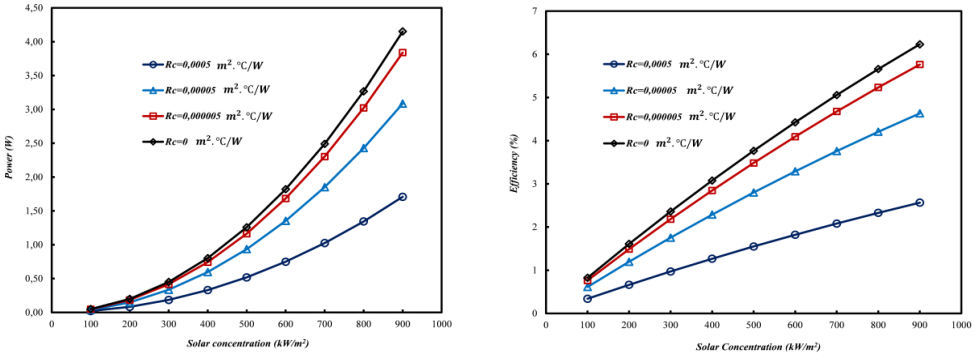

Fig. 5.31: Power generation and efficiency of the TEG versus solar concentration for different thermal contact resistance [232].

CHAPTER 6. CLOSURE

Main conclusions of the thesis are summarized in this chapter. Furthermore, the suggestions and ideas for future work are presented.

6.1 CONCLUSIONS

This dissertation aims to contribute to the waste heat recovery by the TEGs, STEG systems, and CTJ-TEG hybrid systems. The major conclusions of this PhD study are:

For the waste heat recovery by the TEGs:
Experimental investigation on the effect of the different operating conditions on the performance and transient behavior of the TEG system has led to some interesting results. It is found that, Force convection cooling has a substantial impact on the performance of the TEG system in comparison with natural convection heat transfer in the cold side. Though, in order to save the used energy by the cooling fan, lower fan power and volumetric flow rates are recommended to be used. It is indicated that the performance of the TEG system is affected significantly by its operating condition. Volumetric flow rates in both hot and cold sides and the temperatures have a considrable impact on the power generated by the TEG system. In the transient condition, for the small volumetric flow rates, the temperature reduction in the cold side is not significant. The results showed that, enhancing the temperature and the volumetric flow rates on both sides of the TEG system leads to a larger variation in the hot and cold side temperatures.

For the STEG systems:
Experimental investigation and numerical simulation of the oxide-based and Bi-Te based STEG systems are carried out. The main focus was on the transient response of the STEG systems to the variant solar radiations. The results showed that, graphite sheet acts as an absorber and increases the heat flux imposed the both oxide-based and Bi-Te based STEG systems and consequently the generated power by the systems. Although, the ratio of the maximum output power by the oxide-based STEG system using graphite sheet to the system without graphite sheet reduces with enhancement of the concentrated solar radiation. In the transient study, the fluctuations of the electrical output power, the short circuit current, the open circuit voltage and the cold and hot side temperatures of the TEG in both oxide-based and Bi-Te based STEG system are strongly influenced by the sharp variation of the solar radiation.

The numerical model is also developed to predict the performance and conversion efficiency of the oxide-based STEG system in higher temperatures. It is found that due to increment in the figure of merit and the temperature difference, performance and conversion efficiency of the STEG system are enhanced substantially at higher concentrated solar radiations. The numerical model is also used for the Bi-Te based STEG system to evaluate the significance of the impact of the graphite layer on the output power by the system. The results showed that the efficiency of the system with the graphite layer is almost 2.5 times more than the system without the graphite layer. For both oxide-based and Bi-Te based STEG systems it is concluded that for low solar concentration applications, this technique is useful to compensate for the low amount of input energy.

For the CTJ-TEG hybrid systems:

The transient and steady-state behavior of the CTJ-TEG hybrid system is investigated using both experimental and numerical approaches. Parametric study on the impact of some crucial parameters is also carried out. The results indicated that in the transient study, temperatures of different layers are influenced by the quick variation of the solar radiations and power generation by the CTJ cell and TEG module enhances with increasing the solar radiation and concentration ratio. The stepwise variation of the concentration ratio leads to an almost stepwise power generation by the CTJ while the variation of the generated power by the TEG gradually and mostly follows the temperature profiles. It is also found that, the conversion efficiencies of the CTJ and TEG have opposite response to the increment of the solar radiation. The efficiency of the CTJ cell decreases while the efficiency of the TEG module increases and shows that using the TEG module in the CTJ-TEG hybrid system is useful to stabilize the output power by the hybrid system. Furthermore, the substantial impact of the thermal contact resistance on the generated power and conversion efficiency cannot be neglected in the real applications. Increment in the thermal contact resistance cause to a considerable drop in the power generations and conversion efficiencies of the CTJ cell and TEG module. It is also indicated that the contribution of the generated power by the TEG module in the overall output power by the CTJ-TEG hybrid system enhances with increasing the solar concentration.

6.2 OUTLOOK

As future work, the following suggestions for different studied concepts in this thesis are given below.

Regarding waste heat recovery by the TEGs, the following ideas for future studies are suggested:

- Different configurations for the TEGs can be examined.
- A broader range of the temperatures and volumetric flow rates and consequently different operating conditions can be applied to the system.
- The numerical study can be done in future to validate the experimental results and optimize the system to maximize the generated power and efficiency of the system.
- Impact of using different heat sinks and heat sources of the performance of the system can be investigated.

Regarding the STEG systems, the following ideas for future studies are suggested:

- The performance analysis of using other TEG modules with different material properties for various ranges of the temperatures can be studied.
- The STEG systems can be studied under higher ranges of the solar concentrations using a more efficient heat sink.
- STEG system can be examined in the real weather condition to see the actual transient response of the system during the day.
- Geometrical optimization for the STEG system can be done to maximize the efficiency and generated power by the STEG system.

Regarding the CTJ-TEG hybrid systems, the following ideas for future studies are suggested:

- Geometrical and material optimization can be done to acquire the peak generated power by the CTJ-TEG hybrid system with the maximum stability.
- There is a contradiction in the working status of the CTJ cell and TEG module in the hybrid CTJ-TEG system. This concept can be considered to design a hybrid system with the optimum working condition for both CTJ cell and TEG module.
- In order to minimize the energy cost, a study on the optimum value for the convective heat transfer coefficient can be carried out.

- In order to see the actual transient response of the CTJ-TEG hybrid system during the day, the hybrid system can be tested in the real weather condition.
- Different configurations of the PV-TEG hybrid system can be considered to have the maximum utilization of the whole light spectrum. For instance, using spectral beam splitter that is an optical device which can split an incident light beam into two or more beams. The beams with the short wavelengths are more appropriate for PV cell and beams with long wavelengths can be used for the TEG module.

LITERATURE LIST

[1] HoSung Lee, THERMOELECTRICS DESIGN AND MATERIALS, John Wiley & Sons, 2016.

[2] T. Seebeck, "Magnetische Polarisation der Metalle und Erze durch Temperatur-Differenz," Abhandlungen der Deutschen Akademie der Wissenschaften zu Berlin, pp. 265-373, 1823.

[3] Rowe DM. General Principles and Basic Considerations. Thermoelectr. Handb. Macro to Nano, Boca Raton, USA: Taylor & Francis Group; 2006, p. 1–1 – 1–15.

[4] J. Peltier, "Nouvelles Experiences sur la Caloriecete des Courans Electrique," Ann. Chim., vol. LVI, pp. 371-387, 1834.

[5] W. Thomson, "On a Mechanical Theory of Thermoelectric Currents," Proceedings of the Royal Society of Edinburgh, pp. 91-98, 1851.

[6] Decher, R. (1997) Direct Energy Conversion, Oxford University Press.

[7] Sutton, G.W. (ed.) (1966) Direct Energy Conversion, Inter-University Electronics Series, vol. 3, McGraw-Hill Book Company.

[8] Kaye, J. and Welsh, J.A. (eds) (1960) Direct Conversion of Heat to Electricity, John Wiley & Sons, Inc.

[9] Angrist, S.W. (1965) Direct Energy Conversion, Allyn and Bacon, Inc., Boston, MA.

[10] Fleurial J-P, Bux S, Huang C-K, Cheng BJ, Vo T, Allmen Pvon, et al. Advanced High Temperature Bulk Thermoelectric Materials. In: Society A nuclear, editor. Proceedings of Nuclear and Emerging Technologies for Space 2011.

[11] Voyager, the interstellar mission n.d. <http://voyager.jpl.nasa.gov/spacecraft/index.html> [accessed September 24, 2015].

[12] Cataldo RL, Bennett GL. U.S. space radioisotope power systems and applications: past, present and future, radioisotopes - applications in physical sciences; 2011.

[13] Radioisotope Thermoelectric Generator n.d. <http://solarsystem.nasa.gov/ rps/rtg.cfm> [accessed September 24, 2015].

[14] Schwartz LI, Shure HJ. Survey of electric power plants for space applications. In: Fifty-Eight National Meeting of the American Institute of Chemical Engineers Philadelphia, Pennsylvania, December 5–9, 1965.

[15] Caillat T, Sakamoto J, Jewell A, Huang CK, Cheng J, Paik J, et al. Status of skutterudite-based segmented thermoelectric technology components development at JPL. In: STAIF 23rd Symposium on Space Nuclear Power and Propulsion. Albuquerque, New Mexico, Pasadena, CA: Jet Propulsion Laboratory, National Aeronautics and Space Administration; 2006.

[16] Caillat T, Firdosy S, Li B, Chi S, Paik J-A, Huang C-K, et al. Advanced hightemperature thermoelectric devices. In: DOE Thermoelectric Applications Workshop.
[17] Spacecraft Power for Cassini - NASA fact sheet; 1999.
[18] Welcome to Gentherm Global Power Technologies, Gentherm Global Power Technologies n.d. <http://www.genthermglobalpower.com/> [accessed September 24, 2015].
[19] Alimov. Radioisotope Thermoelectric Generators - Bellona n.d. <http://bellona.ru/bellona.org/english_import_area/international/russia/navy/northern_fleet/incidents/31772> [accessed September 24, 2015].
[20] Brignonea M, Ziggiottia A. Impact of novel thermoelectric materials on automotive applications. In: 9th European conference on thermoelectrics. Fiat Research Center; 2011.
[21] Maranville C. Overview of ford-DOE thermoelectric programs: waste heat recovery and climate control. In: 2nd Thermoelectrics Applications Workshop 2011. Ford; 2011.
[22] Eder A, Linde M. Efficient and dynamic the BMW group roadmap for the application of thermoelectric generators. In: 2nd Thermoelectrics Applications Workshop. BMW Group; 2011.
[23] Meisner GP. Advanced thermoelectric materials and generator technology for automotive waste heat at GM. In: 2nd Thermoelectrics Applications Workshop 2011.
[24] Aixala L, Monnet V. Conclusion of RENOTER project (Waste Heat Recovery for Trucks and Passenger Cars). In: Junsch D, editor. Thermoelectrics Goes Automotive II; 2012. p. 241–59.
[25] Magnetto D, Vidiella G. Reduced energy consumption by massive thermoelectric waste heat recovery in light duty trucks. AIP Conf Proc 2012;1449:471–4. http://dx.doi.org/10.1063/1.4731598.
[26] Frobenius F, Gaiser G, Rusche U, Weller B. Thermoelectric generators for the integration into automotive exhaust systems for passenger cars and commercial vehicles. J Electron Mater 2015:1–8. http://dx.doi.org/10.1007/ s11664-015-4059-z.
[27] Brunetti M, Cogliati A, Iannucci D, Scandroglio A. Aircraft capable of hovering having an exhaust duct with thermoelectric conversion circuit. Google Patents; 2015.
[28] Kwok DW, Huang JP, Skorupa JA, Smith JW. Thermoelectric generation system. Google Patents; 2009.
[29] Chabas J. European Commission : CORDIS : Projects & Results Service : Final Report Summary – THETAGEN (Thermoelectric generator for engine control system) n.d. <http://cordis.europa.eu/result/rcn/164433_en.html> [accessedDecember 15, 2015].
[30] Wallace TT. Development of marine thermoelectric heat recovery systems. In: 2nd Thermoelectrics Applications Workshop 2011.

[31] Kristiansen NR, Nielsen HK. Potential for usage of thermoelectric generators on ships. J Electron Mater 2010;39:1746–9. http://dx.doi.org/10.1007/ s11664-010-1189-1.
[32] Wallace T, Bailey M, Starbird N, Blackman A, Wallace C, Logus J, et al. Thermoelectric generator development efforts at the maine maritime academy. Thermoelectrics applications 2009; 2009.
[33] Geradts K, Sonnleitner W. Operation of an internal combustion engine. Google Patents; 2013.
[34] Kaibe H, Makino K, Kajihara T, Fujimoto S, Hachiuma H. Thermoelectric generating system attached to a carburizing furnace at Komatsu Ltd., Awazu Plant. AIP Conf Proc 2012;1449:524–7. http://dx.doi.org/10.1063/1.4731609.
[35] Aranguren P, Astrain D, Rodriguez A, Martinez A. Experimental investigation of the applicability of a thermoelectric generator to recover waste heat from a combustion chamber. Appl Energy 2015;152:121–30. http://dx.doi.org/ 10.1016/j.apenergy.2015.04.077.
[36] Kuroki T, Kabeya K, Makino K, Kajihara T, Kaibe H, Hachiuma H, et al. Thermoelectric generation using waste heat in steel works. J Electron Mater 2014;43:2405–10. http://dx.doi.org/10.1007/s11664-014-3094-5.
[37] Luo Q, Li P, Cai L, Zhou P, Tang D, Zhai P, et al. A thermoelectric waste-heat recovery system for Portland cement rotary kilns. J Electron Mater 2015;44:1750–62. http://dx.doi.org/10.1007/s11664-014-3543-1.
[38] IEA – Energy access database n.d. <http://www.worldenergyoutlook.org/ resources/energydevelopment/energyaccessdatabase/> [accessed March 7, 2016].
[39] Nuwayhid RY, Rowe DM, Min G. Low cost stove-top thermoelectric generator for regions with unreliable electricity supply. Renewable Energy 2003;28:205–22. http://dx.doi.org/10.1016/S0960-1481(02)00024-1.
[40] Nuwayhid RY, Hamade R. Design and testing of a locally made loop-type thermosyphonic heat sink for stove-top thermoelectric generators. Renewable Energy 2005;30:1101–16. http://dx.doi.org/10.1016/j. renene.2004.09.008.
[41] Mastbergen D, Willson B. Generating light from stoves using a thermoelectric generator. In: ETHOS 2005 Engineers in Technical and Humanitarian Opportunities of Service international stove research conference.
[42] Molina MG, Juanicó LE, Rinalde GF. Design of innovative power conditioning system for the grid integration of thermoelectric generators. Int J Hydrogen Energy 2012;37:10057–63. http://dx.doi.org/10.1016/j.ijhydene.2012.01.177.
[43] Champier D, Rivaletto M, Strub F. TEGBioS :a prototype of thermoelectric power generator for biomass stoves. In: ECOS 2009, 22nd Internacional conference on efficiency, cost, optimization, simulation, and environmental impact of energy systems ; 2009.

[44] Champier D, Bédécarrats JP, Kousksou T, Rivaletto M, Strub F, Pignolet P. Study of a TE (thermoelectric) generator incorporated in a multifunction wood stove. Energy 2011;36:1518–26. http://dx.doi.org/10.1016/j. energy.2011.01.012.
[45] Najjar YSH, Kseibi MM. Heat transfer and performance analysis of thermoelectric stoves. Appl Therm Eng 2016;102:1045–58. http://dx.doi. org/10.1016/j.applthermaleng.2016.03.114.
[46] Hoftberger E, Moser W, Aigenbauer SW, Friedl G, Haslinger W. Grid autarchy of automated pellets combustion systems by the means of thermoelectric generators. Konferenz Automotive Goes Thermoelectrics 2010.
[47] Montecucco A, Siviter J, Knox AR. A combined heat and power system for solid-fuel stoves using thermoelectric generators. Energy Procedia 2015;75:597–602. http://dx.doi.org/10.1016/j.egypro.2015.07.462.
[48] Ecofan - Caframo Lifestyle Solutions; 2016. <http://www.caframolifestyle solutions.com/ecofan/> [accessed March 17, 2016].
[49] Codecasa M, Fanciulli C, Gaddi R, Passaretti F. Design and development of a TEG cogenerator device integrated in self standing gas heaters. In: 9th European conference on thermoelectrics.
[50] Codecasa MP, Fanciulli C, Gaddi R, Gomez-Paz F, Passaretti F. Design and development of a TEG cogenerator device integrated into a self-standing natural combustion gas stove. J Electron Mater 2015;44:377–83. http://dx. doi.org/10.1007/s11664-014-3297-9.
[51] Nextreme Laird. Microscale Thermal and Power Management n.d. <http:// www.lairdtech.com/products/thermobility-wpg-1> [accessed May 31, 2016].
[52] Emerson Process Management - Wireless Power Module | Smart Wireless Battery | Emerson n.d. <http://www2.emersonprocess.com/en-us/brands/ rosemount/wireless/smartpower-solutions/pages/index.aspx> [accessed June 1, 2016].
[53] Wang W, Cionca V, Wang N, Hayes M, O'Flynn B, O'Mathuna C. Thermoelectric energy harvesting for building energy management wireless sensor networks. Int J Distrib Sens Netw 2013;2013:14.
[54] Samson D, Kluge M, Fuss T, Schmid U, Becker T. Flight test results of a thermoelectric energy harvester for aircraft. J Electron Mater 2012;41:1134–7. http://dx.doi.org/10.1007/s11664-012-1928-6.
[55] Elefsiniotis A, Weiss M, Becker T, Schmid U. Efficient power management for energy-autonomous wireless sensor nodes for aeronautical applications. J Electron Mater 2013;42:1907–10. http://dx.doi.org/10.1007/s11664-012- 2468-9.
[56] Elefsiniotis A, Becker T, Schmid U. Thermoelectric energy harvesting using phase change materials (PCMs) in high temperature environments in aircraft. J Electron Mater 2014;43:1809–14. http://dx.doi.org/10.1007/s11664-013- 2880-9.

[57] Shi Y, Wang Y, Deng Y, Gao H, Lin Z, Zhu W, et al. A novel selfpowered wireless temperature sensor based on thermoelectric generators. Energy Convers Manage 2014;80:110–6. http://dx.doi.org/10.1016/j. enconman.2014.01.010.

[58] Leonov V, Torfs T, Vullers R, Van Hoof C. Hybrid thermoelectric-photovoltaic generators in wireless electroencephalography diadem and electrocardiography shirt. J Electron Mater 2010;39:1674–80.

[59] Siddique MR, Wang W, Madeo F, Hayes M, O'Flynn B, Walsh M, et al. Body heat thermoelectric energy harvesting for self-powered wearable electronics. ICST 2014. http://dx.doi.org/10.4108/icst.bodynets.2014.257119.

[60] Torfs T, Leonov V, Yazicioglu RF, Merken P, Hoof CV, Vullers RJM, et al. Wearable autonomous wireless electro-encephalography system fully powered by human body heat. Sensors. IEEE; 2008. p. 1269–72. http://dx. doi.org/10.1109/ICSENS.2008.4716675.

[61] Leonov V, Fiorini P, Torfs T, Vullers RJM, Hoof CV. Thermal matching of a thermoelectric energy harvester with the environment and its application in wearable self-powered wireless medical sensors. In: Thermal investigations of ICs and systems, 2009. THERMINIC 2009. 15th International Workshop on. p. 95–100.

[62] Kraemer D, Poudel B, Feng H-P, Caylor JC, Yu B, Yan X, et al. High-performance flat-panel solar thermoelectric generators with high thermal concentration. Nat Mater 2011;10:532–8. http://dx.doi.org/10.1038/nmat3013.

[63] Kraemer D, McEnaney K, Chiesa M, Chen G. Modeling and optimization of solar thermoelectric generators for terrestrial applications. Sol Energy 2012;86:1338–50. http://dx.doi.org/10.1016/j.solener.2012.01.025.

[64] Chen W-H, Wang C-C, Hung C-I, Yang C-C, Juang R-C. Modeling and simulation for the design of thermal-concentrated solar thermoelectric generator. Energy 2014;64:287–97. http://dx.doi.org/10.1016/j.energy. 2013.10.073.

[65] Attivissimo F, Di Nisio A, Lanzolla AML, Paul M. Feasibility of a photovoltaic thermoelectric generator: performance analysis and simulation results. Instrum Measur, IEEE Transact 2015;64:1158–69. http://dx.doi.org/ 10.1109/TIM.2015.2410353.

[66] Makki A, Omer S, Su Y, Sabir H. Numerical investigation of heat pipe-based photovoltaic–thermoelectric generator (HP-PV/TEG) hybrid system. Energy Convers Manage 2016;112:274–87. http://dx.doi.org/10.1016/j. enconman.2015.12.069.

[67] Daniel Champier, Thermoelectric generators: A review of applications, Energy Conversion and Management 140 (2017) 167–181.

[68] Riffat, S.D. and Ma, X. (2003) Thermoelectrics: a review of present and potential applications. Appl. Therm. Eng., 23 (8), 913–935.

[69] Minnich, A.J., Dresselhaus, M.S., Ren, Z.F., and Chen, G. (2009) Bulk nanostructured thermoelectric materials: current research and future prospects. Energy Environ. Sci., 2 (5), 466–479.
[70] Sootsman, J.R., Chung, D.Y., and Kanatzidis, M.G. (2009) New and old concepts in thermoelectric materials. Angew. Chem. Int. Ed., 48 (46), 8616–8639.
[71] Birkholz, U. (1984) Thermoelektrische Bauelemente, in Amorphe und polykristalline Halbleiter, Halbleiterelektronik, vol. 18 (ed. W. Heywang), Springer-Verlag.
[72] Jansch, D. (ed.) (2011) Thermoelectrics Goes Automotive: Thermoelektrik, II, Expert Verlag - IAV.
[73] Tritt, T.M. (ed.) (2000) Recent Trends in Thermoelectric Materials Research I, Semiconductors and Semimetals, vol. 69, Academic Press, San Diego, CA,.
[74] Tritt, T.M. (ed.) (2001) Recent Trends in Thermoelectric Materials Research III, Semiconductors and Semimetals, vol. 71, Academic Press, San Diego, CA.
[75] Shakouri, A. and Zebarjadi, M. (2009) Nanoengineered materials for thermoelectric energy conversion, in Thermal Nanosystems and Nanomaterials, Topics in Applied Physics, vol. 118 (ed. S. Volz), Springer-Verlag, Berlin / Heidelberg, pp. 225–299.
[76] Vineis, C.J., Shakouri, A., Majumdar, A., and Kanatzidis, M.G. (2010) Nanostructured thermoelectrics: Big efficiency gains from small features. Adv. Mater., 22 (36), 3970–3980.
[77] Zebarjadi, M., Esfarjani, K., Dresselhaus, M.S., Ren, Z.F., and Chen, G. (2012) Perspectives on thermoelectrics: from fundamentals to device applications. Energy Environ. Sci., 5 (1), 5147–5162.
[78] Dario Narducci, Peter Bermel, Bruno Lorenzi, Ning Wang, Kazuaki Yazawa, Hybrid and Fully Thermoelectric Solar Harvesting Springer Series in Materials Science Volume 268, 2018.
[79] Lauryn L. Baranowski, G. Jeffrey Snyder and Eric S. Toberer, Concentrated solar thermoelectric generators, Energy Environ. Sci., 2012, 5, 9055.
[80] Advantages and disadvantages of solar energy Archived 26 December 2013 at the Wayback Machine.. Retrieved on 25 December 2013.
[81] Study Sees Solar Cost-Competitive In Europe By 2015. Solar Cells Info (16 October 2007). Retrieved on 3 June 2012.
[82] Bushong, Steven. "Advantages and disadvantages of a solar tracker system". Solar Power World. Retrieved 20 August 2016.
[83]"Cloud Cover and Solar Radiation" (PDF). Scool.larc.nasa.gov. Retrieved 30 December2017.
[84] http://www.alternative-energy-tutorials.com/energy-articles/solar-cell-i-v-characteristic.html.

[85] Eduardo Lorenzo (1994). Solar Electricity: Engineering of Photovoltaic Systems. Progensa. ISBN 84-86505-55-0.
[86] Antonio Luque & Steven Hegedus (2003). Handbook of Photovoltaic Science and Engineering. John Wiley and Sons. ISBN 0-471-49196-9.
[87] Jenny Nelson (2003). The Physics of Solar Cells. Imperial College Press. ISBN 978-1-86094-340-9.
[88] Building Integrated Photovoltaics, Wisconsin Public Service Corporation, accessed: 23 March 2007. Archived 2 February 2007 at the Wayback Machine.
[89] "Solar panels keep buildings cool". University of California, San Diego. Retrieved 19 May2015.
[90] "Global Market Outlook for Photovoltaics 2014–2018" (PDF). EPIA – European Photovoltaic Industry Association. p. 45. Archived from the original (PDF) on 12 June 2014. Retrieved 19 May 2015.
[91] Mojiri, A.; Taylor, R.; Thomsen, E.; Rosengarten, G. (2013). "Spectral beam splitting for efficient conversion of solar energy—A review". Renewable and Sustainable Energy Reviews. 28: 654–663. doi:10.1016/j.rser.2013.08.026.
[92] Pathak, M. J. M.; Sanders, P. G.; Pearce, J. M. (2014). "Optimizing limited solar roof access by exergy analysis of solar thermal, photovoltaic, and hybrid photovoltaic thermal systems". Applied Energy. 120: 115–124. CiteSeerX 10.1.1.1028.406. doi:10.1016/j.apenergy.2014.01.041.
[93] Off grid solutions for remote poor. ebono.org. (26 February 2008).
[94] How 3D Printers Are Boosting Off-The-Grid, Underdeveloped Communities – MotherBoard, Nov. 2014
[95] King, Debbie L.; Babasola, Adegboyega; Rozario, Joseph; Pearce, Joshua M. (2014). "Mobile Open-Source Solar-Powered 3-D Printers for Distributed Manufacturing in Off-Grid Communities". Challenges in Sustainability. 2. doi:10.12924/cis2014.02010018.
[96] Erickson, Jon D.; Chapman, Duane (1995). "Photovoltaic Technology: Markets, Economics, and Development". World Development. 23 (7): 1129–1141. doi:10.1016/0305-750x(95)00033-9.
[97] "Solar water pumping". builditsolar.com. Retrieved 16 June 2010.
[98] Philadelphia's Solar-Powered Trash Compactors. MSNBC (24 July 2009). Retrieved on 3 June 2012.
[99] Solar-Powered Parking Meters Installed. 10news.com (18 February 2009). Retrieved on 3 June 2012.
[100] "Solar-powered parking meters make downtown debut". Impactnews.com. 22 July 2009. Retrieved 19 September 2011.

[101] AT&T installing solar-powered charging stations around New York Retrieved 28 June 2013.
[102] Chevrolet Dealers Install Green Zone Stations Retrieved 28 June 2013.
[103] Miller, Ross (13 January 2009) Next-gen Prius now official, uses solar panels to keep car cool. engadget.com.
[104] "World's largest solar-powered boat completes its trip around the world". Gizmag.com. Retrieved 30 December 2017.
[105] Khan, B. H. (2006) Non-Conventional Energy Resources, TMH Publications
[106] NASA JPL Publication: Basics of Space Flight Archived 8 December 2006 at the Wayback Machine., Chapter 11. Typical Onboard Systems, Propulsion Subsystems.
[107]https://www.gaas.fullsuns.com/cuxiao/gaas.html?55url&gclid=CjwKCAiA9K3gBRA4EiwACEhFe6kwAKzryY2RWcuA4OWNVjcox9EUuWf19hqJoSQK4kkQynuacpzchoCPrAQAvD_BwE.
[108] M. Green, The Physics of Solar Cells: Third Generation Photovoltaics (Imperial College Press, New York, 2003)
[109] https://www.sif.it/static/SIF/resources/public/files/va2014/Centro.pdf, [accessed: December 2018].
[110]https://www.ise.fraunhofer.de/content/dam/ise/de/documents/publications/studies/cpv-report-ise-nrel.pdf, [accessed: December 2018].
[111] Fraunhofer ISE, Levelized Cost of Electricity - Renewable Energy Technologies, www.ise.fraunhofer.de/de/veroeffentlichungen/veroeffentlichungen-pdf-dateien/studien-und-onzeptpapiere/studie-stromgestehungskosten-erneuerbare-energien.pdf (2013).
[112] James W. Stevens, Performance factors for ground-air thermoelectric power generators, Energy Conversion and Management 2013;68:114–123.
[113] Rezania A, Rosendahl LA. A comparison of micro-structured flat-plate and cross-cut heat sinks for thermoelectric generation application. Energy Convers. Manag 2015;101:730-7.
[114] Miranda AG, Chen TS, Hong CW. Feasibility study of a green energy powered thermoelectric chip based air conditioner for electric vehicles. Energy 2013;59:633-41.
[115] Wang Y, Dai C, Wang S. Theoretical analysis of a thermoelectric generator using exhaust gas of vehicles as heat source. Appl Energy 2013;112:1171-80.
[116] Ding LC, Akbarzadeh A, Date A. Performance and reliability of commercially available thermoelectric cells for power generation. Appl. Therm. Eng 2016;102:548-56.
[117] Chen WH, Liao CY, Hung CI, Huang WL. Experimental study on thermoelectric modules for power generation at various operating conditions. Energy 2012;45:874-81.
[118] Yu S, Du Q, Diao H, Shu G, Jiao K. Effect of vehicle driving conditions on the performance of thermoelectric generator. Energy Convers. Manag 2015;96:363-76.

[119] Hsiao YY, Chang WC, Chen SL. A mathematic model of thermoelectric module with applications on waste heat recovery from automobile engine. Energy 2010;35:1447-54.
[120] Hsu CT, Huang GY, Chu HS, Yu B, Yao DJ. Experiments and simulations on low-temperature waste heat harvesting system by thermoelectric power generators. Appl Energy 2011;88:1291-7.
[121] Aranguren P, Astrain D, Pérez MG. Computational and experimental study of a complete heat dissipation system using water as heat carrier placed on a thermoelectric generator. Energy 2014;74:346–58. http://dx.doi.org/ 10.1016/j.energy.2014.06.094.
[122] Jia X-D, Wang Y-J, Gao Y-W. Numerical simulation of thermoelectric performance of linear-shaped thermoelectric generators under transient heat supply. Energy 2017;130:276–85.
[123] Blandino JR, Lawrence DJ. Transient response of a thermoelectric generator subjected to spatially non-uniform heating: Implications for heat and IR sensing applications. Measurement 2016;80:125–37.
[124] Alatam M, Al-Nimr MA, Naji M. Transient Behavior of a Thermoelectric Device under the Hyperbolic Heat Conduction Model. International Journal of Thermophysics. 2003;24(6):1753–68.
[125] Naji M, Alata M, Al-Nimr MA. Transient Behavior of a Thermoelectric Device. Proceedings Of The Institution Of Mechanical Engineers Part A-Journal of power and energy 2003;217(A6):615–22.
[126] Nguyen NQ, Pochiraju KV. Behavior of thermoelectric generators exposed to transient heat sources. Applied Thermal Engineering 2013;51:1–9.
[127] Fisac M, Villasevil FX, Lopez AM. Design of a thermoelectric generator with fast transient response. Renewable Energy 2015;81:658–63.
[128] Savani I, Waage HM, Borset M, Kjelstrup S, Wilhelmsen O. Harnessing thermoelectric power from transient heat sources: Waste heat recovery from silicon production. Energy Conversion and Management 2017;138:171–82.
[129] Crane DT. An Introduction to System-Level, Steady-State and Transient Modeling and Optimization of High-Power-Density Thermoelectric Generator Devices Made of Segmented Thermoelectric Elements. Journal of Electronic Materials 2011;40(5):561–569.
[130] Crane DT, Koripella CR, Jovovic V. Validating Steady-State and Transient Modeling Tools for High-Power-Density Thermoelectric Generators, Journal of Electronic Materials 2012;41(6):1524–1534.
[131] M. Telkes, Solar thermoelectric generators, J. Appl. Phys. 25 (1954) 765.
[132] Dent. C, Cobble. M, 1982. A solar thermoelectric generator experiments and analysis. In: Proceedings of 4th International Conference on Thermoelectric Energy Conversion, pp. 75–78.

[133] Rockendorf. G., Sillmann. R, Podlowski. L, Litzenburger. B, 1999. PV hybrid and thermoelectric collectors. Solar Energy 67, 227–237.
[134] Vatcharasathien. N, Hirunlabh. J, Khedari. J, Daquenet. M, 2005. Design and analysis of solar thermoelectric power generation system. International Journal of Sustainable Energy 24, 115–127.
[135] Li. P, Cai. L, Zhai. P, Tang. X, Zhang. Q, Niino. M, 2010. Design of a concentration solar thermoelectric generator. Journal of Electronic Materials 39, 1522–1530. doi:10.1007/s11664-010-1279-0.
[136] Gang Chen, Theoretical efficiency of solar thermoelectric energy generators, JOURNAL OF APPLIED PHYSICS 109, 104908 (2011).
[137] Daniel Kraemer, Bed Poudel, Hsien-Ping Feng, J. Christopher Caylor, Bo Yu, Xiao Yan, Yi Ma, Xiaowei Wang, Dezhi Wang, Andrew Muto, Kenneth McEnaney, Matteo Chiesa, Zhifeng Ren and Gang Chen, High-performance flat-panel solar thermoelectric generators with high thermal concentration, Nat. Mater. 10 (2011) 532–53.
[138] Daniel Kraemer, Kenneth McEnaney, Matteo Chiesa, Gang Chen, Modeling and optimization of solar thermoelectric generators for terrestrial applications, Sol. Energy. 86 (2012) 1338–1350.
[139] Daniel Kraemer, Qing Jie, Kenneth McEnaney, Feng Cao,Weishu Liu, Lee A.Weinstein, James Loomis, Zhifeng Ren and Gang Chen, Concentrating solar thermoelectric generators with a peak efficiency of 7.4%, Nat. Energy. (2016) DOI: 10.1038/NENERGY.2016.153.
[140] H. A. MADKHALI, A. HAMIL and H. LEE, Validation, Optimization and Simulation of a Solar Thermoelectric Generator Model, J. Electron. Mater. (2017) DOI: 10.1007/s11664-017-5723-2.
[141] Kenneth McEnaney, Daniel Kraemer, Zhifeng Ren, and Gang Chen, Modeling of concentrating solar thermoelectric generators, JOURNAL OF APPLIED PHYSICS 110, 074502 (2011).
[142] Lei Liu, Xue Sen Lu, Mao Lei Shi, Ya Kun Ma, Jian Ying Shi, Modeling of flat-plate solar thermoelectric generators for space applications, Solar Energy 132 (2016) 386–394.
[143] Aaditya A. Candadai, V. Praveen Kumar,Harish C. Barshilia, Performance evaluation of a natural convective-cooled concentration solar thermoelectric generator coupled with a spectrally selective high temperature absorber coating, Sol. Energy Mater. Sol. Cells. 145 (2016) 333-341.
[144] NAVEED UR REHMAN and MUBASHIR ALI SIDDIQUI, Critical Concentration Ratio for Solar Thermoelectric Generators, Journal of ELECTRONIC MATERIALS, Vol. 45, No. 10, 2016.

[145] Dongfang Sun, Limei Shen, Yu Yao, Huanxin Chen, Shiping Jin, Hong He, The real-time study of solar thermoelectric generator, Applied Thermal Engineering 119 (2017) 347-359.

[146] Wei-Hsin Chen, Chien-Chang Wang, Chen-I Hung, Chang-Chung Yang, Rei-Cheng Juang, Modeling and simulation for the design of thermal-concentrated solar thermoelectric generator, Energy 64 (2014) 287-297.

[147] D. N. Kossyvakis, C. G. Vossou, C. G. Provatidis, E.V. Hristoforou, Computational analysis and performance optimization of a solar thermoelectric generator, Renewable Energy 81 (2015) 150-161.

[148] A. Weidenkaff, R. Robert, M. H. Aguirre, L. Bocher, T. Lippert, and S. Canulescu, Development of Thermoelectric Oxides for Renewable Energy Conversion Technologies, Renewable Energy. 2008;33:342-347.

[149] A. Pereira, T. Caroff, G. Lorin, T. Baffie, K. Romanjek, S. Vesin, K. Kusiaku, H. Duchemin, V. Salvador, N. Miloud-Ali, L. Aixala, J. Simon, High temperature solar thermoelectric generator- Indoor characterization method and modeling, Energy. 2015;84: 485–492.

[150] LAURYN L. BARANOWSKI, EMILY L. WARREN and ERIC S. TOBERER, High-Temperature High-Efficiency Solar Thermoelectric Generators, Journal of ELECTRONIC MATERIALS, Vol. 43, No. 6, 2014.

[151] P. Tomeš, M. Trottmann, C. Suter, M. H. Aguirre, A. Steinfeld, P. Haueter and A. Weidenkaff, Thermoelectric Oxide Modules (TOMs) for the Direct Conversion of Simulated Solar Radiation into Electrical Energy, Materials. 2010;3: 2801-2814.

[152] P. Tomeš, R. Robert, L. Bocher, M. Trottmann, M. H. Aguirre, A. Weidenkaff, P. Haueter, A. Steinfeld, and J. Hejtmánek, Direct conversion of simulated solar radiation into electrical energy by a perovskite thermoelectric oxide module (TOM), Proc. Materials Science and Technology Conference and Exhibition, MS&T08. 1 (2008) 429-435.

[153] Lauri Kutt, John Millar, Matti Lehtonen, Maido Marss, Optimization of concentrated solar thermoelectric generator system for highest yearly electric output, 56th international scientific conference on power and electrical engineering of Riga Technical University, 2015.

[154] D. M. Rowe, A High Performance Solar Powered Thermoelectric Generator, Appl. Energy. 8 (1981) 269-273.

[155] P. LI, L. CAI, P. ZHAI, X. TANG, Q. ZHANG, and M. NIINO, Design of a Concentration Solar Thermoelectric Generator, J. Electron. Mater. Vol. 39 No. 9, (2010) DOI: 10.1007/s11664-010-1279-0.

[156] T. YANG, J. XIAO, P. LI, P. ZHAI, and Q. ZHANG, Simulation and Optimization for System Integration of a Solar Thermoelectric Device, J. Electron. Mater. Vol. 40, No. 5 (2011) DOI: 10.1007/s11664-010-1471-2.

[157] A. Rezania, D. Sera, L.A. Rosendahl, Coupled thermal model of photovoltaic-thermoelectric hybrid panel for sample cities in Europe, Renewable Energy 99 (2016) 127-135.

[158] Dallan BS, Schumann J, Frédéric JL. Performance evaluation of a photoelectric–thermoelectric cogeneration hybrid system. Sol. Energy 2015;118:276–85.

[159] D. T. Cotfas, P. A. Cotfas, O. M. Machidon, D. Ciobanu, Investigation of the photovoltaic cell/ thermoelectric element hybrid system performance, Materials Science and Engineering 2016; 133: 012037.

[160] Trevor Hocksun Kwan, Xiaofeng Wu, Power and mass optimization of the hybrid solar panel and thermoelectric generators, Applied Energy 2016; 165: 297–307.

[161] Kraemer D, Hu L, Muto A, Chen X, Chen G, Chiesa M. Photovoltaic-thermoelectric hybrid systems: A general optimization methodology. Appl. Phys. Lett 2008;92:243503–1.

[162] W.G.J.H.M. van Sark, Feasibility of Photovoltaic – Thermoelectric hybrid modules, Applied Energy 2011; 88: 2785–2790.

[163] Kossyvakis DN, Voutsinas GD, Hristoforou EV. Experimental analysis and performance evaluation of a tandem photovoltaic–thermoelectric hybrid system. Energy Convers Manage 2016; 117: 490–500.

[164] Urbiola EAC, Vorobiev YV, Bulat LP. Solar hybrid systems with thermoelectric generators. Sol. Energy 2012; 86: 369–78.

[165] Pradeepkumar Sundarraj, Dipak Maity, Susanta Sinha Roy and Robert A. Taylor, Recent advances in thermoelectric materials and solar thermoelectric generators – a critical review, RSC Adv., 2014, 4, 46860–46874.

[166] Ershuai Yin, Qiang Li, Yimin Xuan, Thermal resistance analysis and optimization of photovoltaic- thermoelectric hybrid system, Energy Conversion and Management 143 (2017) 188–202.

[167] Tae-Hyeon Kil, Sanghyeon Kim, Dae-Han Jeong, Dae-Myeong Geum, Sooseok Lee, Sung-Jin Jung, Sangtae Kim, Chan Park, Jin-Sang Kim, Jeong Min Baik, Ki-Suk Lee, Chang Zoo Kim, Won Jun Choi, Seung-Hyub Baek, A highly-efficient, concentrating-photovoltaic/thermoelectric hybrid generator, Nano Energy 37 (2017) 242–247.

[168] Jin Zhang, Yimin Xuan, Investigation on the effect of thermal resistances on a highly concentrated photovoltaic-thermoelectric hybrid system, Energy Conversion and Management 129 (2016) 1–10.

[169] Ravita Lamba, S.C. Kaushik, Modeling and performance analysis of a concentrated photovoltaic– thermoelectric hybrid power generation system, Energy Conversion and Management 115 (2016) 288–298.
[170] Xinqiang Xu, Siyi Zhou, Mark M. Meyers, Bahgat G. Sammakia, Bruce T. Murray, Performance Analysis of a Combination System of Concentrating Photovoltaic/ Thermal Collector and Thermoelectric Generators, Journal of Electronic Packaging, 136 (2014) 0410041-7.
[171] R. Kiflemariam, M. Almas, and C. Lin, Modeling Integrated Thermoelectric Generator-Photovoltaic Thermal (TEG-PVT) System, Excerpt from the Proceedings of the 2014 COMSOL Conference in Boston.
[172] Wu YY, Wu SY, Xiao L. Performance analysis of photovoltaic–thermoelectric hybrid system with and without glass cover. Energy Convers. Manage 2015; 93: 151–9.
[173] Jin Zhang, Yimin Xuan, Lili Yang. Performance estimation of photovoltaic-thermoelectric hybrid systems. Energy 2014; 78: 895-903.
[174] Tianjun Liao, Bihong Lin, Zhimin Yang, Performance characteristics of a low concentrated Photovoltaic-thermoelectric hybrid power generation device, International Journal of Thermal Sciences 77 (2014) 158–164.
[175] Zhang J, Xuan Y, Yang L. Performance estimation of photovoltaic-thermoelectric hybrid Systems. Energy 2014;78:895-903.
[176] Dianhong Li, Yimin Xuan, Qiang Li, Hui Hong. Exergy and energy analysis of photovoltaic-thermoelectric hybrid Systems. Energy 2017; 126: 343-51.
[177] Ju X, Wang Z, Flamant G, Li P, Zhao W. Numerical analysis and optimization of a spectrum splitting concentration photovoltaic-thermoelectric hybrid system. Sol. Energy 2012; 86:1941–54.
[178] Tracy K.N. Sweet, Matthew H. Rolley, Martin J. Prest and Gao Min, Novel Hybrid III: V Concentrator Photovoltaic- Thermoelectric Receiver Designs, AIP Conference Proceedings 1881, 080009 (2017).
[179] T. K. N. Sweet, M. H. Rolley, W. Li, M. C. Paul, M. Gao and A. R. Knox, Experimental characterization and multi-physics simulation of a triple-junction cell in a novel hybrid III: V concentrator photovoltaic- thermoelectric receiver design with secondary optical element, Energy Procedia 142 (2017) 809–814.
[180] Daniel T. Cotfas, Petru A. Cotfas, Laura Floroian, Dan I. Floroian, Study of combined photovoltaic cell/thermoelectric element/solar collector in medium concentrated light, Optimization of Electrical and Electronic Equipment (OPTIM) & 2017 Intl Aegean Conference on Electrical Machines and Power Electronics (ACEMP), 2017 International Conference on Date of Conference: 25-27 May 2017 Brasov, Romania, 978-1-5090-4489-4/17/$31.00 ©2017 IEEE.

[181] Ryo Tamaki, Takeshi Toyoda, Yoichi Tamura, Akinari Matoba, Toshiharu Minamikawa, Masayuki Tokuda, Megumi Masui, and Yoshitaka Okada, Hybrid photovoltaic and thermoelectric module for high concentration solar system, AIP Conference Proceedings 1881, 100002 (2017); doi: 10.1063/1.5001453.
[182] Ofer Beeri, Oded Rotem, Eden Hazan, Eugene A. Katz, Avi Braun, and Yaniv Gelbstein, Hybrid photovoltaic-thermoelectric system for concentrated solar energy conversion: Experimental realization and modeling, Journal of Applied Physics 118, 115104 (2015); doi: 10.1063/1.4931428.
[183] A. Rezania, L.A. Rosendahl, Feasibility and parametric evaluation of hybrid concentrated photovoltaic-thermoelectric system, Applied Energy 187 (2017) 380–389.
[184] S. Mahmoudinezhad, A. Rezania, A. A. Ranjbar, L. A. Rosendahl. Transient Behavior of the Thermoelectric Generators to the Load Change; An Experimental investigation, Energy Procedia 147 (2018) 537–543.
[185] Sajjad Mahmoudinezhad, Alireza Rezaniakolaei, Lasse Aistrup Rosendahl. Experimental Study on Effect of Operating Conditions on Thermoelectric Power Generation. Energy Procedia 142 (2017) 558–563.
[186] Kline SJ. The purpose of uncertainty analysis. ASME J Heat Transfer 1985;117:153-60.
[187] Coleman HW, Steele Jr WG. Experimentation and uncertainty analysis for engineers. New York:Wiley; 1989.
[188] Zhang G, Jiao K, Niu Z, Diao H, Du Q, Tian H, et al. Power and efficiency factors for comprehensive evaluation of thermoelectric generator materials. Int. J. Heat Mass Transfer 2016;93:1034-7.
[189] Zhang G, Fan L, Niu Z, Jiao K, Diao H, Du Q, et al. A comprehensive design method for segmented thermoelectric generator. Energy Convers. Manage 2015;106:510-9.
[190] J. Petrasch, P. Coray, A. Meier et al, A novel 50 kW 11,000 suns high-flux solar simulator based on an array of xenon arc lamps, ASME Journal of Solar Energy Engineering. vol. 129, no. 4 (2007) pp. 405–411.
[191] I. Alxneit and H. Schmit, Spectral characterization of PSI's high-flux solar simulator, J. Sol. Energy Eng. vol. 134, no. 1 (2012) Article ID 011013.
[192] Daniel Tudor Cotfas, Petru Adrian Cotfas, Dan Ion Floroian, and Laura Floroian, Accelerated Life Test for Photovoltaic Cells Using Concentrated Light, International Journal of Photoenergy Volume 2016, Article ID 9825683.
[193] Thermal Electronics Corp. Part# CMO-25-42S, http://espressomilkcooler.com/wp-content/uploads/2014/06/CMO-25-42S-OXIDE-NEW.pdf, [accessed: July 2018].
[194] Panasonic "PGS" Graphite Sheets, http://docs-europe.electrocomponents.com/webdocs/0e70/0900766b80e702d3.pdf, [accessed: July 2018].

[195] S. Mahmoudinezhad , P. A. Cotfas, D. T. Cotfas, A. Rezania, L. A. Rosendahl, Performance evaluation of a high-temperature thermoelectric generator under different solar concentrations, Energy Procedia 147 (2018) 624–630.
[196] S. Mahmoudinezhad, A. Rezania, P.A. Cotfas, D.T. Cotfas, L.A. Rosendahl, Transient Behavior of Concentrated Solar Oxide Thermoelectric Generator, Energy, Vol. 168, 2018, p. 823-832..
[197] Supasit Paengson, Panida Pilasuta, Kunchit Singsoog, Wanatchaporn Namhongsa, Wairut Impho, Tosawat Seetawan, Improvement in thermoelectric properties of CaMnO3 by Bi doping and hot pressing, Materials Today: Proceedings 4 (2017) 6289–6295.
[198] Richard Tuley and Kevin Simpson, ZT Optimization: An Application Focus, Materials 2017, 10, 309; doi:10.3390/ma10030309.
[199] Patankar SV. Numerical heat transfer and fluid flow. USA: Taylor & Francis; 1980.
[200] M. Backhaus- Ricoult, J. Rustad, L. Moore, C. Smith, J. Brown, Semiconducting large bandgap oxides as potential thermoelectric materials for high-temperature power generation, Appl. Phys. A (2014) 116:433–470.
[201] Hongchao Wang, Wenbin Su, Jian Liu, Chunlei Wang, Recent development of n-type perovskite thermoelectrics, J Materiomics 2 (2016) 225-236.
[202] Nowak H. The sky temperature in net radiant heat loss calculations from low-sloped roofs. Infrared Phys 29 (1989) 231–2.
[203] http://tecteg.com/wp-ontent/uploads/2014/09/Spec-TEG2-07025HT-SS-rev1-1.pdf.
[204] S. Mahmoudinezhad, P.A. Cotfas, A. Rezania, D.T. Cotfas, L.A. Rosendahl. Transient Response of Bi-Te Based Thermoelectric Generator to Variant Solar radiation; An Experimental and Numerical study, paper is submitted to the Renewable Energy journal.
[205]http://thermoelectric-generator.com/wp-content/uploads/2014/07/Ingot-Raw-Material-BiTe-N-and-P.pdf, [Cited: December 2018].
[206] Sajjad Mahmoudinezhad, Shaowei Qing, Alireza Rezaniakolaei, Lasse Aistrup Rosendahl, Transient Model of Hybrid Concentrated Photovoltaic with Thermoelectric Generator, Energy Procedia 2017; 142: 564-569.
[207] S. Mahmoudinezhad, A. Rezania, L.A. Rosendahl, Behavior of hybrid concentrated photovoltaic-thermoelectric generator under variable solar radiation, Energy Conversion and Management 2018; 164: 443-452.
[208] AZUR SPACE Solar Power GmbH. Concentrator triple junction solar cell, Cell Type: 3C42-10 _ 10mm2. Data Sheet (HNR 0003877–00-00). [Cited: October 2018].
[209] Micheli L, Sarmah N, Reddy KS, Luo X, Mallick TK. Design, development, and analysis of a densely packed 500x concentrating photovoltaic cell assembly on insulated metal substrate. Int J Photoenergy 2015; 2015:341032.

[210] Cotal H, Frost J. Heat transfer modeling of concentrator multijunction solar cell assemblies using finite difference techniques. Photovoltaic Specialists Conference (PVSC), 35th IEEE 2010:213–8.
[211] Xiaolong Gou, Huifeng Ping, Qiang Ou, Heng Xiao, Shaowei Qing. A novel thermoelectric generation system with thermal switch. Applied Energy 2015; 160: 843–52.
[212] Meng F, Chen L, Sun F. A numerical model and comparative investigation of a thermoelectric generator with multi-irreversibilities. Energy 2011; 36(5):3513–22.
[213] Chen Min, Rosendahl Lasse, Bach Inger, Condra Thomas, Pedersen John. Irreversible transfer processes of thermoelectric generators. Am J Phys 2007; 75(9):815–20.
[214] Evans DL. Simplified method for predicting photovoltaic array output. Sol Energy 1981; 27: 555–60.
[215] Notton G, Cristofari C, Mattei M, Poggi P. Modelling of a double-glass photovoltaic module using finite differences. Appl Therm Eng 2005; 25: 2854–77.
[216] Mi Z, Chen J, Chen N, Bai Y, Wu W, Fu R, Liu H. Performance Analysis of a Grid-connected High Concentrating Photovoltaic System under Practical Operation Conditions. Energies 2016; 9, 117; doi:10.3390/en9020117.
[217] Çengel. Introduction to Thermodynamics and Heat Transfer, McGraw−Hill Primis, 2008; ISBN: 0−390−86122−7.
[218] S. Mahmoudinezhad, S. Ahmadi Atouei, P.A. Cotfas, D.T. Cotfas, L.A. Rosendahl, A. Rezania. Transient Experimental and Numerical Study on the Transient Behavior of Multi-Junction Solar Cell-Thermoelectric Generator Hybrid System. Paper is submitted to the journal of Energy Conversion and management.
[219] https://solaerotech.com/wp-content/uploads/2018/03/CTJ-Datasheet.pdf [Cited: October 2018].
[220] http://thermoelectric-generator.com/wp-content/uploads/2014/07/Ingot-Raw-Material-BiTe-N-and-P.pdf [Cited: December 2018].
[221] Pilar Espinet-González, Carlos Algora, Neftalí Núñez, Vincenzo Orlando, Manuel Vázquez, Jesús Bautista, and Kenji Araki, Evaluation of the reliability of commercial concentrator triple-junction solar cells by means of accelerated life tests (ALT), AIP Conference Proceedings 1556, 222 (2013); doi: 10.1063/1.4822236.
[222] Xiao-Dong Wang, Yu-Xian Huang, Chin-Hsiang Cheng, David Ta-Wei Lin, Chung-Hao Kang, A three-dimensional numerical modeling of thermoelectric device with consideration of coupling of temperature field and electric potential field, Energy 47 (2012) 488-497.
[223] Cirocco L, Belusko M, Bruno F, Boland J, Pudney P. Optimisation of storage for concentrated solar power plants. Challenges 2014; 5: 473-503.

[224] Khamooshi M, Salati H, Egelioglu F, Hooshyar Faghiri A, Tarabishi J, Babadi S. A review of solar photovoltaic concentrator. Int J Photoenergy 2014;2014:17.
[225] S. Mahmoudinezhad, A. Rezania, D.T. Cotfas, P.A. Cotfas, L.A. Rosendahl, Experimental and numerical investigation of hybrid concentrated photovoltaic - Thermoelectric module under low solar concentration, Energy 159 (2018) 1123-1131.
[226] Efstratios I. Batzelis and Stavros A. Papathanassiou, A Method for the Analytical Extraction of the Single-Diode PV Model Parameters, IEEE TRANSACTIONS ON SUSTAINABLE ENERGY, VOL. 7, NO. 2, 2016.
[227] Meetarani Tripathy, Manish Kumar, P.K. Sadhu, Photovoltaic system using Lambert W function-based technique, Solar Energy 158 (2017) 432–439.
[228] J. Appelbaum, A.Peled, Parameters extraction of solar cells – A comparative examination of three methods, Solar Energy Materials & Solar Cells 122(2014)164–173.
[229] Hassan Fathabadi, Lambert W function-based technique for tracking the maximum power point of PV modules connected in various configurations, Renewable Energy 74 (2015) 214-226.
[230] Xiao W, Lind MGJ, Dunford WG, Capel A. Real-time identification of optimal operating points in photovoltaic power systems. IEEE TRANSACTIONS ON INDUSTRIAL ELECTRONICS, 2006, VOL. 53, NO. 4.
[231] Assaf Ben Or, Joseph Appelbaum, Dependence of multi-junction solar cells parameters on concentration and temperature, Solar Energy Materials & Solar Cells 130 (2014) 234–240.
[232] Sajjad Mahmoudinezhad, Alireza Rezaniakolaei, Lasse Aistrup Rosendahl, Numerical parametric study on the performance of CPV-TEG hybrid system, 10th International Conference on Applied Energy (ICAE2018), 22-25 August 2018, Hong Kong, China.

APPENDIX: PAPERS

PAPER 1: REFERENCE [185]

Experimental Study on Effect of Operating Conditions on Thermoelectric Power Generation

Sajjad Mahmoudi Nezhad, Alireza Rezania, Lasse Rosendahl

The paper has been published in
Energy Procedia 142 (2017) 558-563.

Available online at www.sciencedirect.com

ScienceDirect

Energy Procedia 142 (2017) 558–563

Energy Procedia

www.elsevier.com/locate/procedia

9th International Conference on Applied Energy, ICAE2017, 21-24 August 2017, Cardiff, UK

Experimental Study on Effect of Operating Conditions on Thermoelectric Power Generation

Sajjad Mahmoudinezhad[a], Alireza Rezaniakolaei[a,]*, Lasse Aistrup Rosendahl[a]

[a]*Department of Energy Technology, Aalborg university, Pontoppidanstræde 101, Aalborg DK-9220, Denmark*

Abstract

Effect of boundary conditions of thermal reservoirs on power generation of thermoelectric modules (TEMs) is examined experimentally. To realize the characteristics of the power generation by the TEMs, the system performance is studied over various volumetric flow rates and flow temperatures of the hot gas and in the heat sink over a wide range of electrical load. The results show a significant influence of forced convection produced by an axial fan in the heat sink in comparison with natural convection. Also, both of the temperature and volumetric flow rate of the hot gas have a substantial effect on power generation by the TEMs. Lower volumetric flow rate in the heat sink is suggested to save fan power because it is found that higher volumetric flow rates on the cold side after the optimal flow rate does not have much effect on the power generation by TEMs. The maximum power produced by tested TEMs is 4.59 W at temperature difference equal to 133.78°C.

Peer-review under responsibility of the scientific committee of the 9th International Conference on Applied Energy.

*Keywords:*Forced and Natural Covection; Thermoelectric Module; Experimental Study; Power Generation.

1. Introduction

Some special features like having no moving parts, having long life time, being highly reliable, silent operation and being environmentally friendly make TEMs a good alternative energy technology to decrease dependency on fossil fuels. As TEMs do not need fuel supply and also their low maintenance requirements they can be a good choice for energy harvesting via the direct recovery of waste heat and conversion into useful electrical energy. Applying TEMs to improve the efficiency of waste heat recovery by using different heat sources such as geothermal

* Corresponding author. Tel.: +4521370284; fax: +4598151411.
E-mail address: alr@et.aau.dk

1876-6102
Peer-review under responsibility of the scientific committee of the 9th International Conference on Applied Energy.
10.1016/j.egypro.2017.12.087

energy, power plants, automobiles and other industrial heat-generating process is an interesting subject in studies [1–4]. Hsiao et al [5] developed a mathematic model of TEM to comprehend the characteristics of thermoelectric generator (TEG), and the effects of engine speed and coolant temperature of radiator on the TEM. Output power and thermal efficiency of TEG at different coolant temperatures were presented. Commercially available Bi_2Te_3 thermoelectric cells were examined by Ding et al [6] in different operating conditions. Performance and reliability of TEGs for power generation were presented. Performance of these TEGs when subjected to thermal cycling and continuous operation at hot side temperature of about 160°C was also investigated. The results showed that commercially available TEG tested is reliable to be used under thermally cycled hot side temperature <90°C and cooled at ambient temperature, for at least 500 cycles as tested. An experimental and numerical study on low-temperature waste heat harvesting with 24 TEGs to convert heat from the exhaust pipe of an automobile to electrical energy was carried out by Hsu et al [7]. Open circuit voltage and output power of the system were presented for variant temperature differences. The performances of TEMs at different operating conditions were investigated by Chen et al [8]. Flow patterns, heating temperatures, flow rates of water and numbers of modules were examined experimentally. They found that heating temperature is the most important parameter in the performance of the TEMs and the effect of the other factors are not significant. Rezania et al [9] studied and optimized a micro plate-fin heat exchanger applied to a TEG to maximize the output power and the cost performance of generic TEG systems. They showed that there is a unique pumping power that delivers the maximum cost performance for the TEG systems. To study the effect of complex vehicle driving conditions on the TEG performance, a numerical model of TEG based on vehicle waste heat recovery was developed by Yu et al [10]. They found that the performance variation of TEGs becomes more remarkable with faster acceleration or deceleration. Meanwhile in deceleration the transient response of the hot and cold side temperatures, voltage and power is less significant in comparison with acceleration.

This experimental study aims to find TEMs electrical response to variation of thermal boundary conditions. The effect of volumetric flow rate and the temperature of the exhaust gas, and the effect of variation of the volumetric flow rate in the cold side of the TEMs are tested. Furthermore, in the cold side a comparison between natural and force convection has been studied.

2. Experimental setup

The schematic diagram of the experiment setup is shown in Fig. 1(a). An axial fan with variable power supply is used for cooling the cold side and a hybrid system including a hot gas supplier and a constant temperature reservoir is applied for heating the hot side of TEMs. T-type thermocouples are used for measuring temperatures of the hot and cold sides and also the ambient temperature. Four thermocouples are located on each side of the finned plates just behind of the modules. All the temperatures are monitored continuously in a PC by a data acquisition system. A programmable DC electronic load device is used for applying load to the TEMs. The test section consists of a thermoelectric generator made of four TEMs connected electrically in series. The commercially available Bi_2Te_3 based thermoelectric modules with a module size 30mm×30mm×4.2mm is used for the experiments. As it is shown in Fig. 1(b), TEMs are inserted between two finned plates as conventional heat sink and heat source with the same areas (100×100 mm). The finned surface consists of 17 fins with thickness 2 mm and height 30 mm. The gap between the fins is 2 mm.

3. Results and discussion

Corresponding to equation 1, for obtaining the absolute value of the internal resistance of the TEG, the slope of the V-I linear lines should be calculated. Fig. 2(a) shows the V-I curves in different temperature differences.

$$V = RI \tag{1}$$

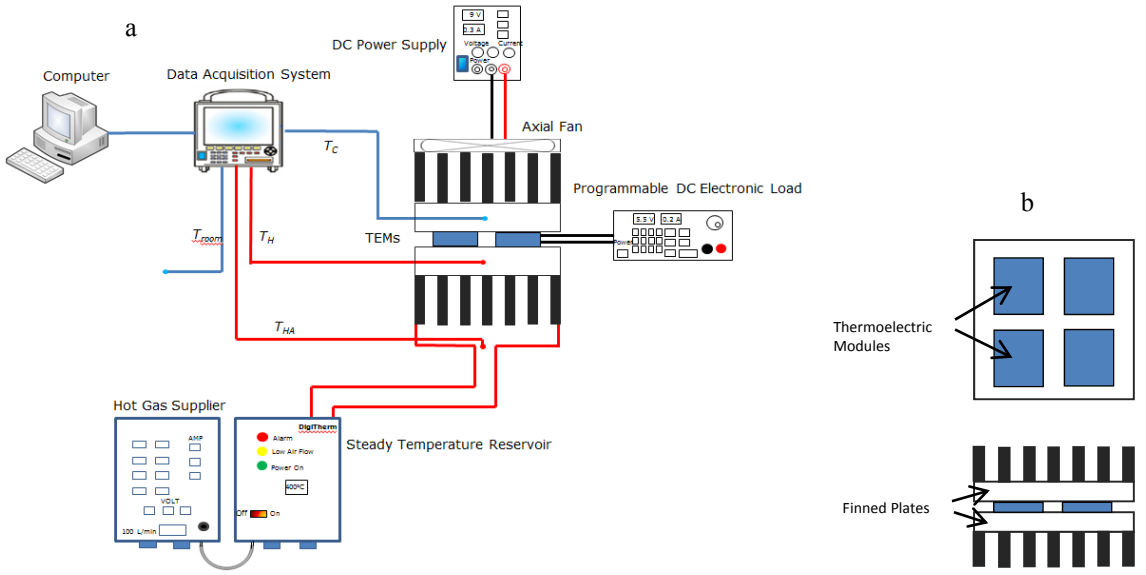

Fig. 1. (a) Schematic diagram of the experiment setup; (b) Schematic diagram of the test section.

It can be seen that the internal resistance for four TEMs is varied between 10.29 Ω to 14.54 Ω. Subsequently the maximum power should occur when the electric load resistance is approximately equal to 12.41 Ω. As it can be seen, the V-I curve slope is slightly increases with increasing the temperature difference. As it is mentioned before, the gradient of the V-I curve is equal to the electrical resistance of the TEG and as the electrical conductance of a material changes with temperature [11-12], thus with increasing the average temperature of the TEG, the electrical resistance of the TEG also should increases.

The variation of output power against current for different ΔT is presented in fig. 2(b). As it can be seen, there is a maximum electrical power output for every value of ΔT. These maximum values are used to create Fig. 3(a). The maximum power produced by the TEG for a given ΔT is:

$$P_{max} = \frac{V_{OC} I_{SC}}{4} = (\alpha \Delta T)^2 / 4R \tag{2}$$

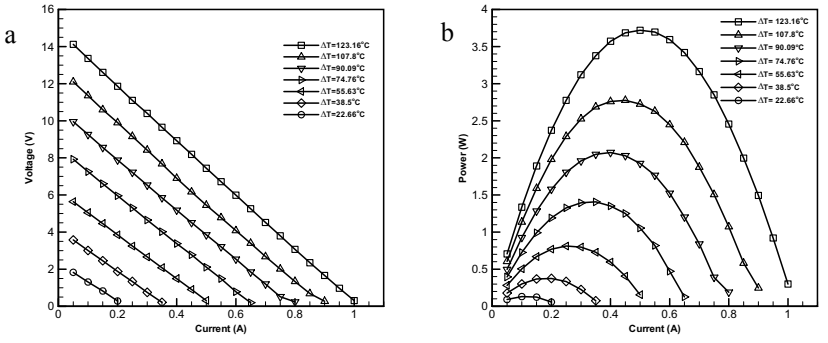

Fig. 2. (a) V-I curves; (b) P-I curves for different temperature differences and with Q_h=90 Lit/min and Q_c=406.3 Lit/min.

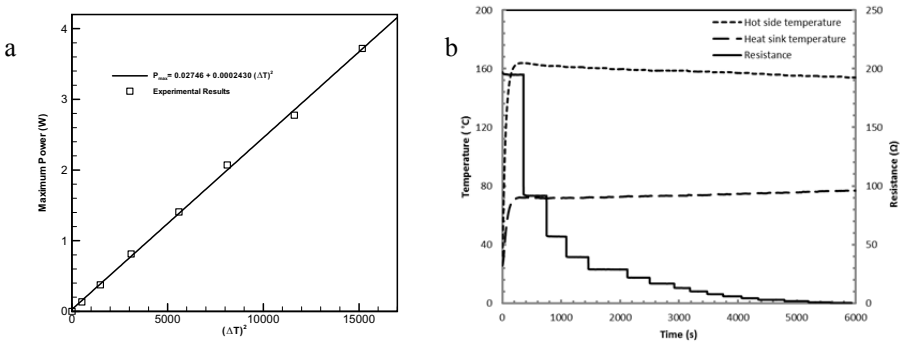

Fig. 3. (a) Maximum power versus ΔT^2; (b) Hot and cold side temperatures and resistance of TEG for Q_h=90 Lit/min and Q_c=406.3 Lit/min.

Where, V_{OC} and I_{SC} are the open circuit voltage and short circuit current. Then based on the equation (2) the power-current relation should have a parabolic form. Fig. 3(a) shows the variation of maximum power of TEMs versus ΔT^2. By using equation 2, the slope of the P_{max}- ΔT^2 curve is equal to $\alpha^2/4R$. As it can be seen in the fig. 3(a) the slope of the line is 0.0002430, then by considering the internal resistance 12.41 Ω, the value of Seebek coefficient will be 0.1098 V/K. As it can be seen in fig. 3(b), with increasing the current, the resistance decreases by the time. Joule heating effect can be seen in the variation of the hot and cold side temperatures. With passing the time, hot side temperature decreases slightly and in the opposite, cold side temperature is increased gradually.

3.1. Effect of the natural and force convection in the cold side

As it can be seen the temperatures of the hot side of TEG and surface of CPV are almost the same and the temperature of the cold side of TEG is also varied in a same manner but by a time delay. This delay is because of the time which heat passes through the CPV and the components of TEG. All of the temperatures are changed by variation of sun radiation which presented in fig. 2(a). Obviously by increasing the sun radiation during the time, all temperatures are increased and vice versa. One another important point in the fig. 2(b) is related to the low sun radiations. As it can be seen, in the small sun radiations, all the temperatures are very close to each other. It is clearly due to low amount of heat transfer through the hybrid system.

Fig. 4(a) and 4(b) show the V-I and P-I curves for different volumetric flow rates of the fan in the cold side, respectively. To observe the substantial effect of the fan and force convection cooling on the power generation by TEMs, figs 4(a) and 4(b) can be compared with figs 5(a) and 5(b). The voltage and power output by the TEMs when natural convection is used for cooling the cold side are illustrated in figs 5(a) and 5(b).

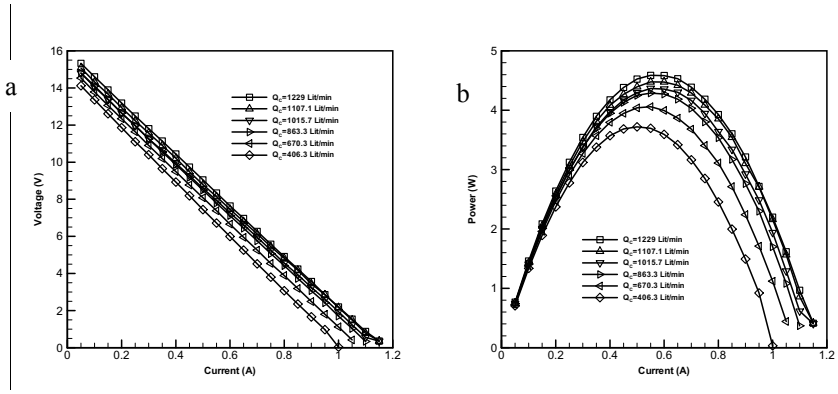

Fig. 4. (a) V-I; (b) P-I curves, both for different volumetric flow rates of the fan in the cold side.

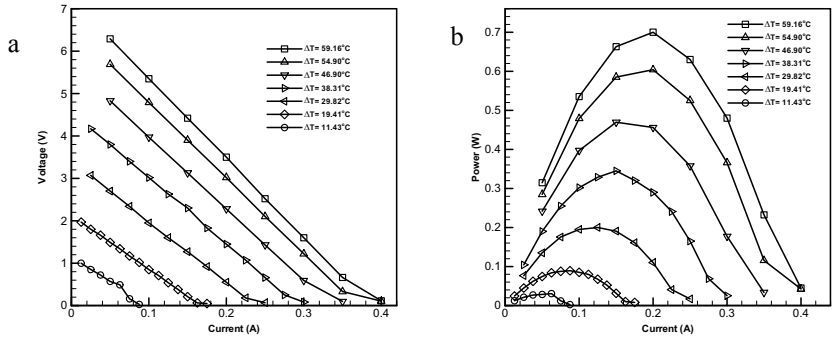

Fig. 5. (a) V-I; (b) P-I curves, both for different temperature differences and Q_h=90 Lit/min (natural convection cooling).

As it can be seen, when there is no fan and thus natural convection heat transfer exists in the cold side, the value of the output voltage and also output power are very small. By running the axial fan, the force convection cooling leads to increasing in the value of the voltage and power significantly. As it can be seen in both figures 4(b) and 5(b) maximum power produced by TEMs increases while temperature difference is increasing. As it is illustrated in figures 4(a) and 4(b) the variation of volumetric flow rate of the fan has not much effect on output voltage and power. So, lower value of the volumetric flow rates is suggested for cooling the cold side. Because, in this way more power could be save.

Table 1 shows the values of the temperatures at different points of the set up for natural and force cooling conditions when the temperature of steady temperature reservoir is 300°C. It can be seen that with increasing of the volumetric flow rate produced by the fan, the temperatures of the cold side and hot side are decreased. But totally the temperature difference ΔT will increases and it leads to increment of voltage and power output.

Table 1.Temperatures at different points in the system for constant T_{STR}= 300 ℃.

	T_{HA} (^oC)	T_H (^oC)	T_C (^oC)	ΔT (^oC)	V_{OC} (V)	P_{max} (W)
Natural convection	267.22	236.9	177.74	59.16	7.2	0.7
Q_c=406.3 Lit/min	266.51	211.6	88.44	123.16	14.96	3.72
Q_c=670.3 Lit/min	263.82	202.14	74.33	127.81	15.35	4.06
Q_c=863.3 Lit/min	262.38	198.97	68.66	130.31	15.55	4.29
Q_c=1015.7 Lit/min	261.07	197.61	66.17	131.44	15.61	4.37
Q_c=1107.1 Lit/min	260.22	196.47	63.65	132.82	15.86	4.48
Q_c=1229 Lit/min	259.6	195.31	61.53	133.78	16.10	4.59

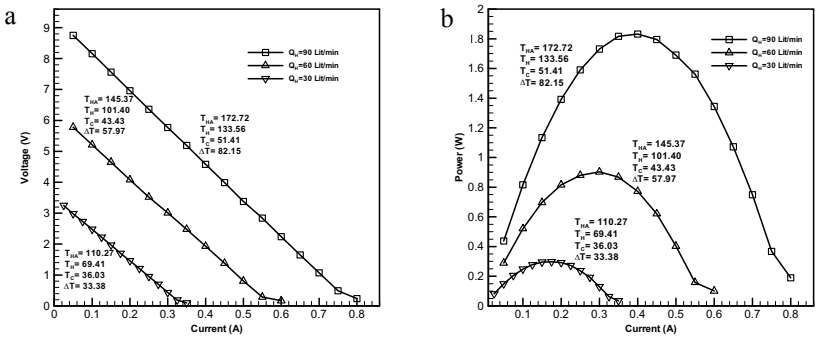

Fig. 6. (a) V-I; (b) P-I curves, both for different volumetric flow in the hot side and Q_c=1015.7 Lit/min.

3.2. Effect of volumetric flow rate of the hot gas

Figs 6(a) and 6(b) show V-I and P-I curves at a constant temperature (T_{STR}=200°C) and for different volumetric flow rates provided by hot gas supplier. As it can be seen, because of the heat loss during the path of the hot gas, the temperature in the hot side is decreased. This falling in temperature value is very depended on the volumetric flow rate applied by hot gas supplier. With increasing the volumetric flow rate, higher force convection heat transfer is produced in the hot side and it leads to having higher temperature in the hot side. The value of temperatures in different points of setup is presented in figs 6(a) and 6(b). It can be seen the volumetric flow rate has a very significant effect on the temperature difference in the hot and cold sides of TEMs and obviously on the voltage and power generated by the TEMs.

4. Conclusions

The effect of different parameters such as temperature and volumetric flow rate in the cold and hot reservoirs, on power generation by four TEMs is investigated experimentally. A comparison between power generation for natural and force convection heat transfer in the cold side is also accomplished. The results show significant influence of using forced convection cooling on the power generation. Variation of the fan power or volumetric flow rate in the cold side at high fan speed does not affect the power generation by TEMs. Therefore, a lower fan speed and volumetric flow rate is recommended to net power. Average Seebeck coefficient of the is obtained by using P_{max}-$(\Delta T)^2$ curve. Finally, the significant effect of the volumetric flow rate of the hot gas on power generation by the TEMs is also studied. It is found that by increment in hot gas flow rate, the temperature difference across the TEMs enhances, and therefore the power generation increases noticeably.

Acknowledgements

The authors would like to acknowledge Center for Thermoelectric Energy Conversion funded in part by the Danish Council for Strategic Research, Programme Commission on Energy and Environment, under Grant No. 63607.

References

[1] Kraemer D, McEnaney K, Chiesa M, Chen G. Modeling and optimization of solar thermoelectric generators for terrestrial applications. Sol Energy 2012;86(5):1338-50.
[2] Rezania A, Rosendahl LA. A comparison of micro-structured flat-plate and cross-cut heat sinks for thermoelectric generation application. Energy Convers. Manag 2015;101:730-7.
[3] Miranda AG, Chen TS, Hong CW. Feasibility study of a green energy powered thermoelectric chip based air conditioner for electric vehicles. Energy 2013;59:633-41.
[4] Wang Y, Dai C, Wang S. Theoretical analysis of a thermoelectric generator using exhaust gas of vehicles as heat source. Appl Energy 2013;112:1171-80.
[5] Hsiao YY, Chang WC, Chen SL. A mathematic model of thermoelectric module with applications on waste heat recovery from automobile engine. Energy 2010;35:1447-54.
[6] Ding LC, Akbarzadeh A, Date A. Performance and reliability of commercially available thermoelectric cells for power generation. Appl. Therm. Eng 2016;102:548-56.
[7] Hsu CT, Huang GY, Chu HS, Yu B, Yao DJ. Experiments and simulations on low-temperature waste heat harvesting system by thermoelectric power generators. Appl Energy 2011;88:1291-7.
[8] Chen WH, Liao CY, Hung CI, Huang WL. Experimental study on thermoelectric modules for power generation at various operating conditions. Energy 2012;45:874-81.
[9] Rezania A, Yazawa K, Rosendahl LA, Shakouri A. Co-optimized design of microchannel heat exchangers and thermoelectric generators. Int. J. Therm. Sci 2013;72:73-81.
[10] Yu S, Du Q, Diao H, Shu G, Jiao K. Effect of vehicle driving conditions on the performance of thermoelectric generator. Energy Convers. Manag 2015;96:363-76.
[11] Zhang G, Jiao K, Niu Z, Diao H, Du Q, Tian H, et al. Power and efficiency factors for comprehensive evaluation of thermoelectric generator materials. Int. J. Heat Mass Transfer 2016;93:1034-7.
[12] Zhang G, Fan L, Niu Z, Jiao K, Diao H, Du Q, et al. A comprehensive design method for segmented thermoelectric generator. Energy Convers. Manage 2015;106:510-9.

PAPER 2: REFERENCE [184]

Transient Behavior of the Thermoelectric Generators to the Load Change; an Experimental Investigation

Sajjad Mahmoudi Nezhad, Alireza Rezania, Ali Akbar Ranjbar, Lasse Rosendahl

The paper has been published in
Energy Procedia 147 (2018) 537-543.

Available online at www.sciencedirect.com

ScienceDirect

Energy Procedia 147 (2018) 537–543

Energy Procedia

www.elsevier.com/locate/procedia

International Scientific Conference "Environmental and Climate Technologies", CONECT 2018

Transient behavior of the thermoelectric generators to the load change; an experimental investigation

Sajjad Mahmoudinezhad[a]*, Alireza Rezania[a], Ali A. Ranjbar[b], Lasse A. Rosendahl[a]

[a]*Department of Energy Technology, Aalborg University, Pontoppidanstræde 101, Aalborg ,DK-9220, Denmark*
[b]*Department of Mechanical Engineering, Babol University of Technology, Babol, P.O. Box 484, Iran*

Abstract

Thermoelectric generators (TEGs) are environmentally friendly and have become a promising technology for different waste heat recovery applications. An experimental study is carried out to examine the performance of four TEGs that are connected in series used for electric power generation over a range of different operating conditions and resistance loads. After obtaining I-V-P curves, the transient thermal response of the TEGs to a load change is investigated. The significance of the impact of volumetric flow rate in the hot and cold sides of the TEGs and the temperature in the constant temperature reservoir on power generation and transient behavior of the TEGs are determined and discussed in details. The results show the substantial effect of the volumetric flow rate and temperature in the power generation and transient thermal behavior of the TEGs.

Keywords: transient response; thermoelectric generator; experimental investigation; variable load

1. Introduction

Having no moving parts and long lifetime, silent operation and low maintenance costs make thermoelectric generators (TEG) a promising technology for waste heat recovery. TEGs convert waste heat into electricity

* Corresponding author. Tel.: +459-35-62-145; fax: +459-81-51-411.
E-mail address: sma@et.aau.dk

10.1016/j.egypro.2018.07.068

directly [1–5]. Due to depletion of conventional energy resources, replacement of them by clean and renewable energies is very crucial. TEGs are small, robust and compact devices that make them an appropriate choice for different applications. There are a lot of studies that considered TEGs under transient conditions. Alata and Naji [6, 7] used an analytical model to investigate the transient performance of thermoelectric cooler (TEC). Generally, mathematical modeling of transient heat conduction problems involves a complex treatment. Due to thermoelectric multi-physics effect in the TEG, the condition is more challenging. Jia et al. [8] established a finite element model to investigate the transient response of linear-shaped TEGs. The results indicated reducing the time to reach steady condition, the entire generated electric power and conversion efficiency can be increased.

Savani et al. [9] studied the behavior of a Bi-Te based TEG under the transient condition of a silicon production plant. The results showed that by increasing the cooling capacity, it would be more advantageous to use the TEG with a higher fractional area and locate it as close as possible to the silicon melt. Blandino and Lawrence [10] investigated both numerically and experimentally transient response of a TEG exposed to spatially non-uniform heating, resulting in small temperature gradients across its thickness. They found that in such application it is crucial to use a highly efficient heat sink over the whole back area of the module.

To minimize the response time of the TEG and then higher working frequency, Fisac et al. [11] developed a TEG structure. The performance of the new TEG's structure is validated by comparing numerical simulation and experimental results. The finite-difference method is used by Nguyen and Pochiraju [12] to solve a transient TEG model subjected to an unsteady state heat source on the hot side. It has found that Thompson effect has a substantial impact on power generation by the TEG. The steady-state and transient models for a gas/liquid cylindrical TEG presented and validated by Crane et al. [13, 14]. The transient model can simulate a wide range of working circumstances.

One of the main advantages of the TEGs is that they are environmentally friendly and can recycle wasted heat energy and convert it into the reusable form of energy. There are many studies on different models and prototypes for different applications of waste heat recovery that have been established and validated with very promising outcomes. Most of them have been examined under steady-state conditions. However, in the real applications, we face unsteady situations, and this transient condition leads to substantial deviation in TEG performance. This experimental work presents an analysis of the transient electrical and thermal behavior of a TEG system to a load change. Moreover, mutual electrical and thermal response of the TEG system under transient condition will be discussed.

2. Experimental setup

Fig. 1 shows a view of the test rig. Power generation by the TEG system is obtained by data derived from experiments. Four 30 mm·30 mm·4.2 mm Bi-Te based TEGs are used in the experiments that electrically connected in series. Force convection cooling of the cold side of the TEG is provided by an axial fan. A DC power supply is used to apply different fan powers and different mass flow rates in the heat sink. For the hot side of the TEGs, a hot gas supplier and a constant temperature reservoir is used. The temperature and mass flow rate of the hot side of the TEG can be controlled by the constant temperature reservoir and hot gas supplier, respectively. Four T-type thermocouples are placed just behind of the TEGs. A programmable DC electronic load device is used for applying different loads to the TEGs. Temperatures in the different points, volumetric flow rates, and output voltage are the main parameters recorded during experiments. All experimental data are collected by LXI (34972A) data acquisition system.

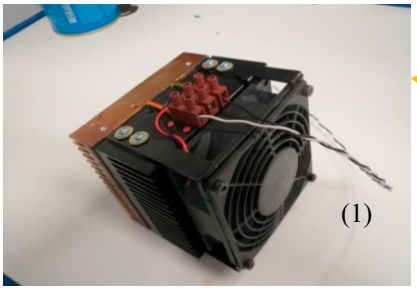

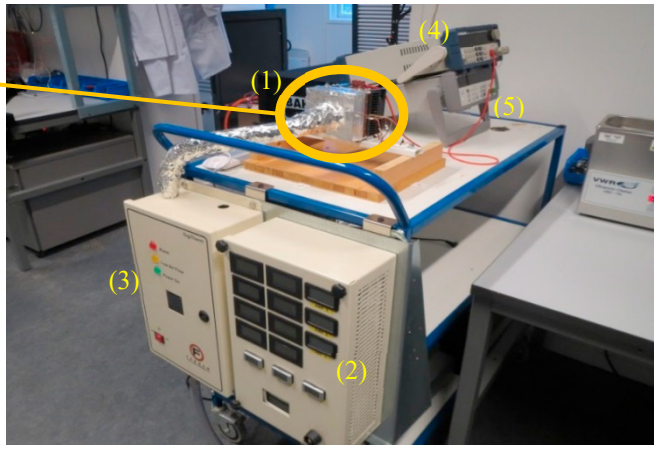

(1) Test section
(2) Constant Temperature reservoir
(3) Flow Rate Supplier
(4) Programmable DC Electronic Load
(5) Data Acquisition System

Fig. 1. A view of the TEG test rig.

2.1. Uncertainty analysis

Uncertainty analysis has been carried out using the method proposed in [15, 16]. To ascertain the accuracy of the equipment, they were calibrated before experiments. The measuring value and the resolutions of all the devices are presented in Table 1. The relative uncertainty of the devices is calculated by [15]:

$$\textit{Relative uncertainty} = 0.5 \cdot \textit{resolution} \cdot \textit{measuring value}^{-1} \tag{1}$$

As it can be seen, the maximum relative uncertainty of the equipment is 2 %.

Table 1. List of equipment relative uncertainties.

Equipment	Measuring range	Resolution	Relative uncertainty
Hot gas supplier	30–90 L/min	0.1 L/min	0.17 %
Constant temperature reservoir	100–400 °C	0.1 °C	0.05 %
DC power supply (for voltage)	3–13 V	0.00125	0.02 %
Programmable DC electronic load (for electric current)	0.025–1.2 A	0.001 A	2.00 %

An error analysis of experiments also is carried out. For a typical test, results for temperature in the different points of the system, voltage, and current are shown in Table 3. The mean value ($\overline{X}$) and the standard deviation (S_X) of the data are defined by [16]:

$$\overline{X} = n^{-1}\sum_{i=1}^{n} X_i \tag{2}$$

$$S_X = \left[(n-1)^{-1}\sum_{i=1}^{n} X_i - \overline{X})^2\right]^{\frac{1}{2}} \tag{3}$$

Then the uncertainty (S_J) is:

$$S_J = S_X \cdot (\overline{X})^{-1} \cdot 100 \tag{4}$$

As it can be seen in Table 2, the maximum uncertainty is 1.98 % which is less than 6 %. It shows that the experiments are reliable.

Table 2. List of experiment uncertainties.

Variable	1st	2nd	3rd	Mean value	Sample standard deviation	Uncertainty
T_{HA} (°C)	215.1 °C	216.39 °C	217.84 °C	216.44 °C	1.37 °C	0.63 %
T_H (°C)	165.37 °C	166.52 °C	163.91 °C	165.26 °C	1.31 °C	0.79 %
T_C (°C)	65.86 °C	63.3 °C	64.46 °C	64.54 °C	1.28 °C	1.98 %
V_{OC} (V)	11.8747 V	11.9194 V	11.9326 V	11.9089 V	0.0303 V	0.25 %
V (V) (@P_{max})	5.7635 V	5.6979 V	5.7241 V	5.7285 V	0.0330 V	0.58 %
I (A) (@P_{max})	0.4513 A	0.4502 A	0.4489 A	0.4501 A	0.0012 A	0.27 %

3. Results and discussion

Four Bi-Te based TEGs are tested under different operating conditions. In the experiments, the volumetric flow rate of the fan in the heat sink and temperature, and volumetric flow rate of the air flow on the hot side are changing to provide different working circumstances. The volumetric flow rate of the fan (Q_c) and hot gas supplier (Q_h) are varied between 406.3 L/min to 1229 L/min and 30 L/min to 90 L/min, respectively.

The variations of the open circuit voltage with the temperature difference for different volumetric flow rates are obtained. Due to electrical resistance in the wires, switches, connections and other devices, the measured open circuit voltage is always less than the actual value, but if TEG produces high voltage and low current, this error is almost negligible [17]. The Seebeck coefficient of a material depends on the temperature [18, 19] but in this framework the open circuit graphs are linear, and it shows that in the tested temperature range, the magnitude of the Seebeck coefficient is approximately constant. From Eq. (5), the value of the Seebeck coefficient can be measured by using the open circuit voltage and the temperature difference between hot side and cold side of the TEGs.

$$V_{oc} = \alpha \Delta T = \alpha (T_h - T_c) \tag{5}$$

where

V_{oc} the open circuit voltage;

α the Seebeck coefficient;

T_h and T_c the temperatures of the hot and cold side of the TEG, respectively.

Using Eq. (5) shows that the Seebeck coefficient values for tested material and in this temperature range are varied between 0.104 V/K and 0.121 V/K for four TEGs.

V-I, R-I and P-I curves for four TEGs at a specific temperature difference (ΔT = 107.8 °C) and with Q_c = 406.3 L/min are illustrated in Fig. 2.

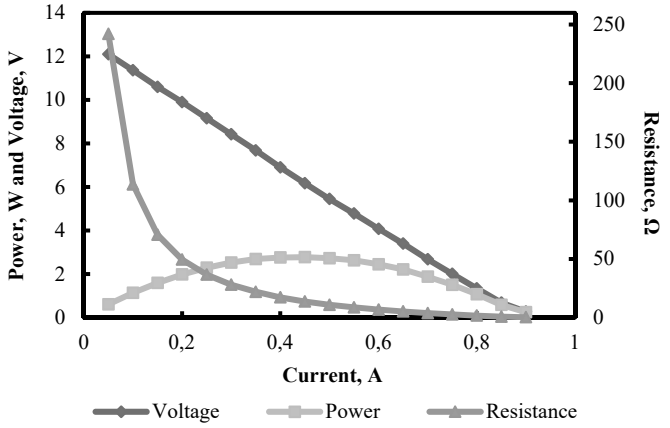

Fig. 2. V-I, R-I and P-I curves for (ΔT = 107.8 °C), Q_h = 90 L/min and Q_c = 406.3 L/min.

The focus of this investigation is on the transient thermal response of the system to an electrical load change. After reaching the steady state condition, the I-V-P curves for all the operating conditions are obtained. Then the equivalent voltage for the maximum power can be achieved. The same operating condition is applied again to the system with open circuit voltage. This time the voltage suddenly drops to the equivalent voltage of the maximum power which is obtained before. Fig. 3 displays the thermal response of the TEGs to the load change for Q_h = 30 L/min and Q_c = 406.3 L/min and T_{TSR} = 250 °C, T_{TSR} is the temperature of the constant temperature reservoir.

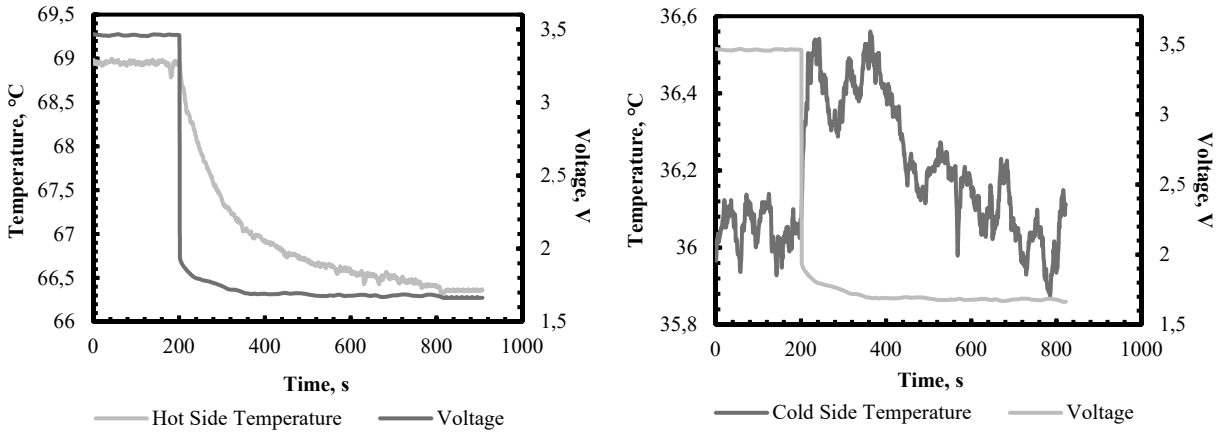

Fig. 3. Variation of the hot and cold side temperatures and voltage versus time for Q_h = 30 L/min and Q_c = 406.3 L/min and T_{TSR} = 250 °C.

As can be observed, the open circuit voltage is equal to V_{oc} = 3.45 V. By applying equivalent current for the maximum power $I_{@Pmax}$ = 0.175 A, the equivalent voltage for the maximum power is $V_{@Pmax}$ = 1.66 V. In this condition, the temperature of the hot side of the TEG drops around 2.5 °C, but the cold side temperature does not change a lot. This variation is owing to the Peltier effect that is working against power generation and deviates the peak working point from the generally known maximum power point (MPP). As a matter of fact, the heat transfer across the TEG from the hot to the cold side varies with the load current produced by the TEG according to the Peltier effect.

By increasing the volumetric flow rate in the hot and cold sides of the TEG, these variations are more sensible. Fig. 4 shows the same graphs for higher volumetric flow rates and the same temperature in the constant temperature reservoir. The open circuit voltage is V_{oc} = 8.67 V and equivalent current and voltage for maximum power are $I_{@Pmax}$ = 0.4 A and $V_{@Pmax}$ = 3.98 V, respectively. Fig. 4 indicates that the drop in the hot side temperatures is around 5 °C, while the cold side temperature enhances 1 °C.

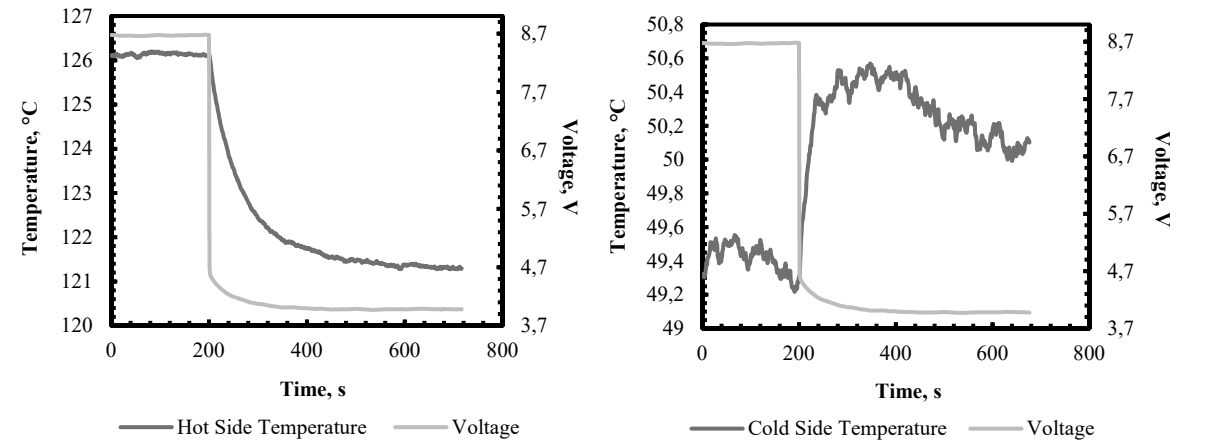

Fig. 4. Variation of hot and cold side temperatures and voltage versus time for Q_h = 90 L/min and Q_c = 1015.7 L/min and T_{TSR} = 250 °C.

Fig. 5 illustrates that increment in the value of the temperature of the constant temperature reservoir has a substantial effect on the characteristics of the TEGs. As can be seen, in this condition the open circuit voltage reaches V_{oc} = 15.05 V. When the current is increased to $I_{@Pmax}$ = 0.55 A, the equivalent voltage for reaching the maximum power is $V_{@Pmax}$ = 7.42 V. In this operating condition, the hot side temperature decreases more than 7.5 °C and the cold side temperature enhances around 2.5 °C.

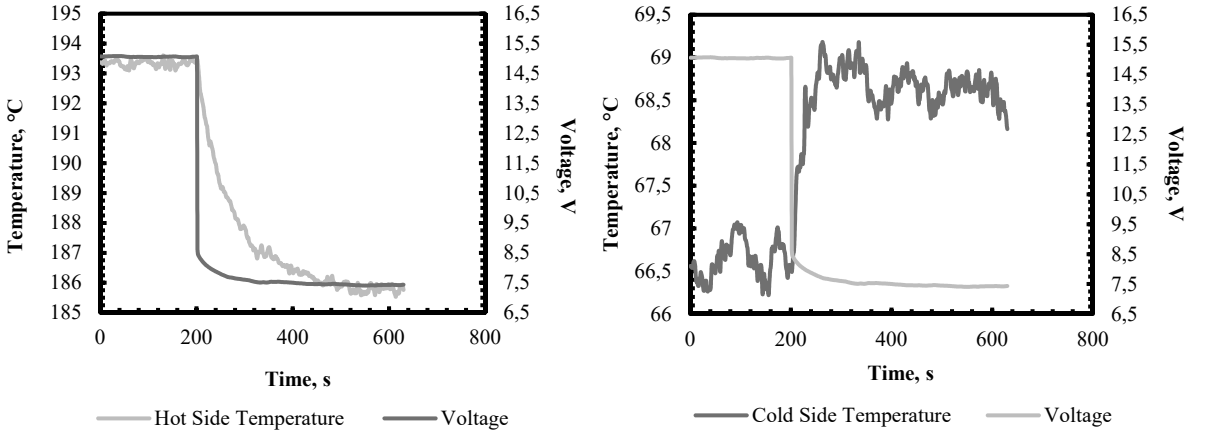

Fig. 5. Variation of hot and cold side temperatures and voltage versus time for Q_h = 90 L/min and Q_c = 1015.7 L/min and T_{TSR} = 400 °C.

The significant effect of volumetric flow rate in the heat source can be observed in Fig. 6. Identical condition with the Fig. 5 is considered except the volumetric flow rate in the hot side that is decreased to Q_h = 30 L/min. A huge drop in the open circuit voltage can be seen. In this working circumstance, by increasing the current from 0 to $I_{@Pmax}$ = 0.275 A, the voltage drops from V_{oc} = 5.70 V to $V_{@Pmax}$ = 2.65 V. The hot side temperature drop is around 4 °C and the variation of the temperature in the cold side is small.

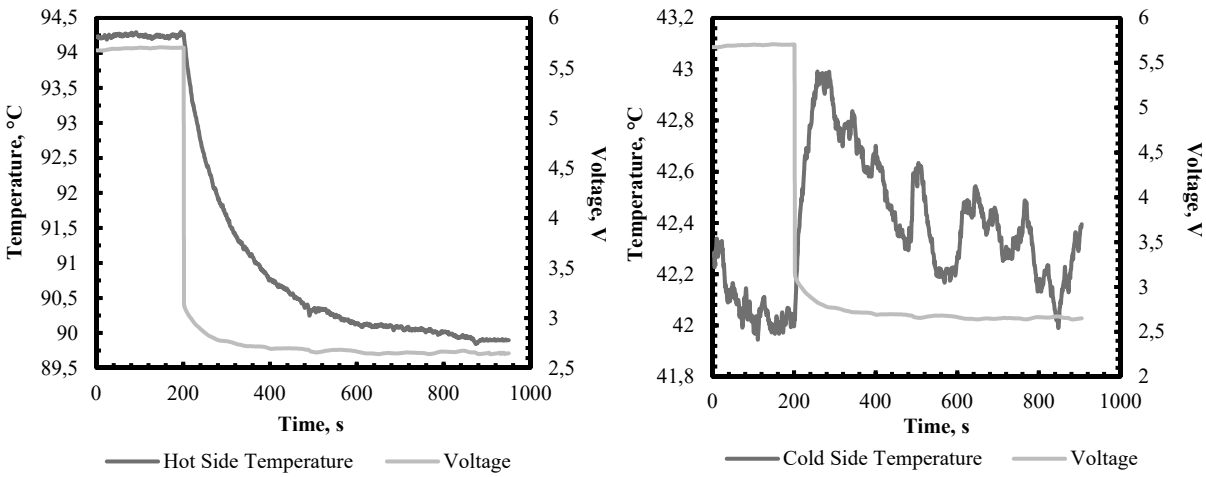

Fig. 6. Variation of hot and cold side temperatures and voltage versus time for Q_h = 30 L/min, Q_c = 1015.7 L/min and T_{TSR} = 400 °C.

4. Conclusion

Four Bi-Te based TEGs are examined experimentally. I-V-P curves in different operating condition are obtained. The impact of different parameters has been considered. Thermal response of the system to a load change from the

open circuit voltage to the equivalent voltage for maximum power is discussed. The results indicate that in the low volumetric flow rate values of the heat source, the variation of the temperature of the cold side is small. With increasing the volumetric flow rate on both sides of the TEG, the temperature drop on the hot side and the enhancement of the temperature on the cold side is increased. The maximum variation in the temperatures is related to the higher temperature in the constant temperature reservoir and higher volumetric flow rate on both sides of the TEG.

Acknowledgements

The authors would like to acknowledge Center for Thermoelectric Energy Conversion funded in part by the Danish Council for Strategic Research, Programme Commission on Energy and Environment, under Grant No. 63607.

References

[1] Hsiao YY, Chang WC, Chen SL. A mathematic model of thermoelectric module with applications on waste heat recovery from automobile engine. Energy 2010;35:1447–54.
[2] Mahmoudinezhad S, Qing S, Rezaniakolaei A, Rosendahl LA. Transient Model of Hybrid Concentrated Photovoltaic with Thermoelectric Generator, Energy Procedia 2017;142:564–9.
[3] Rahbar N, Asadi A. Solar intensity measurement using a thermoelectric module; experimental study and mathematical modelling. Energy Conversion and Management 2016;129:344–53.
[4] Nezhad SM, Rezaniakolaei A, Rosendahl LA. Experimental Study on Effect of Operating Conditions on Thermoelectric Power Generation. Energy Procedia 2017;142:558–63.
[5] Mahmoudinezhad S, Rezania A, Rosendahl LA. Behavior of hybrid concentrated photovoltaic-thermoelectric generator under variable solar radiation. Energy Conversion and Management 2018;164:443–52.
[6] Alatam M, Al-Nimr MA, Naji M. Transient Behavior of a Thermoelectric Device under the Hyperbolic Heat Conduction Model. International Journal of Thermophysics. 2003;24(6):1753–68.
[7] Naji M, Alata M, Al-Nimr MA. Transient Behavior of a Thermoelectric Device. Proceedings Of The Institution Of Mechanical Engineers Part A-Journal of power and energy 2003;217(A6):615–22.
[8] Jia X-D, Wang Y-J, Gao Y-W. Numerical simulation of thermoelectric performance of linear-shaped thermoelectric generators under transient heat supply. Energy 2017;130:276–85.
[9] Savani I, Waage HM, Borset M, Kjelstrup S, Wilhelmsen O. Harnessing thermoelectric power from transient heat sources: Waste heat recovery from silicon production. Energy Conversion and Management 2017;138:171–82.
[10] Blandino JR, Lawrence DJ. Transient response of a thermoelectric generator subjected to spatially non-uniform heating: Implications for heat and IR sensing applications. Measurement 2016;80:125–37.
[11] Fisac M, Villasevil FX, Lopez AM. Design of a thermoelectric generator with fast transient response. Renewable Energy 2015;81:658–63.
[12] Nguyen NQ, Pochiraju KV. Behavior of thermoelectric generators exposed to transient heat sources. Applied Thermal Engineering 2013;51:1–9.
[13] Crane DT. An Introduction to System-Level, Steady-State and Transient Modeling and Optimization of High-Power-Density Thermoelectric Generator Devices Made of Segmented Thermoelectric Elements. Journal of Electronic Materials 2011;40(5):561–569.
[14] Crane DT, Koripella CR, Jovovic V. Validating Steady-State and Transient Modeling Tools for High-Power-Density Thermoelectric Generators, Journal of Electronic Materials 2012;41(6):1524–1534.
[15] Kline SJ. The purpose of uncertainty analysis. ASME J Heat Transfer 1985;117:153–60.
[16] Coleman HW, Steele Jr WG. Experimentation and uncertainty analysis for engineers. New York: Wiley; 1989.
[17] Orr B, Taglieri J, Ding LC, Akbarzadeh A. Validating an alternative method to predict thermoelectric generator performance. Energy Conversion and Management 2016;116:134–41.
[18] Zhang G, Jiao K, Niu Z, Diao H, Du Q, Tian H, et al. Power and efficiency factors for comprehensive evaluation of thermoelectric generator materials. Int J Heat Mass Transf 2016;93:1034–7.
[19] Zhang G, Fan L, Niu Z, Jiao K, Diao H, Du Q, et al. A comprehensive design method for the segmented thermoelectric generator. Energy Convers Manage 2015;106:510– 9.

PAPER 3: REFERENCE [195]

Performance Evaluation of a High-Temperature Thermoelectric Generator under Different Solar Concentrations

Sajjad Mahmoudi Nezhad, Petru Adrian Cotfas, Daniel Tudor Cotfas, Alireza Rezania, Lasse Rosendahl

The paper has been published in
Energy Procedia 147 (2018) 624–630.

Available online at www.sciencedirect.com

ScienceDirect

Energy Procedia 147 (2018) 624–630

Energy Procedia

www.elsevier.com/locate/procedia

International Scientific Conference "Environmental and Climate Technologies", CONECT 2018

Performance evaluation of a high-temperature thermoelectric generator under different solar concentrations

Sajjad Mahmoudinezhad[a]*, Petru A. Cotfas[b], Daniel T. Cotfas[b], Alireza Rezania[a], Lasse A. Rosendah[a]

[a]*Department of Energy Technology, Aalborg University, Pontoppidanstræde 101, Aalborg, DK-9220, Denmark*
[b]*Electrical Engineering and Computer Science Faculty, Transilvania University of Brasov, Brasov, 500036, Romania*

Abstract

Due to some special features like being highly reliable and having long lifetime, solar thermoelectric generators (STEGs) are appropriate to convert solar energy into electrical energy directly. In this investigation, an oxide-based TEG is examined under different solar concentrations. To increase the energy absorbance by the TEG, a self-adhesive graphite sheet is attached to the surface of the TEG. For both STEG systems, the variation of the temperatures on the hot and cold sides of the TEG, open circuit voltage and short circuit current are obtained and compared. I-V-P curves for both STEG systems are achieved and discussed. The results indicate the significant effect of using graphite sheet in the STEG system on the power generation and all abovementioned parameters.

Keywords: solar thermoelectric generator; experimental investigation; graphite sheet; solar concentration; power generation

* Corresponding author. Tel.: +45-93-562-145; fax: +45-98-151-411.
E-mail address: sma@et.aau.dk

10.1016/j.egypro.2018.07.080

1. Introduction

Fast depletion of the fossil fuels makes clean and renewable alternative energies very important. Sun is an unlimited source of energy. Solar energy can be converted to electricity by different devices. STEGs are promising devices which can be used for harvesting solar energy. TEGs have no moving parts and working silently with high reliability, therefore, TEGs have been used in different applications like waste heat recovery [1, 2], low power remote applications [3, 4], space probes [5], hybrid solar-TEG systems [6–8] and so on. Using low-temperature TEGs in STEG systems have been investigated in many references but there are fewer studies on the application of high-temperature TEGs in STEG systems. One of the first studies with remarkable results has been presented by Telks [9]. The efficiency of the STEG system for the solar concentration less than 50 reached to 3.35 %. In the recent years, new investigations of different aspects of STEG systems have been done. Kraemer et al. [10] presented a STEG system which was arrived at 4.6 % conversion efficiency. This efficiency is more than 7 times higher than the formerly obtained maximum value for a flat-panel STEG. Later in another study, Kraemer et al. [11] suggested a numerical model and an optimization approach for the terrestrial STEGs. The conversion efficiency was reached to 5 % in the new design of the STEG system.

With the development of the high-temperature TEGs, the capability of using concentrated solar radiation has been investigated [12] and a new category of the STEG systems have been established. A general model for power generation and efficiency of the STEG systems has been offered by Cai et al. [13]. Impact of different parameters including input energy, the thermal conductivity, the absorptivity and emissivity of the heat collector, and the cooling water were investigated. The results illustrated that increasing input energy and absorptivity, enhance the performance of the STEG while low emissivity of the heat collector is beneficial to achieve a high-performance STEG system. Kutt et al. [14] optimized a concentrated STEG system. The optimum number of commercial TEGs that should be used in the STEG system is determined.

Baranowski et al. [15] divided the STEG into two subsystems including TEG and solar absorber in the modeling procedure. To achieve 85 % efficiency for the absorber they used two different methods that are using the solar selective absorber and thermally insulating cavities. The predicted efficiency for the used TEG materials and for solar concentration between 250 to 300 suns was 15 %. A SiGe-based STEG system was examined by Pereira et al. [16] under high solar concentration values (>100) and high-temperature condition (>450 °C). The maximum efficiency of the system was obtained 1.8 % which is for the lowest emissivity value. The feasibility of direct transformation of concentrated high-temperature solar radiation into electricity was investigated experimentally by Tomes et al [17]. The impact of coated graphite layer on the hot side of the TEG on the temperature difference, maximum power generation by the system and the efficiency of the system are also determined. The results showed that coating the graphite layer on the hot surface leads to having a higher temperature difference between hot and cold sides of the TEG and the maximum power and efficiency of the system improves substantially.

Oxide-based STEGs are appropriate for working under high solar concentrations and high-temperature conditions. These materials are more efficient in the high-temperature ranges. In this study, an oxide-based STEG system is examined experimentally under different solar concentration values. In the next step, to increase the absorbance of the STEG system, a self-adhesive graphite sheet is attached to the top surface of the TEG. An inclusive evaluation of the performance of both STEG systems with and without graphite sheet is carried out. The temperature gradient between the hot and cold side of the TEG, open circuit voltage, short circuit current, and maximum output power are obtained and compared for both STEG systems.

2. Experimental setup

Flat plates, parabolic troughs, Fresnel lenses and parabolic dishes are mostly used as the solar collector in the experiments. In this investigation, a high-flux solar simulator consists of 10 xenon arc lamps cooled with high-pressure water (see Fig. 1) is used to provide the concentrated light. Very high solar concentration (until 11000 suns) can be simulated in the focal point [18, 19]. To deliver a uniform light over the surface of the TEG, an optical mixer located in front of the STEG system. In order to produce 0 to 338 suns, just 6 lamps are used in the experiments. All the experimental results are taken in Solar Technology Laboratory of Paul Scherrer Institute (PSI).

Before starting the experiments, a thermogage is used to measure and calibrate the distribution of the solar radiation. Thus, the most homogeneous heat flux over the area of 42 mm·42 mm can be found and TEG can be located in that area.

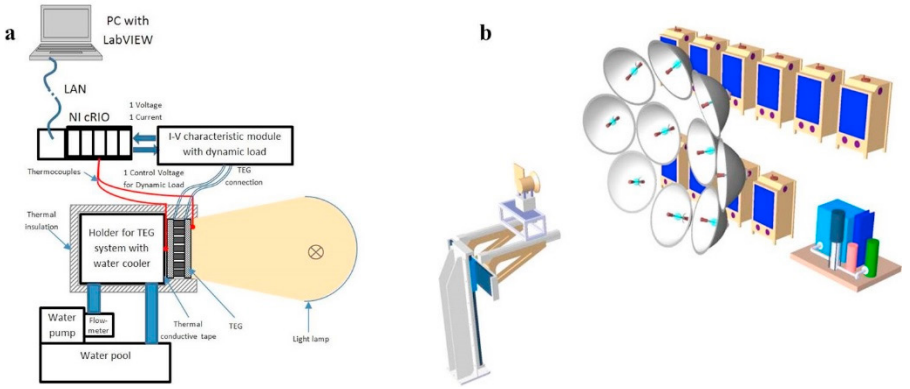

Fig. 1. (a) Schematic of experimental setup; (b) solar simulator used in this study [20].

A commercial oxide TEG model CMO-25-42S with 50 uni-couples and size of 42 mm·42 mm, Fig. 2(a), which the materials of N-Type and P-Type are $CaMnO_3$ (Mn-113) and $Ca_3Co_4O_3$ (Co-349) [21] respectively, is used in the experiments. In order to enhance the energy absorbed from the solar simulator, a self-adhesive graphite sheet [22] is attached to the surface of the TEG. Fig. 2(b) shows the schematic of the STEG system including TEG with graphite layer on top and heat exchanger with water, as the working fluid.

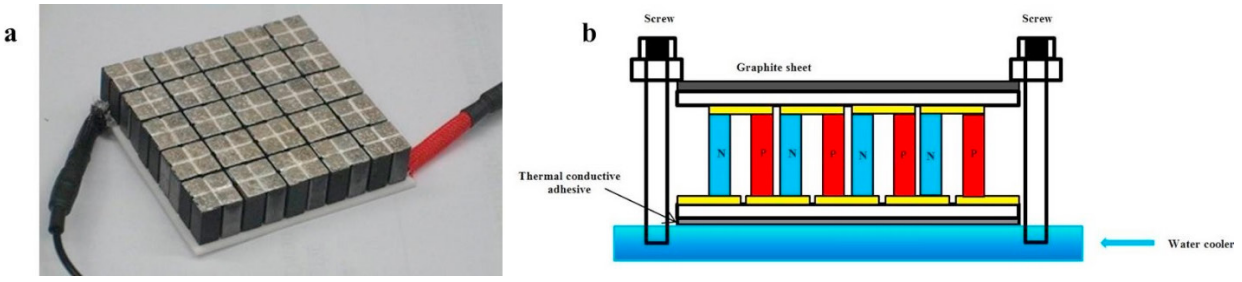

Fig. 2. (a) Oxide TEGs used in experiments; (b) physical model of the STEG system.

The mass flow rate of the water in the heat sink is 5 Lit/min that is constant during all experiments. All the temperatures and I-V-P curves are recorded with a data acquisition and control systems based on National Instruments cRIO. 2 T-type thermocouples are used to measure the temperatures on the hot side. For the cold side and ambient temperature, 3 and 1 T-type thermocouples are used, respectively.

3. Results and discussion

The temperature gradient across the TEG and figure of merit of the TEG are two main parameters in power generation by the TEG. In the first step of experiments, TEG without graphite layer on top is examined. In this condition due to having more reflection from the top surface of the TEG, less input energy can be absorbed; therefore, higher solar radiation can be applied to the STEG system. In the next step, a self-adhesive graphite sheet is attached to the hot side of the TEG and consequently, TEG has more absorbance rather than when there is no graphite sheet. In this situation, the solar radiation that can be applied to the system is less than STEG system without graphite sheet. As mentioned before, 6 lamps are used in the experiments that all of them are kept on during the tests and the magnitude of the solar concentration is controlled by a shutter that is located in front of the lamps. Table 1 shows the values of the solar concentrations that are applied to the both STEG systems along with the open-rate percentage of the shutter.

Table. 1. Solar radiation on the TEGs versus open-rate percentage of the shutter.

Shutter percentage, %	5	10	15	20	25	30	40	50	60	70
Solar radiation for STEG without Gr, kW/m^2	30	56	-	107	-	155	205	252	292	338
Solar radiation for STEG with Gr, kW/m^2	30	56	74	107	128	-	-	-	-	-

The maximum solar concentration that is applied to the STEG system with graphite layer is 128 suns. The reason is that the maximum temperature that the graphite sheet can tolerate to stay attached to the hot surface of the TEG is 400 °C. Fig. 3 illustrates the hot and cold side temperatures of the TEG in both STEG systems.

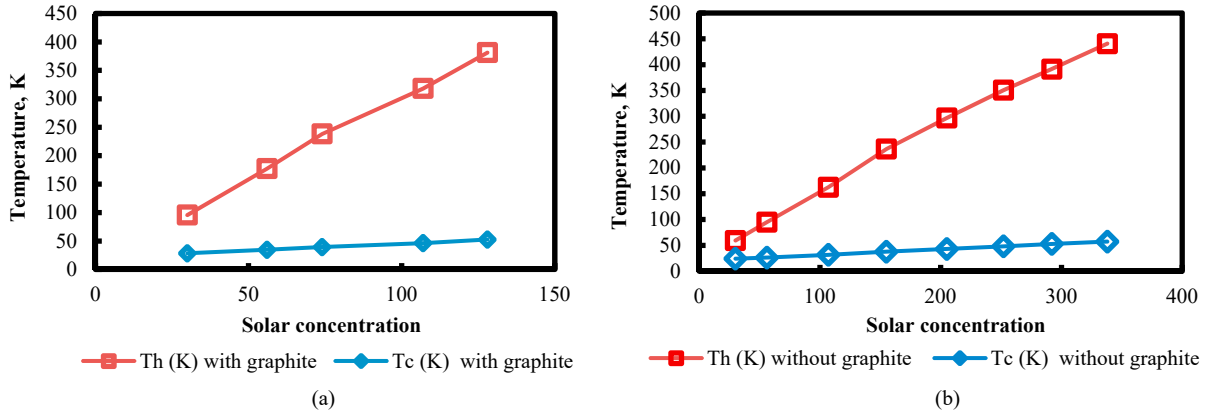

Fig. 3. Hot and cold side temperatures of the STEG: (a) with graphite sheet; (b) without graphite sheet, versus solar concentration.

With increasing the solar radiation and therefore the heat flux through the TEG, the temperature of the hot and cold sides will enhance. The rate of increment of the hot side temperature is more than cold side temperature, therefore, the temperature difference increases as well. Due to the higher rate of energy absorbed from the simulator and consequently higher heat flux across the TEG, the temperature of the STEG system with graphite layer increases in the lower solar concentrations. For solar concentration 128 suns, the temperatures of the hot and cold sides of the TEG in the STEG system with graphite sheet is almost the same with STEG system without graphite sheet and solar concentration 292 suns.

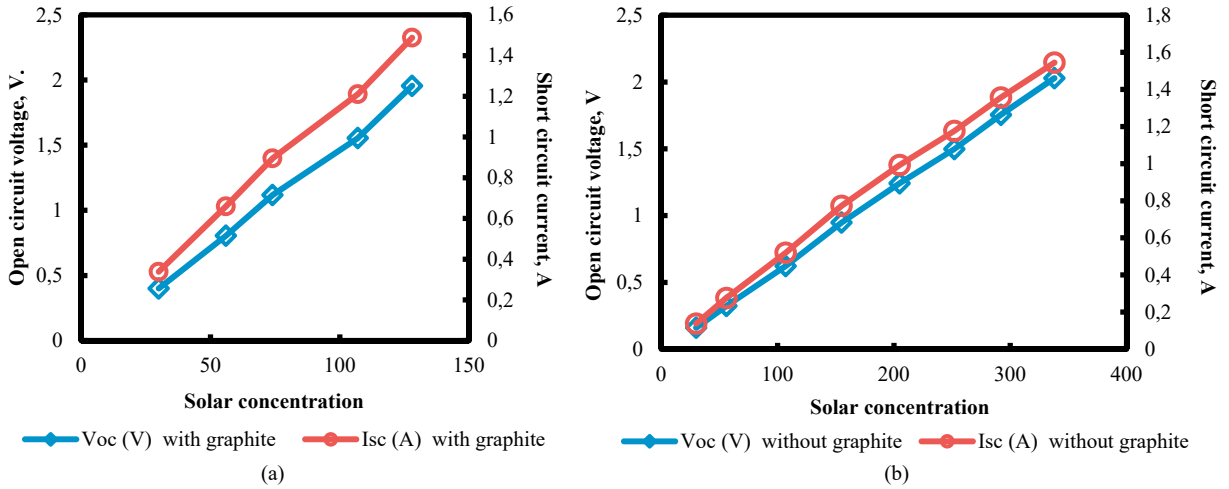

Fig. 4. Open circuit voltage and short circuit current versus solar concentration for STEG: (a) with graphite sheet; (b) without graphite sheet.

Fig. 4 illustrates open circuit voltage and short circuit current for both STEG systems. As can be seen, for both with and without graphite sheet systems, open circuit voltage and short circuit current have the same linear trend and with increasing the solar concentration, the open circuit voltage and short circuit current are enhancing as well. Due to the higher energy absorbed by the TEG when graphite sheet is attached, in lower solar concentration the value of open circuit voltage and short circuit current are almost the same with open circuit voltage and short circuit current without graphite layer and in higher solar concentrations. The value of the open circuit voltage and short circuit current in STEG system with graphite sheet and solar concentration 107 are 1.56 V and 1.21 A, respectively while these values for the system without graphite sheet and solar concentration 252 are 1.5 V and 1.18 A.

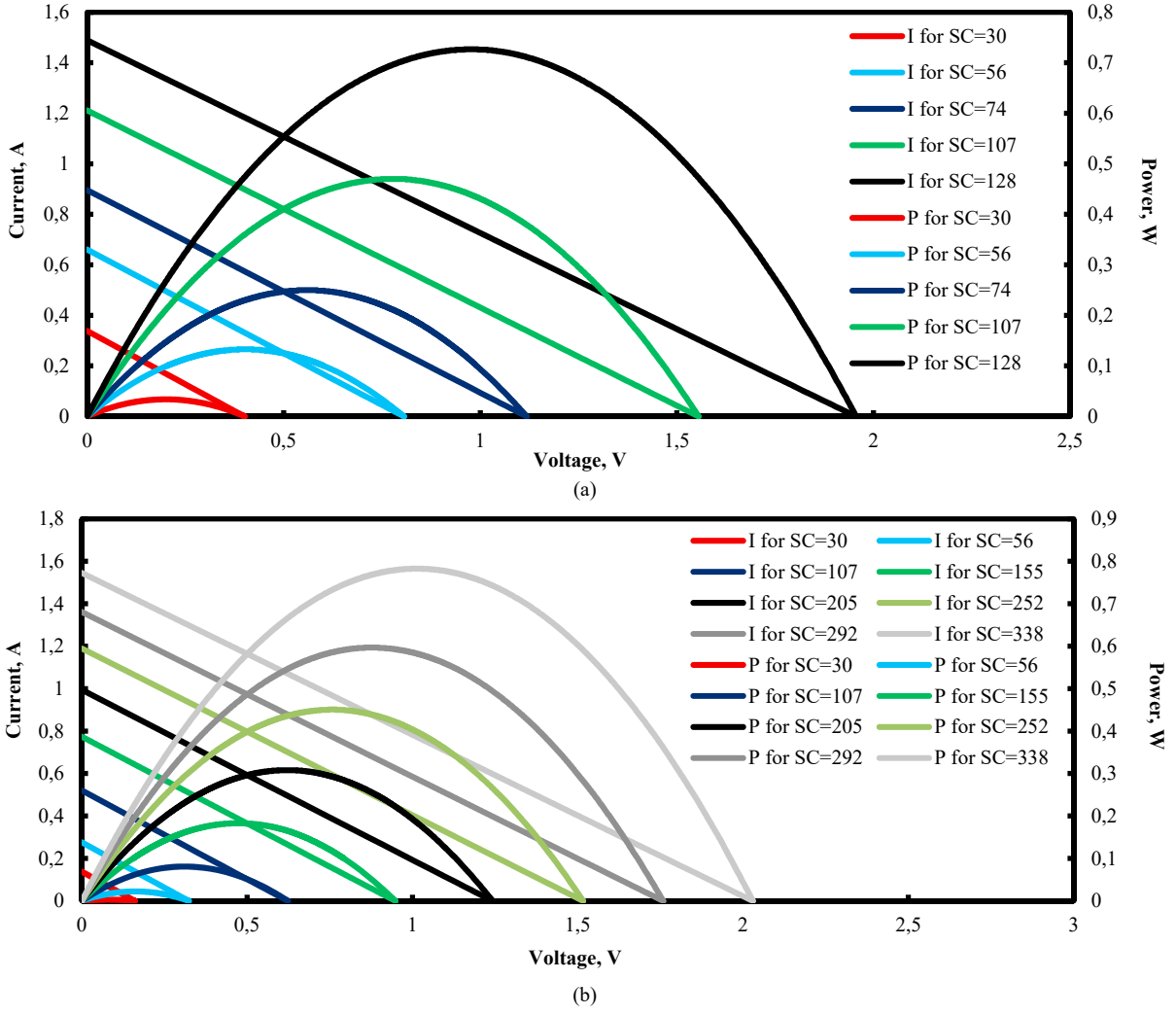

Fig. 5. I-V-P curves for the STEG system: (a) with graphite sheet; (b) without graphite sheet, and different solar concentrations.

The variation of the power and current versus voltage for different solar concentration are shown in Fig. 5. It can be seen that for the same solar concentration the power generated from the TEG with attached graphite is much higher that TEG without graphite sheet. It shows the substantial effect of the graphite sheet on the power generation by the system. This technique is very useful in the low concentration applications to compensate the low amount of input energy. Comparing Fig. 5(a) and Fig. 5(b) shows that for the same solar concentrations, the power generation by the system with graphite sheet is much more than the system without graphite sheet. Fig. 6 illustrates that by

increasing the solar concentration, the ratio of the maximum power of the system with graphite sheet to the system without graphite sheet is decreasing slightly but this amount for the solar concentration 107 is still 5.8 and it shows the significant effect of the graphite sheet.

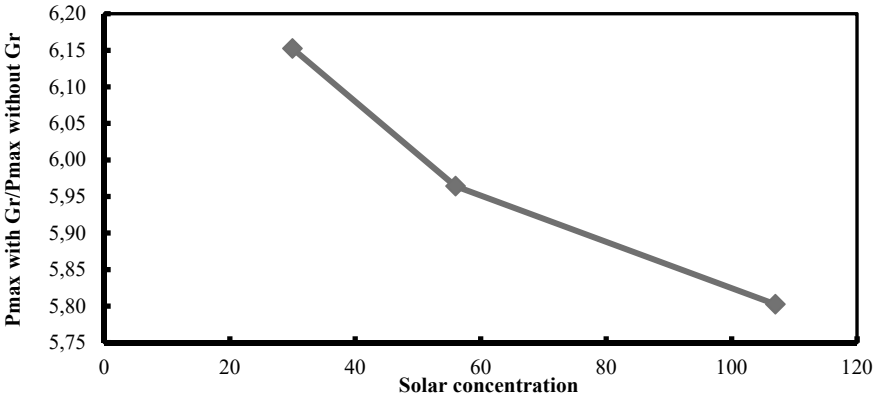

Fig. 6. The ratio of the maximum power for the STEG with graphite sheet to the STEG without graphite sheet versus solar concentration.

4. Conclusion

The performance of an oxide-based STEG system is examined under different solar concentrations. The temperature of the hot and cold sides of the TEG, open circuit voltage, short circuit current, and I-V-P carves are obtained. In the next step of the experiments, a self-adhesive graphite sheet is attached to the hot side of the TEG and all abovementioned are obtained and compared with the TEG without graphite sheet. The results show the huge impact of using the graphite sheet in the STEG system which plays the role of an absorber to increase the amount of absorbed energy from the solar simulator. Furthermore, the ratio of the maximum power in the system with graphite sheet to the system without graphite sheet decreases with increasing the solar concentration.

Acknowledgements

The authors would like to acknowledge financial support from Access to Research Infrastructures activity under 7th Framework Programme, SFERA 2, Grant Agreement n. 312643. The authors are thankful to the team from the Solar Technology Laboratory of Paul Scherrer Institute, Villigen, Switzerland (Ms.Y. Baeuerle, Mr. D. Wuillemin, Mr. V. Schnetzler and Mr. C. Wieckert), where all the measurements of this study were performed.

References

[1] Rahbar N, Esfahani JA, Asadi A. An experimental investigation on productivity and performance of a new improved design portable asymmetrical solar still utilizing thermoelectric modules. Energy Conversion and Management 2016;118:55–62.
[2] Nezhad SM, Rezaniakolaei A, Rosendahl LA. Experimental Study on Effect of Operating Conditions on Thermoelectric Power Generation. Energy Procedia 2017;142:558–63.
[3] Singh R, Tundee S, Akbarzadeh A. Electric power generation from solar pond using combined thermosyphon and thermoelectric modules. Solar Energy 2011;85:371–8.
[4] Stevens JW. Performance factors for ground-air thermoelectric power generators. Energy Conversion and Management 2013;68:114–23.
[5] Kimura R, Yoshida T. Design study of molten-salt-type reactor for powering space probes and its automated start-up. Journal of Nuclear Science and Technology 2013;50(10):998–1010.
[6] Mahmoudinezhad S, Rezania A, Rosendahl LA. Behavior of hybrid concentrated photovoltaic-thermoelectric generator under variable solar radiation. Energy Conversion and Management 2018;164:443–52.
[7] Rezania A, Rosendahl LA. Feasibility and parametric evaluation of hybrid concentrated photovoltaic-thermoelectric system. Appl Energy 2017;187:380–9.
[8] Mahmoudinezhad S, Qing S, Rezaniakolaei A, Rosendahl LA. Transient Model of Hybrid Concentrated Photovoltaic with Thermoelectric Generator. Energy Procedia 2017;142:564–9.

[9] Telkes M. Solar thermoelectric generators. J. Appl. Phys. 1954;25:765.
[10] Kraemer D, Poudel B, Feng H-P, Caylor JC, Yu B, Yan X, Ma Y, Wang X, Wang D, Muto A, McEnaney K, Chiesa M, Ren Z, Chen G. High-performance flat-panel solar thermoelectric generators with high thermal concentration. Nat. Mater. 2011;10:532–53.
[11] Kraemer D, McEnaney K, Chiesa M, Chen G. Modeling and optimization of solar thermoelectric generators for terrestrial applications. Sol. Energy. 2012;86:1338–50.
[12] Weidenkaff A, Robert R, Aguirre MH, Bocher L, Lippert T, Canulescu S. Development of Thermoelectric Oxides for Renewable Energy Conversion Technologies. Renewable Energy 2008;33:342–7.
[13] Cai Y, Xiao J, Zhao W, Tang X, Zhang Q. A General Model for the Electric Power and Energy Efficiency of a Solar Thermoelectric Generator. Journal of Electronic Materials 2011;40(5):1238–43.
[14] Kutt L, Millar J, Lehtonen M, Marss M. Optimization of concentrated solar thermoelectric generator system for highest yearly electric output. The 56th international scientific conference on power and electrical engineering of Riga Technical University, Latvia, Riga, October 14, 2015.
[15] Baranowski LL, Warren EL, Toberer ES. High-Temperature High-Efficiency Solar Thermoelectric Generators. Journal of Electronic Materials 2014;43(6):2348–55.
[16] Pereira A, Caroff T, Lorin G, Baffie T, Romanjek K, Vesin S, Kusiaku K, Duchemin H, Salvador V, Miloud-Ali N, Aixala L, Simon J. High temperature solar thermoelectric generator – Indoor characterization method and modeling. Energy 2015;84:485–92.
[17] Tomes P, Trottmann M, Suter C, Aguirre MH, Steinfeld A, Haueter P, Weidenkaff A. Thermoelectric Oxide Modules (TOMs) for the Direct Conversion of Simulated Solar Radiation into Electrical Energy. Materials 2010;3:2801–14.
[18] Petrasch J, Coray P, Meier A, Brack M, Haberling P, Wuillemin D, Steinfeld A. A novel 50 kW 11,000 suns high-flux solar simulator based on an array of xenon arc lamps. ASME Journal of Solar Energy Engineering 2007;129(4):405–11.
[19] Alxneit I, Schmit H. Spectral characterization of PSI's high-flux solar simulator. J. Sol. Energy Eng 2012;134(1).
[20] Cotfas DT, Cotfas PA, Floroian DI, Floroian L. Accelerated Life Test for Photovoltaic Cells Using Concentrated Light. International Journal of Photoenergy 2016.
[21] TEC. Solidstate Power Generation. Part# CMO-25-42S. Available: http://espressomilkcooler.com/wp-content/uploads/2014/06/CMO-25-42S-OXIDE-NEW.pdf.
[22] RS. Selvklæbende Termisk kontaktfladeark, Grafit, 1000W/m·K, 115x90mm. Available: http://dk.rs-online.com/web/p/varmeledende-spaltefyldende-underlag/7123920/?searchTerm=712-3920&relevancy.

PAPER 4: REFERENCE [196]

Transient Behavior of Concentrated Solar Oxide Thermoelectric Generator

Sajjad Mahmoudi Nezhad, Alireza Rezania, Petru Adrian Cotfas, Daniel Tudor Cotfas, Lasse Rosendahl

The paper has been published in
Energy 168 (2018) 823-832.

Transient Behavior of Concentrated Solar Oxide Thermoelectric Generator

S. Mahmoudinezhad[1], A. Rezania[*, 1], P.A. Cotfas[2], D.T. Cotfas[2], L.A. Rosendahl[1]

[1]*Department of Energy Technology, Aalborg University, Pontoppidanstræde 111, Aalborg DK-9220, Denmark*

[2]*Electrical Engineering and Computer Science Faculty, Transilvania University of Brasov, 500036 Brasov, Romania*

Abstract

Solar thermoelectric generators (STEGs) can directly harness solar energy for power generation. Experimental and numerical studies on the transient response of an oxide thermoelectric generator (TEG) to variation of solar radiation in semi-cloudy weather are carried out. In the first phase, performance of a STEG is investigated under variable solar radiation. Furthermore, effect of a self-adhesive graphite sheet attached to the hot surface of the STEG on enhancement of thermal and electrical performance is studied. In order to evaluate the system performance at high solar concentrations and high operation temperatures, numerical simulation is performed using finite volume method (FVM). I-V-P curves for both STEG systems, with and without the graphite sheet, are obtained. Variation of the hot and cold side temperatures of the TEG and maximum output power variations versus the time are presented and discussed. The results show that, the graphite absorber has a substantial effect on the power generation by the TEG by enhancement of absorbed radiation. This impact is more noticeable at higher solar concentrations and higher temperatures.

Keywords: Solar Radiation, Solar Simulator, Oxide Thermoelectric Generator, Transient response, Graphite absorber.

1. Introduction

Sun is an unlimited source of energy, and solar energy is one of the promising kinds of energies, which can be used instead of the fossil fuel energy. Due to environmental and energy security concerns, harvesting energy of the sun could be an interesting topic to investigate, where many studies are being conducted in this field.

Thermoelectric generators (TEGs) with high reliability, long lifetime and no moving parts [1-2] are an appropriate choice for harvesting solar energy [3-4]. As a TEG locates between a solar absorber and a heat

* Corresponding author: Alireza Rezania. E-mail: alr@et.aau.dk

sink, called solar thermoelectric generators (STEGs), a temperature difference creates across the TEG and produces electrical power. Although, there are many studies for characterizing the STEGs at low temperature, there is lack of study transient behavior of the STEG under variable concentrated solar radiations in medium and high-temperature ranges.

Nomenclature

Abbreviation	
CS	Contact surface
EMF	Electromotive force
Gr	Graphite sheet
SC	Solar concentration
STEG	Solar thermoelectric generator
TE	Thermoelectric
TEG	Thermoelectric generator
ZT	Figure of merit

Greek script	
α	Absorptivity
ε	Emissivity
η	Conversion efficiency, %
σ	Stefan-Boltzmann constant, W/m^2 K^4
Δ	Increment
τ	Thomson coefficient, V/K
ρ	Density (kg/m^3)
γ	Electrical conductivity

Latin script	
A	Area, m^2
C	Specific heat capacity, J/ kg. K
E	Electromotive force, V
G	Solar radiation, W/m^2
h	Heat transfer coefficient, W/ m^{2}K
I	Current, A
K	Thermal conductivity, W/mK
L	length, m
m	Number of control volumes of the thermoelements
n	Number of thermocouples
P	Power, W
Q	Heat loss/ heat transfer, W
r	Resistance, Ω
S	Seebeck coefficient, V/K
T	Temperature, K
t	Time, S
U	Overall Heat transfer coefficient, W/ m^{2}K
V	Voltage, V
x	Heat transfer direction

Subscripts	
i	Contact surface numbers
c	Cold junction
f	Cooling fluid
Gr	Graphite
h	Hot junction
hx	Heat exchanger
ccs	Copper conduction strip
max	Maximum
OC	Open circuit
rad	Radiation
ref	Reference
sc	Semiconductor
sky	Sky
sl	Solder layer
TEG	Thermoelectric generator

superscripts	
b	The bottom contact surface
t	The top contact surface

Telkes [5] reported an outstanding design of STEG system with an efficiency of 3.35% in 1954. The results of his work made a tendency, among many researchers, to apply TEG as solar thermal energy conversion [6-8]. Other notable experimental results by Kraemer et al. [9-10] reported a maximum efficiency of 4.6 % for a STEG system. They proposed an advanced STEG system using a flat-panel spectrally selective absorber, which also acted as a thermal concentrator. Madkhali et al. [11] used both theoretical and numerical methods that confirm Kraemer's study. Later in 2016, Kraemer et al. [12] improved performance of the STEG to 7.4% by an optically concentrated normal solar irradiance of 211 kW/m^2.

Li et al. [13] presented a theoretical model for concentration solar thermoelectric generator, to evaluate system performance based on properties of different bulk thermoelectric materials including Bi_2Te_3, skutterudite and silver antimony lead telluride alloys. The results illustrate that the maximum possible efficiency of the proposed design can reach 9.8%, 13.5% and 14.1% for the mentioned materials, respectively. Eswararmoorthy and Shanmugam [14] thermodynamically examined a parabolic dish joined with a Bi-Te module with a solar-to-electricity efficiency of 2.81% at the temperature of 280 °C. Performance of a STEG system using optical concentration under vacuum conditions with a spectrally selective absorber surface ($\alpha = 0.954$, $\varepsilon = 0.13$) was examined by Cheruvu et al. [15]. The results showed that the ideal range of operation of the absorber is between 200 °C and 370 °C for Bi_2Te_3 TE module.

With emersion of efficient thermoelectric materials enduring high temperatures, thermoelectric conversion of highly concentrated solar radiation has been examined [16]. A three-dimensional finite-element model of a solar thermoelectric device (STED) based on high-performance thermoelectric materials was developed and analyzed by Yang et al. [17]. They found that heat losses and contact resistance have a substantial effect on the total efficiency of the STED. With neglecting these parameters, the overall efficiency of the STED for operation between 300 K and 700 K could attain 9.95%. Rowe [18] studied a high performance solar powered TEG and found out that the theoretical solar-to-electricity efficiency of Si-Ge alloys operating at 1000 K is 12%, which shows the benefit of reaching high temperatures to provide higher efficiencies.

The direct conversion of highly concentrated solar radiation was experimentally illustrated by directly irradiated TE modules working at 900 K on the hot side and achieving solar-to-electricity efficiencies <1% [19-20]. Pereira et al. [21] presented an experimental investigation on a $Si_{80}Ge_{20}$ thermoelectric material based STEG system which was working under high concentration ratio and high temperature. They also developed a numerical model to predict STEG system efficiency for higher temperatures. Candadai et al. [22] focused on the considering the performance of the solar absorber subsystem in a STEG system which was exposed to solar irradiation flux at different optical concentration ratios (10–100).

A vacuumed enclosure was used by Sudharshan et al. [23] for maximizing power generation of the STEG system. The influence of different enclosure pressures on convective heat loss from the solar selective substrate was examined. They also studied the significance of using a large area absorber and discussed the

effect of these parameters on the open circuit voltage, output power and efficiency of the STEG system. The system performance evaluation was studied numerically by Kossyvakis et al. [24] under different operating conditions followed by a discussion on different approaches to increase output power and to improve system operation based on the solar irradiation intensities. Chen et al. [25] developed a numerical model for a thermal-concentrated STEG system which was considered temperature-dependent properties for thermoelectric materials. They determined and discussed effects of substrate area, thermoelectric element geometry and heat sink efficiency on the power generation by TEG module.

Since the weather condition and consequently daily solar irradiance may vary with the time, the temperature of the TEG, and therefore the power generation and efficiency of the STEG system fluctuate. Oxide TEGs are popular for high-temperature waste heat recovery applications, and Oxide-based materials are more efficient at the high range of temperatures, which makes them suitable for highly concentrated solar radiations.Since there is lack of comprehensive study in literature on investigation of transient behavior of the STEG systems, dynamic response of a high-temperature oxide TEG under different concentrated lights and transient solar radiation, representing semi cloudy weather condition is investigated experimentally. A numerical model is also developed to validate the results and to predict performance of the STEG system at higher solar concentrations and temperatures. This study, furthermore, aims to investigate significant effects of the graphite layer on electrical performance of the STEG. Variation of the hot and cold side temperatures of the TEG, voltage and current generation, and maximum power generation by the TEG is presented and discussed for the STEG modules with and without graphite layer.

2. Experimental procedure

Generally, in the real cases, STEGs comprise a solar collector, a TEG and a heat sink. There are several options for the collector such as flat plate, parabolic troughs, Fresnel lenses and parabolic dishes. In this study concentrated light were provided by a solar simulator. This high-flux solar simulator consists of 10 xenon arc lamps cooled with high-pressure water (see Figure 1). The highly concentrated light, similar to the solar radiation, is obtained in the focal plane using the lamps [26-27]. The solar simulator can simulate up to

11000 suns ($11000\ kW/m^2$) on a focal point. In this study, 6 lamps were used to simulate 0 to 338 suns. In order to create a uniform light over the area of the TEG, shown in Figure 2, an "optical mixer" located horizontally is used, where the STEG module was placed behind it.

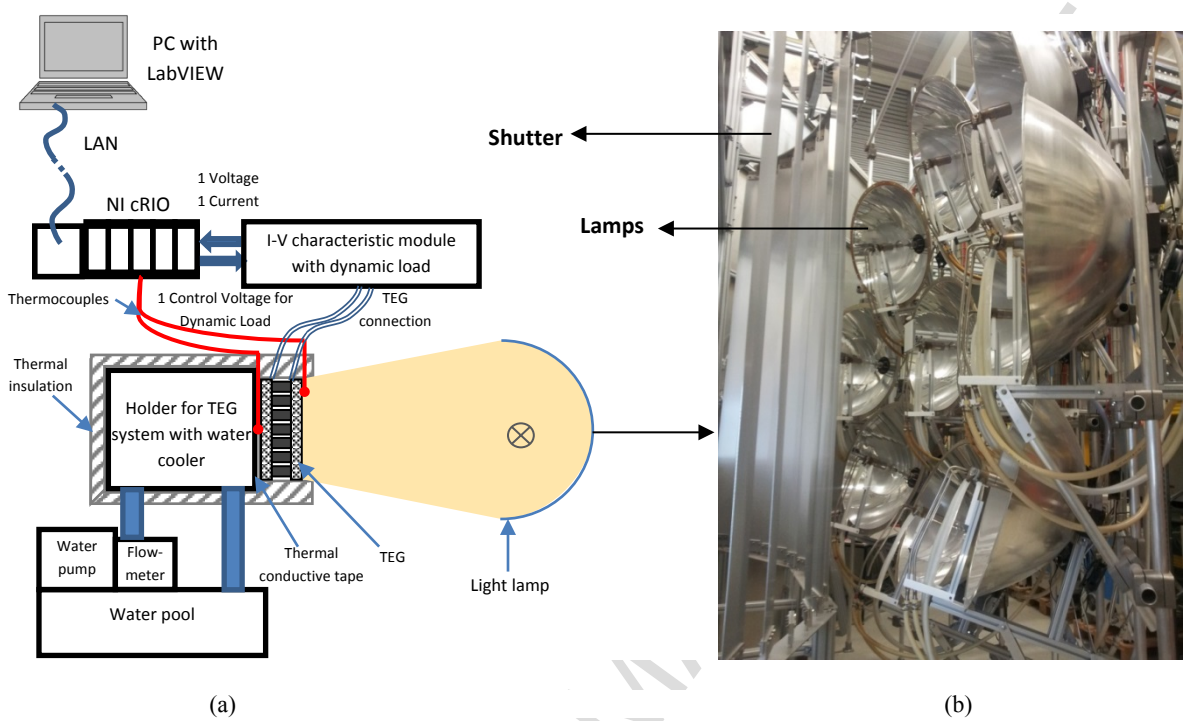

(a) (b)

Figure 1, (a) Schematic of the experimental setup, (b) solar simulator used in current study.

In order to realize a solar intensity map, before evaluation of the performance of the STEGs, radiative flux distribution was measured and calibrated by a thermogage sensor on the exit plane of the mixer for different operation conditions. This was important to select area $(42mm \times 42mm)$ with the most homogenous heat flux received from the solar radiance simulator.

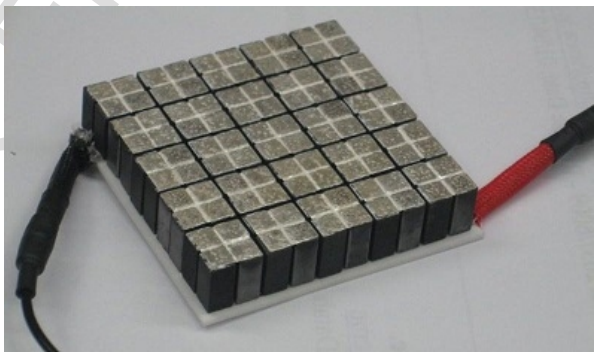

Figure 2, Oxide TEGs used in experiments [28].

The experiments were carried out for high-temperature oxide TEG model CMO-25-42S with 50 uni-couples and size of $42mm \times 42mm$, which the N-Type and P-Type materials are made of $CaMnO_3$ (Mn-113) and $Ca_3Co_4O_3$ (Co-349), respectively [28]. The graphite sheet [29] was attached on the hot side ceramic layer in order to improve absorbance of the solar radiation. Heat exchanger with water, as the working fluid, is used to dissipate heat from the cold side of the TEGs. The volumetric flow rate of the water is kept constant and equal to 5 L/min. I-V variation and the temperatures are measured using data acquisition and control systems based on National Instruments cRIO. Totally, 6 thermocouples were used to measure the temperatures on the hot side (2 thermocouples), cold side (3 thermocouples) and ambient temperature. The imposed dynamic electrical load is based on the dynamic impedance of a capacitor in the charging process (see Figure 3). The capacitor C is connected to the TEG which acts as a voltage source. In order to avoid the connection circuit resistance, the capacitor is pre-charged using the V voltage source with the K switch in the position 2. After the pre-charging process and by closing the K switch (in position 1), at first the capacitor discharges through TEG, and then it starts charging until the capacitor voltage reaches the V_{OC} value. In this manner, it is assured that the entire I-V characterization process is measured from $V_{TEG}=0$ to $V_{TEG}=V_{OC}$.

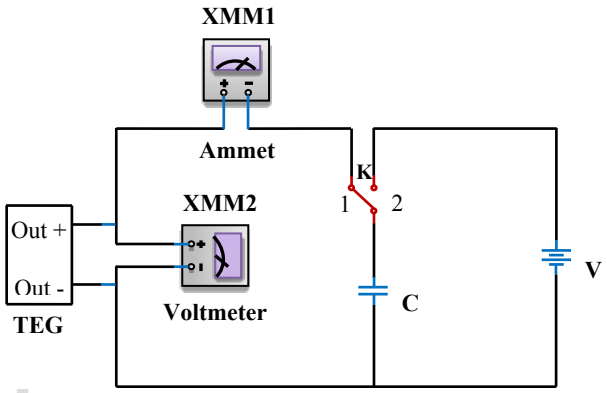

Figure 3, Simplified schematic of the dynamic electrical load.

In order to assess quality of the measurements, uncertainty study is carried out for the method suggested in Ref. [30-31]. To establish precise measurements, the devices were calibrated in advance. Range of the measurements and accuracy of the equipment are illustrated in Table 1. The relative uncertainty of the equipment is as follows [30]:

$$\text{Relative uncertainty} = \frac{0.5 \times \text{resolution}}{\text{measuring value}} \quad (1)$$

Table 1. List of equipment relative uncertainties.

Error sources	Measuring device	Measuring range	Resolution	Relative uncertainty
Temperature	NI 9211 and NI 9213	37.1 °C -499.2 °C and 32.8 °C -371.5 °C	0.07 °C and 0.02 °C	0.09% and 0.03%
Voltage	NI 9215	0.38V -1.98 V	0.002 V	0.26%
Current	NI 9227	0.32A -1.48 A	0.015 A	2.34%

In Table 1 the current has the highest relative uncertainty that is 2.34 %. In addition, an error analysis of the tests is carried out. For solar concentration of 338 suns and in the steady state condition, results for the maximum power, voltage, current and the temperatures are presented in table 2. The mean value ($\overline{X}$) is defined as [31]:

$$\overline{X} = \frac{1}{n}\sum_{i=1}^{n} X_i \quad (2)$$

and the standard deviation (S_X) of the data is given by [31]:

$$S_X = \left[\frac{1}{n-1}\sum_{i=1}^{n}\left(X_i - \overline{X}\right)^2\right]^{1/2} \quad (3)$$

Therefore, the uncertainty (S_J) is:

$$S_J = \frac{S_X}{\overline{X}} \times 100 \quad (4)$$

Results presented in Table 2 illustrate the highest uncertainty is related to the maximum power and is equal to 2.87 %.

Table 2. List of experiment uncertainties.

Variable	1st	2nd	3rd	4th	Mean value	Sample standard deviation	Uncertainty
T_h (ºC)	495.2 °C	498.1 °C	500.8 °C	496.7 °C	497.7 °C	2.38 °C	0.48%
T_c (ºC)	57.7 °C	58.5 °C	59.2 °C	57.2 °C	58.15 °C	0.88 °C	1.51%
V_{OC} (V)	1.96 V	2.00 V	1.99 V	1.97	1.98 V	0.018 V	0.92%
I_{SC} (A)	1.49 A	1.47 A	1.51 A	1.46	1.48 A	0.022 A	1.49%

3. Results of experiment

One particular aspect of this study is to evaluate transient response of the STEG system under variant concentrated solar radiations, representing areas with cloudy condition weather. Accomplishing the experiments in real and random cloudy weather, make it problematic to analyze behavior of the power and efficiency of the STEG system. Therefore, the experiments are carried out using solar simulator, which can provide precise and controlled concentrated solar radiation. Data produced under indoor examinations is, moreover, helpful to check validity of the numerical simulation under the transient boundary condition.

High-temperature oxide-based TEG is examined under variant concentrated solar radiations. The radiative lamps were permanently on during each experiment, while radiation density was regulated by a shutter, as shown in Figure 1. Equivalent radiated solar radiation on the TEGs versus percentage of open-rate of the shutter is shown in Table 3.

Table 3. Solar radiation on the TEGs versus open-rate percentage of the shutter.

Shutter percentage (%)	5	10	15	20	25	30	35	40	45	50	55	60	65	70
Solar radiation (kW/m^2)	30	56	74	107	128	155	176	205	228	252	271	292	315	338

3. 1. STEG without graphite absorber

Figure 4a shows the variation of applied solar radiation, which is time-dependent, representing semi cloudy weather conditions. In order to examine the effect of the solar radiation fluctuation rate on the STEG performance, time interval between each variation of the solar radiation was set to 1 minute. Figure 4a also shows the variation of the hot and cold side temperatures of the STEG with one-minute time interval while the system is already under steady state condition. As can be seen, dynamic responses of the temperatures indicates that temperature distribution in the STEG is directly affected by the rate of the solar radiation. Both of the cold and hot side temperatures follow variations of the solar radiation. Moreover, the cold side temperature follows temperature variation of the hot side but with a delay. Critical material properties in the transient heat transfer, e.g., heat capacity, density and thermal conductivity, caused such delay that the cold side of the STEG senses the effect of the solar fluctuation with few seconds delay.

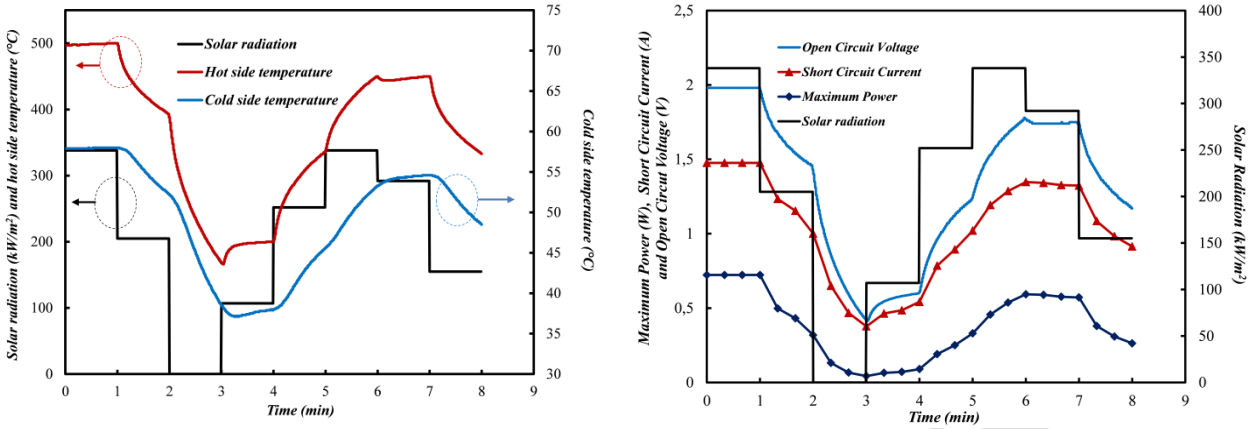

(a) (b)

Figure 4, (a) Solar radiation and hot and cold side temperatures variation, (b) Solar radiation, Open circuit voltage, short circuit current and maximum power for the STEG without graphite layer.

The temperature variations and the delayed response of the cold side temperature to the heat flux fluctuation affect the profile of the electrical potential generated by the STEG. Figure 4b shows the variation of the open circuit voltage, short circuit current and maximum power of the STEG versus time. The open circuit voltage was measured and recorded every 200 milliseconds while the short circuit current and maximum power generations were recorded every 20 seconds. The considered electrical parameters have the same trend and follow the temperature profile. For 1 minute time interval, even at the same solar radiation value (338 suns), the open circuit voltage and short circuit current cannot reach to the peak point in the next cycles since 1 minutes is short for the system to reach the thermally steady state condition.

3. 2. STEG with graphite absorber

Before considering the transient study, the system ran to reach to steady state condition, while the measurements are taken with 1 minute interval. Figure 5 shows the evolution of the I-V-P curves for the solar radiation $107 kW/m^2$ since the radiation began until the STEG reached the steady state condition. In this study, the nominal steady state condition is considered when the variation of the parameters is less than 1% of the mean measured values. The temperature difference between the hot and cold sides of the oxide TEG becomes quasi constant after five minutes.

Power generation of the STEG systems depends on temperature gradient across the TEG module. Therefore

it is important to maximize this parameter to enhance both conversion efficiency and heat flux across the module. Increasing absorbed energy from the solar radiation and, furthermore, reduction of the heat loss from the system are two key parameters to achieve this purpose. In the second part of this investigation, the first parameter is taken into consideration by attaching a graphite sheet on the hot surface. Figure 5b displays the evolution of the I-V-P curves for the solar radiation 107 kW/m^2 from the time when the radiation began until reaching the steady state condition.

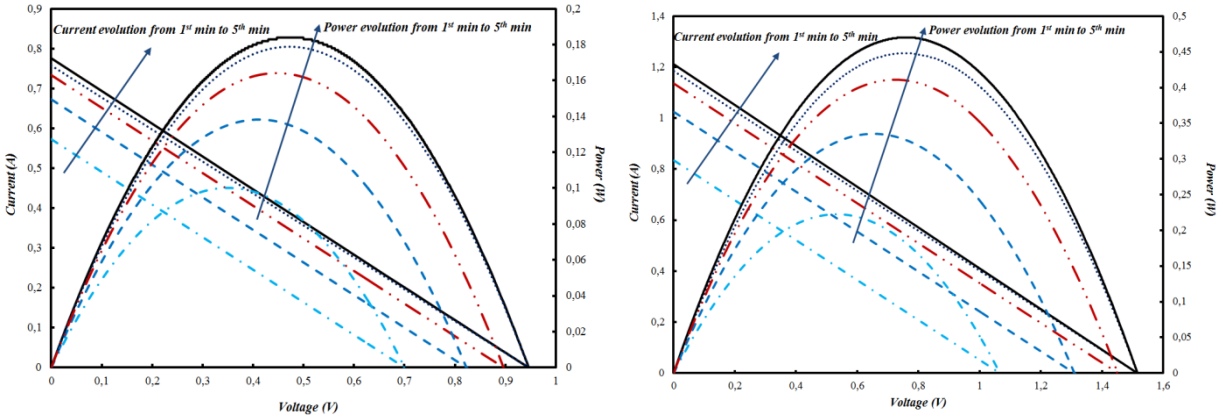

(a) (b)

Figure 5, I-V-P curves for STEG (a) Without graphite layer (b) With graphite layer and solar radiation 107 kW/m^2.

It is worthy to indicate that with attaching cheap graphite sheet on the hot surface of the TEG, power generation increases significantly at the same solar radiation 107 kW/m^2. The graphite layer enhances absorbance coefficient of the radiation, while ceramic substrate of the TEG without the graphite sheet has higher reflection coefficient compared to the TEG with the graphite layer. As can be seen in Figure 5b, power generation in the TEG with the graphite layer is 2.5 times higher than that one in the TEG without the graphite layer (See Figure 5a). Consequently, the efficiency (which is defined as ratio of the output power to the input solar radiation) of the STEG module with graphite sheet (0.25%) is 2.5 times of the STEG system without the graphite sheet (0.1%).

To determine transient response of the STEG systems, the same patterns with different values of the solar radiation are considered. The graphite sheet used in the experiments was self-adhesive, where the adhesive could tolerate maximum 400 °C. The imposed solar radiation should have been managed in a way that the

temperature on the hot side of the TEG does not exceed 400 °C (See Figure 6a). Therefore, for each time step, solar radiation on the STEG with the graphite sheet was taken 1/3 of the solar radiation on the STEG without the graphite sheet (See Figure 6). Therefore the maximum imposed solar radiation which was fixed 117.3 suns in this study.

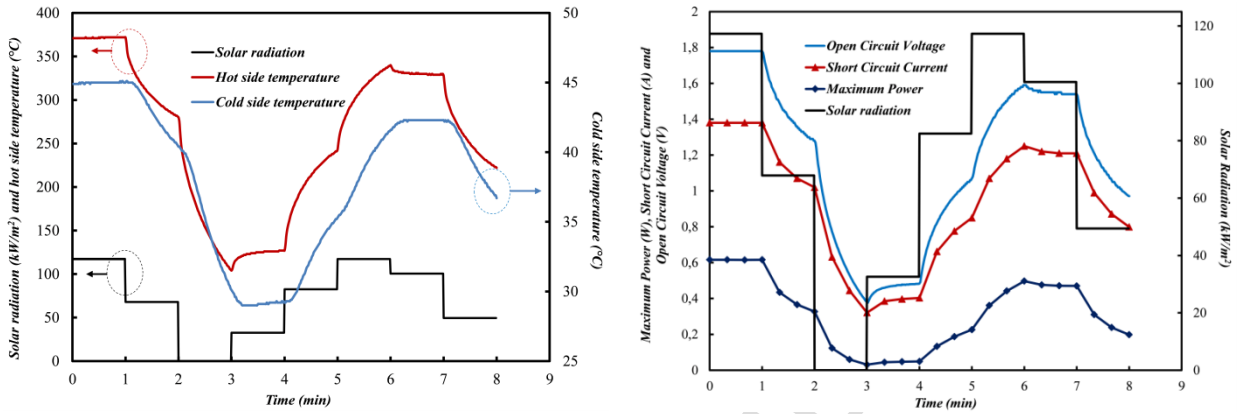

(a) (b)

Figure 6, (a) Solar radiation and hot and cold side temperatures variation, (b) Solar radiation, Open circuit voltage, short circuit current and maximum power for the STEG with graphite layer.

Figure 6b illustrates the variations of the open circuit voltage, short circuit current and maximum power versus time. By comparison the results of this figure and those shown in Figure 4b, it can be observed that, the magnitude of these parameters are close to each other for the both cases, for the STEGs with and without the graphite layer. It is worthy to note that the applied solar radiation on the STEG without the graphite layer is higher than that one of the STEG with graphite layer. This enhancement shows the substantial effect of the graphite layer, which can absorb more input energy. For low solar concentration application but high-temperature STEGs, this technique is useful to compensate the low input energy and obtain higher power generation.

4. Modeling and simulation

As known, due to higher figure of merit at higher temperatures, oxide-based TEGs perform with higher efficiency and power generation when the operating temperature increases [32-33]. In the second part since increment of the STEG hot temperature was limited to the adhesive paste of the graphite sheet, an unsteady-

state one-dimensional heat transfer model is developed in this section to predict performance of the STEG at high solar radiations. Finite volume method [34] was applied to solve the obtained partial differential equations using energy conservation law. All elementary and accessorial effects of the TEG including the Seebeck effect, Peltier effect, Thomson effect, Joule effect and Fourier effect are considered in the derived equations. Unlike conventional and simple models of thermoelectric materials in Multi-physics modeling, where thermoelectric properties of the energy materials are taken constant [35-37], in current work properties of the P-Type and N-Type thermoelectric material including the Seebeck coefficient, thermal and electrical conductivities and, as a result, figure of the merit are considered temperature dependent [38-39]. The physical model of the STEG system is displayed in Figure 7.

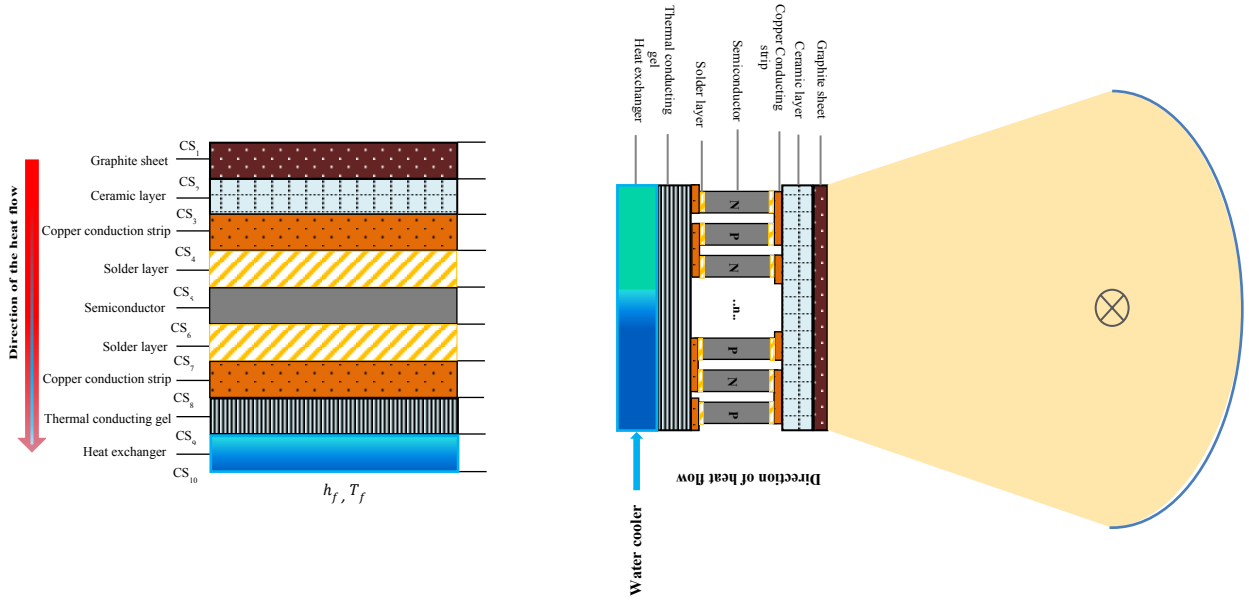

Figure 7, One-dimensional heat transfer physical model of the STEG system.

Different layers of the STEG considered in the calculation are shown in Figure 7. A group of non-linear equations is acquired applying energy conservation law for each contact surface of the STEG system. Considering all the effects in a TEG leads equations for the different layers of the TEG as follow:

On the top surface of the graphite layer (CS1) [3]:

$$\rho_{Gr} c_{Gr} V_{Gr} \frac{\partial T_{Gr}}{\partial t} = \alpha \times SC \times G \times A_{Gr} - Q_{rad} + KA\left(\frac{\partial T}{\partial x}\right)\Big|_{x = CS_1^b} \qquad (5)$$

where, Q_{rad} is the radiation loss from the top layer of the STEG and could be obtained by equation (6) [40]:

$$Q_{rad} = \varepsilon\sigma A_{Gr}\left(T_{Gr^t}{}^4 - T_{sky}{}^4\right) \quad (6)$$

where $\sigma = 5.67 \times 10^{-8} W/m^2K^4$ and T_{sky} is defined as a function of the ambient temperature based on an investigation by Nowak [41].

For the contact surfaces, 2 to 5, equation 7 with corresponding constants that are presented in table 4 is used.

$$\rho_i c_i V_i \frac{\partial T_i}{\partial t} = C_1 k_{(i-1)} n_{(i-1)} A_{(i-1)} \left(\frac{\partial T}{\partial x}\right)\Big|_{x=CS_i^t} - C_2 \frac{n_{(i-1)} I^2 r_{(i-1)}}{2} - C_3 k_i n_i A_i \left(\frac{\partial T}{\partial x}\right)\Big|_{x=CS_i^b} + C_4 n_i S_{i,h} I T_{i,h} - C_5 \frac{n_i I^2 r_{i,l}}{2} - C_6 \frac{n_i \tau_l I\left(T_{i,h} - T_{i,2}\right)}{2} \quad (7)$$

Table 4. Corresponding constants for different layers in the equation (7).

i	C_1	C_2	C_3	C_4	C_5	C_6
2	1	0	1	0	0	0
3	1	0	1	0	1	0
4	1	1	1	0	1	0
5	1	1	1	1	1	1

For the contact surfaces, 6 to 9, equation 8 with corresponding constants that are shown in table 5 is used.

$$\rho_i c_i V_i \frac{\partial T_i}{\partial t} = C_7 k_i n_i A_i \left(\frac{\partial T}{\partial x}\right)\Big|_{x=CS_i^b} - C_8 n_i S_{i,h} I T_{i,h} - C_9 \frac{n_i I^2 r_{i,m}}{2} - C_{10} \frac{n_i \tau_m I\left(T_{i,m} - T_{i,c}\right)}{2} - C_{11} k_{(i+1)} n_{(i+1)} A_{(i+1)} \left(\frac{\partial T}{\partial x}\right)\Big|_{x=CS_i^t} + C_{12} \frac{n_{(i+1)} I^2 r_{(i+1)}}{2} \quad (8)$$

Table 5. Corresponding constants for different layers in the equation (8).

i	C_7	C_8	C_9	C_{10}	C_{11}	C_{12}
6	1	1	1	1	1	1
7	1	0	1	0	1	-1
8	1	0	1	0	1	0
9	1	0	0	0	1	0

On contact surface between the heat exchanger base and the working fluid (CS10) [3]:

$$\rho_{hx} c_{hx} V_{hx} \frac{\partial T_{hx}}{\partial t} = k_{hx} A_{hx} \left(\frac{\partial T}{\partial x}\right)\Big|_{x=CS_{10}^t} + h_f A_f \left(T_{hx,2} - T_f\right) \quad (9)$$

Solving the abovementioned equations leads to having time-dependent temperatures of different contact surfaces in the TEG module. Therefore, considering the influence of the Thomson effect, the electromotive force (EMF) of the TEG device is [3]:

$$E = n_{sc}\left[S_{sc,h}T_{sc,h} - S_{sc,c}T_{sc,c} - \sum_{i=1}^{m-1}\tau_i(T_i - T_{i+1})\right] \quad (10)$$

The electrical resistance of the copper conduction strip, solder layer, and semiconductors are composed the internal electrical resistance of the TEG module, therefore [3]:

$$R_i = \left(n_{ccs}r_{ccs} + n_{sl}r_{sl} + n_{sc}\sum_{i=1}^{m}r_{sc,i}\right) \quad (11)$$

and the output power will be defined as [3]:

$$P_{TEG} = \left(E/(R_i + R_L)\right)^2 R_L = \left[n_{sc}\left[S_{sc,h}T_{sc,h} - S_{sc,c}T_{sc,c} - \sum_{i=1}^{m-1}\tau_i(T_i - T_{i+1})\right]\right]^2 R_L \Big/ \left[\left(n_{ccs}r_{ccs} + n_{sl}r_{sl} + n_{sc}\sum_{i=1}^{m}r_{sc,i}\right) + R_L\right]^2 \quad (12)$$

Therefore, the instantaneous efficiency of the TEG can be calculated as follows [42]:

$$\eta_{TEG} = {}^{P_{TEG}}/\left(SC \times G \times A - Q_{rad}\right) \quad (13)$$

In the numerical model, the TEG is assumed thermally insulated. Therefore, excluding the heat transfer from the upper surface of the STEG system by radiation, heat loss from the STEG to the ambient is neglected. Moreover, the convective and radiative heat transfers between TE elements in the TEG module are taken zero. The input heat flux changes by variation of the solar radiation. Identical patterns for the solar radiation are applied to the both experimental procedure and numerical study. In the other word, based on equation 5, the boundary condition on the STEG top surface depends on the solar concentration and consequently the solar radiation inserted to the STEG system. Since the set time step for variation of the solar concentration is one minute, the insert solar radiation to the system changes every minute.

The boundary condition in the cold side of the STEG system is considered as convective heat transfer with the overall heat transfer coefficient of U. As mentioned, a parallel-pipe copper heat sink with dimensions 9cm × 9cm × 1cm using water as the coolant fluid is utilized in the experiments. The overall heat transfer coefficient, U, can be achieved using the input heat flux, mass flow rate, inlet temperature and outlet

temperature of the heat sink as follows [43]:

$$U = \frac{q}{A\Delta T_{lm}} \tag{14}$$

where

$$\Delta T_{lm} = \frac{\Delta T_1 - \Delta T_2}{\ln(\Delta T_1/\Delta T_2)} \tag{15}$$

In this equation, ΔT_{lm} is the log mean temperature difference. By equalizing the heat flux introduced in equation 14 with the last term in equation 9, the heat transfer coefficient used for the numerical model can be estimated.

5. Results of performance analysis

In order to predict and evaluate the performance of the STEG system at higher solar concentrations, a numerical model is developed. The existing model can trace the temperature fluctuation for every variation of the solar radiations. In order to validate the numerical results, the solar radiation pattern of Figure 6 is used as input to the model. Figure 8 shows the numerical and experimental results for the mentioned pattern. As can be seen, the numerical simulation results are in a close agreement with the experimental ones. The average error between the numerical simulation and experimental results is 7 %.

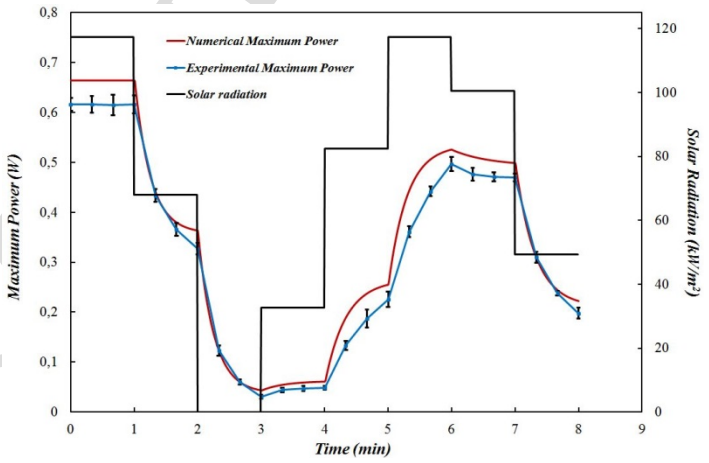

Figure 8, Numerical and experimental results of the maximum power versus time for the STEG with the graphite layer.

In order to express the potential errors related to each measurement, the error bars are shown in Figure 8. As

can be seen in Table 6, four duplications are carried out for each experimental set and values for the maximum power are obtained and presented in this table. The error bars illustrated in Figure 8 represent the standard deviation (SD) of the data set. The narrow SD bars in this figure indicate that the experimental data are clumped around the mean value with low scatter. Therefore, the mean value, as a representative number for the data set, has high accuracy and reliability. It can be seen that, for the 4th and 7th minutes, the SD error bars are overlapped, indicating that the differences are not statistically significant for these moments.

In order to evaluate the estimated population parameter rather than a single value or a point estimation, the confidence intervals are, furthermore, obtained. Table 6 presents 95% confidence interval obtained from equation 16 [44] as the most common confidence level.

$$95\%\ Confidence\ Interval = \overline{X} \pm 1.96 \times \frac{S_X}{\sqrt{n}} \tag{16}$$

Table 6. Mean values, standard deviations and 95 % confidence intervals for the maximum power.

Time (min)	trial 1	trial 2	trial 3	trial 4	Mean value	standard deviation	Maximum 95 % Confidence Interval	Minimum 95 % Confidence Interval
0	0.624 W	0.610 W	0.621 W	0.608 W	0.616 W	0.008	0.624 W	0.608 W
0.333	0.630 W	0.603 W	0.631 W	0.601 W	0.616 W	0.016	0.632 W	0.600 W
0.667	0.633 W	0.599 W	0.632 W	0.595 W	0.615 W	0.021	0.635 W	0.595 W
1.000	0.629 W	0.605 W	0.633 W	0.597 W	0.616 W	0.018	0.633 W	0.599 W
1.333	0.444 W	0.425 W	0.446 W	0.420 W	0.434 W	0.013	0.447 W	0.421 W
1.667	0.372 W	0.361 W	0.380 W	0.351 W	0.366 W	0.013	0.378 W	0.354 W
2.000	0.341 W	0.322 W	0.331 W	0.314 W	0.327 W	0.012	0.338 W	0.316 W
2.333	0.136 W	0.116 W	0.127 W	0.113 W	0.123 W	0.011	0.133 W	0.113 W
2.667	0.061 W	0.055 W	0.066 W	0.057 W	0.060 W	0.005	0.065 W	0.055 W
3.000	0.029 W	0.034 W	0.035 W	0.027 W	0.031 W	0.004	0.035 W	0.027 W
3.333	0.045 W	0.039 W	0.049 W	0.043 W	0.044 W	0.004	0.048 W	0.040 W
3.667	0.053 W	0.050 W	0.044 W	0.041 W	0.047 W	0.005	0.052 W	0.042 W
4.000	0.046 W	0.052 W	0.044 W	0.052 W	0.049 W	0.004	0.053 W	0.044 W
4.333	0.128 W	0.142 W	0.122 W	0.139 W	0.133 W	0.009	0.142 W	0.124 W
4.667	0.173 W	0.193 W	0.171 W	0.210 W	0.187 W	0.018	0.205 W	0.169 W
5.000	0.215 W	0.240 W	0.211 W	0.239 W	0.226 W	0.015	0.241 W	0.211 W
5.333	0.348 W	0.368 W	0.355 W	0.372 W	0.361 W	0.011	0.372 W	0.350 W
5.667	0.431 W	0.450 W	0.433 W	0.448 W	0.441 W	0.010	0.450 W	0.431 W
6.000	0.490 W	0.505 W	0.482 W	0.513 W	0.498 W	0.014	0.511 W	0.484 W
6.333	0.485 W	0.467 W	0.489 W	0.463 W	0.476 W	0.013	0.488 W	0.464 W
6.667	0.461 W	0.475 W	0.466 W	0.482 W	0.471 W	0.009	0.480 W	0.462 W
7.000	0.463 W	0.480 W	0.471 W	0.464 W	0.470 W	0.008	0.477 W	0.462 W
7.333	0.302 W	0.320 W	0.299 W	0.318 W	0.310 W	0.011	0.320 W	0.299 W
7.667	0.237 W	0.239 W	0.232 W	0.243 W	0.238 W	0.005	0.242 W	0.233 W
8.000	0.210 W	0.186 W	0.192 W	0.204 W	0.198 W	0.011	0.209 W	0.187 W

In order to reach the higher temperatures, the input solar radiation should be increased. In this study, the maximum temperature for the oxide-based TEG is limited to 950 °C, while the simulation has capability to evaluate the system performance at higher temperatures. Figure 9 shows the imposed solar radiation and calculated power generation in the numerical study compared to the results presented in Figure 8. As shown, the power generation by the STEG system, using the black pattern, causes a significant increment in power generation by the TEG. Increment in the heat flux and temperature and, consequently, the figure of merit of the oxide-based TEG, as key parameters in power generation, causes such a substantial enhancement in the power generation.

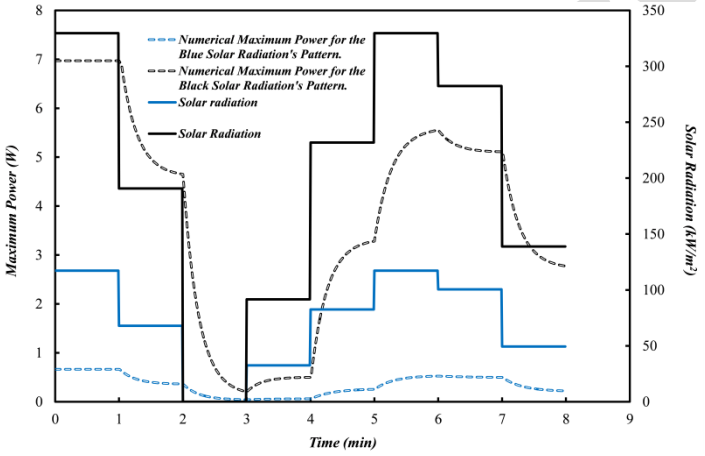

Figure 9, Numerical power generation by the STEG with graphite layer for different solar radiation patterns versus time.

Although this study aims to evaluate transient behavior of the oxide-based and high-temperature STEG system, a steady-state analysis is performed over a wide range of solar radiations in order to valid results of the considered STEG system, and furthermore to compare the results with other investigations. Efficiency of an oxide -based STEG system studied by Tomes et al. [19] was less than 1 % for the temperatures up to 900 °C. Pereira et al. [21] found maximum theoretical efficiency of 1.8 % for a $Si_{80}Ge_{20}$ STEG system. Figure 10 indicates variation of the maximum power and efficiency of the STEG system with the graphite sheet, for different solar radiations. Power generation and efficiency corresponding to solar radiation of $329\ kW/m^2$ are 6.97 W and 1.2 %, respectively, while these values are 0.62 W and 0.3 %, respectively at solar radiation of $117\ kW/m^2$. It shows that both output power and efficiency of the system increase with enhancement in

the solar radiation.

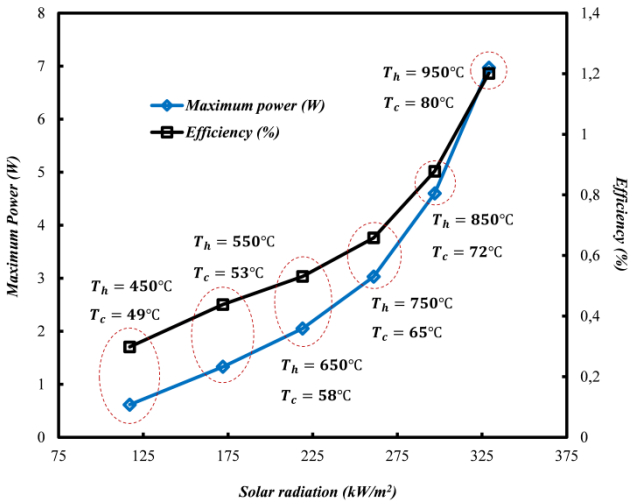

Figure 10, Numerical results of maximum power and efficiency of the STEG system versus solar radiation.

6. Conclusions

Influence of a graphite layer on critical electrical output parameters of oxide-based high-temperature STEG was examined under transient solar radiations. I-V-P characteristics, hot and cold side temperatures, open circuit voltage, short circuit current and maximum power generated by the STEG with graphite layer were obtained, discussed, and compared with those one of the STEG without the graphite layer. For the both STEGs same radiation pattern, but different values of solar radiation, were considered to simulate semi cloudy weather condition. The I-V-P plots show that both systems reach to the steady state after 5 minutes. The hot and cold side temperatures of the STEGs and the electrical output are strongly affected by the sharp fluctuation of the solar radiation. The results show that by attaching the graphite layer on the hot surface of the TEG, the output power increases 2.5 times at the same level of solar radiation. Numerical simulation is, moreover, carried out to predict performance of the STEG system with graphite sheet at high level of solar concentrations and temperatures. The results indicate that the power generation and efficiency of the system increase significantly at high solar radiations.

Acknowledgment

The authors would like to acknowledge financial support from Access to Research Infrastructures activity under 7th Framework Programme, SFERA 2, Grant Agreement n. 312643. The authors are thankful to the team from the Solar Technology Laboratory of Paul Scherrer Institute, Villigen, Switzerland (Ms.Y. Baeuerle, Mr. D. Wuillemin, Mr. V. Schnetzler and Mr. C. Wieckert), where all the measurements of this study were performed.

References

[1] Sajjad Mahmoudi Nezhad, Alireza Rezaniakolaei, Lasse Aistrup Rosendahl, Experimental Study on Effect of Operating Conditions on Thermoelectric Power Generation, Energy Procedia 142 (2017) 558–563.

[2] S. Mahmoudinezhad, A. Rezania, A.A. Ranjbar, L.A. Rosendahl, Transient behavior of the thermoelectric generators to the load change; an experimental investigation, Energy Procedia 147, 537-543.

[3] S. Mahmoudinezhad, A. Rezania, L. A. Rosendahl, Behavior of hybrid concentrated photovoltaic-thermoelectric generator under variable solar radiation, Energy Conversion and Management 164 (2018) 443–452.

[4] Sajjad Mahmoudinezhad, Shaowei Qing, Alireza Rezaniakolaei, Lasse Aistrup Rosendahl, Transient Model of Hybrid Concentrated Photovoltaic with Thermoelectric Generator, Energy Procedia 142 (2017) 564–569.

[5] M. Telkes, Solar thermoelectric generators, J. Appl. Phys. 25 (1954) 765.

[6] H. Goldsmid, J. Giutronich and M. Kaila, Solar thermoelectric generation using bismuth telluride alloys, Sol. Energy. 24 (1980) 435–440.

[7] Petr Tomeš, Matthias Trottmann, Clemens Suter, Myriam Heidi Aguirre, Aldo Steinfeld, Philipp Haueter and Anke Weidenkaff, Thermoelectric Oxide Modules (TOMs) for the Direct Conversion of Simulated Solar Radiation into Electrical Energy, Materials 3 (2010) 2801-2814; doi:10.3390/ma3042801.

[8] S. Mahmoudinezhad, P.A. Cotfas, D.T. Cotfas, A. Rezania, L.A. Rosendah, Performance evaluation of a high-temperature thermoelectric generator under different solar concentrations, Energy Procedia 147, 624-630.

[9] Daniel Kraemer, Bed Poudel, Hsien-Ping Feng, J. Christopher Caylor, Bo Yu, Xiao Yan, Yi Ma, Xiaowei Wang, Dezhi Wang, Andrew Muto, Kenneth McEnaney, Matteo Chiesa, Zhifeng Ren and Gang Chen, High-performance flat-panel solar thermoelectric generators with high thermal concentration, Nat. Mater. 10 (2011) 532–53.

[10] Daniel Kraemer, Kenneth McEnaney, Matteo Chiesa, Gang Chen, Modeling and optimization of solar thermoelectric generators for terrestrial applications, Sol. Energy. 86 (2012) 1338–1350.

[11] H. A. MADKHALI, A. HAMIL and H. LEE, Validation, Optimization and Simulation of a Solar Thermoelectric Generator Model, J. Electron. Mater. (2017) DOI: 10.1007/s11664-017-5723-2.

[12] Daniel Kraemer, Qing Jie, Kenneth McEnaney, Feng Cao, Weishu Liu, Lee A.Weinstein, James Loomis, Zhifeng Ren and Gang Chen, Concentrating solar thermoelectric generators with a peak efficiency of 7.4%, Nat. Energy. (2016) DOI: 10.1038/NENERGY.2016.153.

[13] P. LI, L. CAI, P. ZHAI, X. TANG, Q. ZHANG, and M. NIINO, Design of a Concentration Solar Thermoelectric Generator, J. Electron. Mater. Vol. 39 No. 9, (2010) DOI: 10.1007/s11664-010-1279-0.

[14] M. Eswararmoorthy and S. Shanmugam, Thermodynamic analysis of solar parabolic dish thermoelectric generator, Int. J. Renewable Energy Technology. 1 (2010) 348-360.

[15] P. Cheruvu, V. P. Kumar & H. C. Barshilia, Experimental analysis and evaluation of a vacuum enclosed concentrated solar thermoelectric generator coupled with a spectrally selective absorber coating, Int. J. Sustainable Eng. (2017) DOI: 10.1080/14786451.2017.1365866.

[16] A. Weidenkaff, R. Robert, M. H. Aguirre, L. Bocher, T. Lippert, and S. Canulescu, Development of Thermoelectric Oxides for Renewable Energy Conversion Technologies, Renewable Energy. 33 (2008) 342-347.

[17] T. YANG, J. XIAO, P. LI, P. ZHAI, and Q. ZHANG, Simulation and Optimization for System Integration of a Solar Thermoelectric Device, J. Electron. Mater. Vol. 40, No. 5 (2011) DOI: 10.1007/s11664-010-1471-2.

[18] D. M. Rowe, A High Performance Solar Powered Thermoelectric Generator, Appl. Energy. 8 (1981) 269-273.

[19] P. Tomeš, M. Trottmann, C. Suter, M. H. Aguirre, A. Steinfeld, P. Haueter and A. Weidenkaff, Thermoelectric Oxide Modules (TOMs) for the Direct Conversion of Simulated Solar Radiation into Electrical Energy, Materials. 3 (2010) 2801-2814.

[20] P. Tomeš, R. Robert, L. Bocher, M. Trottmann, M. H. Aguirre, A. Weidenkaff, P. Haueter, A. Steinfeld, and J. Hejtmánek, Direct conversion of simulated solar radiation into electrical energy by a perovskite thermoelectric oxide module (TOM), Proc. Materials Science and Technology Conference and Exhibition, MS&T08. 1 (2008) 429-435.

[21] A. Pereira, T. Caroff, G. Lorin, T. Baffie, K. Romanjek, S. Vesin, K. Kusiaku, H. Duchemin, V. Salvador, N. Miloud-Ali, L. Aixala, J. Simon, High temperature solar thermoelectric generator- Indoor characterization method and modeling, Energy. 84 (2015) 485–492.

[22] Aaditya A. Candada, V. Praveen Kumar, Harish C. Barshilia, Performance evaluation of a natural convective-cooled concentration solar thermoelectric generator coupled with a spectrally selective high temperature absorber coating, Sol. Energy Mater. Sol. Cells. 145 (2016) 333–341.

[23] K. Y. Sudharshan, V. Praveen Kumar, Harish C. Barshilia, Performance evaluation of a thermally concentrated solar thermo-electric generator without optical concentration, Sol. Energy Mater. Sol. Cells. 157 (2016) 93–100.

[24] D. N. Kossyvakis, C. G. Vossou, C. G. Provatidis, E.V. Hristoforou, Computational analysis and performance optimization of a solar thermoelectric generator, Renewable Energy. 81 (2015) 150–161.

[25] Wei-Hsin Chen, Chien-Chang Wang, Chen-I Hung, Chang-Chung Yang, Rei-Cheng Juang, Modeling and simulation for the design of thermal-concentrated solar thermoelectric generator, Energy. 64 (2014) 287–297.

[26] J. Petrasch, P. Coray, A. Meier et al, A novel 50 kW 11,000 suns high-flux solar simulator based on an array of xenon arc lamps, ASME Journal of Solar Energy Engineering. vol. 129, no. 4 (2007) pp. 405–411.

[27] I. Alxneit and H. Schmit, Spectral characterization of PSI's high-flux solar simulator, J. Sol. Energy Eng. vol. 134, no. 1 (2012) Article ID 011013.

[28] Thermal Electronics Corp. Part# CMO-25-42S, http://espressomilkcooler.com/wp-content/uploads/2014/06/CMO-25-42S-OXIDE-NEW.pdf, [accessed: October 2018].

[29] Panasonic "PGS" Graphite Sheets, https://www.alliedelec.com/m/d/33d2b002cce5b5a6aceddaf0748811b6.pdf, [accessed: October 2018].

[30] Kline SJ. The purpose of uncertainty analysis. ASME J Heat Transfer 1985;117:153-60.

[31] Coleman HW, Steele Jr WG. Experimentation and uncertainty analysis for engineers. New York:Wiley; 1989.

[32] Supasit Paengson, Panida Pilasuta, Kunchit Singsoog, Wanatchaporn Namhongsa, Wairut Impho, Tosawat Seetawan, Improvement in thermoelectric properties of $CaMnO_3$ by Bi doping and hot pressing, Materials Today: Proceedings 4 (2017) 6289–6295.

[33] Richard Tuley and Kevin Simpson, ZT Optimization: An Application Focus, Materials 2017, 10, 309; doi:10.3390/ma10030309.

[34] Patankar SV. Numerical heat transfer and fluid flow. USA: Taylor & Francis; 1980.

[35] A. Rezania, L. A. Rosendahl, Evaluating thermoelectric power generation device performance using a rectangular microchannel heat sink, Journal of Electronic Materials, 40(5) (2011), pp. 481-488.

[36] A. Rezania, L. A. Rosendahl, A comparison of micro-structured flat-plate and cross-cut heat sinks for thermoelectric generation application, Energy Conversion and Management 101 (2015) 730-737.

[37] A. Rezania, L. A. Rosendahl, New configurations of micro plate-fin heat sink to reduce coolant pumping power, Journal of Electronic Materials, 41(6) (2012), pp. 1298-1304.

[38] M. Backhaus- Ricoult, J. Rustad, L. Moore, C. Smith, J. Brown, Semiconducting large bandgap oxides as potential thermoelectric materials for high-temperature power generation, Appl. Phys. A (2014) 116:433–470.

[39] Hongchao Wang, Wenbin Su, Jian Liu, Chunlei Wang, Recent development of n-type perovskite thermoelectrics, J Materiomics 2 (2016) 225-236.

[40] S. Mahmoudinezhad, A. Rezania, D.T. Cotfas, P.A. Cotfas, L.A. Rosendahl, Experimental and Numerical Investigation of Hybrid Concentrated Photovoltaic–Thermoelectric Module under Low Solar Concentration. Energy 159 (2018) 1123-1131.

[41] Nowak H. The sky temperature in net radiant heat loss calculations from low-sloped roofs. Infrared Phys 29 (1989) 231–2.

[42] Rezania A, Rosendahl LA. Feasibility and parametric evaluation of hybrid concentrated photovoltaic-thermoelectric system. Appl Energy 187 (2017) 380–9.

[43] Afgan, N., M. Carvalho, A. Bar-Cohen, D. Butterworth, and W. Roetzel, eds., 1994, New Developments in Heat Exchangers, Gordon & Breach, New York.

[44] "Checking Out Statistical Confidence Interval Critical Values – For Dummies", www.dummies.com, Retrieved: 2016-02-11.

PAPER 5: REFERENCE [204]

Transient Response of Bi-Te Based Thermoelectric Generator to Variant Solar Radiation; an Experimental and Numerical Study

Sajjad Mahmoudi Nezhad, Petru Adrian Cotfas, Alireza Rezania, Daniel Tudor Cotfas, Lasse Rosendahl

The paper is under review in the Renewable Energy Journal

Transient Response of Thermoelectric Generators to Bi_2Te_3 and Zn_4Sb_3 Energy Harvester Materials under Variant Solar Radiation

S. Mahmoudinezhad[1], P.A. Cotfas[2], D.T. Cotfas[2], L.A. Rosendahl[1], A. Rezania[1]

[1]*Department of Energy Technology, Aalborg University, Pontoppidanstræde 111, Aalborg DK-9220, Denmark*

[2]*Electrical Engineering and Computer Science Faculty, Transilvania University of Brasov, 500036 Brasov, Romania*

Abstract

Some special features like having no moving parts and long lifetime and being highly reliable make thermoelectric generators (TEGs) a proper choice to convert solar energy into electricity. In this work, performance of Bi_2Te_3 and Zn_4Sb_3 solar thermoelectric generators (STEGs) are studied using both experimental and numerical approaches. Variation of the temperatures of the hot and cold sides of the TEGs, open circuit voltage, short circuit current and maximum power generation are obtained and discussed. Effect of thermoelectric material properties and geometry of the thermoelectric elements on performance of the STEGs is examined. Results of the developed numerical model using finite volume method are in good agreement with the experimental data. Performance of the TEG without graphite layer and with the same solar radiation condition is investigated and compared with the TEG with graphite layer. The results shows that, applying the graphite layer significantly enhances performance of the STEGs.

Keywords: Solar Radiation, Thermoelectric Generators, Solar Simulator, Transient Response, Finite Volume Method, Material Properties.

1. Introduction

In the last decades, the use of energy has become a vital concern owing to the quick growth in energy demand. Due to fast depletion and other environmental concerns of the fossil fuels, the demand of clean energy is growing quickly. Since solar energy is free, clean and inexhaustible, it can be an ideal alternative energy resource. Thermoelectric generators are solid state devices with some special features that make them appropriate choice in different applications [1-2]. Solar thermoelectric generator (STEG) technology is promising for power generation, especially with falling costs in recent years.

Nomenclature

Abbreviation	
CS	Contact surface
EMF	Electromotive force
Gr	Graphite
SC	Solar concentration
TE	Thermoelectric
TEG	Thermoelectric generator
ZT	Figure of merit

Greek script	
α	Seebeck coefficient, V/K
ε	Emissivity
η	Conversion efficiency, %
σ	Stefan-Boltzmann constant, $W/m^2 K^4$
Δ	Increment
τ	Thomson coefficient, V/K
ρ	Density, kg/m^3
γ	Electrical conductivity, S m

Latin script	
A	Area, m^2
C	Specific heat capacity, J/ kg. K
G	Solar radiation, W/m^2
h	Heat transfer coefficient, W/ m^2K
I	Current, A
K	Thermal conductivity, W/mK
L	length, m
n	Number of thermocouples
P	Power, W
q	Inner heat source, W
Q	Heat loss/ heat transfer, W
r	Resistance, Ω
T	Temperature, K
t	Time, S
x	Heat transfer direction

Subscripts	
a	Ambient
c	Cold junction
f	Cooling fluid
Gr	Graphite
h	Hot junction
hx	Heat exchanger
ccs	Copper conduction strip
max	Maximum
rad	Radiation
ref	Reference
sky	Sky
TEG	Thermoelectric generator

superscripts	
b	The bottom contact surface
t	The top contact surface

Many studies have been done for characterizing the STEG systems over the medium and high-temperature ranges [3-4] and low-temperature range [5-23]. Telkes [5] presented a STEG system which the maximum efficiency for flat-panel STEG system arrived at 0.63%. For less than 50 times optical concentration, the efficiency was obtained 3.35%. The outcomes of this study made a lot of attractions between the researchers to use TEGs to convert solar energy into electrical power [6-9].

The theoretical efficiency of STEGs is investigated by Chen [10] and it is found that in the low-temperature range (150-250°C) which Bi_2Te_3-based materials are appropriate and in an evacuated environment, STEGs can have high efficiency with little or no optical concentration. McEnaney et al. [11] studied numerically a concentrating STEG system. They found that for a geometric optical concentration ratio of 45 and with current skutterudite and bismuth telluride materials, concentrating STEGs can reach efficiencies more than 10%. Kraemer et al. [12] presented the results of an experimental study of a promising flat-plate STEG system which reached a maximum efficiency of 4.6% under 1 kW/m^2 condition. In another investigation,

Kraemer et al. [13] developed a model and an optimization approach for earth-based STEGs. For the Bi_2Te_3-based STEG which they considered in their model, the efficacy was achieved to 5%. In order to increase the efficiency of the STEG systems Madkhali et al. [14] proposed simulation and optimization of a prototype STEG system. The results indicated that with using two cover glasses and radiation shields, the maximum efficiency of the STEG system will reach to 7%. Later in 2016, Kraemer et al. [15] enhanced efficiency of the STEG to 9.6% by an optically concentrated normal solar irradiance of 211 kW/m^2. However, the obtained system efficiency was 7.4%.

To realize the impact of different loss mechanisms that affect the efficiency of the STEG system, Mazumder [16] established a coupled fluid-thermal-electric three-dimensional computational model of a STEG. It was found that the main parameters for the loss in efficiency are the irreversible losses owing to heat and current conduction and Joule heating. A numerical model of a flat-plate STEG system is developed by Liu et al. [17]. The effect of the thermal concentration ratio and also geometrical parameters of the TEG on the performance of the STEG were examined. They found that the length of the TEG legs and the thermal concentration ratio are the main factors in power generation and efficiency of the STEG system. Chen et al. [18] used both numerical and experimental approaches to examine the performance of a thermal-concentrated STEG system. They tested and evaluated three dissimilar geometry types of TEG. The results show that the smallest TEG has the maximum performance with the efficiency of 4.15%. Candadai et al. [19] considered the performance of a Bi_2Te_3 based STEG system numerically and experimentally. The results indicated the maximum efficiency and power generated from the STEG at various concentration ratios and in the practical temperature range of the thermoelectric module.

The impacts of enclosure pressure and thermal concentration on the open circuit voltage, power generation and efficiency of a STEG system were investigated by Sudharshan et al. [20]. It is found that reducing the enclosure pressure increased the open circuit voltage, output power and efficiency of the STEG system. They also studied the influence of the using a big area absorber. The results showed that the open circuit voltage and output power of the STEG system would be enhanced by using a large surface area absorber. ANSYS Workbench was used by Kossyvakis et al. [21] for a numerical simulation and optimization of a STEG

system. The results indicated that for systems using thermal concentration, the application of low power thermoelectric modules would be more efficient. A numerical and experimental study on a practical flat-panel STEG system under the real condition is presented by Sun et al. [22]. They also provided a method to optimize their STEG system and showed that to obtain the maximum output power from the STEG system, it is essential to have an impedance match between the generator and electrical load. Rehman and Siddiqui [23] established a correlation for critical concentration ratio of solar concentrated thermoelectric generators (SCTEGs). The results showed that the maximum temperature that a module could tolerate had the most substantial influence on the critical concentration ratio.

Almost all of the studies in the field of STEG systems are on the different ways to improve the efficiency and performance of the STEGs. Transient response of the STEG system has not been studied in the literature. As the weather condition and consequently solar irradiance is changing during the day, understanding the behavior and response of the STEG system to the time-dependent solar irradiation can be very helpful for stability and reliability design of the system. To the best of our knowledge, there is no published research in this area which considered the transient behavior of the STEG systems. A very frequently used TEGs for power generation and refrigeration applications is BiTe based TEGs that have low-cost and appropriately strong thermoelectric effect. In this study, dynamic response of a BiTe based TEG to the different concentrated lights and transient solar radiation is investigated. The TEG which is used in the experiments covered by a graphite layer that enhances the absorbed energy from the solar simulator. The experimental results are validated by a numerical simulation using finite volume approach. The temperature variation, open circuit voltage, short circuit current and maximum power generation in transient condition are obtained and evaluated. After validation of the experiments, the numerical simulation for the STEG system without graphite layer is done and the significance of using graphite sheet is discussed. In order to investigate the impact of using different materials, a Zn_4Sb_3 based TEG is considered in the simulation and the maximum generated power is achieved and discussed. The potential of the geometrical optimization of the STEG system is also evaluated by considering different values of the length of the semiconductors.

2. Experimental setup

The experimental study is carried out in Solar Technology Laboratory of Paul Scherrer Institute (PSI). Commonly, flat plate, parabolic troughs, Fresnel lenses and parabolic dishes are using as the solar collector in the STEG systems. In this work, a solar simulator which is consist of 10 xenon arc lamps is used to generate concentrated light (see Figure 1). Extremely concentrated light up to 11000 suns ($11000\ kW/m^2$) can be simulated on focal point [24-25]. In these experiments just 6 lamps were used to simulate 0 to 56 suns. An optical mixer which is placed in front of the TEG is used to produce uniform light over the area of the TEG shown in Figure 2.

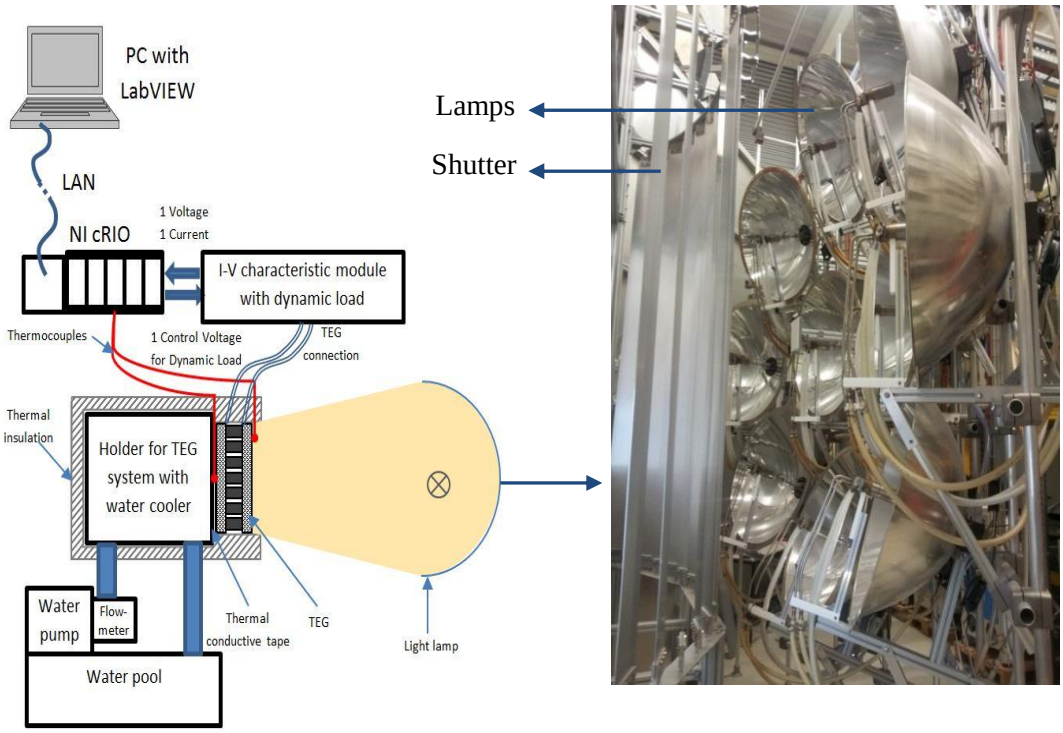

(a) (b)

Fig. 1. (a) Schematic of the experimental setup (b) solar simulator used in this study.

Before starting the experiments and considering the performance of the STEG system, a thermogage sensor which is located on the exit plane of the optical mixer measured and calibrated the radiative flux distribution to determine the solar intensity map. It is necessary to find the $40mm \times 40mm$ zone which heat flux delivered from the solar simulator has the best homogeneity.

Fig. 2. BiTe based TEG used in experiments [26].

The TEG which is used in the experiments was a BiTe based TEG model TEG2-07025HT-SS with 199 uni-couples and size $40\text{mm} \times 40\text{mm}$ [26]. To increase the temperature difference between hot and cold sides of TEG and consequently increasing the power generation by the TEG, a heat exchanger is located behind the TEG module. The mass flow rate of the water, as the working fluid of the heat exchanger, is kept constant and equal to 5 L/min. All the temperatures and I-V characteristics of the TEG are measured using data acquisition and control systems based on National Instruments cRIO. 5 thermocouples are used in the experiments to measure the temperatures of the ambient, hot side of the TEG (2 thermocouples) and cold side of the TEG (2 thermocouples).

The I-V characteristics of the TEG was measured based on the impedance variation of a capacitor during the charging process. When the capacitor is connected to the TEG (the K switch is in the position 1) the capacitor impedance variation starts from very low value (the capacitor is discharged), to very high value (the capacitor is fully charged). The TEG acts as a power source. The simplified schema is shown in Fig.3.

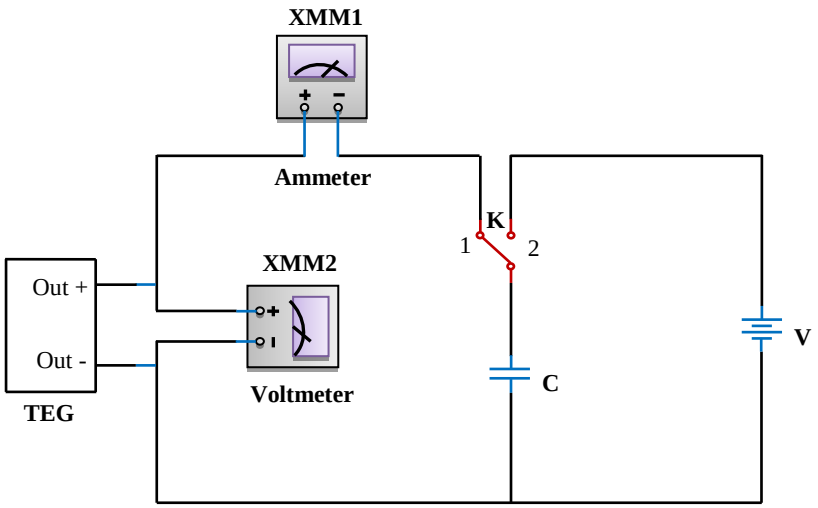

Fig. 3. Simplified schematic of the dynamic electrical load.

The voltage source V is used for pre-charge the capacitor (when the K switch is in position 2) in order to compensate the circuit resistance. In this manner it is assure that the entire I-V characteristics are obtained (from V_{TEG}=0 to V_{TEG}=V_{OC}).

3. Numerical approach

An unsteady-state one-dimensional heat transfer model is proposed using energy conservation law to validate the experimental study. The TEG module is a non-linear system with many ingredients and special properties. Three basic effects of the TEG are Seebeck, Peltier and Thomson effects. In addition, every TEG has two accessorial effects including the Joule and Fourier effects. Seebeck effect generates an electromotive force (EMF). Peltier effect that is not an interface effect cause to Peltier heat which is produced only on the end sides of the semiconductors. Thomson effect and Joule effect produce Thomson heat and Joule heat. Both of them are volumetric effects that are supposed to be equally transferred to the hot and cold junctions of the semiconductor elements [27-28].

Unlike conventional and simple modeling of thermoelectric materials in multiphysics modeling where thermoelectric properties of the materials are taken constant [29-31], in current study all thermoelectric material properties including the thermal and electrical conductivity and Seebeck coefficient and consequently the figure of the merit as the key parameter, are taken as a functions of the temperature.

Some appropriate assumptions are considered in the simulation procedure. The main simplifying assumptions are as follow:

1. The TEG is well thermal insulated, therefore, heat transfer from the TEG system to the surroundings is supposed to be zero except the heat dissipation from the top surface of the TEG by radiation.
2. The convective and radiative heat transfers in the middle of the TE elements in the TEG module are neglected.
3. The same materials are used for N- and P-type semiconductors in the TEG.
4. Electrical and thermal contact resistances are considered negligible owing to assuming that all the components of the TEG are well connected.

One-dimensional physical model of the STEG system which is used in the simulation is illustrated in Figure 4.

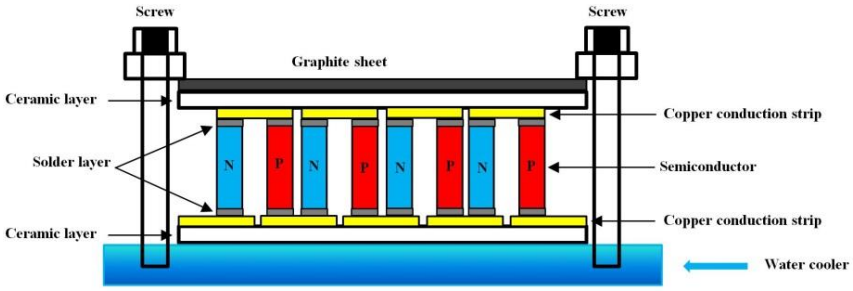

Fig. 4. One-dimensional physical model of the STEG system.

TEG module comprises of the ceramic substrates, copper conduction strips, solder layers, semiconductor thermocouples and thermal insulations. In the first simulation, a thin graphite layer is considered on the top surface of the TEG.

3.1. Governing equations

The behavior of a thermoelectric module is governed by the well-known coupled equations of TE constitutive include both the heat transfer and the continuity of electric charge equations, which are given as follows [32].

Conservation of heat energy:

$$\rho C \frac{\partial T}{\partial t} + \nabla . q'' = Q' \quad (1)$$

Continuity of electric current:

$$\nabla . J = \frac{\partial \rho_c}{\partial t} \quad (2)$$

where ρ_c is the charge density.

The heat flux, q'', and the Joule heating energy, Q', are defined as:

$$q'' = -k\nabla T + P'J \quad (3)$$

$$Q' = J.E \quad (4)$$

In these equations, J is the electric current's flux that is produced by a coupling of the irreversible Joule effect and the reversible Seebeck effect and P' is the Peltier coefficient.

$$P' = \alpha T \quad (5)$$

$$J = -\gamma \nabla V - \gamma \alpha \nabla T \quad (6)$$

Equations (1) and (2) can be rewritten using Equations (3)-(6):

$$\rho C \frac{\partial T}{\partial t} + \nabla . \left(-k\nabla T + \alpha T(-\gamma \nabla V - \gamma \alpha \nabla T)\right) = (-\gamma \nabla V - \gamma \alpha \nabla T)(-\nabla V) \quad (7)$$

$$-\gamma(\nabla^2 V + S\nabla^2 T) = \frac{\partial \rho_c}{\partial t} \quad (8)$$

These equations are appropriate to use for both the transient and steady state condition. For the steady state condition, $\frac{\partial \rho_c}{\partial t} = 0$.

3.2. Boundary conditions

Using energy conservation law for each contact layer of the TEG system leads to obtaining a set of non-linear equations. In order to solve these coupled partial differential equations, finite volume method [33] is used. The corresponding boundary condition on the top surface (CS1) of the graphite sheet is:

$$\rho_{Gr} c_{Gr} V_{Gr} \frac{\partial T_{Gr}}{\partial t} = SC \times G \times A_{Gr} - Q_{rad} + KA \left(\frac{\partial T}{\partial x}\right)\Big|_{x=CS_1^b} \quad (9)$$

In this equation, Q_{rad} is the radiative heat loss from the surface of the TEG and could be calculated by equation (10):

$$Q_{rad} = \varepsilon\sigma A_{Gr}\left({T_{Gr}}^4 - {T_{sky}}^4\right) \quad (10)$$

Where Stefan–Boltzmann constant $\sigma = 5.67 \times 10^{-8}\mathrm{W/m^2K^4}$ and the sky temperature $\mathrm{T_{sky}}$ is considered as a function of the ambient temperature according to a study by Nowak [34].

In this investigation, there are n pairs of P–N junction in the TE module and the thermoelectric elements are divided into m control volumes. On contact surface between heat exchanger base and the cooling fluid (CS10):

$$\rho_{hx}c_{hx}V_{hx}\frac{\partial T_{hx}}{\partial t} = k_{hx}A_{hx}\left(\frac{\partial T}{\partial x}\right)\Big|_{x=CS_{10}^{t}} + h_f A_f\left(T_{hx,2} - T_f\right) \quad (11)$$

Time-dependent and coupled temperatures of each layer in the TEG module are calculated by solving above equations.

3.3. Power generation and efficiency

After solving the coupled equations (1-11), the time-dependent temperatures of different components of the STEG system can be determined. After finding the temperature of the TEG layers, power generation and efficiency of the TEG can be obtained. By taking into account the impact of the Thomson effect, the electromotive force (EMF) of the TEG module is:

$$\mathrm{E} = \mathrm{n_{sc}}\left[\alpha_{\mathrm{sc,h}}\mathrm{T_{sc,h}} - \alpha_{\mathrm{sc,c}}\mathrm{T_{sc,c}} - \sum_{\mathrm{i=1}}^{\mathrm{m-1}}\tau_{\mathrm{i}}(\mathrm{T_i} - \mathrm{T_{i+1}})\right] \quad (12)$$

The internal electrical resistance of the TEG module, which comprises electrical resistance of the copper conduction strip, solder layer, and semiconductors:

$$\mathrm{R_i} = \left(\mathrm{n_{ccs}r_{ccs}} + \mathrm{n_{sl}r_{sl}} + \mathrm{n_{sc}}\sum_{\mathrm{i=1}}^{\mathrm{m}}\mathrm{r_{sc,i}}\right) \quad (13)$$

Consequently, the output power can be computed as follows:

$$\mathrm{P_{TEG}} = (\mathrm{E}/(\mathrm{R_i} + \mathrm{R_L}))^2\mathrm{R_L}$$

$$= \left[\mathrm{n_{sc}}\left[\alpha_{\mathrm{sc,h}}\mathrm{T_{sc,h}} - \alpha_{\mathrm{sc,c}}\mathrm{T_{sc,c}} - \sum_{\mathrm{i=1}}^{\mathrm{m-1}}\tau_{\mathrm{i}}(\mathrm{T_i} - \mathrm{T_{i+1}})\right]\right]^2 \mathrm{R_L}\Big/\left[\left(\mathrm{n_{ccs}r_{ccs}} + \mathrm{n_{sl}r_{sl}} + \mathrm{n_{sc}}\sum_{\mathrm{i=1}}^{\mathrm{m}}\mathrm{r_{sc,i}}\right) + \mathrm{R_L}\right]^2 \quad (14)$$

and instantaneous efficiency of the TEG is defined as:

$$\eta_{TEG} = P_{TEG}/(SC \times G \times A - Q_{rad}) \quad (15)$$

4. Results and discussion

The performance of the STEG system under the transient condition like the cloudy weather is studied. Figure 5 shows the pattern which is considered in the experiments. In order to observe the behavior of the system under the transient condition, experiments are done for two different time intervals, 1 minute and 5 minutes. As mentioned before 6 radiative lamps are used in the experiments which were permanently on during each experiment and radiation density was controlled by the shutter shown in Figure 1. With 6 lamps and 5% and 10% open-rate of the shutter, equivalent radiated solar radiations on the TEG are 30 suns and 56 suns, respectively.

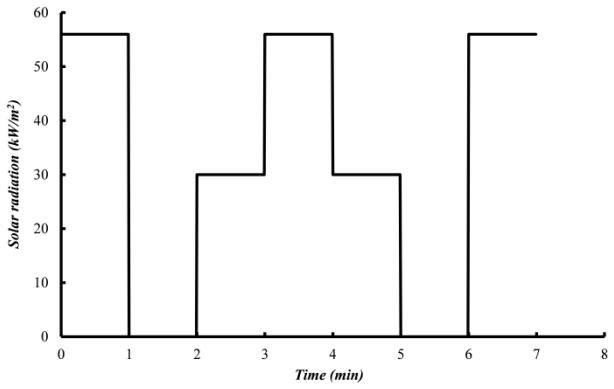

Fig. 5. Applied solar radiation patterns to the STEG.

4.1. Temperature gradient in the STEG

The presented numerical model is capable to trace the temperature fluctuation owing to variation in the solar radiation. The same pattern for solar radiation is also applied as an input in the numerical simulation. The time-dependent temperature of different layers of the TEG including the hot and cold sides of the TEG module can be obtained as results of the simulation process. Figure 6 shows the experimental and numerical dynamic response of the temperatures of the hot and cold sides of the TEG to the fluctuated solar radiation

while the system is already under steady state condition. The temperature gradient across the TEG module is the most important parameter in power generation by a TEG module. It can be seen that the temperatures are directly affected by the sharp instabilities of the solar radiation. As it can be observed the numeric simulation results are in a good agreement with experimental results.

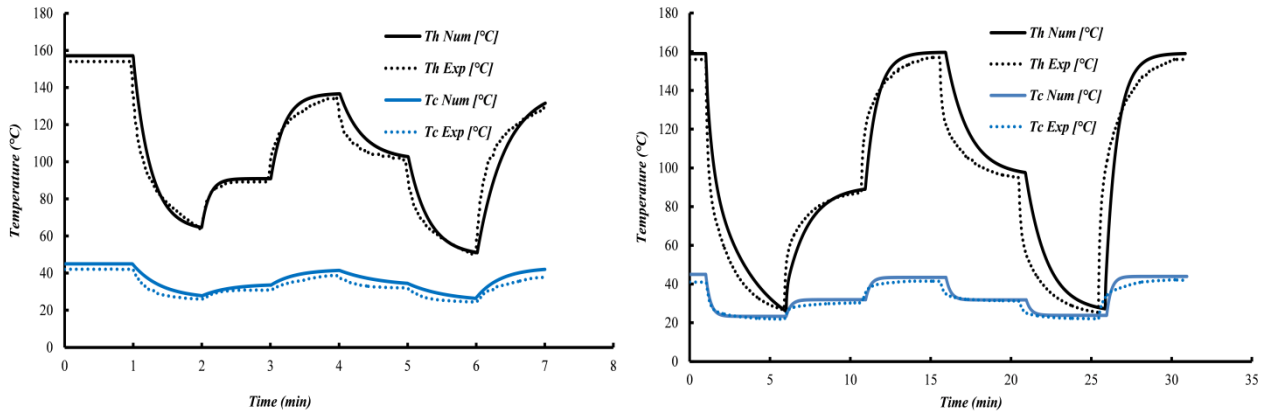

Fig. 6. Hot and cold side temperatures of the STEG for (a) 1-minute time interval, (b) 5 minutes time interval.

4.2. Open circuit voltage and short circuit current

Figure 7 shows the experimental results for the variation of the open circuit voltage and short circuit current of the STEG. For both time intervals, the open circuit voltage was recorded every 200 milliseconds but short circuit current was measured every 20s and 1min for 1min and 5mins time intervals, respectively. For both time intervals, the short circuit current and open circuit voltage have an identical trend and follow the temperature profile. As 1 minute is a short time for the system to reach the thermally steady state condition, even at the similar solar radiation magnitude (56 suns), the short circuit current and open circuit voltage cannot reach to the peak point in the next cycles. On the other hand, 5 minutes time interval is adequate for the voltage and current to practically reach to their steady state condition.

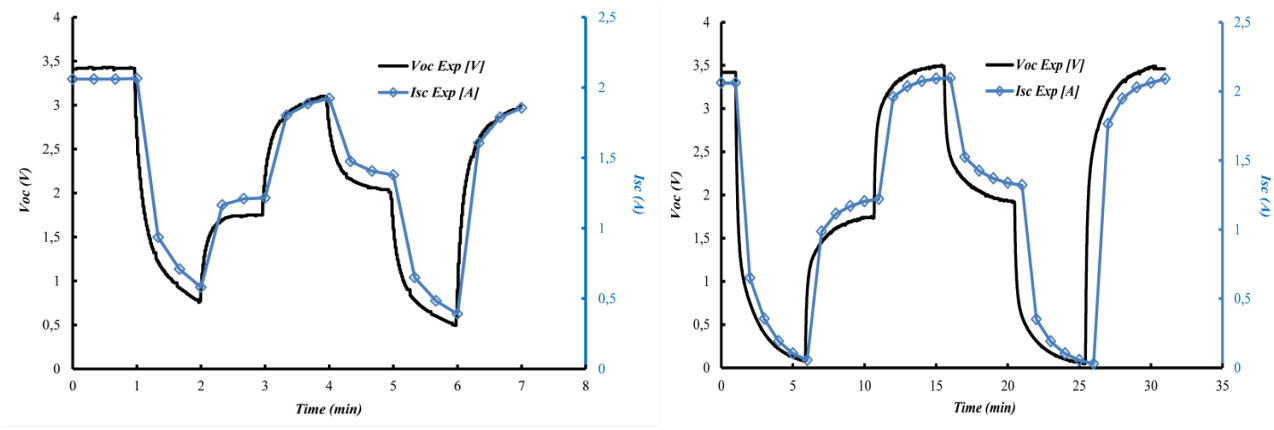

Fig. 7. Open circuit voltage and short circuit current of the TEG for (a) 1-minute time interval, (b) 5 minutes time interval.

4.3. Maximum output power by the STEG system

Experimental and numerical results for the maximum output power versus time are illustrated in figure 8. The most important parameters in power generation by the TEG are the figure of merit and temperature difference between the hot and cold sides of the TEG. In this investigation, a BiTe based TEG is used and due to low-temperature variation, the value of the figure of merit does not change a lot [35]. Therefore, the most dominant parameter in power generation is the temperature difference between hot and cold sides of the TEG. In order to enhance both conversion efficiency and heat flux across the module, it is crucial to maximizing the temperature gradient across the TEG module. As it can be observed in figure 8, with increasing the solar radiation and consequently the temperature gradient across the TEG, the maximum power increases, and vice versa.

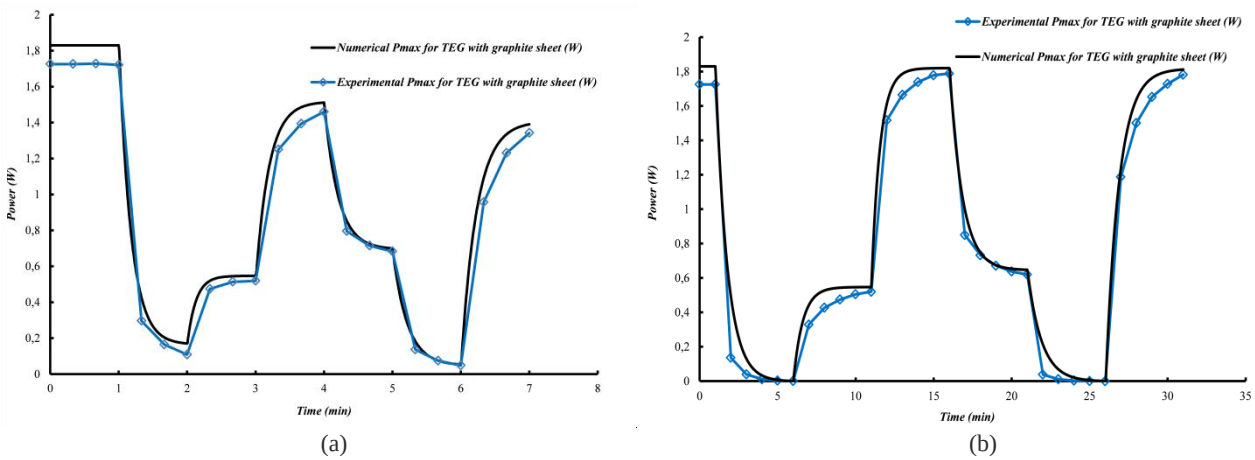

Figure. 8. Maximum power versus time for the STEG with graphite layer for (a) 1min time interval (b) 5mins time interval.

The graphite layer has a substantial effect to enhance the absorbed energy from the solar radiation. In the following section, the significance of the existence of the graphite layer will be investigated.

4.4. Numerical study on the effect of the graphite layer

In the first part of this framework, an experimental study and numerical validation on a STEG system are accomplished. The TEG which is used in the first part is covered with a graphite layer. The graphite layer plays the role of an absorber for the STEG system so it can absorb more energy from the solar simulator. In this part, the numerical simulation for the STEG system without graphite layer is carried out. Apparently, the graphite layer increases absorbance coefficient of the radiation, while the ceramic layer of the TEG without the graphite layer has higher reflection coefficient compared the TEG with the graphite layer.

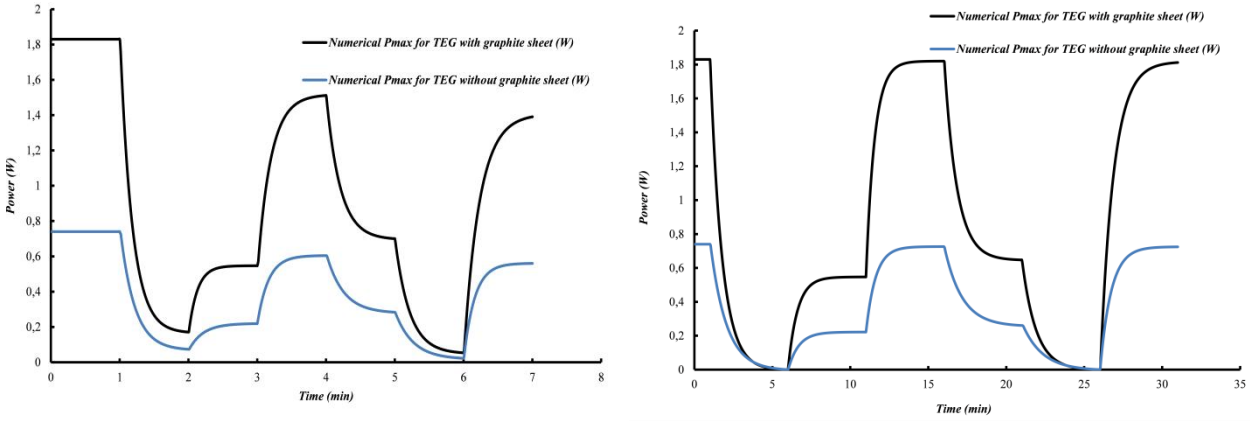

Figure. 9. Maximum power versus time for the STEG with and without graphite layer for (a) 1 min time interval (b) 5 mins time interval.

Figure 9 displayed the maximum output power for both STEG systems, with and without graphite layer. It is worthy to notice that with graphite layer on the hot surface of the TEG, output power enhances substantially at the similar solar radiation. The significant effect of the graphite layer can be observed in this figure. The maximum power generation from the system when graphite layer is attached on the TEG is almost 2.5 times more than without graphite layer's one. It is owing to the higher portion of energy which can be absorbed by the graphite layer. Therefore, the efficiency (which is defined as the ratio of the output power to the input

solar radiation) of the STEG system with graphite layer (3.3%) is 2.53 times of the STEG module without the graphite layer (1.3%). Though the power generation in the STEG system without graphite layer is less than the STEG system with graphite layer the range of the fluctuations in the STEG system without graphite layer is also less than the other one. Consequently, it can be concluded that without graphite layer, more stable power could be obtained.

One of the remarkable consequences of this investigation is that for low solar concentration applications, this technique, using TEG with graphite layer, is fruitful to compensate the low input energy and obtain higher power generation. This result is noticeable for both of the 1 minute and 5 minutes time interval. Electrical impact of the time interval between the solar radiation steps on the maximum output power can be observed in Figures 7 and 8. By enhancing the time interval variation of the short circuit current, open circuit voltage and maximum power occur over a larger range. For instance, with 5 minutes time interval, the minimum output powers which are at minutes 6 and 26 are zero and the maximum output powers which happened at minutes 16 and 31 are close to the steady state condition.

4.5. Material and Geometrical optimization

In order to maximize the generated power by the STEG system, material and geometry of the system should be optimized. In this study, a Zn_4Sb_3 based STEG system is also examined. The material properties of the BiTe based TEG are replaced with the material properties of the Zn_4Sb_3 based TEG [36]. Figure 10 shows the time-dependent variation of the maximum powers of the STEG systems with the same geometries and different TE materials. Although the figure of merit of the Zn_4Sb_3 based TEG is less (varying between 0.3 to 0.48 in the examined temperature range) than the BiTe based TEG (varying between 0.75 to 1.02 in the examined temperature range), the generated powers by the Zn_4Sb_3 based TEG are relatively high. The reason is that, with applying the same patterns of solar radiations, shown in Figure 5, due to the higher thermal resistance of the Zn_4Sb_3 based TEG compare to BiTe based TEG, the temperature difference between hot and cold junctions of the TEG is higher for Zn_4Sb_3 based TEG. It is known that figure of merit and the temperature gradient across the TEG are two key parameters in power generation by the TEGs. Therefore for the Zn_4Sb_3 based TEG, the higher temperature difference between the hot and cold sides compensates the

low amount of the figure of merit.

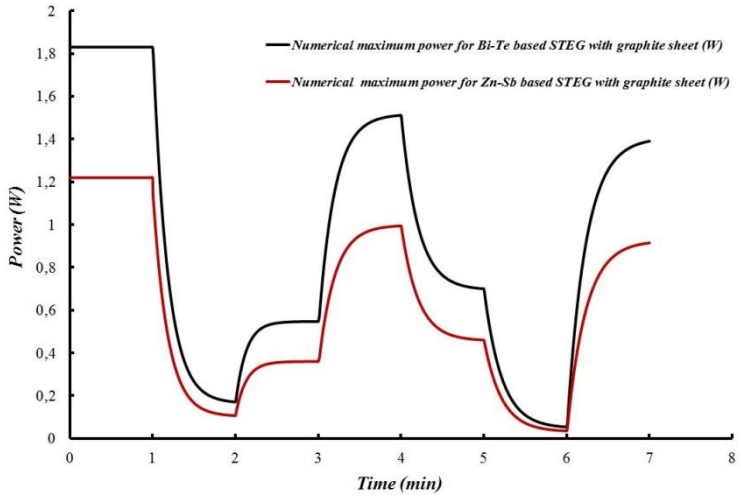

Figure. 10. Maximum power versus time for the BiTe based and Zn_4Sb_3 based STEG systems.

Figure 11 displays the variation of the maximum power and efficiency of both BiTe based and Zn_4Sb_3 based STEG system in the steady state condition and for different solar concentrations. The values of the temperature differences and figure of merits are shown in this figure. Maximum power and efficiency of both of the STEG systems increases when the concentrated solar radiation enhances. For the BiTe based STEG system, the values of the figure of merits are higher than Zn_4Sb_3 based STEG system. While, the temperature differences for the Zn_4Sb_3 based STEG system are higher than BiTe based STEG system. Since the maximum figure of merit for BiTe based TEG occurs at around 380 K [35], at the temperatures higher than this value the figure of merit decreases. Figure of merit of the Zn_4Sb_3 based TEG has opposite manner and enhances with increasing the temperature [36]. As can be observed in Figure 11, for the solar concentration SC=125 suns, the value of the generated power and efficiency of the both STEG systems are very close. Due to decreasing the value of the figure of merit of the BiTe based TEG, the rate of increasing of the power and efficiency of the BiTe based STEG system is less than Zn_4Sb_3 based STEG system. On the other hand, the value of the figure of merit of the Zn_4Sb_3 based TEG has an increasing rate. Therefore, with increasing the solar concentration and consequently the temperature gradient across the TEG, the generated power and efficiency of the Zn_4Sb_3 based STEG system increases. It can be predicted that for higher solar concentrations, Zn_4Sb_3 based STEG system has better performance compare to the BiTe based STEG

system.

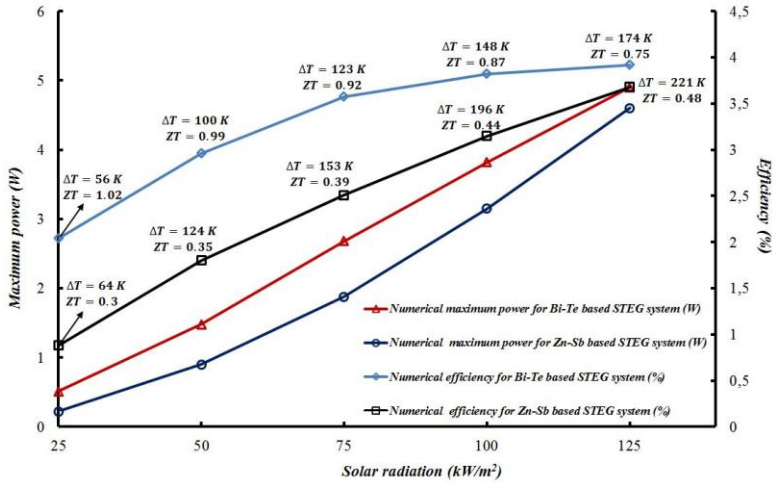

Figure. 11. Maximum powers and efficiencies of the STEG systems versus concentrated solar radiation.

There are different geometrical parameters that can be considered for optimization of the STEG systems. In this study, the impact of variation of the length of the semiconductors as a key parameter is investigated. More detailed study about using different materials in the STEG systems with different geometrical parameters are planned for the future works.

The length of the TEG used in the experiments and the above simulations was L=1.5 mm. Figure 12, illustrates the variation of the maximum powers and efficiencies of the STEG systems for different lengths of the semiconductors of the TEGs and for constant solar concentration SC=56 suns. The thermal resistance of the TEGs increases by enhancing the length of the semiconductors and, consequently, the temperature gradient across the TEG, maximum generated powers and efficiencies are increased. In the studied range, due to having higher figure of merit, the generated power and efficiency of the BiTe based STEG system are higher than Zn_4Sb_3 based STEG system.

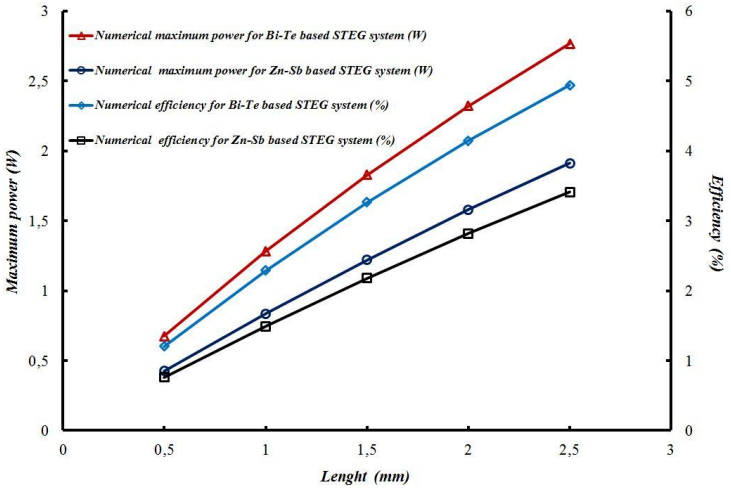

Figure. 12. Maximum powers and efficiencies of the STEG systems versus the length of the semiconductors.

5. Conclusion

In this work, an experimental investigation and numerical simulation were carried out for a STEG system including graphite absorber layer. The hot and cold sides temperatures, short circuit current, open circuit voltage and maximum power produced by the STEG with graphite layer were achieved and discussed. The numerical results were in good agreement with the experiments. The hot and cold side temperatures of the STEGs and the electrical output power are affected by the sharp fluctuations of the solar radiation. It is found that, by applying an identical solar radiation pattern, using a graphite layer increases the power generation and the efficiency around 2.5 times. Furthermore, the numerical simulation is used to evaluate the potential of the STEG system for two types of materials with various geometries. The results show that Zn_4Sb_3 based STEG is more appropriate choice, compared to the BiTe based STEG, for higher solar concentration ratios. The significance of the length effect of the semiconductors is also examined. The results indicate that increasing the length of the semiconductors improves power performance of the both STEG systems.

Acknowledgment

Financial support by the Access to Research Infrastructures activity in the 7th Framework Programme of the EU (SFERA 2 Grant Agreement n. 312643) is gratefully acknowledged. The authors are thankful to the team from the Solar Technology Laboratory of Paul Scherrer Institute, Villigen, Switzerland (Ms.Y. Baeuerle, Mr.

D. Wuillemin, Mr. V. Schnetzler and Mr. C. Wieckert), where all the measurements in concentrated light were performed.

References

[1] S. Mahmoudinezhad, A. Rezaniakolaei, L.A. Rosendahl, Experimental study on effect of operating conditions on thermoelectric power generation, Energy Procedia 142 (2017) 558-563.

[2] S. Mahmoudinezhad, A. Rezania, A.A. Ranjbar, L.A. Rosendahl, Transient behavior of the thermoelectric generators to the load change; an experimental investigation, Energy Procedia 147 (2018) 537-543.

[3] A. Pereira, T. Caroff, G. Lorin, T. Baffie, K. Romanjek, S. Vesin, K. Kusiaku, H. Duchemin, V. Salvador, N. Miloud-Ali, L. Aixala, J. Simon, High temperature solar thermoelectric generator- Indoor characterization method and modeling, Energy 84 (2015) 485–492.

[4] S. Mahmoudinezhad, P.A. Cotfas, D.T. Cotfas, A. Rezania, L.A. Rosendahl, Performance evaluation of a high-temperature thermoelectric generator under different solar concentrations, Energy Procedia 147 (2018) 624-630.

[5] M. Telkes, Solar thermoelectric generators, J. Appl. Phys. 25 (1954) 765.

[6] Dent. C, Cobble. M, 1982. A solar thermoelectric generator experiments and analysis. In: Proceedings of 4th International Conference on Thermoelectric Energy Conversion 75–78.

[7] S. Mahmoudinezhad, A. Rezania, L.A. Rosendahl, Behavior of hybrid concentrated photovoltaic-thermoelectric generator under variable solar radiation, Energy Conversion and Management 164 (2018) 443-452.

[8] Vatcharasathien. N, Hirunlabh. J, Khedari. J, Daquenet. M, Design and analysis of solar thermoelectric power generation system. International Journal of Sustainable Energy 24 (2005) 115–127.

[9] S. Mahmoudinezhad, S. Qing, A. Rezaniakolaei, L.A. Rosendahl, Transient Model of Hybrid Concentrated Photovoltaic with Thermoelectric Generator, Energy Procedia 142 (2017) 564-569.

[10] Gang Chen, Theoretical efficiency of solar thermoelectric energy generators, Journal of Applied Physics 109 (2011) 104908.

[11] Kenneth McEnaney, Daniel Kraemer, Zhifeng Ren, and Gang Chen, Modeling of concentrating solar thermoelectric generators, Journal of Applied Physics 110 (2011) 074502.

[12] Daniel Kraemer, Bed Poudel, Hsien-Ping Feng, J. Christopher Caylor, Bo Yu, Xiao Yan, Yi Ma, Xiaowei Wang, Dezhi Wang, Andrew Muto, Kenneth McEnaney, Matteo Chiesa, Zhifeng Ren and Gang Chen, High-performance flat-panel solar thermoelectric generators with high thermal concentration, Nat. Mater. 10 (2011) 532–53.

[13] Daniel Kraemer, Kenneth McEnaney, Matteo Chiesa, Gang Chen, Modeling and optimization of solar thermoelectric generators for terrestrial applications, Sol. Energy 86 (2012) 1338–1350.

[14] H.A. Madkhali, A. Hamil, H. Lee, Validation, Optimization and smulation of a solar thermoelectric generator model, J. Electron. Mater. 46 (2017) 6756–6768.

[15] Daniel Kraemer, Qing Jie, Kenneth McEnaney, Feng Cao,Weishu Liu, Lee A.Weinstein, James Loomis, Zhifeng Ren and Gang Chen, Concentrating solar thermoelectric generators with a peak efficiency of 7.4%, Nat. Energy 1 (2016) 16153.

[16] Sandip Mazumder, Computational Modeling of a Solar Thermoelectric Generator, Journal of Thermal Science and Engineering Applications 7 (2015) 041004-1.

[17] Lei Liu, Xue Sen Lu, Mao Lei Shi, Ya Kun Ma, Jian Ying Shi, Modeling of flat-plate solar thermoelectric generators for space applications, Solar Energy 132 (2016) 386–394.

[18] Wei-Hsin Chen, Chien-Chang Wang, Chen-I Hung, Chang-Chung Yang, Rei-Cheng Juang, Modeling and simulation for the design of thermal-concentrated solar thermoelectric generator, Energy 64 (2014) 287-297.

[19] Aaditya A. Candadai, V. Praveen Kumar,Harish C. Barshilia, Performance evaluation of a natural convective-cooled concentration solar thermoelectric generator coupled with a spectrally selective high temperature absorber coating, Sol. Energy Mater. Sol. Cells. 145 (2016) 333-341.

[20] K. Y. Sudharshan, V. Praveen Kumar, Harish C. Barshilia, Performance evaluation of a thermally concentrated solar thermo-electric generator without optical concentration, Solar Energy Materials & Solar Cells 157 (2016) 93-100.

[21] D. N. Kossyvakis, C. G. Vossou, C. G. Provatidis, E.V. Hristoforou, Computational analysis and performance optimization of a solar thermoelectric generator, Renewable Energy 81 (2015) 150-161.

[22] Dongfang Sun, Limei Shen, Yu Yao, Huanxin Chen, Shiping Jin, Hong He, The real-time study of solar thermoelectric generator, Applied Thermal Engineering 119 (2017) 347-359.

[23] N. ur Rehman, M.A. Siddiqui, Critical concentration ratio for solar thermoelectric generators, Journal of Electronic Materials 45 (2016) 5285–5296.

[24] J. Petrasch, P. Coray, A.Meier et al, A novel 50 kW 11,000 suns high-flux solar simulator based on an array of xenon arc lamps, ASME Journal of Solar Energy Engineering 129 (2007) 405–411.

[25] I. Alxneit and H. Schmit, Spectral characterization of PSI's high-flux solar simulator, J. Sol. Energy Eng. 134 (2012) 011013.

[26] http://tecteg.com/wp-content/uploads/2014/09/Spec-TEG2-07025HT-SS-rev1-1.pdf. [Cited: November 2018].

[27] Meng F, Chen L, Sun F. A numerical model and comparative investigation of a thermoelectric generator with multi- irreversibilities. Energy 36 (2015) 3513–22.

[28] S Mahmoudinezhad, A Rezania, DT Cotfas, PA Cotfas, LA Rosendahl, Experimental and Numerical Investigation of Hybrid Concentrated Photovoltaic–Thermoelectric Module under Low Solar Concentration, Energy 159 (2018) 1123-1131.

[29] A. Rezania, L. A. Rosendahl, Evaluating thermoelectric power generation device performance using a rectangular microchannel heat sink, Journal of Electronic Materials 40 (2011) 481-488.

[30] A.M. Goudarzi, P. Mazandarani, R. Panahi, H. Behsaz, A. Rezania, L. A. Rosendahl, Integration of thermoelectric generators and wood stove to produce heat, hot water, and electrical power, Journal of Electronic Materials 42 (2013) 2127-2133

[31] A. Rezania, L. A. Rosendahl, New configurations of micro plate-fin heat sink to reduce coolant pumping power, Journal of Electronic Materials, 41 (2012) 1298-1304.

[32] Leisheng Chen, Jaeyoung Lee, Effect of pulsed heat power on the thermal and electrical performances of a thermoelectric generator, Applied Energy 150 (2015) 138–149.

[33] S. V. Patankar. Numerical Heat Transfer and Fluid Flow, (1980) Taylor & Francis, USA.

[34] Nowak H. The sky temperature in net radiant heat loss calculations from low-sloped roofs. Infrared Phys. 29 (1989) 231–2.

[35] http://thermoelectric-generator.com/wp-content/uploads/2014/07/Ingot-Raw-Material-BiTe-N-and-P.pdf. [Cited: November 2018].

[36] T. Dasgupta, C. Stiewe, A. Sesselmann, H. Yin, B. B. Iversen, and E. Mueller, Thermoelectric studies in β-Zn_4Sb_3—the complex interdependence between thermal stability, thermoelectric transport, and zinc content, Journal of Applied Physics 113 (2013) 103708.

PAPER 6: REFERENCE [206]

Transient Model of Hybrid Concentrated Photovoltaic with Thermoelectric Generator

Sajjad Mahmoudi Nezhad, Shaowei Qing, Alireza Rezania, Lasse Rosendahl

The paper has been published in
Energy Procedia 142 (2017) 564-569.

Available online at www.sciencedirect.com

ScienceDirect

Energy Procedia 142 (2017) 564–569

Energy Procedia

www.elsevier.com/locate/procedia

9th International Conference on Applied Energy, ICAE2017, 21-24 August 2017, Cardiff, UK

Transient Model of Hybrid Concentrated Photovoltaic with Thermoelectric Generator

Sajjad Mahmoudinezhad[a], Shaowei Qing[b,c], Alireza Rezaniakolaei[a,*], Lasse Aistrup Rosendahl[a]

[a]*Department of Energy Technology, Aalborg university, Pontoppidanstræde 101, Aalborg DK-9220, Denmark*
[b]*Key Laboratory of Low-grade Energy Utilization Technologies and Systems, Chongqing University, Ministry of Education, China*
[c]*College of Power Engineering, Chongqing University, Chongqing 400044, China*

Abstract

Transient performance of a concentrated photovoltaic thermoelectric (CPV-TEG) hybrid system is modeled and investigated. A heat sink with water, as the working fluid has been implemented as the cold reservoir of the hybrid system to harvest the heat loss from CPV cell and to increase the efficiency and performance of the hybrid module. This investigation is carried out by using a numerical simulation approach with MATLAB software. The governing equations for CPV-TEG hybrid system in transient state is derived and discretized. The results are consisting of the variation of the temperatures, power generation and efficiency of the CPV and TEG with the time in the transient condition.

Peer-review under responsibility of the scientific committee of the 9th International Conference on Applied Energy.

Keywords: Concentrated Photovoltaic Cell; Thermoelectric Generator; Hybrid Syestem; Solar Energy; Transient Model.

1. Introduction

The use of solar energy is an important method to reduce the global greenhouse crisis. Due to better utilization of this source of energy it is important to improve the efficiency of photovoltaic (PV) cell. Even while using high efficiency concentrating multi junction (CMJ) cells, more than half of the solar irradiance is not converted into electricity and is dissipated by heat. Harvesting of this heat for increasing the system's efficiency even more can be

* Corresponding author. Tel.: +4521370284; fax: +4598151411.
E-mail address: alr@et.aau.dk

1876-6102
Peer-review under responsibility of the scientific committee of the 9th International Conference on Applied Energy.
10.1016/j.egypro.2017.12.088

approached by applying thermoelectric devices. CPV-TE hybrid system could be a prospective way to improve the utilization efficiency of solar energy. Several researches have been carried out focusing on improving efficiency of the hybrid CPV–TE [1-4]. Due to the variation of weather condition, considering transient model in heat transfer is very useful and applicable. A TE module was placed thermally in series with a photovoltaic module by Dallan et al. [5]. It was shown that the PV module's power output within the configuration of the PV–TE hybrid system increases up to 39% under fixed thermal input conditions relative to the PV module's operation in absence of the TEM. Beeri et al. [6] have investigated a CPV–TE hybrid demonstrator experimentally and theoretically. They found that, including Peltier cooling effect, the total contribution of the TEG to the hybrid system's efficiency reached a value of almost 40% at a sun concentration level of 200. Energy conversion and heat transfer process of the spectrum splitting CPV-TE hybrid system was investigated by Ju et al. [7], and an energy based numerical model for CPV-TE hybrid systems was presented. Results show that in comparison with PV-only systems the spectrum splitting PV-TE hybrid systems are more appropriate for working under high concentration condition. The effects of a series of parameters on the PV-TE hybrid system of solar energy utilization have been analyzed by Zhang et al. [8]. They found that among these parameters, temperature is one of the dominant factors, which affects the conversion efficiency of such hybrid systems. They also found that a large convection heat transfer coefficient is beneficial to maintain a larger temperature gradient of the thermoelectric module. Kraemer et al. [9] presented a general optimization methodology for the hybrid systems consisting of (PV) and (TE) modules. They developed the optimization method for the hybrid systems operating at low temperature combined. A thermally coupled model of PV/TEG panel was presented to accurately calculate performance of the hybrid system under dissimilar weather conditions by Rezania et al [10]. They found that with current thermoelectric materials, the power generation by the TEG is insignificant in comparison with electrical output by the PV panel, and the TEG plays only a small role on power generation in the hybrid PV/TEG panel. The possibility of using of thermoelectric generators in solar hybrid systems has been investigated by Urbiola et al. [11]. It was found that the TEG's efficiency had almost linear dependence on the temperature difference ΔT between its plates, reaching 4% at $\Delta T = 155^{o}C$ (hot plate at $200^{o}C$) with 3W of power generated over the matched load. A thermodynamic model for analyzing the performance of a (CPV–TEG) hybrid system including Thomson effect in conjunction with Seebeck, Joule and Fourier heat conduction effects was developed by Lamba and Kaushik [12]. It was observed that by considering Thomson effect in TEG module, the power output of the PV, TE and hybrid PV–TEG systems decreases and at C = 1 and 5, it reduces the power output of hybrid system by 0.7% and 4.78% respectively.

According to previous investigations in the fields CPV-TEG hybrid systems, it can be found that hybrid systems are more efficient for harnessing solar energy. Hybrid systems could be optimized in different ways and also different combinations are exists. Due to variation of weather condition during a day for example in cloudy days, power generation and efficiency of hybrid system will changed with the time. Considering this variation can be very important and practical. The aim of this paper is the investigation of thermal behavior, power generation and also efficiency of CPV-TEG hybrid system in the transient condition for different solar radiations. Therefore, we propose a numerical model with considering some logical simplifying assumptions.

2. Numerical model

Fig.1 illustrates physical model of the CPV-TEG system including the heat sink. In order to verify the effect of the new TEG system with CPV cells, a corresponding numerical model algorithm is established. An unsteady-state heat transfer model with applicable simplifications is used to study the performance of the hybrid system. The main simplifying assumptions are as follows:

- The CPV and TEG modules are insulated thermally, therefor, thermal leakage from the modules to the surroundings is assumed to be zero except the hot surface of the CPV cell and heat dissipation from bottom surfaces of the cells, where are specified as heat source and heat sink, respectively.

- The N- and P- type thermoelements in the TEG are identical in dimensions and material properties.

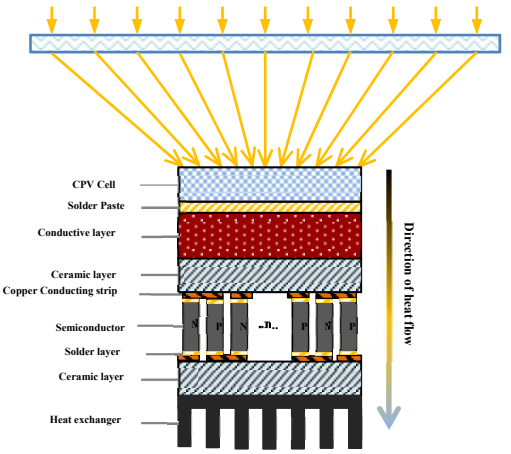

Fig. 1. The physical model of the CPV-TEG hybrid system

- For better consideration of the effect of the sun concentration, all the physical parameters are treated as constant values, except for the Seebeck coefficient, the Thomson coefficient, the electric conductivity and thermal conductivity which are depended on the temperature. And also the figure of the merit of the thermoelectric materials that varies as a key parameter in this study.
- The adjacent end-faces between the components of TEG system are well contacted, so the contact thermal resistance is not considered.

Then, we can construct a one-dimensional unsteady-state heat conduction model:

$$\rho c \frac{\partial T}{\partial t} = \frac{\partial}{\partial x}\left(k \frac{\partial T}{\partial x}\right) + q \tag{1}$$

Where ρ, c, x, k, q and T are the density, specific heat capacity, heat transfer direction, thermal conductivity, inner heat source and temperature of different materials, respectively and also t is the time. The inner heat sources of all the components are equal to zero.

By considering transient energy conservation law for the nodes of the CPV cell shown in Fig. 1, the electrical power generation by the cell and the heat flow through it can be calculated according to created set of nonlinear equations. On the top surface of the CPV cell:

$$\rho c V \frac{\partial T}{\partial t} = SC \times G \times A - Q_{rad} + KA \frac{\partial T}{\partial x} - P_{cpv} \tag{2}$$

Where SC, G, Q_{rad}, P_{cpv} are sun concentration, solar radiation, radiated heat loss from the CPV cell to the ambient and power generation of the CPV cell, respectively. Electrical conversion power of the CPV cell is defined based on the solar irradiation on the cell and its conversion efficiency:

$$P_{CPV} = SC \times G \times A_{CPV} \times \eta_{CPV} \tag{3}$$

Where, the efficiency of photovoltaic cells has been traditionally represented with linear expression [13]:

$$\eta_{CPV} = \eta_{T_{ref}}\left[1 - \beta_{ref}\left(T_{CPV} - T_{ref}\right)\right] \quad (4)$$

Where $\eta_{T_{ref}}$ is electrical conversion efficiency of the CPV cell at the reference temperature ($T_{ref} = 25\,°C$) and reference solar radiation ($G_{ref} = 1000\ W/m^2$) [14] and β_{ref} is CPV cell temperature coefficient at the reference temperature which normally given by the manufacturer. The absolute efficiency reduction is $-0.047\ \%/K$ [15].

Power generation and efficiency of CPV and TEG and can easily be calculated after obtaining the temperature of each contact surfaces. By considering the influence of Thomson effect, the electromotive force (EMF) of the TEG device with n_{mod} TE modules is:

$$E = n_{mod} n_{sc}\left[\alpha_{sc,h} T_{sc,h} - \alpha_{sc,c} T_{sc,c} - \sum_{i=1}^{m-1} \tau_i (T_i - T_{i+1})\right] \quad (5)$$

Where α and τ are coefficient of Seebeck and Thomson; n_{sc} is the numbers of semiconductors; the subscripts h and c are referred to hot and cold side of semiconductors, respectively.

By taking into account the total internal resistance of the TEG system consists of copper conduction strip, solder layer and semiconductor, which can be expressed as:

$$R_i = n_{mod}\left(n_{ccs} r_{ccs} + n_{sl} r_{sl} + n_{sc} \sum_{i=1}^{m} r_{sc,i}\right) \quad (6)$$

Where n_{sl} and n_{sc} and n_{ccs} are numbers of solder layer and semiconductor and copper conduction strip, respectively; r_{sl} and r_{sc} and r_{ccs} are electric resistances of solder layer and semiconductor copper conduction strip, respectively. Then the output power is:

$$P_{TEG} = (E/(R_i + R_L))^2 R_L$$
$$= \left[n_{mod} n_{sc}\left[\alpha_{sc,h} T_{sc,h} - \alpha_{sc,c} T_{sc,c} - \sum_{i=1}^{m-1} \tau_i (T_i - T_{i+1})\right]\right]^2 R_L / \left[n_{mod}\left(n_{ccs} r_{ccs} + n_{sl} r_{sl} + n_{sc} \sum_{i=1}^{m} r_{sc,i}\right) + R_L\right]^2 \quad (7)$$

Also the efficiency of the TEG within a specified interval of Δt, is obtained by:

$$\eta_{TEG} = P_{TEG} / \left(SC \times G \times A - Q_{rad} - P_{cpv}\right) \quad (8)$$

3. Results and discussion

This study prepared a comprehensive method to predict the transient behavior of CPV-TE hybrid systems. The effect of the solar radiation during a typical period of time in wet season [16] on the efficiency of the hybrid module is considered. In the floating condition like cloudy weather, transient heat transfer will be more noticeable and power generation and efficiency of CPV-TEG system become more important. Variation of solar radiation in 15 minutes for a typical cloudy day is shown in Fig. 2(a).

In this investigation, sun concentration (SC) and heat transfer coefficient for the heat sink are considered 200 and $1000\mathrm{W/m^2.K}$ respectively. The dynamic response of the temperatures of hot side and cold side of TEG and also on the surface of CPV cell in the CPV-TEG hybrid system is shown in Fig. 2(b). It can be seen that all the temperatures are directly influenced by the sharp fluctuations of the sun radiation.

As it can be seen the temperatures of the hot side of TEG and surface of CPV are almost the same and the temperature of the cold side of TEG is also varied in a same manner but by a time delay. This delay is because of the time which heat passes through the CPV and the components of TEG. All of the temperatures are changed by variation of sun radiation which presented in fig. 2(a). Obviously by increasing the sun radiation during the time, all temperatures are increased and vice versa. One another important point in the fig. 2(b) is related to the low sun

radiations. As it can be seen, in the small sun radiations, all the temperatures are very close to each other. It is clearly due to low amount of heat transfer through the hybrid system.

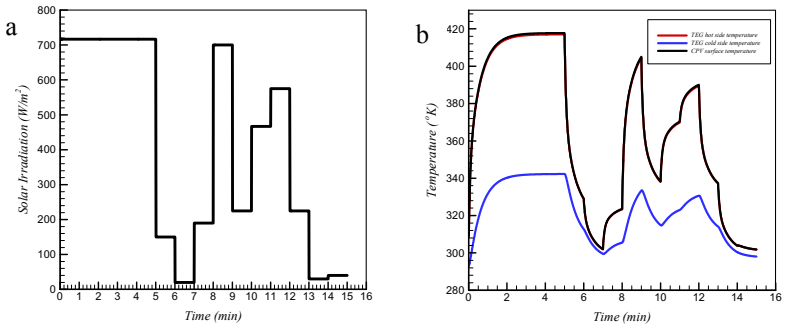

Fig. 2. (a) Variation of solar radiation by the time; (b) Variation of the temperatures of hot side and cold side of TEG and surface of CPV cell

Fig. 3(a) shows the power generation by the CPV during the time. By comparing fig. 2(a) and fig. 3(a) it is very clear that in high sun radiations, there is more power generation and due to dependency of CPV power (P_{CPV}) to the sun radiation it was predictable. Temperature difference between the hot side and cold side of the TEG has the most important effect in the power generation by the TEG. Power output by the TEG is presented in fig. 3(b). By comparing results in the fig. 2(b) and fig. 3(b), the importance of this effect will be approved. As it can be seen, everywhere that temperature difference is high, more power will produced and vice versa.

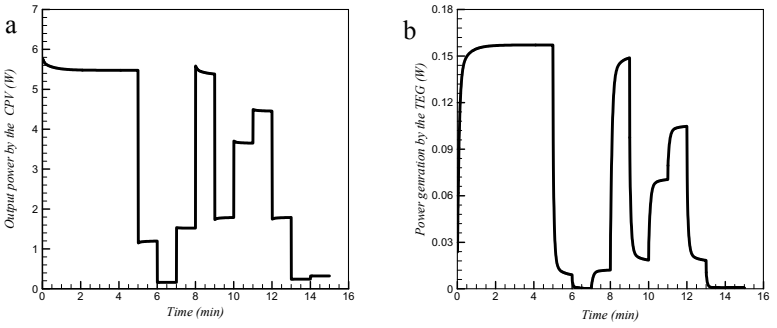

Fig. 3. (a) Power generation by the CPV; (b) Power generation by the TEG

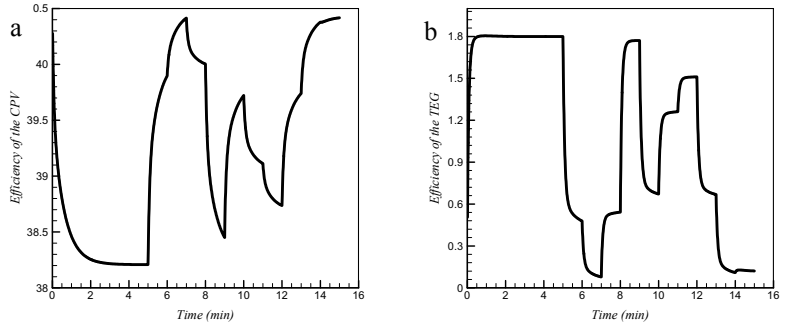

Fig. 4. (a) Efficiency of the CPV; (b) Efficiency of the TEG

Fig. 4(a) illustrates the variation of the efficiency of the CPV as a function of time. By taking into account the variation of the temperature of the CPV cell in the fig. 2(b), by increasing the temperature of the CPV cell, the efficiency will be decreased and vice versa. It is completely compatible with the equation of the efficiency of the CPV. Fig. 4(b) shows the efficiency of the TEG. As it can be observed, due to the low power generation and also small temperature difference between the hot side and cold side of the TEG the amount of the efficiency is not very significant. Although in the higher solar concentrations and temperature differences and also with using materials with higher ZT, the efficiency and power generation by TEG will be increased.

4. Conclusion

Transient power generation and efficiency of a CPV-TEG hybrid system has been investigated. Temperature variation for the CPV and hot side and cold side of TEG also was presented. The results also showed that with increasing the sun radiation, the power generation by CPV and TEG increased. However, the efficiency of the CPV is reduced by increasing the sun radiation. The system could be optimized with optimization of the TEG geometries, thermoelectric materials properties and using a more efficient heat sink.

Acknowledgements

The authors would like to acknowledge Center for Thermoelectric Energy Conversion funded in part by the Danish Council for Strategic Research, Programme Commission on Energy and Environment, under Grant No. 63607.

References

[1] Al-Nimr MA, Tashtoush BM, Jaradat AA. Modeling and simulation of thermoelectric device working as a heat pump and an electric generator under Mediterranean climate. Energy 2015;90(Part 2):1239–50.
[2] Wang N, Han L, He H, et al. A novel high performance photovoltaic– thermoelectric hybrid device. Energy Environ Sci 2011;4(9):3676–9.
[3] Rezania A, Rosendahl LA. Feasibility and parametric evaluation of hybrid concentrated photovoltaic-thermoelectric system. Appl Energy 2017;187:380–9.
[4] Wu YY, Wu SY, Xiao L. Performance analysis of photovoltaic–thermoelectric hybrid system with and without glass cover. Energy Convers. Manage 2015;93:151–9.
[5] Dallan BS, Schumann J, Frédéric JL. Performance evaluation of a photoelectric– thermoelectric cogeneration hybrid system. Sol. Energy 2015;118:276–85.
[6] Beeri O, Rotem O, Hazan E, Katz EA, Braun A, and Gelbstein Y. Hybrid photovoltaic-thermoelectric system for concentrated solar energy conversion: Experimental realization and modeling, J. Appl. Phys 2015; 118: 115104–1.
[7] Ju X, Wang Z, Flamant G, Li P, Zhao W. Numerical analysis and optimization of a spectrum splitting concentration photovoltaic-thermoelectric hybrid system. Sol. Energy 2012; 86:1941–54.
[8] Zhang J, Xuan Y, Yang L. Performance estimation of photovoltaic-thermoelectric hybrid Systems. Energy 2014;78:895-903.
[9] Kraemer D, Hu L, Muto A, Chen X, Chen G, Chiesa M. Photovoltaic-thermoelectric hybrid systems: A general optimization methodology. Appl. Phys. Lett 2008;92:243503–1.
[10] Rezania A, Sera D, Rosendahl LA. Coupled thermal model of photovoltaic-thermoelectric hybrid panel for sample cities in Europe. Renewable Energy 2016;99:127-135.
[11] Urbiola EAC, Vorobiev YV, Bulat LP. Solar hybrid systems with thermoelectric generators. Sol. Energy 2012;86: 369–78.
[12] Lamba R, Kaushik SC. Modeling and performance analysis of a concentrated photovoltaic– thermoelectric hybrid power generation system. Energy Convers. Manage 2016;115: 288–298.
[13] Notton G, Cristofari C, Mattei M, Poggi P. Modelling of a double-glass photovoltaic module using finite differences. Appl. Therm. Eng 2005;25:2854–77.
[14] Evans DL. Simplified method for predicting photovoltaic array output. Sol. Energy 1981;27: 555–60.
[15] AZUR SPACE Solar Power GmbH, Concentrator triple junction solar cell, Cell Type: 3C42-10 × 10 mm^2, Data Sheet (HNR 0003877-00-00), [Cited: June, 2016].
[16] Mi Z, Chen J, Chen N, Bai Y, Wu W, Fu R, Liu H. Performance Analysis of a Grid-connected High Concentrating Photovoltaic System under Practical Operation Conditions. Energies 2016, 9, 117; doi:10.3390/en9020117.

PAPER 7: REFERENCE [207]

Behavior of Hybrid Concentrated Photovoltaic-Thermoelectric Generator under Variable Solar Radiation

Sajjad Mahmoudi Nezhad, Alireza Rezania, Lasse Rosendahl

The paper has been published in
Energy Conversion and Management 164 (2018) 443-452.

Energy Conversion and Management 164 (2018) 443–452

Contents lists available at ScienceDirect

Energy Conversion and Management

journal homepage: www.elsevier.com/locate/enconman

Behavior of hybrid concentrated photovoltaic-thermoelectric generator under variable solar radiation

S. Mahmoudinezhad, A. Rezania*, L.A. Rosendahl

Department of Energy Technology, Aalborg University, Pontoppidanstraede 111, Aalborg DK-9220, Denmark

ARTICLE INFO

Keywords:
Concentrated photovoltaic cell
Thermoelectric generator
Hybrid module
Solar energy
Transient model

ABSTRACT

Transient response of a hybrid system composed of concentrated photovoltaic (CPV) cell and thermoelectric generator (TEG) is investigated in this study. This research is carried out by using a numerical simulation approach thermally coupled between the CPV and TEG. A transient model is established and solved by finite volume algorithm. In spite of temperatures profile in the hybrid CPV-TEG module, as results of variation of solar irradiation, power generation and efficiency of the CPV and TEG under the transient condition are presented. The results show that efficiency of the TEG and CPV varies diversely versus changing the solar radiation and module temperature. Moreover, the thermal response of the TEG stabilizes temperature fluctuation of the hybrid module when the solar radiation rapidly changes. In this work, impact of the thermal contact resistance on the temperature profile and system efficiency is investigated. The model presented in this study provides a fundamental understanding of the thermal and electrical effect of the TEG in hybrid CPV-TEG module under transient conditions.

1. Introduction

With growing population in the world and progress in technology and industry, additional energy sources are needed to be added to the existing energy reserves. Sun is an infinite source of energy, and fortunately, solar energy is a free, clean and abundant source of energy. Concentrated photovoltaic (CPV) cells are solar-based power generating cells which can convert a fraction of solar radiation into electricity with higher efficiency than conventional photovoltaic (PV) cells. Even CPVs dissipate more than half of the solar radiation as wasted thermal energy. By harvesting the dissipated heat into electricity, the efficiency and power generation of the system can be enhanced.

Due to some particular aspects like having no moving parts and long lifetime, being highly reliable, silent operation and being environment-friendly [1] thermoelectric generators (TEGs) have been a good choice for energy harvesting through the direct recovery of waste heat and conversion into useful electrical energy [2–4]. Most of the studies in the area of hybrid photovoltaic-thermoelectric systems considers integration of conventional PV modules with the TEG [5–8], while charectristics of CPV-TEG hybrid systems are examined less in the literature. Hybrid systems have been investigated using both numerical and experimental approaches [5–7]. Rezania et al. [9] found that a combined PV-TEG system is not an appropriate choice for power generation especially when the PV performance drops with increasing the temperature. They indicated that, with existing thermoelectric materials, the power generation by TEG plays only a small role in power generation in the hybrid PV-TEG panel. However in another investigation, Rezania and Rosendahl [10] showed that by increasing the solar radiation and with optimal geometry and material of the TEG, the hybrid CPV-TEG systems can be suitable, applicable and economically reasonable system. Wu et al. [11] presented a thermal and electric theoretical model for glazed/unglazed PV-TEG hybrid system.

A performance comparison between glazed and unglazed system was given. External parameters, such as wind velocity and nanofluid flow rate were investigated, and it was found that the variation of crucial factors can lead to a different system behavior. They also found that, for certain thermoelectric modules, a higher figure of merit, Z, may still cause a reduction in the system overall efficiency. Different aspects of CPV-TEG hybrid systems have been studied with different methods [12–20]. A hybrid system composed of a multi-junction PV cell and a TEG has been investigated experimentally by Beeri et al. [12].

Multi-physics software e.g. Comsol Multiphysics have been used for estimation of the complete influence of the TEG to the hybrid system performance. A theoretical thermodynamic model of an irreversible CPV–TEG hybrid system has been established by Lamba and Kaushik [13], where ideal concentration ratio based on the maximum power output of the hybrid system has been determined. Performance of different hybrid systems generating electricity and thermal energy using

* Corresponding author.
E-mail address: alr@et.aau.dk (A. Rezania).

https://doi.org/10.1016/j.enconman.2018.03.025
Received 20 December 2017; Received in revised form 9 March 2018; Accepted 10 March 2018

Nomenclature

Abbreviation

CPV	concentrated photovoltaic
PV	photovoltaic
SC	solar concentration
TE	thermoelectric
TEG	thermoelectric generator
ZT	figure of merit
EMF	electromotive force
PCM	phase change material
CS	contact surface

Greek script

α	seebeck coefficient, V/K
β	temperature coefficient, $\Delta\eta/\Delta T$, 1/K
ε	emissivity
η	conversion efficiency, %
σ	Stefan-Boltzmann constant, $W/m^2 K^4$
Δ	increment
τ	thomson coefficient, V/K
ρ	density (kg/m^3)
γ	electrical conductivity

Latin script

A	area, m^2
C	specific heat capacity, J/kg K
G	solar radiation, W/m^2
H	heat transfer coefficient, $W/m^2 K$
I	current, A
K	thermal conductivity, W/m K
L	length, m
n	number of thermocouples
P	power, W
q	inner heat source, W
Q	heat loss/heat transfer, W
r	resistance, Ω
T	temperature, K
x	heat transfer direction

Subscripts

1–12	contact surface numbers
a	ambient
c	cold junction
col	conductive layer
cel	ceramic layer
CPV	concentrated photovoltaic
f	cooling fluid
h	hot junction
hx	heat exchanger
ccs	copper conduction strip
max	maximum
rad	radiation
ref	reference
sky	sky
sp	solder paste
TEG	thermoelectric generator

Superscripts

b	the bottom contact surface
t	the top contact surface

TEGs for both non-concentrated and concentrated solar radiation cases has been investigated by Urbiola et al. [14] at relatively low temperatures (below 250 °C).

Ju et al. [15] studied an energy-based numerical model of spectrum splitting applied to PV-TEG hybrid system. Their results indicated that in comparison with the PV-only system the spectrum splitting PV–TE hybrid system is more appropriate for working under high concentration conditions. Energy analysis and exergy analysis approach was used by Li et al. [16] to study the performance of the PV-TE hybrid systems. The energy efficiency, exergy efficiency and the exergy losses of the PV-TE hybrid system were computed. The results showed that at higher concentration ratios and appropriate PV cell used in the PV-TE hybrid system can enhance the system overall conversion efficiency.

A parametric numerical study of the crucial factors in the CPV-TEG hybrid system is presented by Rezania and Rosendahl [10] with an energy cost comparison between CPV and CPV-TEG systems. The results indicated that the contribution of the TEG in power generation increases at high sun concentrations. To minimize energy cost, the optimal value of the heat transfer coefficient in the heat sink was obtained based on the critical design parameters of the CPV and the TEG. Heat flow and temperature distribution in a thermal concentrated PV-TEG hybrid system were investigated theoretically and numerically by Zhu et al. [17] in order to establish a cost and energy lumped model for evaluation of economic practicability of the hybrid technology.

Influence of different parameters like temperature, thermal contact resistance, concentrating ratio and convection heat transfer coefficient were investigated theoretically by Zhang et al. [18] for assessing the efficiency of a CPV-TEG hybrid system. They found that with the increase of cell temperature, the efficiency of polymer PV cell first enhances and then drops, which is appropriate for CPV-TEG hybrid systems. Liao et al. [19] found that the CPV-TEG hybrid system generates more electrical power and also has higher efficiency than a CPV or TEG. Li et al. [20] proposed a concentration solar thermoelectric generator design that used an improved theoretical model to calculate the maximum possible performance of the system.

This paper aims to provide a fundamental understanding of the fast transient behavior of CPV-TEG hybrid module throughout the investigation of the dynamic response of the CPV-TEG components in a hybrid module to the variation of solar radiation under partly cloudy weather conditions. As a matter of fact, since daily solar irradiance is varying with the time, the temperature of the CPV–TEG system, and consequently the power generation and efficiency of the system become unstable. To the best of our knowledge, none of the formerly published studies in this research area considered the transient behavior of the CPV-TEG hybrid system. This paper focuses on the significance of varying weather condition on temperatures, power generation and efficiency of the hybrid CPV-TEG system. This paper proposes an inclusive method to investigate the transient response of components of the hybrid CPV-TEG system to the every time-dependent solar radiation. Since effect of thermal contact resistance between the hybrid module layers can be critical on the system electrical output, influence of the thermal contact resistance at the interfaces between CPV-TEG and TEG-heat sink is, furthermore, evaluated.

2. Modeling and simulation analysis

Fluctuations of the weather condition, especially in the partly cloudy climates, and the effect of the variations on power generation

and efficiency of the hybrid system is a critical issue in order to stabilize the system's electrical response. The considered transient model involves most effective material and design parameters on such a module performance.

2.1. Conceptual model

The physical model of the CPV-TEG hybrid system is displayed in Fig. 1. The CPV-TEG hybrid system consists of the CPV cell, solder paste, conductive layer, ceramic substrates, copper conduction strips, solder layers, semiconductor thermocouples and thermal insulations. The solar irradiance can be concentrated by a concentrator. To increase the temperature difference between the hot and cold sides of the TEG and, simultaneously, to maintain the solar cell temperature below the critical operational temperature a heat exchanger is located underneath the TE modules. Area of the CPV cell and TEG module is 1 cm × 1 cm. The TEG module has 256 thermoelectric elements with cross sectional area of 0.44 mm × 0.44 mm. Geometry and material properties of the system layers can be seen in Table 1.

In this study, not only temperature of each layer in the hybrid module varias under transient solar radiation, there is high temperature variation between the hot and cold surfaces of the TEG. Therefore in this study, the thermoelectric material properties including the Seebeck coefficient, the electrical conductivity and the thermal conductivity, and therefore the figure of the merit as the key parameter, are taken depended on the temperature variation.

2.2. Numerical model

In order to evaluate the power generation and efficiency of the CPV-TEG hybrid system under the transient condition, an unsteady-state one-dimensional heat transfer model is established using energy conservation law. Finite volume method [25] has been used for representing and evaluating partial differential equations in the form of algebraic equations. The TEG module is a non-linear system with many components and effects. Some proper simplifications are used to examine the performance of the CPV-TEG system. The main simplifying assumptions are as follow:

1. The CPV and TEG are well thermal insulated, thus, heat transfer from the hybrid system to the environment is presumed to be zero except the heat loss from the top surface of the CPV cell by radiation and also heat transfer from the bottom surface of the CPV where is considered as a heat source for the TEG.
2. The radiative and convective heat losses between the TE elements in the TEG module are neglected.
3. The N- and P-type semiconductors in the TEG are composed of identical materials.
4. Different components of the TEG and CPV are well connected; so that electrical and thermal contact resistances are taken negligible.

Therefore, the one-dimensional transient conduction heat transfer model can be constructed as:

$$\rho c \frac{\partial T}{\partial t} = \frac{\partial}{\partial x}\left(k \frac{\partial T}{\partial x}\right) + q \tag{1}$$

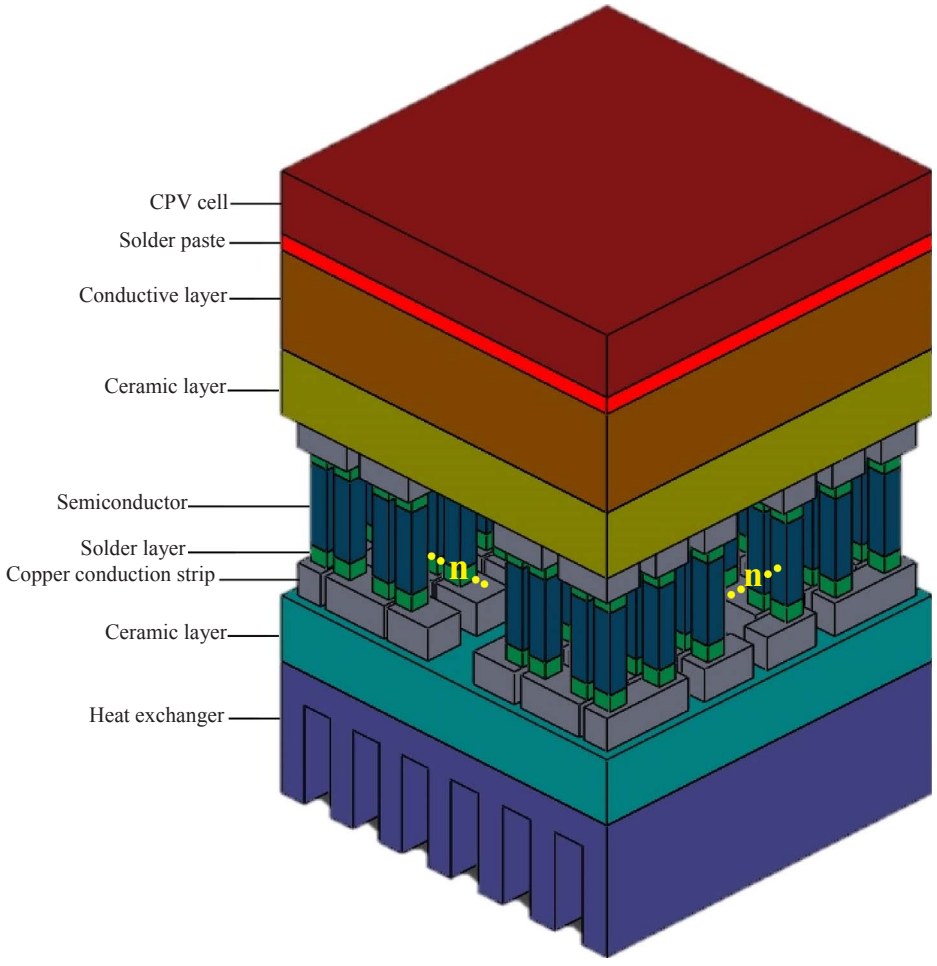

Fig. 1. The physical model of the CPV-TEG hybrid system.

Table 1
Geometry and material properties of different layers in the hybrid system.

Layer	Material	Thickness (mm)	Thermal conductivity (W/m K)	Density (kg/m^3)
CPV cell	GaInP/GaInAs/Ge [21]	0.19 [22]	60	5350
Solder paste	$Sn_{95}Ag_5$ [23]	0.05	37.8	7390
Conductive layer	Cu [23]	0.3	385	8900
Ceramic layer	99.5%Al_2O_3 [23]	0.2	25	3700
Copper conducting strip	Cu	0.1	385	8900
Semiconductor	Bi_2Te_3 [24]	1.00	[a]	7300

[a] $K(T) = 5.32-0.0187T + 2.44\times10^{-5}T^2-3.24\times10^{-10}T^3$ (W/(m K)) [24].

A working TEG comprises three elementary TE effects, including the Seebeck, Peltier and Thomson effects, and two accessorial effects, including the Joule and Fourier effects. The electromotive force (EMF) is produced by the Seebeck effect. Peltier effect, Thomson effect, and Joule effects cause Peltier heat, Thomson heat, and Joule heat, respectively. Although the Peltier effect is not an interface effect, the Peltier heat produces only on the end sides of the semiconductors. Thomson heat and Joule heat production that are volumetric effects are assumed to be equally transferred to the hot and cold junctions of the semiconductor elements [26,27]. Fig. 2 shows the one-dimensional heat transfer physical model of the CPV-TEG module considered in this study.

Cooling condition on the cold side of the TEG is assumed to be free convection heat transfer with water as the working fluid. By using energy conservation law for each contact surface of the system shown in Fig. 1, a set of nonlinear equations were created in order to determine the value of temperature in different layers. Therefore, the power generation and efficiency of the CPV and TEG can be calculated. The corresponding boundary conditions of different elements are listed as follow:

On the top surface of the CPV cell (CS1):

$$\rho_{CPV}c_{CPV}V_{CPV}\frac{\partial T_{CPV}}{\partial t} = SC\times G\times A_{CPV}-Q_{rad}+KA\left(\frac{\partial T}{\partial x}\right)\Big|_{x=CS_1^b}-P_{CPV} \quad (2)$$

Although due to the small area of the CPV cell, the radiation heat loss from the top surface of the CPV is small, it is considered in the calculations and could be obtained by Eq. (3):

$$Q_{rad} = \varepsilon\sigma A_{CPV}(T_{CPV^t}^4-T_{sky}^4) \quad (3)$$

where $\sigma = 5.67\times10^{-8}$ W/m^2 K^4. The sky temperature is taken dependent to the ambient temperature according to a study by Nowak [28].

In Eq. (2), the power generation by the CPV cell is a function of the solar concentration, solar radiation, area of the cell and efficiency of the CPV cell:

$$P_{CPV} = SC\times G\times A_{CPV}\times\eta_{CPV} \quad (4)$$

where the efficiency of the CPV cell and is determined by linear function [29]:

$$\eta_{CPV} = \eta_{T_{ref}}[1-\beta_{ref}(T_{CPV}-T_{ref})] \quad (5)$$

where $\eta_{T_{ref}}$ is electrical conversion efficiency of the CPV cell at the reference temperature (T_{ref} = 25 °C) and reference solar radiation (G_{ref} = 1000 W/m^2) [30]. In Eq. (5), β_{ref} is the CPV cell temperature coefficient at the reference temperature, which is commonly provided by the manufacturer and considered as −0.1%/K [21] in this study.

Conductive heat transfer crossing the boundaries of the CPV cell, solder paste, and the conductive layer is presented in Eqs. (6)–(8).

On the top surface of the solder paste (CS2):

$$\rho_{sp}c_{sp}V_{sp}\frac{\partial T_{sp}}{\partial t} = k_{CPV}A_{CPV}\left(\frac{\partial T}{\partial x}\right)\Big|_{x=CS_2^t}-k_{sp}A_{sp}\left(\frac{\partial T}{\partial x}\right)\Big|_{x=CS_2^b} \quad (6)$$

On the bottom surface of the solder paste (CS3):

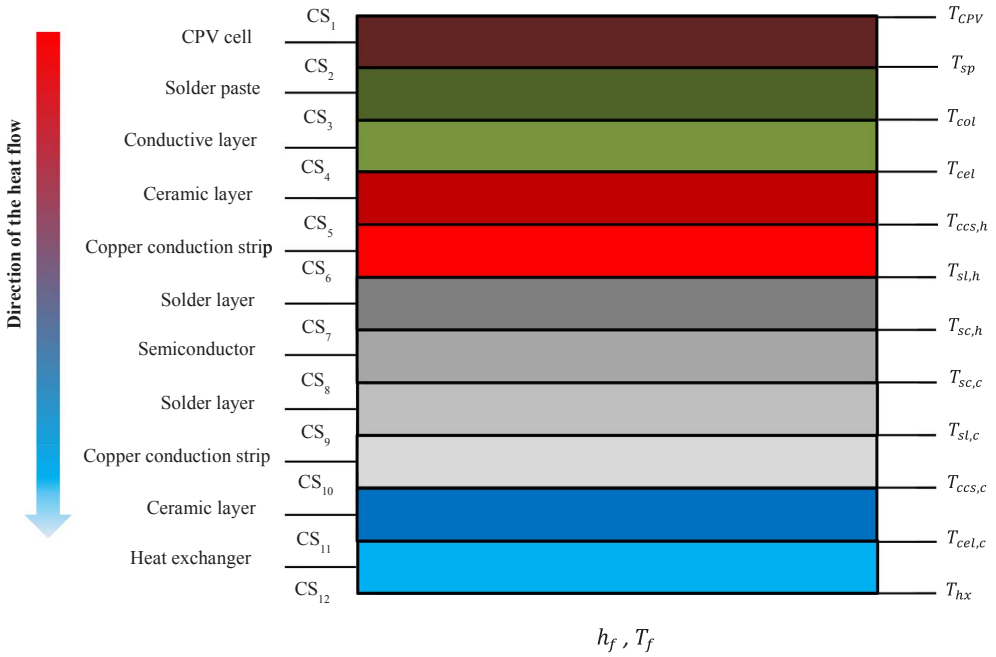

Fig. 2. One-dimensional heat transfer physical model of the CPV-TEG module.

$$\rho_{col}c_{col}V_{col}\frac{\partial T_{col}}{\partial t} = k_{sp}A_{sp}\left(\frac{\partial T}{\partial x}\right)\Big|_{x=CS_3^t} - k_{col}A_{col}\left(\frac{\partial T}{\partial x}\right)\Big|_{x=CS_3^b} \quad (7)$$

On the bottom surface of the conductive layer (CS4):

$$\rho_{cel}c_{cel}V_{cel}\frac{\partial T_{cel}}{\partial t} = k_{col}A_{col}\left(\frac{\partial T}{\partial x}\right)\Big|_{x=CS_4^t} - k_{cel}A_{cel}\left(\frac{\partial T}{\partial x}\right)\Big|_{x=CS_4^b} \quad (8)$$

In this study, there are n pairs of P–N junction in the TE module. The thermoelectric elements are divided into m control volumes. With consideration of the Peltier, Thomson and Joule effects, the corresponding boundary conditions of different ingredients of the TEG are listed as follow:

On the contact surface between the ceramic layer and copper conduction strip (CS5):

$$\rho_{ccs}c_{ccs}V_{ccs}\frac{\partial T_{ccs,h}}{\partial t} = k_{cel}n_{cel}A_{cel}\left(\frac{\partial T}{\partial x}\right)\Big|_{x=CS_5^t} - k_{ccs}n_{ccs}A_{ccs}\left(\frac{\partial T}{\partial x}\right)\Big|_{x=CS_5^b} - \frac{n_{ccs}I^2r_{ccs}}{2} \quad (9)$$

On the contact surface between copper conduction strip and the solder layer (CS6):

$$\rho_{sl}c_{sl}V_{sl}\frac{\partial T_{sl,h}}{\partial t} = k_{ccs}n_{ccs}A_{ccs}\left(\frac{\partial T}{\partial x}\right)\Big|_{x=CS_6^t} - \frac{n_{ccs}I^2r_{ccs}}{2} - k_{sl}n_{sl}A_{sl}\left(\frac{\partial T}{\partial x}\right)\Big|_{x=CS_6^b} - \frac{n_{sl}I^2r_{sl}}{2} \quad (10)$$

On the contact surface between solder layer and semiconductor (CS7):

$$\rho_{sc}c_{sc}V_{sc}\frac{\partial T_{sc,h}}{\partial t} = k_{sl}n_{sl}A_{sl}\left(\frac{\partial T}{\partial x}\right)\Big|_{x=CS_7^t} - \frac{n_{sl}I^2r_{sl}}{2} - k_{sc}n_{sc}A_{sc}\left(\frac{\partial T}{\partial x}\right)\Big|_{x=CS_7^b} + n_{sc}\alpha_{sc,h}IT_{sc,h} - \frac{n_{sc}I^2r_{sc,l}}{2} - \frac{n_{sc}\tau_l I(T_{sc,h}-T_{sc,2})}{2} \quad (11)$$

On the contact surface between semiconductor and solder layer (CS8):

$$\rho_{sc}c_{sc}V_{sc}\frac{\partial T_{sc,c}}{\partial t} = k_{sc}n_{sc}A_{sc}\left(\frac{\partial T}{\partial x}\right)\Big|_{x=CS_8^b} - n_{sc}\alpha_{sc,h}IT_{sc,h} - \frac{n_{sc}I^2r_{sc,m}}{2} - \frac{n_{sc}\tau_m I(T_{sc,m}-T_{sc,c})}{2} - k_{sl}n_{sl}A_{sl}\left(\frac{\partial T}{\partial x}\right)\Big|_{x=CS_8^t} + \frac{n_{sl}I^2r_{sl}}{2} \quad (12)$$

On contact surface between solder layer and copper conduction strip (CS9):

$$\rho_{sl}c_{sl}V_{sl}\frac{\partial T_{sl,c}}{\partial t} = k_{sl}n_{sl}A_{sl}\left(\frac{\partial T}{\partial x}\right)\Big|_{x=CS_9^t} - \frac{n_{sl}I^2r_{sl}}{2} - k_{ccs}n_{ccs}A_{ccs}\left(\frac{\partial T}{\partial x}\right)\Big|_{x=CS_9^b} - \frac{n_{ccs}I^2r_{ccs}}{2} \quad (13)$$

On contact surface between copper conduction strip and ceramic substrate (CS10):

$$\rho_{ccs}c_{ccs}V_{ccs}\frac{\partial T_{ccs,c}}{\partial t} = k_{ccs}n_{ccs}A_{ccs}\left(\frac{\partial T}{\partial x}\right)\Big|_{x=CS_{10}^t} - \frac{n_{ccs}I^2r_{ccs}}{2} - k_{cel}n_{cel}A_{cel}\left(\frac{\partial T}{\partial x}\right)\Big|_{x=CS_{10}^b} \quad (14)$$

On contact surface between ceramic substrate and heat exchanger base (CS11):

$$\rho_{cel}c_{cel}V_{cel}\frac{\partial T_{cel,c}}{\partial t} = k_{cel}n_{cel}A_{cel}\left(\frac{\partial T}{\partial x}\right)\Big|_{x=CS_{11}^t} - k_{hx}A_{hx}\left(\frac{\partial T}{\partial x}\right)\Big|_{x=CS_{11}^b} \quad (15)$$

On contact surface between heat exchanger base and the cooling fluid (CS12):

$$\rho_{hx}c_{hx}V_{hx}\frac{\partial T_{hx}}{\partial t} = k_{hx}A_{hx}\left(\frac{\partial T}{\partial x}\right)\Big|_{x=CS_{12}^t} + h_fA_f(T_{hx,2}-T_f) \quad (16)$$

Time-dependent and coupled temperatures of each layer in the hybrid module are calculated by solving above equations.

2.3. Power generation and efficiency

Corresponding to Eqs. (4) and (5), power generation and efficiency of the CPV cell can be calculated by the temperature of the CPV cell.

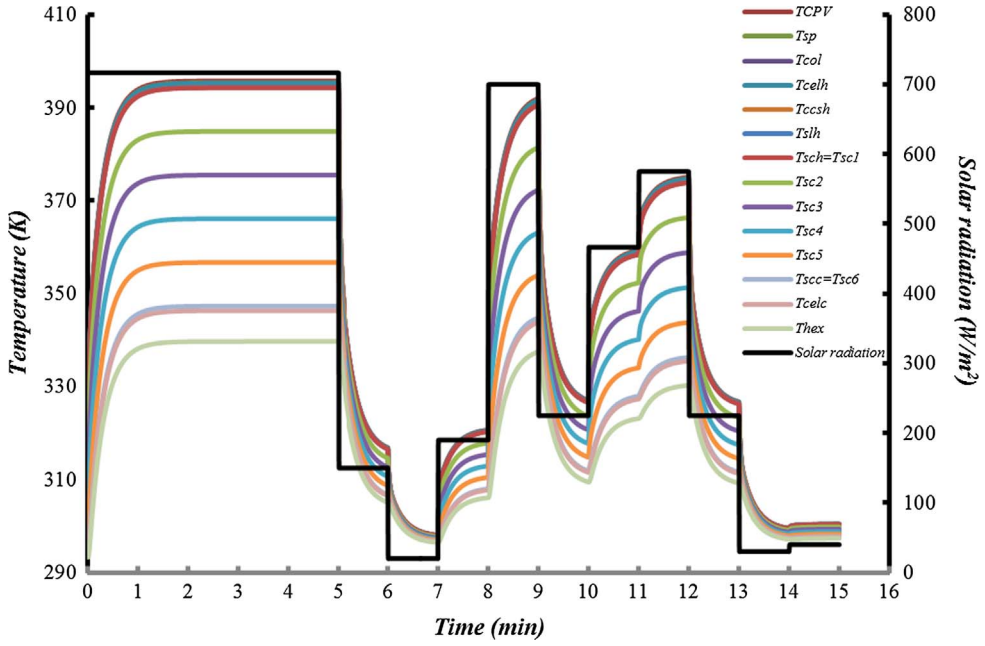

Fig. 3. Variation of solar radiation and the temperatures of hybrid module components versus time.

Since this temperature varies with the variation of the solar irradiation, both of the power generation and efficiency are a function of the time. Power generation and efficiency of the TEG also can be achieved by finding the temperature of the TEG layers. By, taking into consideration the impact of the Thomson effect, the electromotive force (EMF) of the TEG module is:

$$E = n_{sc}\left[\alpha_{sc,h}T_{sc,h} - \alpha_{sc,c}T_{sc,c} - \sum_{i=1}^{m-1}\tau_i(T_i - T_{i+1})\right] \quad (17)$$

The internal electrical resistance of the TEG module, which consists electrical resistance of the copper conduction strip, solder layer, and semiconductors:

$$R_i = \left(n_{ccs}r_{ccs} + n_{sl}r_{sl} + n_{sc}\sum_{i=1}^{m} r_{sc,i}\right) \quad (18)$$

Therefore, the power generation can be calculated as follows:

$$P_{TEG} = (E/(R_i + R_L))^2 R_L = \left[n_{sc}\left[\alpha_{sc,h}T_{sc,h} - \alpha_{sc,c}T_{sc,c} - \sum_{i=1}^{m-1}\tau_i(T_i - T_{i+1})\right]\right]^2 R_L \Bigg/ \left[\left(n_{ccs}r_{ccs} + n_{sl}r_{sl} + n_{sc}\sum_{i=1}^{m} r_{sc,i}\right) + R_L\right]^2 \quad (19)$$

and instantaneous efficiency of the TEG is defined as:

$$\eta_{TEG} = P_{TEG}/(SC \times G \times A - Q_{rad} - P_{cpv}) \quad (20)$$

3. Results and discussion

The presented model in this study is capable to trace the temperature variation due to fluctuation in the solar radiation. Fig. 3 shows the variation of solar radiation under typical partly cloudy weather condition during a period of time in the wet season in locations such as Kunming, China [31] considered in this study.

The time-dependent temperature of the hybrid module's components can be obtained as results of the simulation process. Fig. 3 shows the dynamic response of the temperatures of studied layers in the hybrid module including the temperature of the CPV cell and hot and cold sides of the TEG. Initial temperature for all the components of the hybrid module was taken 293 K. Therefore, here is a startup transient part starting from $t = 0$, which takes around two minutes for the selected solar concentration $SC = 400$ and heat transfer coefficient in the heat sink efficiency $h_f = 2000$ W/m^2 K. Obviously by selecting other values of the solar concentration and heat sink efficiencies, the temperature profile shown in Fig. 3 would be different. All the temperatures are directly affected by the sharp instabilities of the solar radiation. Temperatures of the CPV surface and the TEG hot side are almost equal due to the high thermal conductivity of the CPV cell. Since the thermal conductivity of the TE elements is relatively low and there is a higher resolution in the temperature distribution, the semiconductors are divided to 5 segments and the temperatures of these segments (T_{sc1} to T_{sc6}) are computed. Because of the lower thermal conductivity of the semiconductor material, the temperature difference between the segments is higher than temperature difference through the other components of the hybrid module. The temperatures of all the ingredients fluctuate with the same trend within the short time interval. This delay is caused by the critical considered parameters thermal resistance, density, and heat capacity of the module's components and needed time for passing the heat through the CPV cell and the TEG module. The temperature fluctuations correspond to the variation of the solar radiation shown in Fig. 3. Depending on the heat transfer coefficient in the heat sink, the system reaches to steady state condition after a while. It is worthy to note that, due to the low amount of heat flux across the hybrid module when the solar radiation is low, all the temperatures are close to each other under partly cloudy weather conditions. However, by increasing the solar radiation, the temperatures difference between the hot and cold side of each layer increases.

Temperature plays an essential role in power generation by the CPV cell and TEG module. There is a contradiction in working status of the CPV cell and TEG module for different temperature values. Increment in temperature of the CPV causes dropping in CPV conversion efficienc. On the other hand, it enhances the temperature difference between the hot and cold sides of the TEG; so that the power generation and conversion efficiency of the TEG are enhanced (see Figs. 4 and 6). This reverse bahavior must be considered in design of the hybrid module under practical optimal operating conditions. In the following sections the effect of the temperature, as a vital parameter, along with other parameters on power generation and efficiency of the CPV cell and TEG module will be presented and discussed. An optimized TEG model, which considers this reverse effect of the temperature on the power generation and efficiency of the CPV-TEG module, is required to minimize negative effect of the ambient condition variation on the system performance.

Fig. 4 shows the variation of the CPV cell efficiency versus time. According to Eq. (5), for constant temperature coefficient (β_{ref}), the

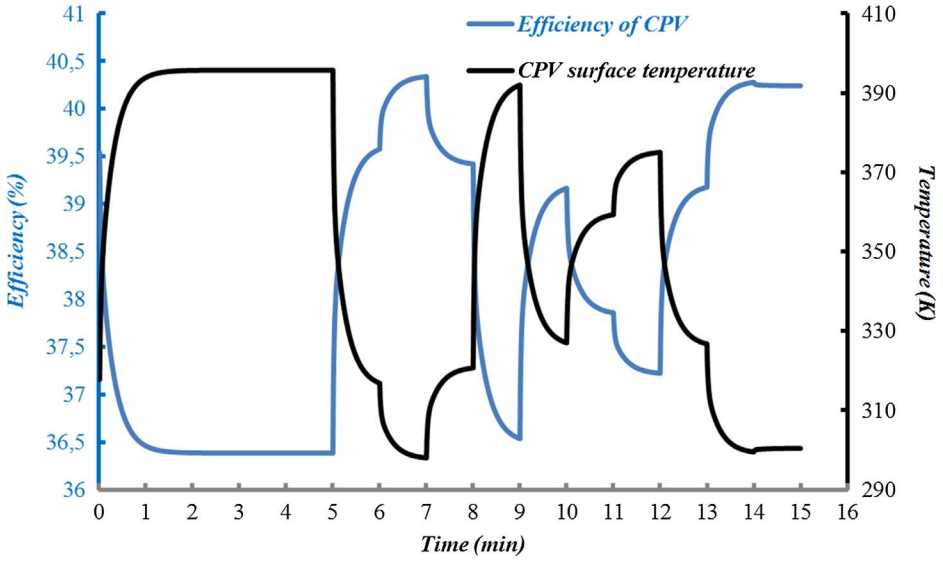

Fig. 4. Variation of efficiency and temperature of the CPV cell versus time.

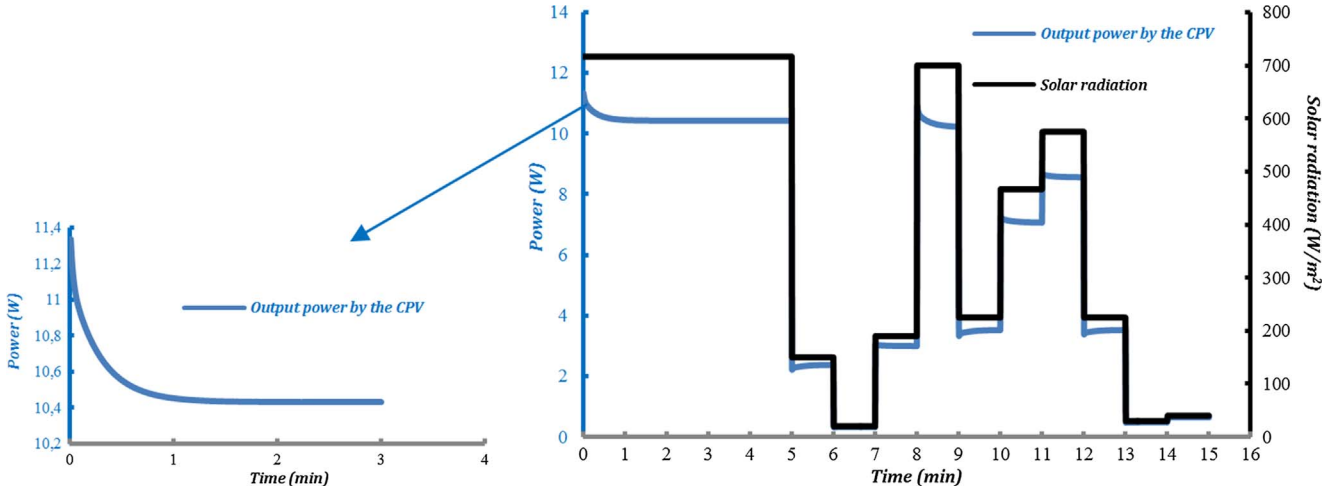

Fig. 5. Power generation by the CPV cell.

efficiency of the CPV has an inversely proportional relationship to its temperature. Consequently, by variation of the solar radiation, the temperature of the CPV cell changes, and the efficiency of the CPV cell also alters.

According to Eq. (4), the temperature of the CPV cell is an important parameter in power generation by the CPV. As shown in Fig. 4, by increasing the solar radiation from fully cloudy condition to the clear sky, the efficiency of the CPV reduces ~ 4%. The effect of the temperature increment, and consequently the efficiency of the CPV, on the cell power generation, can be seen in the very small transient parts of Fig. 5, However, the variation of the solar irradiation has the most significant effect on the power generation. The power generation graph follows the graph of the solar radiation in an almost same manner with non-linear behavior that is due to variation in the temperature of the CPV.

Two of the important parameters in power generation by the TEG are the figure of merit and temperature difference between the hot and cold sides of the TEG. In this study, since value the figure of merit changes within small range due to the small variation of the TEG average temperature, the temperature difference between the hot and cold sides of the TEG is the most dominant factor. Fig. 6 shows the power generation by the TEG and the variation of the temperature difference. It can be seen that, by an increment in the temperature difference, the efficiency and the power produced by the TEG also increases, and vice versa.

As displayed in Fig. 6, by increasing the received solar radiation, and consequently the temperature difference, the power generation enhances. By taking Eq. (20) into consideration, the efficiency of the TEG changes with the power generation with a directly proportional relationship (Fig. 7). Using appropriate TEG materials with higher ZT and providing an optimal design for the TEG and heat sink in order to make higher temperature difference enhances the power generation and efficiency of the TEG.

One of the remarkable outcomes of this study is the way that the CPV and TEG respond to variation of weather condition at the same time. As can be seen in Fig. 8, the CPV and TEG have opposite tendency in response to variation of the solar irradiation. The hybrid module of the CPV-TEG technologies discussed in this study is a worthy aspect for further study because even under an unstable weather condition with fluctuation in the solar radiation, the TEG generates some additional power to the reduced power generation by the CPV. Since the efficiency of the TEG varies inversely to the efficiency of the CPV cell, application of the TEG helps to compensate a fraction of the lost power generation by the CPV. Since geometry of the TEG plays a vital role in the performance of the module, the optimization of the TEG geometry for enhancement of overal efficiency of the hybrid system can be interesting as future study.

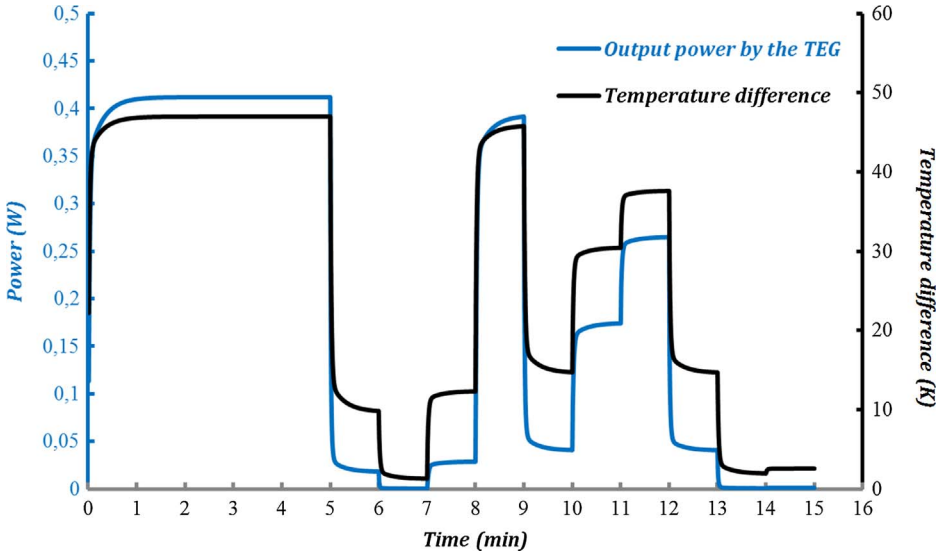

Fig. 6. Power generation by the TEG and temperature difference.

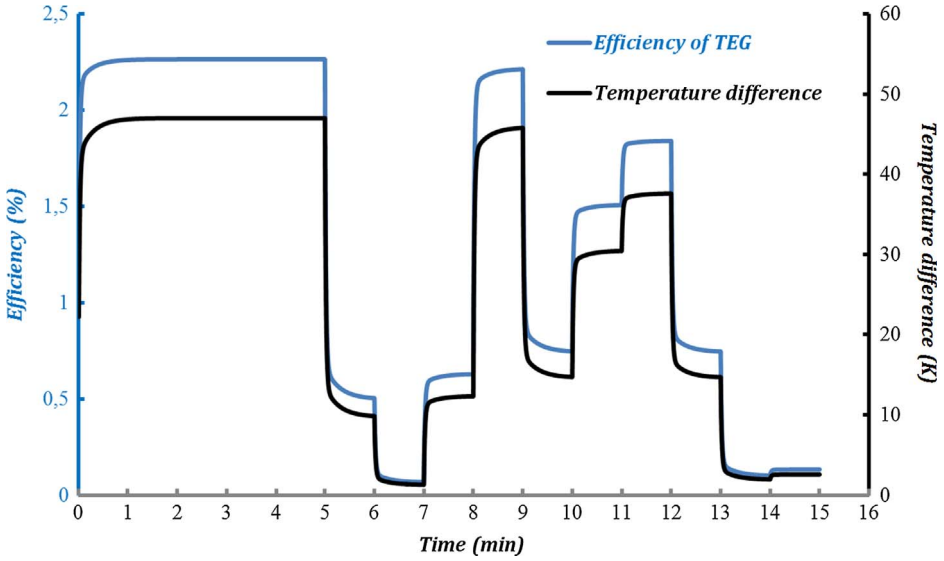

Fig. 7. Variation of the efficiency of the TEG and temperature difference versus time.

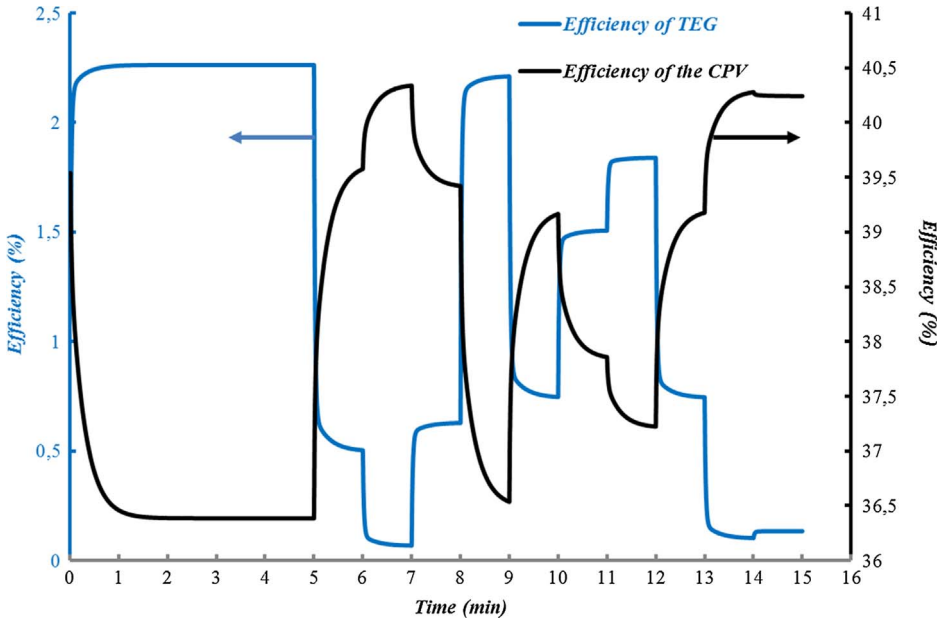

Fig. 8. Variation of the efficiency of the CPV cell and the TEG versus time.

Fig. 9 shows the power generation by the CPV-only and CPV-TEG hybrid system for first 3 min at constant solar radiation. As can be seen, the output power by the CPV cell is varies over range of 10.43 W and 11.33 W, while the output power by the entire hybrid system varies between 10.84 W and 11.44 W. Therefore it can be note that, the existence of the TEG in the hybrid system helps to have more stable output power. This stability enhances when TEGs with higher ZT value are used in the hybrid module. For higher ZT values, power generation from the TEG is enhanced and, therefore, more wasted heat can be recovered and more stable power will be produced by the hybrid system.

In analysis of the heat conduction across the multilayer hybrid module, ideal contact resistance was assumed at the interfaces of the CPV-TEG and the TEG-heat sink. Therefore, no temperature drop accured at the interfaces, as results of the calculations. Although, under practial circumstances, thermal contact resistance can play an critical role in invstigation of the temperature profile across the module and can cause temperature drop at the interfaces. Thermal contact resistance can be defined as ratio between this temperature drop and the average heat flow across the interface, as stated by Eq. (21):

$$R_c = \frac{\Delta T_{interface}}{\dot{Q}/A} \ (\mathrm{m^2.^\circ C/W}) \tag{21}$$

In order to evaluate effect of the thermal contact resistance between the CPV-TEG and TEG-heat sink, the heat transfer equation across the interface can be added to the Eqs. (8) and (15):

$$\dot{Q} = h_c A \Delta T_{interface} \tag{22}$$

where h_c is thermal contact conductance, in inverse to the thermal contact resistance, and $\Delta T_{interface}$ is effective temperature difference at the interface.

Significance of the thermal contact resistance changes with variation of surface roughness, material properties, temperature and pressure at the interface, and type of fluid trapped at the interface. Based on the experimental results, magnitudes of the thermal contact resistance is considered over a wide range of valuses, between 5×10^{-6} and

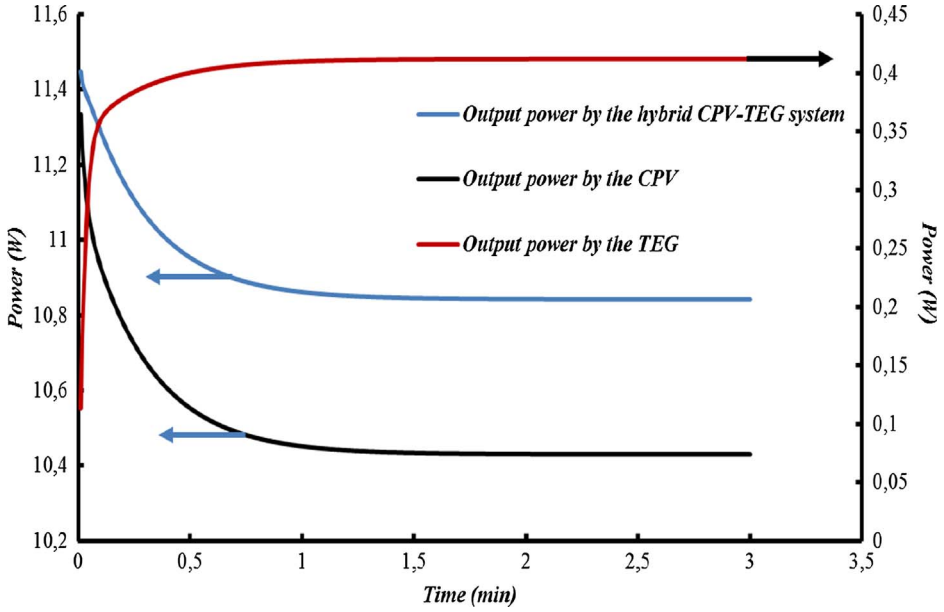

Fig. 9. Variation of the output power by the CPV cell, TEG module and the hybrid system versus time.

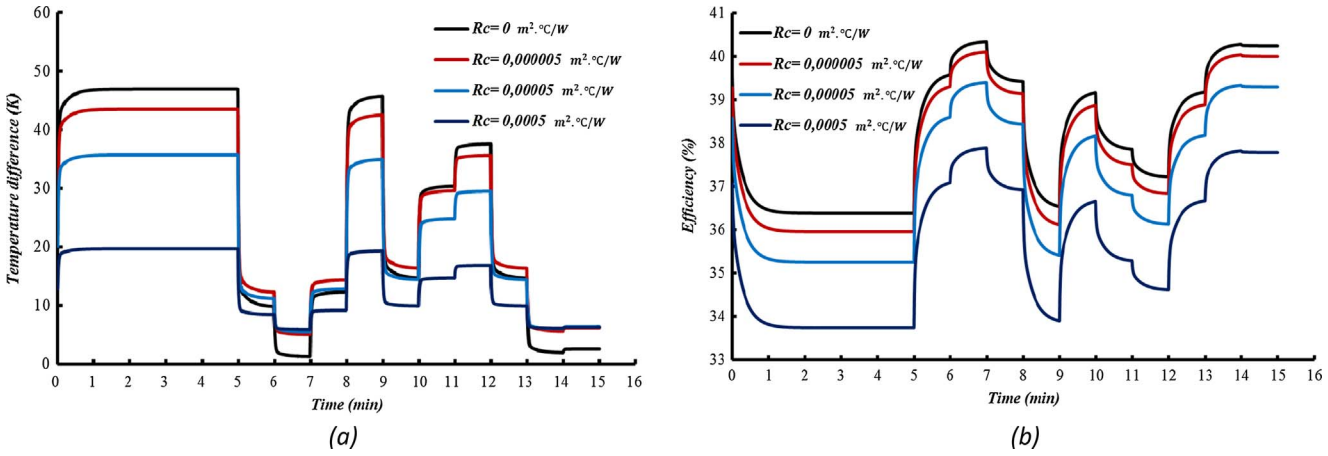

Fig. 10. Variation of the (a) temperature difference across the TEG and (b) efficiency of the CPV versus time for different thermal contact resistances.

5×10^{-4} m².°C/W [32]. Fig. 10(a) shows sensitivity of the temperature difference across the TEG to different values of the thermal contact resistances.

As shown, by increment in the thermal contact resistance from zero (idead contact) to 5×10^{-4} m² °C/W, the temperature difference across the TEG decreases, that causes reduction in TEG conversion efficiency. The sensitivity illustarion of the CPV efficiency in Fig. 10(b) indicates that, at higher thermal contact resistance the thermal conductance between the TEG and the CPV and furthermore betwenn the TEG and heat sink reduces. Concequently, the operating temperature of the CPV increases. Increment in the CPV cell temperature leads to lower efficiency and power generation by the CPV.

4. Conclusions

To evaluate the performance of the CPV-TEG hybrid module under transient solar radiation, one-dimensional, and thermally coupled, a dynamic model is established and solved by finite volume method. The results show that temperatures of all components are directly affected by the sharp fluctuations in the solar radiation. Due to the low thermal conductivity of the semiconductor material, the temperature drop across the thermoelectric elements is more significant compared to the other layers in the hybrid module. An optimization would be needed to consider the opposite effect of the temperature on the power and efficiency of the CPV cell and TEG module. This optimization will be presented in the future study. Increasing the solar radiation reduces the CPV efficiency but increases the TEG efficiency. Application of the TEG causes more stable overall power generation by the hybrid module as the weather condition suddenly changes since the efficiency of the TEG varies inversely to the efficiency of the CPV cell. The model provided a fundamental understanding of the stability of overall output performance by counting TEG effect, that can play an important role in the CPV industry in locations that the weather is partly cloudy and frequently fluctuation of solar radiation causes instability in the power generation. The results show that, the thermal contact resistance has a substantial effect on the temperature profile, power generation and efficiency of the TEG and CPV, and cannot be ignored for optimal design of the hybrid module. Higher thermal contact resistance leads to less efficient TEG and CPV.

References

[1] Nezhad Sajjad Mahmoudi, Rezaniakolaei Alireza, Rosendahl Lasse Aistrup. Experimental study on effect of operating conditions on thermoelectric power generation. Energy Procedia 2017;142:558–63.
[2] Makki Adham, Omer Siddig, Su Yuehong, Sabir Hisham. Numerical investigation of heat pipe-based photovoltaic–thermoelectric generator (HP-PV/TEG) hybrid

system. Energy Convers Manage 2016;112:274–87.
[3] He W, Su YH, Riffat SB, Hou JX, Ji J. Parametrical analysis of the design and performance of a solar heat pipe thermoelectric generator unit. Appl Energy 2011;88:5083–9.
[4] Hsu CT, Huang GY, Chu HS, Yu B, Yao DJ. Experiments and simulations on low-temperature waste heat harvesting system by thermoelectric power generators. Appl Energy 2011;88:1291–7.
[5] Kossyvakis DN, Voutsinas GD, Hristoforou EV. Experimental analysis and performance evaluation of a tandem photovoltaic–thermoelectric hybrid system. Energy Convers Manage 2016;117:490–500.
[6] Vorobiev Yu, Gonzalez-Hernandez J, Vorobiev P, Bulat L. Thermal-photovoltaic solar hybrid system for efficient solar energy conversion. Sol Energy 2006;80:170–6.
[7] Babu Challa, Ponnambalam P. The role of thermoelectric generators in the hybrid PV/T systems: A review. Energy Convers Manage 2017;151:368–85.
[8] Lin Jian, Liao Tianjun, Lin Bihong. Performance analysis and load matching of a photovoltaic–thermoelectric hybrid system. Energy Convers Manage 2015;105:891–9.
[9] Rezania A, Sera D, Rosendahl LA. Coupled thermal model of photovoltaic-thermoelectric hybrid panel for sample cities in Europe. Renew Energy 2016;99:127–35.
[10] Rezania A, Rosendahl LA. Feasibility and parametric evaluation of hybrid concentrated photovoltaic-thermoelectric system. Appl Energy 2017;187:380–9.
[11] Wu YY, Wu SY, Xiao L. Performance analysis of photovoltaic–thermoelectric hybrid system with and without glass cover. Energy Convers Manage 2015;93:151–9.
[12] Beeri O, Rotem O, Hazan E, Katz EA, Braun A, Gelbstein Y. Hybrid photovoltaic-thermoelectric system for concentrated solar energy conversion: experimental realization and modeling. J Appl Phys 2015;118:1151041–8.
[13] Lamba Ravita, Kaushik SC. Modeling and performance analysis of a concentrated photovoltaic– thermoelectric hybrid power generation system. Energy Convers Manage 2016;115:288–98.
[14] Chavez-Urbiola EA, Vorobiev YuV, Bulat LP. Solar hybrid systems with thermoelectric generators. Sol Energy 2012;86:369–78.
[15] Ju Xing, Wang Zhifeng, Flamant Gilles, Li Peng, Zhao Wenyu. Numerical analysis and optimization of a spectrum splitting concentration photovoltaic–thermoelectric hybrid system. Sol Energy 2012;86:1941–54.
[16] Li Dianhong, Xuan Yimin, Li Qiang, Hong Hui. Exergy and energy analysis of photovoltaic-thermoelectric hybrid systems. Energy 2017;126:343–51.
[17] Zhu Wei, Deng Yuan, Wang Yao, Shen Shengfei, Gulfam Raza. High-performance photovoltaic-thermoelectric hybrid power generation system with optimized thermal management. Energy 2016;100:91–101.
[18] Zhang Jin, Xuan Yimin, Yang Lili. Performance estimation of photovoltaic-thermoelectric hybrid systems. Energy 2014;78:895–903.
[19] Liao Tianjun, Lin Bihong, Yang Zhimin. Performance characteristics of a low concentrated photovoltaic-thermoelectric hybrid power generation device. Int J Therm Sci 2014;77:158–64.
[20] Li Peng, Cai Lanlan, Zhai Pengcheng, Tang Xinfeng, Zhang Qingjie, Niino M. Design of a concentration solar thermoelectric generator. J Electron Mater 2010;39(9):1522–30.
[21] AZUR SPACE Solar Power GmbH. Concentrator triple junction solar cell, Cell Type: 3C42-10 _ 10mm2. Data Sheet (HNR 0003877–00-00). [Cited: June, 2016].
[22] Micheli L, Sarmah N, Reddy KS, Luo X, Mallick TK. Design, development, and analysis of a densely packed 500x concentrating photovoltaic cell assembly on insulated metal substrate. Int J Photoenergy 2015;2015:341032.
[23] Cotal H, Frost J. Heat transfer modeling of concentrator multijunction solar cell assemblies using finite difference techniques. In: Photovoltaic specialists conference (PVSC), 35th IEEE 2010:213–8.
[24] Gou Xiaolong, Ping Huifeng, Ou Qiang, Xiao Heng, Qing Shaowei. A novel thermoelectric generation system with thermal switch. Appl Energy 2015;160:843–52.
[25] Patankar SV. Numerical heat transfer and fluid flow. USA: Taylor & Francis; 1980.
[26] Meng F, Chen L, Sun F. A numerical model and comparative investigation of a thermoelectric generator with multi-irreversibilities. Energy 2011;36(5):3513–22.
[27] Min Chen, Lasse Rosendahl, Inger Bach, Thomas Condra, John Pedersen. Irreversible transfer processes of thermoelectric generators. Am J Phys 2007;75(9):815–20.
[28] Nowak H. The sky temperature in net radiant heat loss calculations from low-sloped roofs. Infrared Phys 1989;29:231–2.
[29] Evans DL. Simplified method for predicting photovoltaic array output. Sol Energy 1981;27:555–60.
[30] Notton G, Cristofari C, Mattei M, Poggi P. Modelling of a double-glass photovoltaic module using finite differences. Appl Therm Eng 2005;25:2854–77.
[31] Mi Z, Chen J, Chen N, Bai Y, Wu W, Fu R, et al. Performance analysis of a grid-connected high concentrating photovoltaic system under practical operation conditions. Energies 2016;9:117. http://dx.doi.org/10.3390/en9020117.
[32] Çengel. Introduction to Thermodynamics and Heat Transfer, McGraw – Hill Primis, 2008; ISBN: 0 – 390 – 86122 – 7.

PAPER 8: REFERENCE [218]

Transient Experimental and Numerical Study on the Transient Behavior of Multi-Junction Solar Cell-Thermoelectric Generator Hybrid System

Sajjad Mahmoudi Nezhad, Saeed Ahmadi Atouei, Petru Adrian Cotfas, Daniel Tudor Cotfas, Lasse Rosendahl, Alireza Rezania

The paper is under review in the Energy Conversion and Management journal.

Experimental and Numerical Study on the Transient Behavior of Multi-Junction Solar Cell-Thermoelectric Generator Hybrid System

S. Mahmoudinezhad[*1], S. Ahmadi Atouei[2], P.A. Cotfas[3], D.T. Cotfas[3], L.A. Rosendahl[1], A. Rezania[1]

[1]*Department of Energy Technology, Aalborg University, Pontoppidanstraede 111, Aalborg DK-9220, Denmark*

[2]*Department of Mechanical Engineering, Babol University of Technology, P.O. Box 484, Babol, Iran*

[3]*Electrical Engineering and Computer Science Faculty, Transilvania University of Brasov, 500036 Brasov, Romania*

Abstract

An experimental investigation and numerical verification of the transient behavior of a hybrid concentrating triple junction (CTJ) solar cell-Thermoelectric Generator (TEG) system is presented in this paper. The experimental work is accomplished under varying concentrated solar radiations using a solar simulator, and the numerical study is conducted using COMSOL Multiphysics Modeling Software. An arbitrary pattern for the solar radiation varying between 0 to 39 suns is considered in the experiments and numerical simulation. Time-dependent temperatures of the CTJ and hot and cold sides of the TEG along with short circuit current, open circuit voltage and maximum power of the CTJ and TEG are obtained experimentally. The results indicate that the output power by the CTJ is fluctuating very fast with changing the solar radiation. Due to the thermal capacity and thermal resistance of the TEG, this variation for the temperatures and output power of the TEG is more gradually. The results also indicate that using TEG in the hybrid system leads to having more stable overall output power. Furthermore, the contribution of the TEG in the overall power generation by the system can be enhanced with material and geometrical optimization.

[*] Corresponding author: Sajjad Mahmoudinezhad. E-mail: sma@et.aau.dk

Keywords: *Concentrating triple-junction solar cell; Thermoelectric generator; COMSOL Multiphysics Software; Solar simulator; Transient modeling.*

1. Introduction

Sun is one of the most promising future sources of energy. Solar energy is clean, renewable and inexhaustible energy that produces completely no waste or environmental emissions. Currently, photovoltaic (PV) panels are the main devices to convert sunlight into electricity. In order to reduce the material costs and increase the efficiency and utilization rate of solar energy, multi-junction (MJ) solar cells have been becoming more interesting for different applications. Remarkable improvement has been lately reported about four-junction cells, which have reached record-efficiencies equal to 46% [1-2]. Even with using the most efficient MJ cells, more than half of the input solar energy will be dissipated. Owing to some distinct aspects of the TEGs like having no moving parts and being highly reliable [3-5], TEGs can be an appropriate option for heat recovery from the CTJ cells.

Nowadays, in order to maximize utilization of the solar energy, studying hybrid systems are getting more of interest. Generally, hybrid systems that have been considered in the previous studies can be classified into three categorizations. Most of the studies in the field of hybrid systems have been examined PV-TEG systems under standard illumination condition [6-8]. There are fewer studies that have been considered PV-TEG systems under concentrated light [9-16]. The third category that has been investigated less than two others are CTJ-TEG hybrid systems [17-24].

Lamba and Kaushik [9] developed a thermodynamic model to consider a concentrated photovoltaic-thermoelectric (CPV-TEG) hybrid system. The impact of some key parameters on the performance of the hybrid system is examined. The results showed that in the optimum condition, the percentage enhancement in efficiency of the PV-TEG hybrid system is 13.37% more than the PV-only system. A three-dimensional model considering the thermal resistance of the hybrid system is used by Zhang and Xuan [10] to present different methods to design a CPV-TEG system. They found that the thermal

resistance between TEG and environment has a higher impact on the power generation in comparison with the thermal contact resistance between TEG and PV cell. Yin et al. [11] are also presented a thermal resistance analysis to improve the efficiency and design of a PV-TEG hybrid system. It was found that under the concentrating light, amorphous silicon and polymer PV cells have better performance. In order to enhance the utilization of the solar energy, the photon and thermal management of a PV-TEG hybrid system using for both space and terrestrial applications are offered by Da et al. [12]. The results indicated that the PV-TEG system has better performance for both space and terrestrial applications in lower concentration ratios.

A theoretical model for a low concentrated PV-TEG hybrid system is developed by Liao et al. [13] using energy conservation law. It was found that in spite of generating higher power, PV-TEG hybrid system has more efficiency than the ingredients. A GaAs-based PV cell and a commercial TEG composed the PV-TEG hybrid system that examined by Kil et al. [14] under different solar concentrations ranging 0 to 50 suns. The results showed a 3% increment in the efficiency of PV-TEG hybrid system compares to the PV-only system at 50 suns. COMSOL Multiphysics Software was used by Xu et al. [15] to model a three-dimensional concentrated PV-TEG hybrid system. They found that with the same cooling condition in the heat sink, the temperature of the PV cell in PV-TEG hybrid system is more than the PV-only system, but the temperature has more constant distribution as well. In another study, Kiflemariam et al. [16] developed a two-dimensional steady-state model using COMSOL Multiphysics Software to predict the response of a PV-TEG hybrid system under concentrated light. It was found that reducing the thermal resistance leads to having a lower temperature for the PV cell.

Mahmoudinezhad et al. [17] examined a CTJ-TEG hybrid system under solar concentrations lower than 40 suns and in the steady state condition. The results showed that with increasing the solar concentration, the efficiency of the CTJ decreases while the efficiency of the TEG enhances. Thermal and electrical analysis of a novel CTJ-TEG hybrid system was carried out both numerically and experimentally by sweet et al. [18-19]. The presented results can be applied to increase the performance

and lifetime of the hybrid system and decrease the cost of energy. Tamaki et al. [20] experimentally illustrated that a Bi-Te based TEG could compensate a portion of the waste heat from a triple-junction solar cell in a CTJ-TEG hybrid system. A hybrid CTJ-TEG is examined using both numerical and experimental approaches [21]. The results indicated that the contribution of the TEG in the power generation by the hybrid system increases substantially in higher solar concentrations and reaches to 40% for the solar concentration of 200 suns. This contribution enhancement of the TEG for higher solar concentrations was confirmed in another numerical study by Rezania and Rosendahl [22]. A numerical model of a CTJ-TEG hybrid system is developed by Mahmoudinezhad et al. [23-24] to consider the transient behavior of the hybrid system. The results indicated that integrating TEG with the triple-junction solar cell helps to have a more stable power generation by the hybrid system. The significance of the impact of the thermal contact resistance on power generation by the hybrid system was also evaluated.

In this paper, both experimental and numerical approaches are used to investigate the transient response of the CTJ-TEG hybrid system. The prototype that is used in this investigation offers a basic conception of the thermal and electrical impact of the TEG and CTJ in a hybrid CTJ-TEG device under unsteady solar radiations representing partly cloudy weather condition. Variation of the open circuit voltage, short circuit current and maximum power produced by the CTJ and TEG are obtained and discussed in details. COMSOL Multiphysics Modeling Software is used for the numerical simulation. The experimental and numerical temperatures and maximum powers are achieved and compared. Furthermore, a brief discussion about the feasibility of the optimization of the system to maximize the utilization of the solar energy is presented in the last section of the paper.

2. Experimental Setup

Commonly, in the real applications, different devices like parabolic dishes and Fresnel lenses can be used to concentrate the sun. In this work, in order to achieve accurate solar concentrations with a one-

minute time interval, a solar simulator with ten xenon arc lamps (see Figure 1b) is used. Up to 11000 suns ($11000\,kW/m^2$) can be delivered to the focal point by the solar simulator [25-26]. Due to temperature limitation for the CTJ cell, just two lamps are employed to deliver between 0 to 39 suns on the surface of the CTJ. A shutter controls the variation of the solar concentration while the xenon laps were on during the tests. Figure 1a illustrates the schematic of the experimental rigs. An optical mixer is placed in front of the test section to uniform the concentrated light over the CTJ area. All of the experiments are carried out in Paul Scherrer Institute (PSI), Villigen, Switzerland.

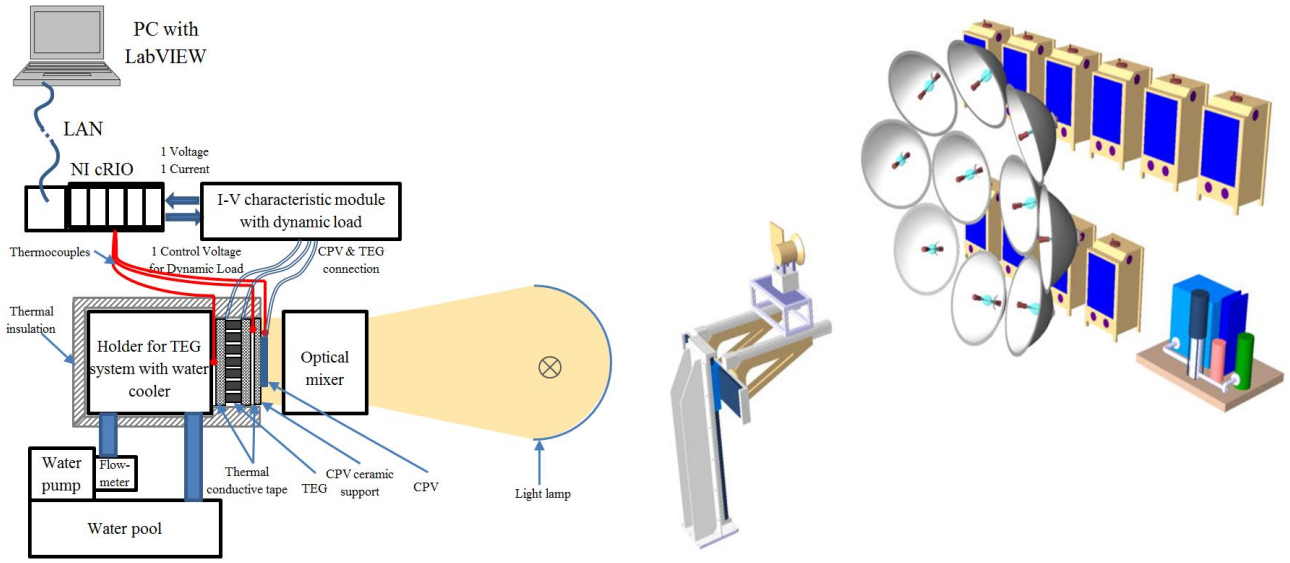

(a) (b)

Figure. 1. (a) Schematic of experimental setup [17]; (b) solar simulator used in this study [27].

Figure 2a displays the diagram of the CTJ-TEG hybrid system. A $10.075\,mm \times 10.68\,mm$ commercially available CTJ photovoltaic cell [28] along with a Bi-Te based TEG [29] with 194 thermoelectric elements and the size of $8.7\,mm \times 8.7\,mm$ are integrated to compose the CTJ-TEG hybrid system (see Figures 2b and 2c). A heat exchanger positioned just behind the hybrid system to drive the heat away from the cold side of the TEG. The operating fluid is water, and the mass flow rate in the heat exchanger is $5\,Lit/min$ that is constant during the experiments. Two thermocouples for each

are applied to obtain the temperatures of the surface of the CTJ cell and the hot and cold sides of the TEG, and one thermocouple is used to measure the ambient temperature.

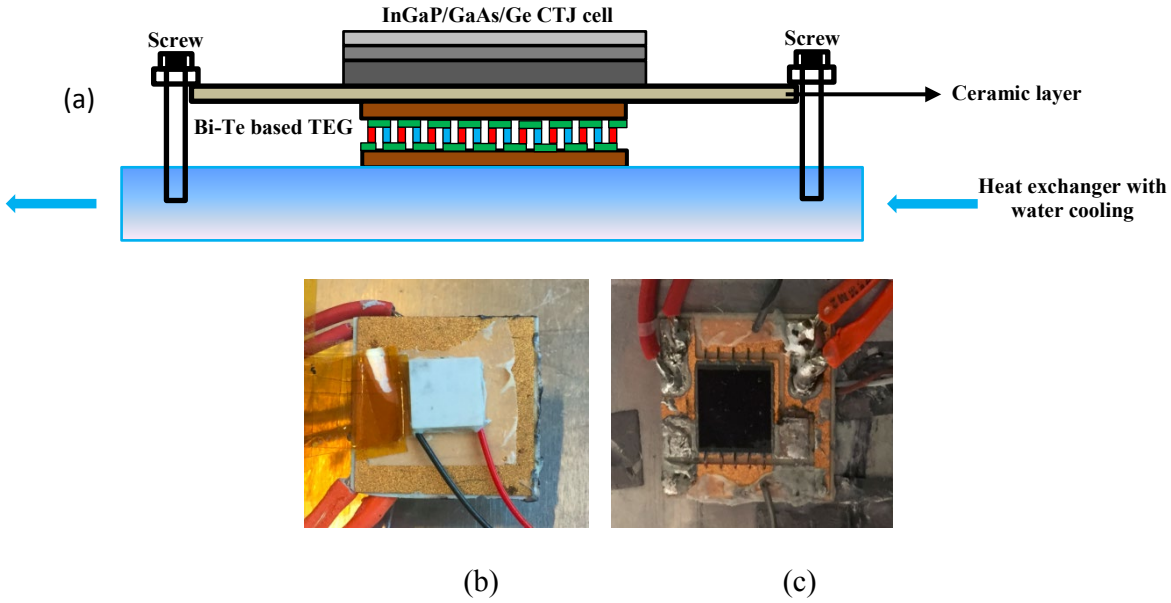

Fig. 2, (a) Schematic of the CTJ-TEG hybrid system, (b) Hybrid CTJ-TEG system, rear view, (c) Hybrid CTJ-TEG system, front view [17].

The temperatures and I-V characteristics of the CTJ and TEG are achieved using data logger and controllers based on National Instrument cRIO-9074 [17] that is an embedded controller appropriate for advanced control and monitoring applications. A dynamic load using the dynamic impedance of a 20 mF capacitor in the charging process was used to obtain the I-V characteristic of the TEG.

3. Modeling and simulation approach

In this study, a 3D finite element analysis in COMSOL Multiphysics 5.2 is employed to simulate the transient behavior of the system. COMSOL as a finite element analysis, solver and simulation software can be used for various physics and engineering applications, especially coupled phenomena or Multiphysics.

The 3D geometric model of the system is firstly created in the software, and then the mesh of the geometry is built using COMSOL pre-defined "fine" mesh (see Figure 3). After defining the properties of the materials, initial values and boundary conditions, the thermal profile of the CTJ-TEG hybrid system is obtained by the solver. The geometry and material properties are presented in Table 1. The surface area of the CTJ and TEG module are considered identical with the real values in the experiments.

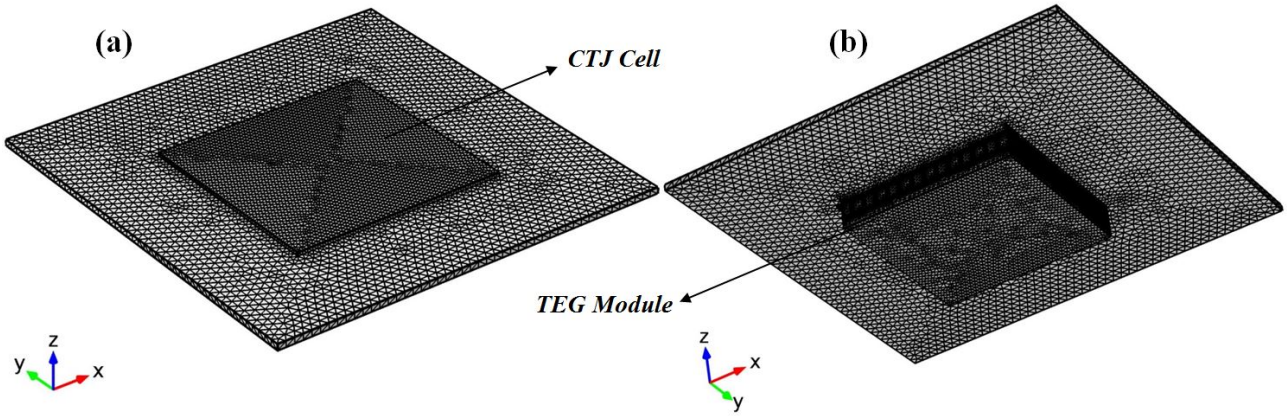

Fig. 3, Pre-defined fine mesh for the CTJ-TEG hybrid system, (a) Front view, (b) Rear view.

Table 1, Geometry and material properties of different layers in the hybrid system [17].

Layer	Material	Thickness, mm	Thermal conductivity, W/m K	Density, Kg/m^3
CTJ cell	GaInP/GaInAs/Ge [28]	0.185 [28]	60	5350
Solder paste	$Sn_{95}Ag_5$ [30]	0.05	37.8	7390
Conductive layer	Cu [30]	0.3	385	8900
Ceramic layer	99.5%Al_2O_3 [30]	0.4	25	3700
Copper conducting strip	Cu	0.1	385	8900
Semiconductor	Bi_2Te_3 [29]	0.7	*	7300

$* K(T) = 5.265 - 0.0283T + 6 \times 10^{-5}T^2 - 4 \times 10^{-8}T^3 \ (W/m.K)$[29]

3.1. Governing Equations an Boundary conditions

The physical phenomena in the TEG system include thermoelectric effect described by the following governing equations which couple the thermal and electrical fields. The governing equations are given as follows [31]:

$$\nabla . \vec{q} = \dot{q} \qquad (1)$$

$$\nabla.\vec{J} = 0 \tag{2}$$

Where $\vec{q}$, $\dot{q}$ and $\vec{J}$ are the heat flux, heat generation and current density vectors, respectively. The heat flux and current density vectors are integrated by [32]:

$$\vec{q} = ST\vec{J} - k\nabla T \tag{3}$$

$$\vec{J} = \frac{1}{\upsilon_e}\left(\vec{E} - S\nabla T\right) = -\frac{1}{\upsilon_e}(\nabla\phi + S\nabla T) \tag{4}$$

$$\vec{E} = -\nabla\phi \tag{5}$$

In Equations (3) and (4), S, k, T and υ_e are the Seebeck coefficient, thermal conductivity temperature, and electrical resistivity of a thermoelectric module, respectively. In Equation (5), $\vec{E}$ is the electric field intensity vector and ϕ is electric scalar potential. With substitution of Equations (3) and (4) in Equations (1) and (2), the coupled electric potential and temperature equations are given by:

$$\nabla.\left(ST\vec{J}\right) - \nabla.(k\nabla T) = \dot{q} \tag{6}$$

$$\nabla.\left(\frac{1}{\upsilon_e}\nabla\phi\right) + \nabla.\left(\frac{S}{\upsilon_e}\nabla T\right) = 0 \tag{7}$$

The input heat flux to the hybrid system is changing with the time. The same pattern with the pattern applied for the experiments is also used in the numerical study, see Figure 4. The boundary condition for the cold side of the TEG in the hybrid system is convective heat transfer and is given by:

$$-n \times (k\nabla T) = h \times (T - T_\infty) \tag{8}$$

In this equation n is the normal vector to the interface, h is the convective heat transfer coefficient and T_∞ is the ambient temperature.

4. Results and discussion

In order to determine the performance of the CTJ-TEG hybrid system under the transient condition, a random time-dependent pattern for the solar concentration is applied to the hybrid system (see Figure 4). The temperature variation of the surface of the CTJ and hot and cold sides of the TEG are illustrated in Figure 4. The temperatures are measured every 20 seconds. All the temperatures vary with the same

trend, and all are following the solar radiation variation. It is worthy to notice that the system was run to reach the steady state condition before and the variation is started after the first minute. Due to the temperature limitation of the CTJ, the input solar radiation is managed in a way that the temperature of the CTJ does not exceed the maximum temperature [33].

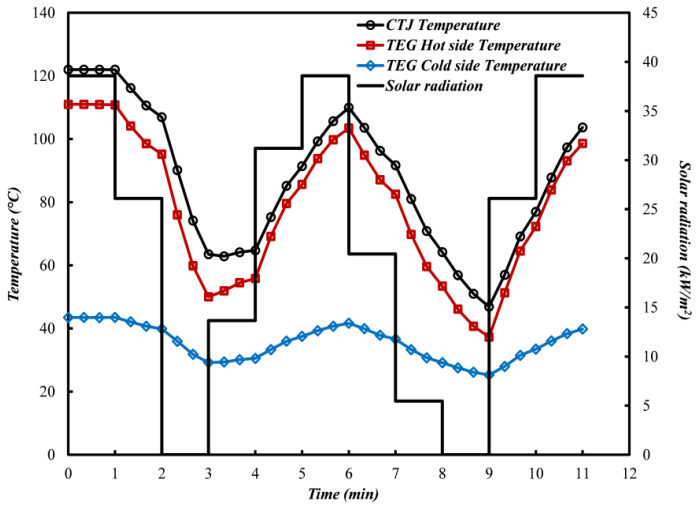

Fig. 4, Variation of the solar radiation and the temperatures of the CTJ and hot and cold sides of the TEG.

Figure 5 displays the variation of the open circuit voltage, short circuit current and maximum power of the CTJ in the hybrid system. As can be observed, the variation of the open circuit voltage is not very significant, and it does not change promptly while, both the short-circuit current and maximum power of the CTJ fluctuate stepwise and completely follow the variation of the solar radiation shown in Figure 4. All the parameters are measured every 20 seconds. The short circuit current of the CTJ reaches to steady state condition very fast, and after 20 seconds it would be almost constant. Area 1 in Figure 5 shows that with decreasing the solar radiation and consequently the temperature of the CTJ, the open circuit voltage increases slightly and it leads to a small increase in maximum power of the CTJ shown in Area 2. The opposite variation can be seen in areas 3 and 4. In these areas, the solar radiation and consequently the temperature of the CTJ are enhanced, and therefore, insignificant decrements in the values of open circuit voltage and maximum power of the CTJ occur.

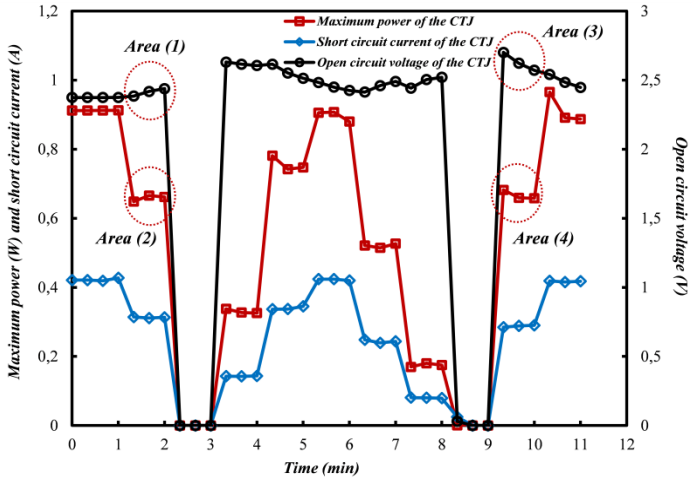

Fig. 5, Open circuit voltage, short circuit current and maximum power of the CTJ versus time.

Time-dependent variations of the open circuit voltage, short circuit current and maximum power of the TEG in the hybrid system are illustrated in Figure 6. Due to the higher thermal capacity and thermal resistance of the TEG than the CTJ, the variation of all the parameters mentioned above that are shown in Figure 6 are not stepwise, and they mostly follow the variation of the temperatures of the hot and cold sides of the TEG displayed in Figure 4 and not the solar radiation. Figure 6 shows that the maximum power generated by the TEG when the system is in the steady condition is almost 2.1% of the maximum power generated by the CTJ. By using TEGs with more efficient materials and optimized geometry, this value can be increased in future, but this amount of power also helps to have a more stable power generation by the system [23].

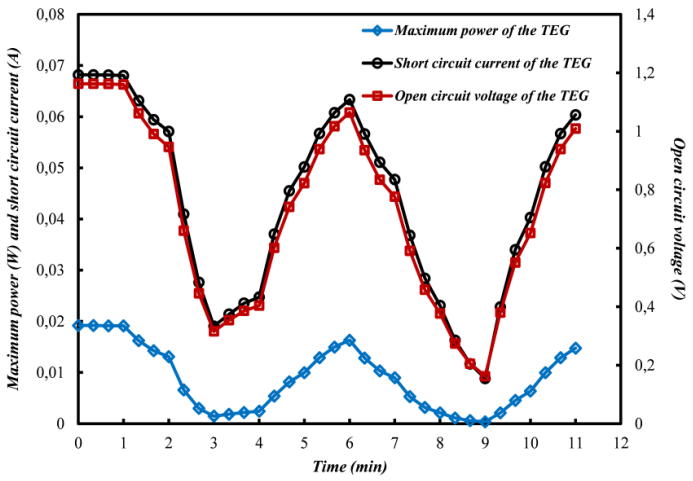

Fig. 6, Open circuit voltage, short circuit current and maximum power of the TEG versus time.

As it is mentioned before COMSOL Multiphysics Modeling Software is used to simulate the hybrid CTJ-TEG hybrid system under transient condition. Figure 7 displays the variation of the temperature contour of the hybrid system during one arbitrary minute (6^{th} minute). The temperature propagation from the CTJ to the TEG can be observed in Figure 7. The maximum and minimum temperatures of the hybrid system that are related to the CTJ cell and cold side of the TEG varies between 88.9°C and 32.6°C for the t=300s and between 107°C and 36.2°C for the t=360s.

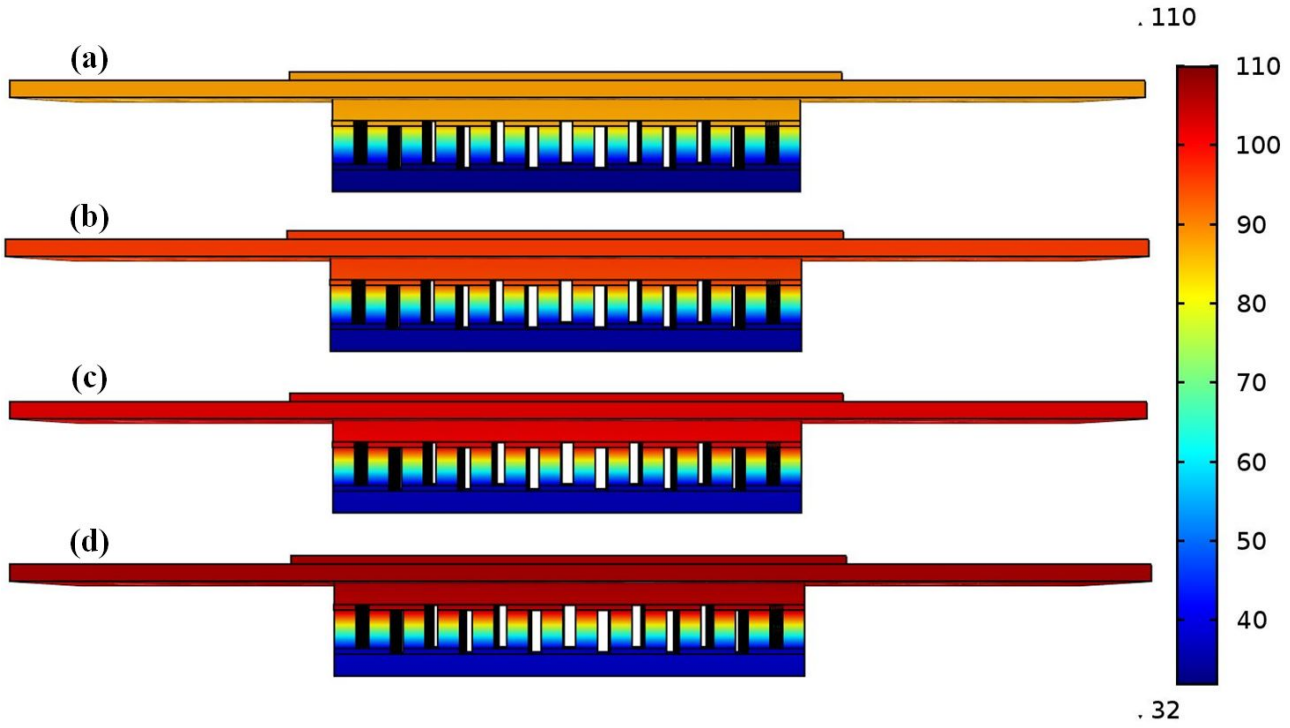

Fig. 7, Temperature contours for (a) t=300 s (b) t=320 s (c) t=340 s (d) t=360 s.

Temperature field and electric potential field are coupled within semiconductors. The three-dimensional electric potential distribution in the TEG is illustrated in Figure 8. Generally, the current flowing through the semiconductors and the temperature gradient owing to the Seebeck effect are two parameters in generating the electric potential in the semiconductors [34]. By increasing the temperature

difference between the hot and cold sides of the TEG, the electric potential enhances. The maximum electric potentials of the TEG are 0.96V and 1.23V for t=300s and t=360s, respectively.

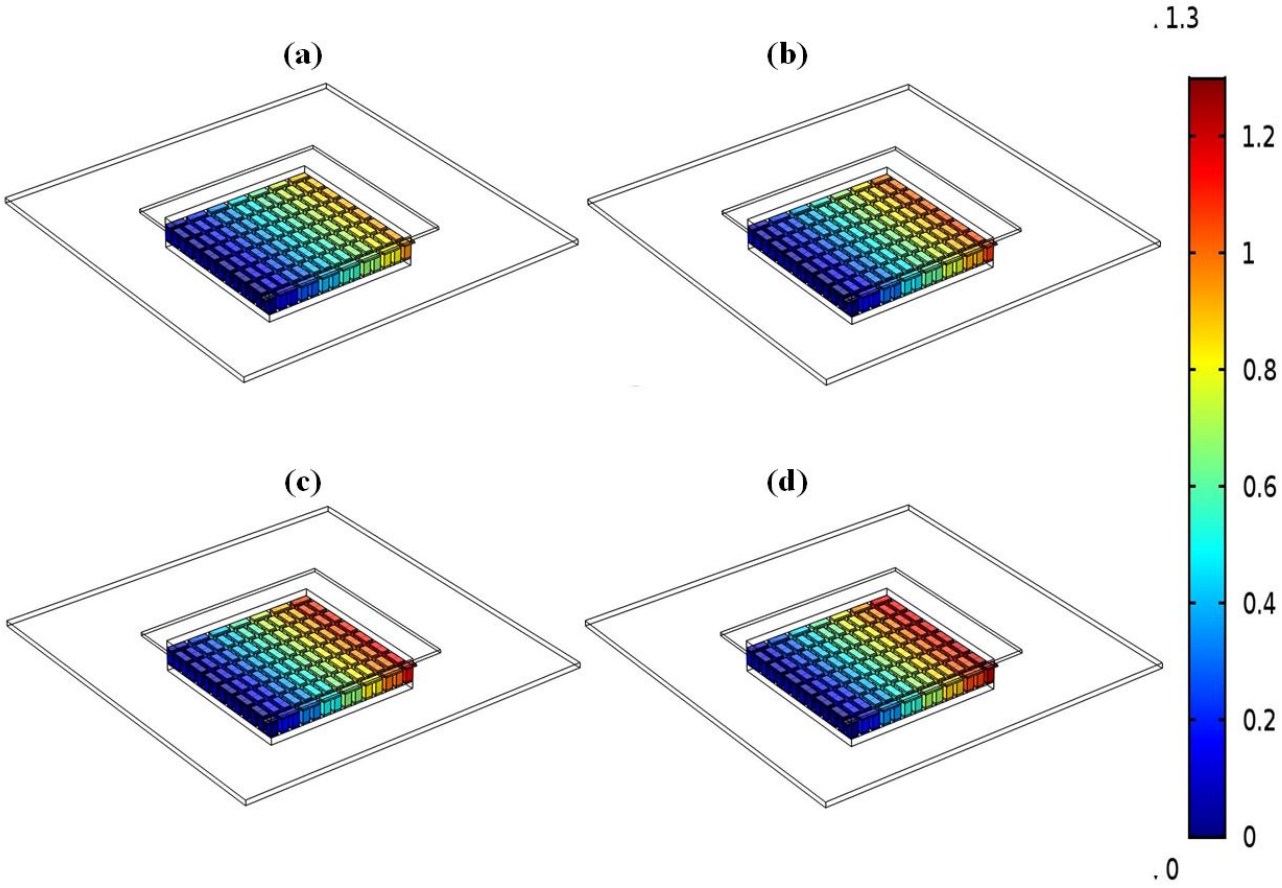

Fig. 8, Electric potential of the TEG for (a) t=300 s (b) t=320 s (c) t=340 s (d) t=360 s.

A comparison between the simulated and experimentally measured power generation by the CTJ in the CTJ-TEG hybrid system is illustrated in Figures 9. By stepwise changing of the solar concentration, the power generation by the CTJ is varying significantly due to variation in the input heat flux to the hybrid system. Furthermore, when the solar concentration drops, due to decreasing the temperature of the CTJ, a small increment in the power generation by the CTJ occurs that is displayed for the second minute in area 1. The opposite variation of the CTJ power generation can be observed in area 2 that is for the tenth minute. It indicates that with increasing the solar concentration and consequently the CTJ temperature, the output power drops slightly.

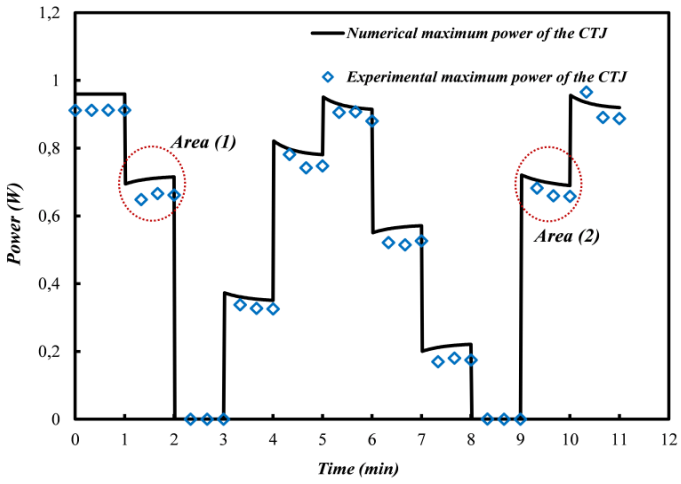

Fig. 9, Experimental and numerical maximum power generated by the CTJ versus time.

The experimental and numerical results for the power generation by the TEG are displayed in Figure 10. Due to the small variation of the material properties of the TEG in the temperature range shown in Figure 4, the variation of the figure of merit of the TEG is not significant. Consequently, the temperature difference between the hot and cold sides of the TEG is the most dominant parameter in the power generation by the TEG. Figure 10 shows that the variation of the output power by the TEG completely follows the variation of the temperature difference between the hot and cold sides of the TEG. One of the most vital benefits of using the CTJ-TEG hybrid system is the effect of the TEG in stabilizing the overall output power by the system. Noticing areas 1 and 2 in Figure 10 and comparing with areas 1 and 2 in Figure 9 shows that for the second and tenth minutes, the variation of the output powers by the TEG and CTJ have reverse manner and it helps to stabilize the total output power. In the other word, power generated by the TEG can compensate a portion of the CTJ output power variation.

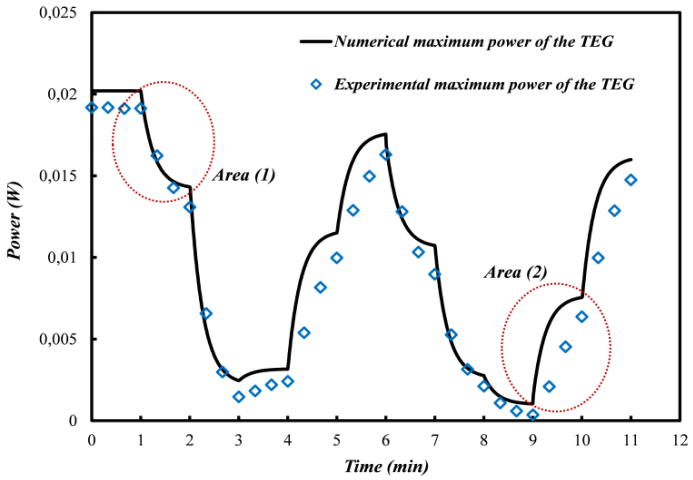

Fig. 10, Experimental and numerical maximum power generated by the TEG versus time.

Very close agreement between the numerical and experimental results can be seen in Figures 9 and 10. There is an overestimation for the power generation by both CTJ and TEG. The reason is that the obtained temperature from the numerical simulation for the CTJ is less than the experimental values and it leads to having higher values for power generation as well. Although the temperatures of the hot and cold sides of the TEG are also less than experimental values but the temperature differences obtained from numerical work are higher, and consequently, the output powers measured in numerical simulation are also higher than experimental ones.

In order to investigate the impact of the geometrical optimization on the performance of the hybrid system, the length of the thermoelements as one of the key parameter in power generation is considered. For the applied TEG in the current study, the maximum power generated by the CTJ in the steady state condition and solar concentration 39 suns is $P_{max} = 0.96\,W$ while this value for the TEG is $P_{max} = 0.02\,W$. This values are for the thermoelement length $l = 0.7\,mm$, see Table 1. For the constant solar concentration 39 suns, the impact of the thermoelements length on the power generation by the TEG and CTJ is illustrated in Figure 11. By increasing the length of the thermoelements, the temperature difference between the hot and cold sides of the TEG enhances and concequently the generated power by the TEG will increases.

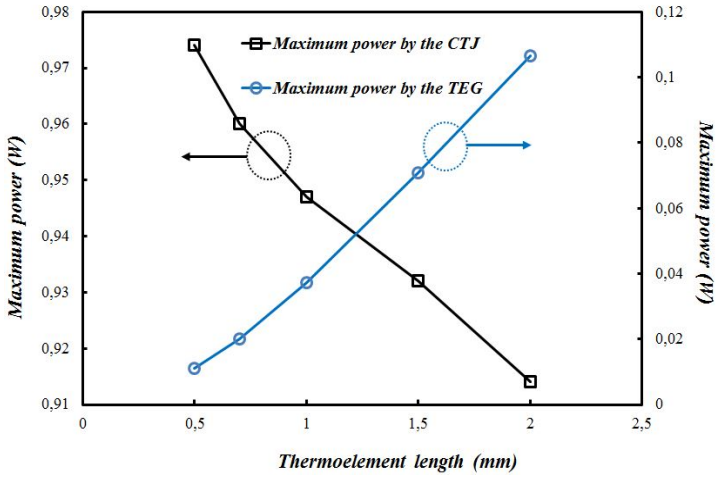

Fig. 11, Maximum power of the TEG and CTJ for different thermoelement lengths and solar concentration 39 suns.

The thermal resistance of the hybrid system enhances by increasing the length of the thermoelements. Therefore, for the same cooling system and input heat flux, the temperature of the CTJ cell increases and its causes to decrease the maximum power generated by the CTJ cell. It is worthy to note that the ratio of the maximum generated power by the TEG to the maximum generated power by the CTJ increases for higher thermoelement lengths, see Figure 12. As mentioned before, this ratio for the thermoelement length $l = 0.7\ mm$ is 2.1% but Figure 12 indicates that this ratio can be increased to 11.67% for the thermoelement length $l = 2\ mm$. It illustrates the potential of the TEG to play a more substantial role in the overall power generation by the hybrid system.

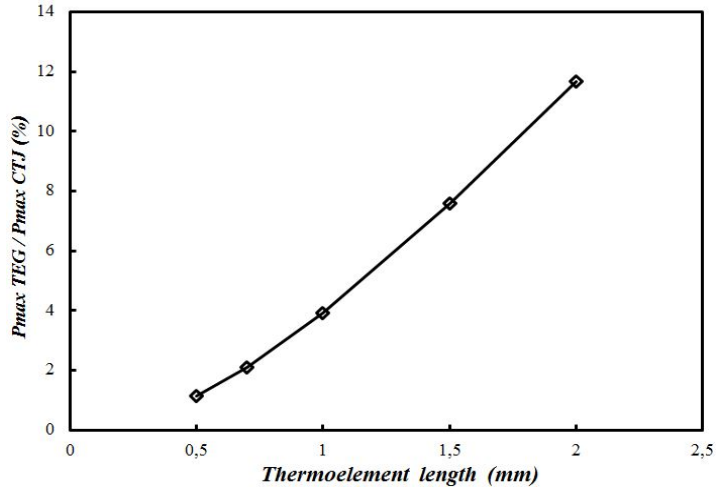

Fig. 12, Ratio of the maximum power of the TEG to CTJ versus the length of the thermoelements.

In the current study, the length of the thermoelements is the only parameter that is investigated to show the importance of the optimization. Different parameters can affect the performance of the CTJ-TEG hybrid system. In order to maximize the generated power by the hybrid system with the highest stability, material and geometrical optimization of the TEG and CTJ is planned for the future study.

5. Conclusion

Transient behavior of the CTJ-TEG hybrid system under variant solar concentrations is investigated using both experimental and numerical approaches. Temperatures of the CTJ cell and hot and cold sides of the TEG along with the variation of the open circuit voltage, short circuit current and maximum power versus time for both CTJ and TEG in CTJ-TEG hybrid system are obtained experimentally and discussed in details. A three-dimensional numerical model is developed using COMSOL Multiphysics Modeling Software. The results illustrate a close agreement between numerical and experimental results. It is found that when solar concentration fluctuates stepwise, the output power by the CTJ also alters very fast and with the same trend but the variation of the output power by the TEG is more gradually and almost follows the temperature variation. The power generation by the TEG for solar concentration 39 suns and thermoelement length $l = 0.7\ mm$ is 2.1% of the output power by the CTJ. Using numerical simulation shows that this ratio can be reached to 11.67% for the thermoelement length $l = 2\ mm$. It is indicated that integrating TEG with the CTJ cell helps to produce more stable power. Using more efficient materials with optimum geometry for the TEG can enhance the power generation by the TEG, and it helps to compensate a higher portion of the power reduction by the CTJ and have a more stable overall power.

Acknowledgment

The authors would like to acknowledge financial support from Access to Research Infrastructures activity under the 7th Framework Programme, SFERA 2, Grant Agreement n. 312643. The authors are thankful to the team from the Solar Technology Laboratory of Paul Scherrer Institute, Villigen, Switzerland (Ms.Y. Baeuerle, Mr. D. Wuillemin, Mr. V. Schnetzler, and Mr. C. Wieckert), where all the measurements of this study were performed.

References

[1] New world record for solar cell efficiency at 46% French-German cooperation confirms competitive advantage of European photovoltaic industry, in, Fraunhofer ISE report, Freiburg, 2014.

[2] M.A. Green, K. Emery, Y. Hishikawa, W. Warta, E.D. Dunlop, Solar cell efficiency tables (version 47), Prog. Photovolt. Res. Appl. 24 (2016).

[3] S. Mahmoudinezhad, A. Rezania, A. A. Ranjbar, L. A. Rosendahl, Transient Behavior of the Thermoelectric Generators to the Load Change; An Experimental investigation, Energy Procedia 147 (2018) 537-543.

[4] Sajjad Mahmoudinezhad, Alireza Rezaniakolaei, Lasse Aistrup Rosendahl, Experimental Study on Effect of Operating Conditions on Thermoelectric Power Generation, Energy Procedia 2017; 142: 558–563.

[5] S. Mahmoudinezhad, P. A. Cotfas, D. T. Cotfas, A. Rezania, L. A. Rosendahl, Performance evaluation of a high-temperature thermoelectric generator under different solar concentrations, Energy Procedia 147 (2018) 624-630.

[6] D. T. Cotfas, P. A. Cotfas, D. Ciobanu, O. Machidon, Characterization of Photovoltaic–Thermoelectric–Solar Collector Hybrid Systems in Natural Sunlight Conditions, Journal of Energy Engineering 143(6) (2017): 04017055.

[7] A. Rezania, D. Sera, L.A. Rosendahl, Coupled thermal model of photovoltaic-thermoelectric hybrid panel for sample cities in Europe, Renewable Energy 99 (2016) 127-135.

[8] Milad Mohsenzadeh, M.B. Shafii, H. Jafari mosleh, A novel concentrating photovoltaic/thermal solar system combined with thermoelectric module in an integrated design, Renewable Energy 113 (2017) 822-834.

[9] Ravita Lamba, S.C. Kaushik, Modeling and performance analysis of a concentrated photovoltaic–thermoelectric hybrid power generation system, Energy Conversion and Management 115 (2016) 288–298.

[10] Jin Zhang, Yimin Xuan, Investigation on the effect of thermal resistances on a highly concentrated photovoltaic-thermoelectric hybrid system, Energy Conversion and Management 129 (2016) 1–10.

[11] Ershuai Yin, Qiang Li, Yimin Xuan, Thermal resistance analysis and optimization of photovoltaic-thermoelectric hybrid system, Energy Conversion and Management 143 (2017) 188–202.

[12] Yun Da, Yimin Xuan, Qiang Li, From light trapping to solar energy utilization: A novel Photovoltaic-thermoelectric hybrid system to fully utilize solar spectrum, Energy 95 (2016) 200–210.

[13] Tianjun Liao, Bihong Lin, Zhimin Yang, Performance characteristics of a low concentrated Photovoltaic-thermoelectric hybrid power generation device, International Journal of Thermal Sciences 77 (2014) 158–164.

[14] Tae-Hyeon Kil, Sanghyeon Kim, Dae-Han Jeong, Dae-Myeong Geum, Sooseok Lee, Sung-Jin Jung, Sangtae Kim, Chan Park, Jin-Sang Kim, Jeong Min Baik, Ki-Suk Lee, Chang Zoo Kim, Won Jun Choi, Seung-Hyub Baek, A highly-efficient, concentrating-photovoltaic/thermoelectric hybrid generator, Nano Energy 37 (2017) 242–247.

[15] Xinqiang Xu, Siyi Zhou, Mark M. Meyers, Bahgat G. Sammakia, Bruce T. Murray, Performance Analysis of a Combination System of Concentrating Photovoltaic/ Thermal Collector and Thermoelectric Generators, Journal of Electronic Packaging, 136 (2014) 0410041-7.

[16] R. Kiflemariam, M. Almas, and C. Lin, Modeling Integrated Thermoelectric Generator-Photovoltaic Thermal (TEG-PVT) System, Excerpt from the Proceedings of the 2014 COMSOL Conference in Boston.

[17] S. Mahmoudinezhad, A. Rezania, D.T. Cotfas, P.A. Cotfas, L.A. Rosendahl, Experimental and Numerical Investigation of Hybrid Concentrated Photovoltaic–Thermoelectric Module under Low Solar Concentration. Energy 159 (2018) 1123-1131.

[18] T. K. N. Sweet, M. H. Rolley, W. Li, M. C. Paul, M. Gao and A. R. Knox, Experimental characterization and multi-physics simulation of a triple-junction cell in a novel hybrid III: V concentrator photovoltaic- thermoelectric receiver design with secondary optical element, Energy Procedia 142 (2017) 809–814.

[19] Tracy K.N. Sweet, Matthew H. Rolley, Martin J. Prest and Gao Min, Novel Hybrid III: V Concentrator Photovoltaic- Thermoelectric Receiver Designs, AIP Conference Proceedings 1881, 080009 (2017).

[20] Ryo Tamaki, Takeshi Toyoda, Yoichi Tamura, Akinari Matoba, Toshiharu Minamikawa, Masayuki Tokuda, Megumi Masui, and Yoshitaka Okada, Hybrid photovoltaic and thermoelectric module for high concentration solar system, AIP Conference Proceedings 1881, 100002 (2017); doi: 10.1063/1.5001453.

[21] Ofer Beeri, Oded Rotem, Eden Hazan, Eugene A. Katz, Avi Braun, and Yaniv Gelbstein, Hybrid photovoltaic-thermoelectric system for concentrated solar energy conversion: Experimental realization and modeling, Journal of Applied Physics 118, 115104 (2015); doi: 10.1063/1.4931428.

[22] A. Rezania, L.A. Rosendahl, Feasibility and parametric evaluation of hybrid concentrated photovoltaic-thermoelectric system, Applied Energy 187 (2017) 380–389.

[23] S. Mahmoudinezhad, A. Rezania, L.A. Rosendahl, Behavior of hybrid concentrated photovoltaic-thermoelectric generator under variable solar radiation, Energy Conversion and Management 164 (2018) 443–452.

[24] Sajjad Mahmoudinezhad, Shaowei Qing, Alireza Rezaniakolaei, Lasse Aistrup Rosendahl, Transient Model of Hybrid Concentrated Photovoltaic with Thermoelectric Generator, Energy Procedia 2017; 142: 564-569.

[25] J. Petrasch, P. Coray, A. Meier et al, A novel 50 kW 11,000 suns high-flux solar simulator based on an array of xenon arc lamps, ASME Journal of Solar Energy Engineering. vol. 129, no. 4 (2007) pp. 405–411.

[26] I. Alxneit and H. Schmit, Spectral characterization of PSI's high-flux solar simulator, J. Sol. Energy Eng. vol. 134, no. 1 (2012) Article ID 011013.

[27] Daniel Tudor Cotfas, Petru Adrian Cotfas, Dan Ion Floroian, and Laura Floroian, Accelerated Life Test for Photovoltaic Cells Using Concentrated Light, International Journal of Photoenergy Volume 2016, Article ID 9825683.

[28] https://solaerotech.com/wp-content/uploads/2018/03/CTJ-Datasheet.pdf [Cited: November 2018].

[29] http://thermoelectric-generator.com/wp-content/uploads/2014/07/Ingot-Raw-Material-BiTe-N-and-P.pdf [Cited: November 2018].

[30] Cotal H, Frost J. Heat transfer modeling of concentrator multijunction solar cell assemblies using finite difference techniques. In: Photovoltaic specialists conference (PVSC). 35th. IEEE; 2010. p. 213-8.

[31] Chen WH, Liao CY, Hung CI. A numerical study on the performance of miniature thermoelectric cooler affected by Thomson Effect. Appl Energy 2012;89:464–73.

[32] Wang XD, Huang YX, Cheng CH, Lin DTW, Kang CH. A three-dimensional numerical modeling of thermoelectric device with consideration of coupling of temperature field and electric potential field. Energy 2012; 47:488–97.

[33] Pilar Espinet-González, Carlos Algora, Neftalí Núñez, Vincenzo Orlando, Manuel Vázquez, Jesús Bautista, and Kenji Araki, Evaluation of the reliability of commercial concentrator triple-junction solar cells by means of accelerated life tests (ALT), AIP Conference Proceedings 1556, 222 (2013); doi: 10.1063/1.4822236.

[34] Xiao-Dong Wang, Yu-Xian Huang, Chin-Hsiang Cheng, David Ta-Wei Lin, Chung-Hao Kang, A three-dimensional numerical modeling of thermoelectric device with consideration of coupling of temperature field and electric potential field, Energy 47 (2012) 488-497.

PAPER 9: REFERENCE [225]

Experimental and Numerical Investigation of Hybrid Concentrated Photovoltaic - Thermoelectric Module under Low Solar Concentration

Sajjad Mahmoudi Nezhad, Alireza Rezania, Daniel Tudor Cotfas, Petru Adrian Cotfas, Lasse Rosendahl,

The paper has been published in
Energy 159 (2018) 1123-1131.

Energy 159 (2018) 1123–1131

Contents lists available at ScienceDirect

Energy

journal homepage: www.elsevier.com/locate/energy

Experimental and numerical investigation of hybrid concentrated photovoltaic – Thermoelectric module under low solar concentration

S. Mahmoudinezhad [a], A. Rezania [a, *], D.T. Cotfas [b], P.A. Cotfas [b], L.A. Rosendahl [a]

[a] Department of Energy Technology, Aalborg University, Pontoppidanstræde 111, Aalborg, DK, 9220, Denmark
[b] Electrical Engineering and Computer Science Faculty, Transilvania University of Brasov, 500036 Brasov, Romania

ARTICLE INFO

Article history:
Received 20 February 2018
Accepted 26 June 2018
Available online 27 June 2018

Keywords:
Concentrated photovoltaic
Thermoelectric generator
Solar simulator
Lambert W function
Newton–raphson algorithm

ABSTRACT

The quick progress in solar energy technology has made it one of the most promising alternatives to conventional energy systems in recent years. In this work, in order to make efficient use of the solar energy, a hybrid system composed of the concentrated photovoltaic cell and thermoelectric generator (CPV-TEG) is studied using both experimental and numerical approaches. The experimental study is carried out under concentrated radiation of a solar simulator, and the numerical simulation is accomplished using finite volume method. The results are presented for various solar concentration (SC) values ranging from 8 suns to 37 suns. The variation of the temperatures, open circuit voltage, and short circuit current are discussed. I-V-P curves for both CPV and TEG are obtained and evaluated experimentally and numerically. The results show that contribution of the TEG in the total electrical power produced by the hybrid system enhances with increasing the solar radiation. Furthermore, the experimental results indicate that the maximum and minimum efficiency of the CPV is reached to 35.33% and 23.02%, while these values for the TEG are 1.20% and 0.63%, respectively.

1. Introduction

Nowadays, replacement of fossil fuels with renewable energies has become a vital need, where a significant global challenge is to encounter future energy demand in a renewable and sustainable way. Solar energy is a free, abundant and inexhaustible source of clean renewable energy that can be used to reduce the dependency on conventional fuels. In spite of the great improvement in photovoltaic (PV) technologies, the conversion efficiencies of PV systems need to be further improved. Due to higher efficiency in a smaller area, concentrated photovoltaics (CPVs) have attracted great attention from researchers recent years. The CPV cells can have high conversion efficiencies under concentrated sunlight. For instance, the efficiency of the four-junction cell of Fraunhofer Institute has reached to 46% at 508 suns [1,2]. Nevertheless, more than half of the radiation is lost that can be recovered by thermoelectric generator (TEG). Having long lifetime and no moving parts and being highly reliable makes TEG an appropriate choice for energy harvesting from CPV cells [3].

Many studies have been considered the feasibility of using TEGs for harvesting the dissipated heat from the PV cells [4–8], but few studies considered coupled effect of CPV-TEG hybrid systems. Sweet et al. [9] investigated a hybrid CPV-TEG system, and found that using the thermoelectric module for cooling, improves CPV cell efficiency, fill factor and power generation. Rezania et al. [10] investigated a hybrid PV-TEG system and showed that, with present thermoelectric materials the contribution of the TEG power in overall power produced by the PV-TEG system is very small. Although, in another study, Rezania and Rosendahl [11] demonstrated that, especially in the high solar concentrations and with an optimized TEG, CPV-TEG is an applicable and also, economically, is a practical hybrid system.

Sundarraj et al. [12] reviewed latest progress in thermoelectric materials and solar thermoelectric generators, and predicted that hybrid CPV-TEG systems enable to make a significant change in renewable technologies in the close future. Beeri et al. [13] experimentally studied a hybrid CPV/TEG system and found that the impact of the TEG in overall power generation by the system increases with higher sun concentration. In addition, with using more advanced CPV cells and thermoelectric materials, the conversion efficiency can reach 50%. In another investigation, Tamaki et al. [14] found that, the TEG can compensate a part of the power generation loss in the CPV at high operating temperatures.

* Corresponding author.
E-mail address: alr@et.aau.dk (A. Rezania).

https://doi.org/10.1016/j.energy.2018.06.181
0360-5442/

Nomenclature

Abbreviation

CPV	Concentrated photovoltaic
CS	Contact surface
EMF	Electromotive force
EXP	Experimental
NUM	Numerical
PV	Photovoltaic
SC	Solar concentration
TEG	Thermoelectric generator
ZT	Figure of merit

Latin script

A	Area, m^2
C	Specific heat capacity, J/kg K
G	Solar radiation, W/m^2
h	Heat transfer coefficient, W/m^2K
I	Current, A
K	Thermal conductivity, W/m K
k	Boltzmann's constant, J/K
L	Length, m
n	Number of thermocouples
P	Power, W
q	Elementary charge, C
Q	Heat loss/heat transfer, W
R	Electrical resistance, Ω
T	Temperature, K
V	Voltage, V
x	Heat transfer direction

Greek script

α	Seebeck coefficient, V/K
ε	Emissivity
η	Conversion efficiency, %
σ	Stefan-Boltzmann constant, $W/m^2\ K^4$
Δ	Increment
τ	Thomson coefficient, V/K
ρ	Density, kg/m^3
γ	Electrical conductivity, S/m

Subscripts

1–12	Contact surface numbers
a	Ambient
c	Cold junction
col	Conductive layer
cel	Ceramic layer
CPV	Concentrated photovoltaic
f	Cooling fluid
h	Hot junction
hx	Heat exchanger
ccs	Copper conduction strip
max	Maximum
PH	Photogenerated
rad	Radiation
ref	Reference
S	series
SH	shunt
sky	Sky
sp	Solder paste
TEG	Thermoelectric generator

superscripts

b	The bottom contact surface
t	The top contact surface

Liao et al. [15] presented some applicable points for the optimum parametric design of the hybrid CPV-TEG system changing with the device output current. They indicated that the CPV-TEG hybrid system is more efficient than CPV-only systems. Kil et al. [16] used a single junction, GaAs-based solar cell and a commercial TEG in a hybrid CPV-TEG system, and illustrated that efficiency of the hybrid system is 3% more the CPV-only at the solar concentration of 50 suns. Mahmoudinezhad et al. [17,18] numerically studied transient response of a hybrid CPV-TEG system to the transient variation of solar radiation during a cloudy day.

CPV-cells have smaller area compared to PV cells, nonetheless, offers higher conversion efficiency. Enhancement of the efficiency is one of the crucial issue in order to reduce the cost of the solar power production. CPV technology has potential to enhance cost performance of energy production and, moreover, to diminish area and land required for the renewable energy system. Although hybrid PV-TEG systems have been studied in the literature, there is lack of comprehensive coupled model to predict performance of CPV-TEG hybrid systems. Therefore, a practical inclusive evaluation of the CPV-TEG hybrid system which should consider critical electrical and thermal aspects of the CPV and TEG is considered in this study. Furthermore, feasibility of achieving high efficiency and power for a CPV-TEG hybrid system is examined. An experimental prototype hybrid CPV-TEG system is considered under low solar concentration ratios (less than 40 suns [19,20]). In order to predict electrical response of the hybrid module to the solar radiation, one-dimensional model is developed using energy conservation law, and finite volume method [21] is used for discretization of the coupled equations. Since there are some limitations and challenges to evaluate performance of such a system with small-scale energy conversion elements, this study aims to provide a fundamental milestone for investigation of hybrid CPV-TEG systems.

2. Experimental setup

The experimental work is accomplished in Paul Scherrer Institut (PSI), Villigen, Switzerland. In order to deliver wide range of solar irradiation, the simulator consists of 10 xenon arc lamps (see Fig. 1). By means of the xenon lamps, highly concentrated light can be obtained in the focal plane [22,23]. The solar simulator can provide up to 11000 suns on the focal point. In this investigation, just 2 lamps were used to simulate 8 to 37 suns. While, the radiative lamps were operating during the experiments, a shutter, shown in Fig. 1, was used to control the radiation density on the hybrid module. Equivalent radiated solar radiation on the CPV surface versus open-rate percentage of the shutter is presented in Table 1.

As Fig. 2 shows, an optical mixer which is located horizontally in front of the hybrid CPV-TEG system was used to generate identical light over surface of the CPV cell. Before mounting and testing the CPV-TEG module, a thermogage sensor located on the exit plane of the optical mixer was used to measure and calibrate the radiative flux distribution. Therefore the most homogenous radiation received from the solar simulator on the CPV surface ($10.075mm \times 10.68mm$) was found.

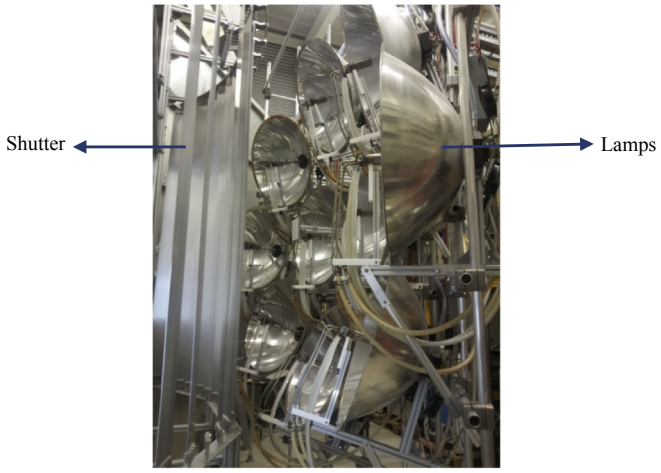

Fig. 1. Solar simulator used in this study.

A concentrating triple-junction InGaP/InGaAs/Ge solar cell [24] is used in this study. A Bi-Te based TEG module [25] with area of 8.7mm × 8.7mm which has 194 thermoelectric elements with the cross-sectional area of 0.4mm × 0.4mm is used in the experiments. Geometry and material properties of the hybrid system layers are tabulated in Table 2, and physical model of the CPV-TEG hybrid system is displayed in Fig. 3(a).

A heat exchanger with water, as the working fluid, was located on the cold side of the TEG to dissipate the heat. The mass flow rate of the coolant water was kept constant and equal to 5 L/min. A data acquisition and control systems based on National Instruments cRIO 9074 was used to measure the I-V variation and the temperatures. Totally, 7 thermocouples were used to measure the temperatures of the CPV cell (2 thermocouples), hot side of the TEG (2 thermocouples), cold side of the TEG (2 thermocouples) and ambient. Schematic of the experimental set up is illustrated in Fig. 4. The NI cRIO 9074 platform is based on a 400MHz processor and an FPGA Spartan-3 chip. The NI cRIO I/O modules used for measurements are:

1. NI 9215: an analog input module with 16bits resolution and ±10V input range was used for TEG voltage measurement.
2. NI 9225: a module with 24bits resolution and $5A_{RMS}$ input range was used for TEG current measurement.
3. NI 9211 and NI 9213: two modules with 24bits resolution and ± 80mV input range and with 24bits resolution and ±78.125mV input range, respectively. The modules are used for measuring the temperature using K type thermocouples.

In order to measure the I-V characteristic of the TEG, a dynamic load based on a capacitor was used. I-V characteristic is measured during the charging process of a 20mF capacitor directly connected to the TEG which acts as an energy source.

3. Numerical approach

Performance of the CPV-TEG is evaluated based on temperature of different layers of the hybrid module under different operating conditions. A steady-state one-dimensional heat transfer model based on the energy conservation law is developed. The coupled equations for all the components are obtained and solved implicitly. Finite volume method is used to discretize the equations and to represent them in the algebraic form. MATLAB software is used to solve the obtained equations.

Table 1
Solar radiation on the CPV versus open-rate percentage of the shutter.

Shutter percentage (%)	3	6	9	12	15	18
Solar radiation (kW/m^2)	8	17	22	27	32	37

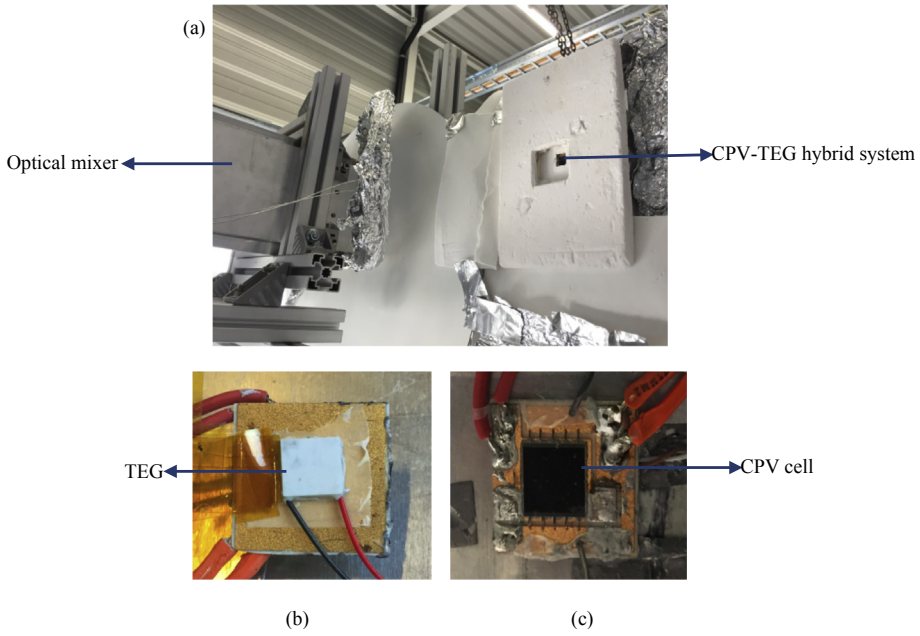

Fig. 2. (a) Mounted experimental setup, (b) Hybrid CPV-TEG system, rear view, (c) Hybrid CPV-TEG system, front view.

Table 2
Geometry and material properties of different layers in the hybrid system.

Layer	Material	Thickness, mm	Thermal conductivity, W/m K	Density, Kg/m^3
CPV cell	GaInP/GaInAs/Ge [24]	0.185 [24]	60	5350
Solder paste	$Sn_{95}Ag_5$ [26]	0.05	37.8	7390
Conductive layer	Cu [26]	0.3	385	8900
Ceramic layer	99.5%Al_2O_3 [26]	0.4	25	3700
Copper conducting strip	Cu	0.1	385	8900
Semiconductor	Bi_2Te_3 [25]	0.7	[a]	7300

[a] $K(T) = 5.265 - 0.0283T + 6\times10^{-5}T^2 - 4\times10^{-8}T^3 (W/m.K)$ [25].

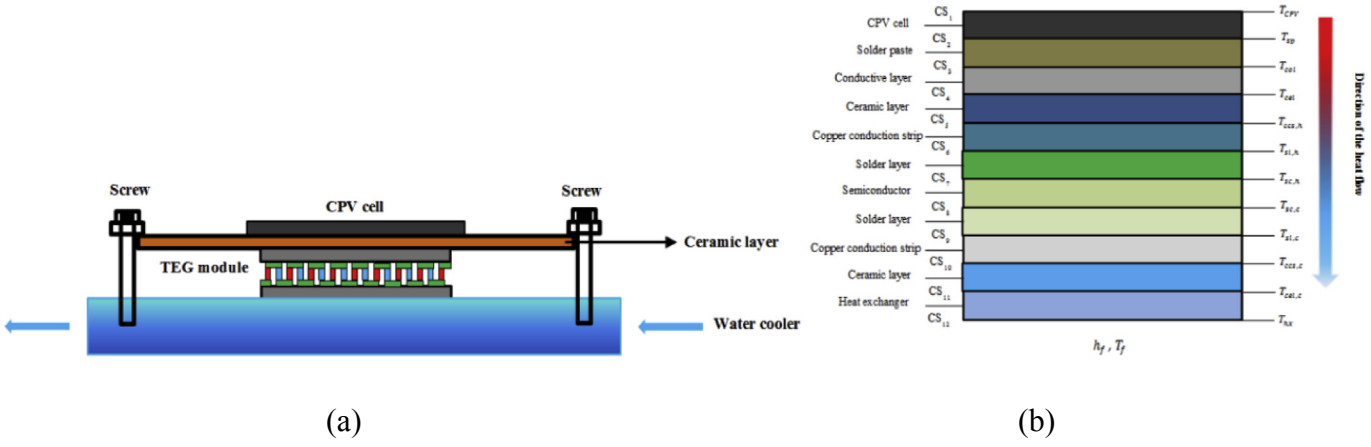

Fig. 3. (a) Schematic of the CPV-TEG hybrid system. (b) One-dimensional heat transfer physical model of the CPV-TEG module.

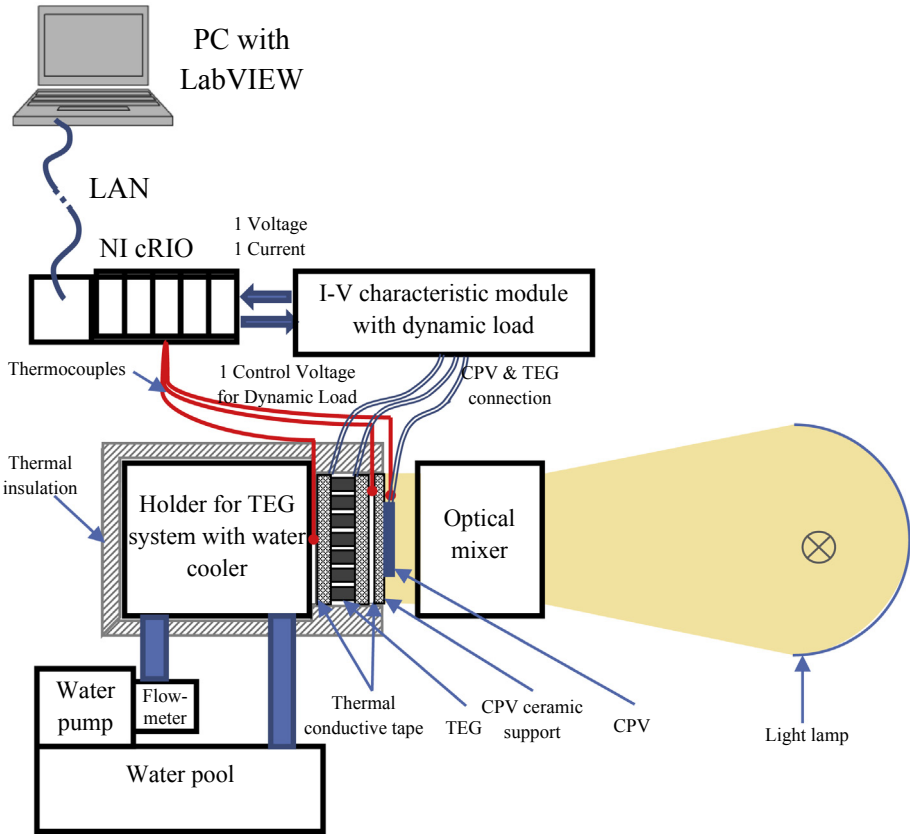

Fig. 4. Schematic of the experimental setup.

To investigate the performance and characteristics of the hybrid CPV-TEG system, some reasonable simplifications are considered. The main assumptions are:

1. Hybrid CPV-TEG system is thermally well insulated, therefore heat transfer to the environment is assumed to be zero excluding the heat loss from the top surface of the CPV cell by radiation and also heat transfer from the bottom surface of the CPV; where is considered as a heat source for the TEG.
2. The radiative and convective heat losses between the TE elements in the TEG module are neglected.
3. Identical materials are used for the N- and P-type semiconductors in the TEG.
4. All ingredients of the CPV-TEG hybrid system are well connected. Therefore the electrical and thermal contact resistances are neglected.

Seebeck, Peltier and Thomson effects are three basic effects of a working TEG. In addition, Joule and Fourier's effects are two accessorial effects. Seebeck effect produces an electromotive force (EMF). Peltier heat, Thomson heat, and Joule heat are generated from Peltier effect, Thomson effect, and Joule effect respectively. Peltier effect is the existence of heating or cooling at an electrified junction of two different conductors, therefore, the Peltier heat produces only on the end sides of the semiconductors. Thomson heat and Joule heat are volumetric effects that are presumed to be equally transmitted to the hot and cold junctions of the semiconductor elements [27,28]. Fig. 3(b) illustrates the 1-D heat transfer numerical model of the CPV-TEG hybrid system used in this study.

Energy conservation law is applied for each contact surface of the hybrid system. To calculate the temperature of different layers of the hybrid system, which is a key parameter for evaluating power generation and efficiency of the CPV and TEG, a set of nonlinear equations are derived. The corresponding equations of different components are listed as follow:

On the top surface of the CPV cell (CS1):

$$SC \times G \times A_{CPV} - Q_{rad} + KA\left(\frac{\partial T}{\partial x}\right)\Big|_{x=CS_1^b} - P_{CPV} = 0 \tag{1}$$

The radiation heat loss from the top surface of the CPV could be obtained by Eq. (2):

$$Q_{rad} = \varepsilon\sigma A_{CPV}\left(T_{CPV^t}^4 - T_{sky}^4\right) \tag{2}$$

where$\sigma = 5.67 \times 10^{-8} W/m^2K^4$. The sky temperature is considered as a function of the ambient temperature according to a study by Nowak [29].

Conductive heat transfer crossing the boundaries of the CPV cell, solder paste, and the conductive layer is presented in Equations (3)–(5).

On the top surface of the solder paste (CS2):

$$k_{CPV}A_{CPV}\left(\frac{\partial T}{\partial x}\right)\Big|_{x=CS_2^t} = k_{sp}A_{sp}\left(\frac{\partial T}{\partial x}\right)\Big|_{x=CS_2^b} \tag{3}$$

On the bottom surface of the solder paste (CS3):

$$k_{sp}A_{sp}\left(\frac{\partial T}{\partial x}\right)\Big|_{x=CS_3^t} = k_{col}A_{col}\left(\frac{\partial T}{\partial x}\right)\Big|_{x=CS_3^b} \tag{4}$$

On the bottom surface of the conductive layer (CS4):

$$k_{col}A_{col}\left(\frac{\partial T}{\partial x}\right)\Big|_{x=CS_4^t} = k_{cel}A_{cel}\left(\frac{\partial T}{\partial x}\right)\Big|_{x=CS_4^b} \tag{5}$$

With considering the Peltier, Thomson and Joule effects, the corresponding boundary conditions of different components of the TEG are listed as follow:

On the contact surface between the ceramic layer and copper conduction strip (CS5):

$$k_{cel}n_{cel}A_{cel}\left(\frac{\partial T}{\partial x}\right)\Big|_{x=CS_5^t} = k_{ccs}n_{ccs}A_{ccs}\left(\frac{\partial T}{\partial x}\right)\Big|_{x=CS_5^b} - \frac{n_{ccs}I^2r_{ccs}}{2} \tag{6}$$

where n is the pairs of P–N junction in the TE module.

On the contact surface between copper conduction strip and the solder layer (CS6):

$$k_{ccs}n_{ccs}A_{ccs}\left(\frac{\partial T}{\partial x}\right)\Big|_{x=CS_6^t} - \frac{n_{ccs}I^2r_{ccs}}{2} = k_{sl}n_{sl}A_{sl}\left(\frac{\partial T}{\partial x}\right)\Big|_{x=CS_6^b} - \frac{n_{sl}I^2r_{sl}}{2} \tag{7}$$

On the contact surface between solder layer and semiconductor (CS7):

$$k_{sl}n_{sl}A_{sl}\left(\frac{\partial T}{\partial x}\right)\Big|_{x=CS_7^t} - \frac{n_{sl}I^2r_{sl}}{2} = k_{sc}n_{sc}A_{sc}\left(\frac{\partial T}{\partial x}\right)\Big|_{x=CS_7^b} + n_{sc}\alpha_{sc,h}IT_{sc,h} - \frac{n_{sc}I^2r_{sc,l}}{2} - \frac{n_{sc}\tau_l I\left(T_{sc,h} - T_{sc,2}\right)}{2} \tag{8}$$

On the contact surface between semiconductor and solder layer (CS8):

$$k_{sc}n_{sc}A_{sc}\left(\frac{\partial T}{\partial x}\right)\Big|_{x=CS_8^b} - n_{sc}\alpha_{sc,h}IT_{sc,h} - \frac{n_{sc}I^2r_{sc,m}}{2} - \frac{n_{sc}\tau_m I\left(T_{sc,m} - T_{sc,c}\right)}{2} = k_{sl}n_{sl}A_{sl}\left(\frac{\partial T}{\partial x}\right)\Big|_{x=CS_8^t} + \frac{n_{sl}I^2r_{sl}}{2} \tag{9}$$

Due to low thermal conductivity of the semiconductors, the thermoelectric elements are divided into m control volumes.

On contact surface between solder layer and copper conduction strip (CS9):

$$k_{sl}n_{sl}A_{sl}\left(\frac{\partial T}{\partial x}\right)\Big|_{x=CS_9^t} - \frac{n_{sl}I^2r_{sl}}{2} = k_{ccs}n_{ccs}A_{ccs}\left(\frac{\partial T}{\partial x}\right)\Big|_{x=CS_9^b} - \frac{n_{ccs}I^2r_{ccs}}{2} \tag{10}$$

On contact surface between copper conduction strip and ceramic substrate (CS10):

$$k_{ccs}n_{ccs}A_{ccs}\left(\frac{\partial T}{\partial x}\right)\Big|_{x=CS_{10}^t} - \frac{n_{ccs}I^2r_{ccs}}{2} = k_{cel}n_{cel}A_{cel}\left(\frac{\partial T}{\partial x}\right)\Big|_{x=CS_{10}^b} \tag{11}$$

On contact surface between ceramic substrate and heat exchanger base (CS11):

$$k_{cel}n_{cel}A_{cel}\left(\frac{\partial T}{\partial x}\right)\Big|_{x=CS_{11}^{t}} = k_{hx}A_{hx}\left(\frac{\partial T}{\partial x}\right)\Big|_{x=CS_{11}^{b}} \quad (12)$$

On contact surface between heat exchanger base and the cooling fluid (CS12):

$$k_{hx}A_{hx}\left(\frac{\partial T}{\partial x}\right)\Big|_{x=CS_{12}^{t}} = h_f A_f\left(T_{hx,2} - T_f\right) \quad (13)$$

Coupled temperatures of each layer in the hybrid module are calculated by solving above equations.

3.1. Power generation and efficiency of the CPV and TEG

In this study, a single diode model [30] is considered for the PV module, (see Fig. 5). Based on this model, the PV module current is expressed as a function of the PV module voltage as:

$$I = I_{PH} - \frac{V + IR_S}{R_{SH}} - I_0\left[exp\left(\frac{V + IR_S}{nV_T}\right) - 1\right] \quad (14)$$

where the thermal voltage $V_T = kT/q$, I_0 is the reverse saturation current and n is the diode ideality factor which for ideal diode is equal to 1.

When R_S is not zero, the current cannot be obtained directly from equation (14), but it can be solved using the Lambert W function [31–33]. Therefore equation (14) can be expanded as follows:

$$I = \frac{(I_{PH} + I_0) - V/R_{SH}}{1 + R_S/R_{SH}} - \frac{nV_T}{R_S}W\left(\frac{I_0R_S}{nV_T(1 + R_S/R_{SH})}exp\left(\frac{V}{nV_T}\left(1 - \frac{R_S}{R_S + R_{SH}}\right) + \frac{(I_{PH} + I_0)R_S}{nV_T(1 + R_S/R_{SH})}\right)\right) \quad (15)$$

where the voltage of the CPV is:

$$V = (I_{PH} + I_0)R_{SH} - I(R_S + R_{SH}) - nV_TW\left(\frac{I_0R_{SH}}{nV_T}exp\left(\frac{(I_{PH} + I_0 - I)R_{SH}}{nV_T}\right)\right) \quad (16)$$

Power generation by the CPV can be obtained by:

$$P_{CPV} = VI \quad (17)$$

Therefore, the efficiency of the CPV is defined as:

$$\eta_{CPV} = \frac{P_{CPV}}{SC \times G \times A_{CPV}} \quad (18)$$

After solving the coupled equations and obtaining the temperatures of different layers of the TEG, power generation and efficiency of the TEG can be determined. The electromotive force (EMF) of the TEG module can be achieved by considering Thomson effect:

$$E = n_{sc}\left[\alpha_{sc,h}T_{sc,h} - \alpha_{sc,c}T_{sc,c} - \sum_{i=1}^{m-1}\tau_i(T_i - T_{i+1})\right] \quad (19)$$

The internal electrical resistance of the TEG module, which is a function of the electrical resistance of the copper conduction strip, solder paste, and semiconductors, can be defined as:

$$R_i = \left(n_{ccs}r_{ccs} + n_{sl}r_{sl} + n_{sc}\sum_{i=1}^{m}r_{sc,i}\right) \quad (20)$$

Therefore, the power generation by the TEG module can be considered as follows:

$$P_{TEG} = (E/(R_i + R_L))^2R_L = \left[n_{sc}\left[\alpha_{sc,h}T_{sc,h} - \alpha_{sc,c}T_{sc,c} - \sum_{i=1}^{m-1}\tau_i(T_i - T_{i+1})\right]\right]^2 R_L \Big/ \left[\left(n_{ccs}r_{ccs} + n_{sl}r_{sl} + n_{sc}\sum_{i=1}^{m}r_{sc,i}\right) + R_L\right]^2 \quad (21)$$

and the efficiency of the TEG is defined as:

$$\eta_{TEG} = P_{TEG}/(SC \times G \times A - Q_{rad} - P_{cpv}) \quad (22)$$

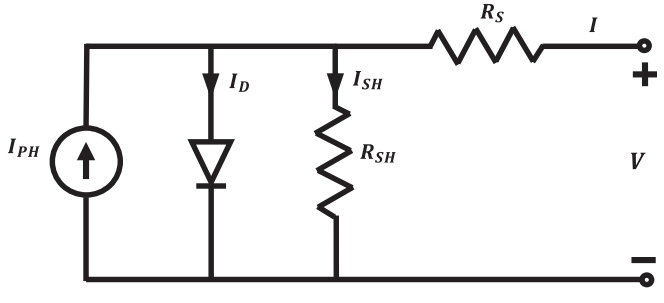

Fig. 5. The equivalent circuit of CPV module with a single-diode system [31].

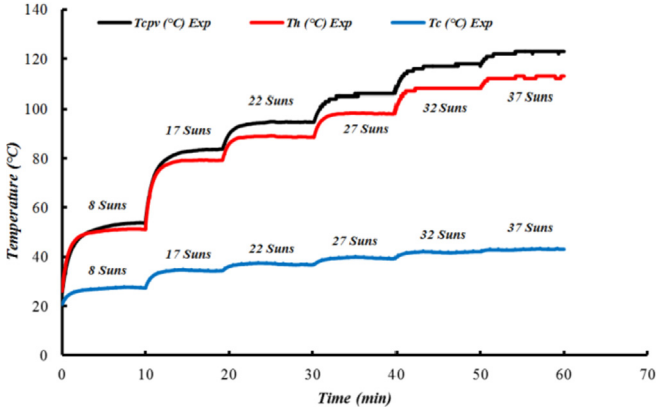

Fig. 6. Temperature variation of the CPV and hot and cold side of the TEG.

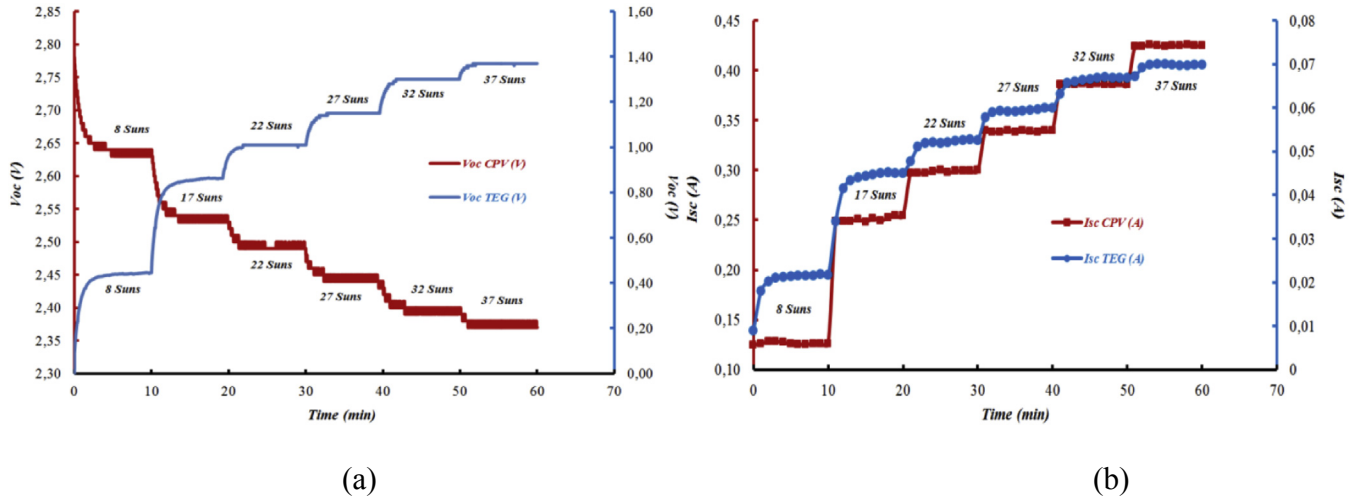

Fig. 7. (a) Open circuit voltage and (b) short circuit current of the CPV and TEG.

4. Results and discussion

The power generation and efficiency of the CPV and TEG, in this study, are defined based on the temperature of the CPV and hot and cold sides of the TEG. Fig. 6 shows the variation of the temperatures of the CPV cell and hot and cold sides of the TEG versus time. The experiments are done for 10 min for every constant solar concentration varying between 8 suns to 37 suns. Figs. 6 and 7 show that, for different given values of solar concentrations, 10 min is adequate time for the system to reach its steady state condition.

The open circuit voltage and short circuit current for the CPV and TEG is illustrated in Fig. 7. During the experiments, the open circuit voltage is measured and recorded every second and short circuit current is measured and recorded every minute. With increasing the solar radiation and also the temperature difference between the hot and cold side of the TEG, both of the open circuit voltage and short circuit current of the TEG increase. Although for the CPV, with increasing the solar radiation and the temperature, the open circuit voltage decreases and the short-circuit current increases, which will be discussed in details later.

Fig. 8 shows the I-V and P-V curves for different solar concentrations for the experimental and numerical results. In the numerical simulation, Lambert W function is used to obtain the I-V characteristics of the CPV, and Newton–Raphson algorithm [34] is applied to the curve fitting procedure of the experimental data. The solar concentration and temperature are playing a very important role in the I-V-P characteristics of a CPV cell. The amount of photogenerated current I_{PH} rises slightly with increment of the temperature because of an increase in the number of thermally produced carriers in the cell. As is known, the photogenerated current I_{PH} is almost equal to the short circuit current I_{SC}, therefore it can be concluded that the solar concentration is the only key factor in increasing the short circuit current of the CPV, and the temperature has less influence on the I_{SC}. The effect of the temperature is more visible in the open circuit voltage that reduces when the temperature increases. It can be seen that, the experimental results and numerical simulation are in close agreement. In the P-V curve, the maximum power in the experiments for 8 suns and 37 suns are obtained 0.283 W and 0.852 W respectively, while these values for numerical simulation are 0.314 W and 0.902 W, respectively.

Fig. 9 illustrates the I-V and P-V variation of the TEG for different solar concentrations. Two key parameters in the I-V characteristics and power generation by the TEG are the figure of merit of the TEG

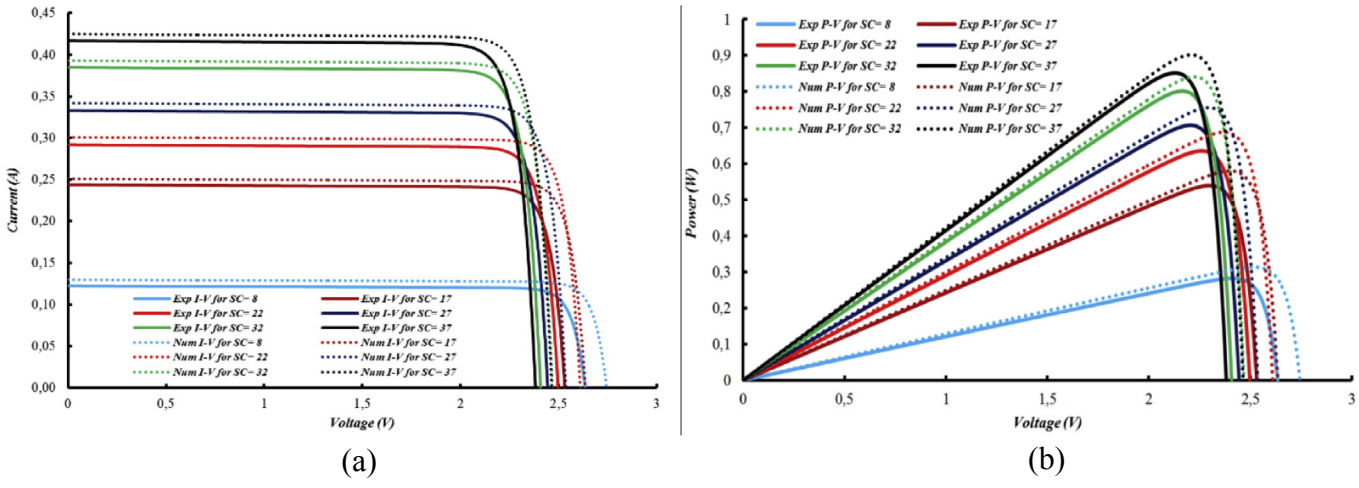

Fig. 8. (a) I-V curve (b) P-V curve for the CPV in hybrid CPV-TEG system.

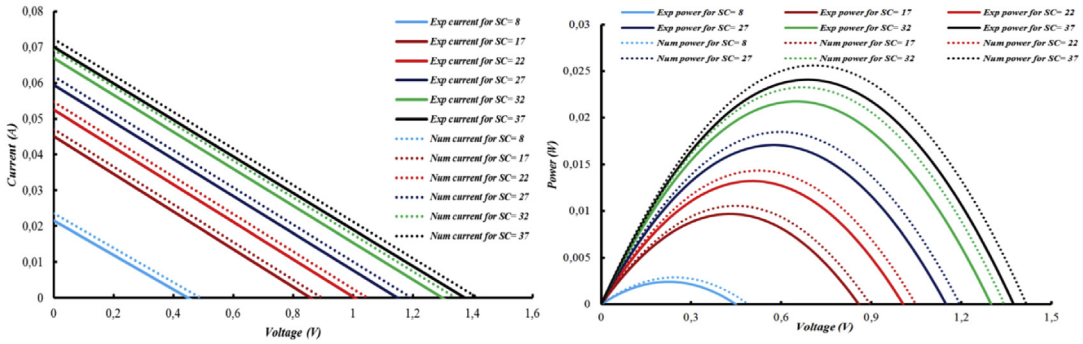

Fig. 9. (a) I-V curve (b) P-V curve for the TEG in hybrid CPV-TEG system.

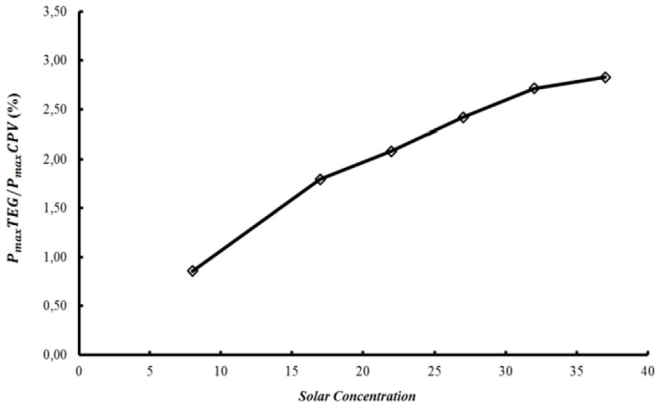

Fig. 10. Ratio of the maximum power of the TEG to CPV versus solar concentration.

and the temperature difference between the hot and cold sides of the TEG. With raising the solar concentration, the temperatures of the hot and cold sides of the TEG and also the temperature difference increases. The figure of merit of the TEG used in this study decreases slightly as the temperatures increase [25]. Therefore, the effect of the temperatures is more dominant and, consequently, the power generation by the TEG enhance. The maximum power for 8 suns is obtained 2.43 mW and 2.89 mW for the experimental and numerical studies, respectively. For 37 suns these values for the experiments and numerical simulation are 24.1 mW and 25.6 mW, respectively.

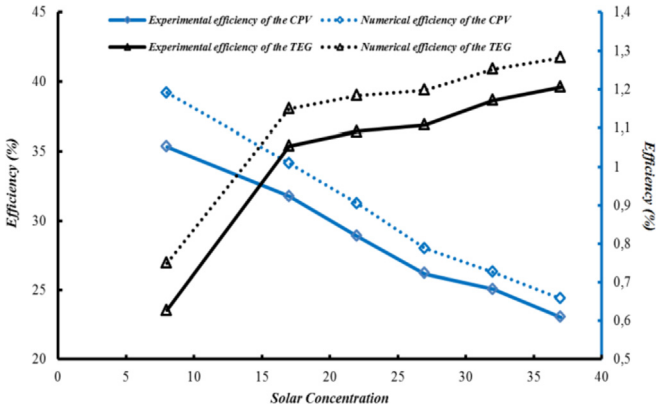

Fig. 11. Variation of the efficiencies of the CPV and the TEG in hybrid CPV-TEG system versus solar concentration.

The ratio of the maximum power produced by the TEG to the maximum power generated by the CPV is shown in Fig. 10. For the lower solar concentrations, the contribution of the TEG in power generation by the hybrid system is smaller, while at higher the solar concentration, the TEG has more contribution in the total power generation. As can be seen in Fig. 10, the maximum power of the TEG is 0.86% and 2.83% of the maximum power of CPV for 8 suns and 37 suns, respectively.

Solar concentration and temperature are playing the most crucial role in performance of the CPV and TEG. For the CPV, the temperature is the more dominant parameter that affects the efficiency than solar concentration [35]. As shown in Fig. 11, by using similar cooling condition in all the experiments, as the solar concentration increases the temperature of the CPV cell increases, and consequently the efficiency of the CPV cell decreases. The maximum and minimum efficiencies of the CPV in the experimental results are 35.33% and 23.02% that are related to 8 suns and 37 suns, respectively. These values in the numerical simulation are obtained 39.21% and 24.38%, correspondingly. The consistent over prediction of the numerical results rather than experimental results is because of under prediction of the temperature of the CPV-cell obtained by the numerical simulation. Numerical model is one-dimensional with considering some assumptions that cause lower temperature for the CPV- cell than the temperature achieved by the experiments.

Since the figure of merit of the applied material in this study decreases gradually by increasing the temperature [25] then, the temperature difference plays the most substantial role in the efficiency of the TEG. Fig. 6 illustrates that by increasing the solar concentration, the temperature difference is increasing as well and accordingly the efficiency of the TEG will be increased, see Fig. 11. The minimum efficiency of the TEG is for the 8 suns which are obtained 0.63% and 0.75% for the experimental work and numerical simulation, respectively. The maximum efficiency is taking place for 37 suns which are equal to 1.20% and 1.28% for the experimental and numerical results, respectively. Furthermore, the hot and cold side temperatures of the TEG, obtained by the numerical study, are less than the experimental values. Nevertheless, the temperature difference is higher and, consequently, the power generation by the TEG is also higher in the numerical evaluation.

5. Conclusion

In this study, feasibility of the hybrid CPV-TEG system for the low solar concentrations is investigated both experimentally and numerically. Variation of the temperatures, open circuit voltage

and short circuit current for different components of the hybrid system are presented and discussed. I-V-P curves for the CPV and TEG for the both experimental results and numerical simulation are obtained and compared. It is observed that the numerical simulation is in a good agreement with the experimental results. The maximum and minimum experimental efficiency of the CPV is reached to 35.33% and 23.02% which are for 8 suns and 37 suns, respectively. These values for the TEG are obtained 1.20% and 0.63% for the 37 suns and 8 suns, respectively. The results showed that by increasing the solar concentration, the ratio of the maximum power generation by the TEG to the CPV increases and, therefore, the impact of the TEG on overall power generation by the hybrid system enhances at higher solar concentrations.

Acknowledgment

The authors would like to acknowledge financial support from Access to Research Infrastructures activity under 7th Framework Programme, SFERA 2, Grant Agreement n. 312643. The authors are thankful to the team from the Solar Technology Laboratory of Paul Scherrer Institute, Villigen, Switzerland (Ms.Y. Baeuerle, Mr. D. Wuillemin, Mr. V. Schnetzler and Mr. C. Wieckert), where all the measurements of this study were performed.

References

[1] New world record for solar cell efficiency at 46% French-German cooperation confirms competitive advantage of European photovoltaic industry. In: Fraunhofer ISE report, Freiburg; 2014.
[2] Green MA, Emery K, Hishikawa Y, Warta W, Dunlop ED. Solar cell efficiency tables (version 47). Prog. Photovolt. Res. Appl. 2016;24.
[3] Nezhad Sajjad Mahmoudi, Rezaniakolaei Alireza, Rosendahl Lasse Aistrup. Experimental study on effect of operating conditions on thermoelectric power generation. Energy Procedia 2017;142:558–63.
[4] Bjork R, Nielsen KK. The performance of a combined solar photovoltaic (PV) and thermoelectric generator (TEG) system. Sol Energy 2015;120:187–94.
[5] Cotfas DT, Cotfas PA, Machidon OM, Ciobanu D. Investigation of the photovoltaic cell/thermoelectric element hybrid system performance. Mater Sci Eng 2016;133:012037.
[6] Teffah Khaled, Zhang Youtong. Modeling and experimental research of hybrid PV-thermoelectric system for high concentrated solar energy conversion. Sol Energy 2017;157:10–9.
[7] Soltani Shohreh, Kasaeian Alibakhsh, Sarrafha Hamid, Wen Dongsheng. An experimental investigation of a hybrid photovoltaic/thermoelectric system with nanofluid application. Sol Energy 2017;155:1033–43.
[8] Cotfas Daniel Tudor, Cotfas Petru Adrian, Ciobanu Daniela, Machidon Octavian Mihai. Characterization of photovoltaic–thermoelectric–solar collector hybrid systems in natural sunlight conditions. J Energy Eng 2017;143(6): 04017055.
[9] Sweet Tracy KN, Rolley Matthew H, Prest Martin J, Min Gao. Novel hybrid III: V concentrator photovoltaic- thermoelectric receiver designs. In: AIP conference proceedings 1881; 2017. p. 080009.
[10] Rezania A, Sera D, Rosendahl LA. Coupled thermal model of photovoltaic-thermoelectric hybrid panel for sample cities in Europe. Renew Energy 2016;99:127–35.
[11] Rezania A, Rosendahl LA. Feasibility and parametric evaluation of hybrid concentrated photovoltaic-thermoelectric system. Appl Energy 2017;187: 380–9.
[12] Sundarraj Pradeepkumar, Maity Dipak, Roy Susanta Sinha, Taylor Robert A. Recent advances in thermoelectric materials and solar thermoelectric generators – a critical review. RSC Adv 2014;4:46860–74.
[13] Beeri O, Rotem O, Hazan E, Katz EA, Braun A, Gelbstein Y. Hybrid photovoltaic-thermoelectric system for concentrated solar energy conversion: experimental realization and modeling. J Appl Phys 2015;118:1151041–8.
[14] Tamaki Ryo, Toyoda Takeshi, Tamura Yoichi, Matoba Akinari, Minamikawa Toshiharu, Tokuda Masayuki, Masui Megumi, Okada Yoshitaka. Hybrid photovoltaic and thermoelectric module for high concentration solar system. In: AIP conference proceedings 1881; 2017. p. 100002.
[15] Liao Tianjun, Lin Bihong, Yang Zhimin. Performance characteristics of a low concentrated Photovoltaic-thermoelectric hybrid power generation device. Int J Therm Sci 2014;77:158–64.
[16] Kil Tae-Hyeon, Kim Sanghyeon, Jeong Dae-Han, Geum Dae-Myeong, Lee Sooseok, Jung Sung-Jin, Kim Sangtae, Park Chan, Kim Jin-Sang, Baik Jeong Min, Lee Ki-Suk, Kim Chang Zoo, Choi Won Jun, Baek Seung-Hyub. A highly-efficient, concentrating-photovoltaic/thermoelectric hybrid Generator. Nano Energy 2017;37:242–7.
[17] Mahmoudinezhad Sajjad, Qing Shaowei, Rezaniakolaei Alireza, Rosendahl Lasse Aistrup. Transient model of hybrid concentrated photovoltaic with thermoelectric generator. Energy Procedia 2017;142:564–9.
[18] Mahmoudinezhad S, Rezania A, Rosendahl LA. Behavior of hybrid concentrated photovoltaic-thermoelectric generator under variable solar radiation. Energy Convers Manag 2018;164:443–52.
[19] Cirocco L, Belusko M, Bruno F, Boland J, Pudney P. Optimisation of storage for concentrated solar power plants. Challenges 2014;5:473–503.
[20] Khamooshi M, Salati H, Egelioglu F, Hooshyar Faghiri A, Tarabishi J, Babadi S. A review of solar photovoltaic concentrator. Int J Photoenergy 2014;2014:17.
[21] Patankar SV. Numerical heat transfer and fluid flow. USA: Taylor & Francis; 1980.
[22] Petrasch J, Coray P, A.Meier, et al. A novel 50 kW 11,000 suns high-flux solar simulator based on an array of xenon arc lamps. ASME J Solar Energy Eng 2007;129(4):405–11.
[23] Alxneit I, Schmit H. Spectral characterization of PSI's high-flux solar simulator. J Sol Energy Eng 2012;134(1). Article ID 011013.
[24] https://solaerotech.com/solaerotech/wp-content/uploads/2018/03/CTJ-Datasheet.pdf [Cited: May 2018].
[25] http://thermoelectric-generator.com/wp-content/uploads/2014/07/Ingot-Raw-Material-BiTe-N-and-P.pdf [Cited: May 2018].
[26] Cotal H, Frost J. Heat transfer modeling of concentrator multijunction solar cell assemblies using finite difference techniques. In: Photovoltaic specialists conference (PVSC). 35th. IEEE; 2010. p. 213–8.
[27] Meng F, Chen L, Sun F. A numerical model and comparative investigation of a thermoelectric generator with multi-irreversibilities. Energy 2011;36(5): 3513–22.
[28] Min Chen, Rosendahl Lasse, Bach Inger, Condra Thomas, Pedersen John. Irreversible transfer processes of thermoelectric generators. Am J Phys 2007;75(9):815–20.
[29] Nowak H. The sky temperature in net radiant heat loss calculations from low-sloped roofs. Infrared Phys 1989;29:231–2.
[30] Batzelis Efstratios I, Papathanassiou Stavros A. A method for the analytical extraction of the single-diode PV model parameters. IEEE Trans Sustain Energy 2016;7(2).
[31] Tripathy Meetarani, Kumar Manish, Sadhu PK. Photovoltaic system using Lambert W function-based technique. Sol Energy 2017;158:432–9.
[32] Appelbaum J, Peled A. Parameters extraction of solar cells – a comparative examination of three methods. Sol Energy Mater Sol Cells 2014;122:164–73.
[33] Fathabadi Hassan. Lambert W function-based technique for tracking the maximum power point of PV modules connected in various configurations. Renew Energy 2015;74:214–26.
[34] Xiao W, Lind MGJ, Dunford WG, Capel A. Real-time identification of optimal operating points in photovoltaic power systems. IEEE Trans Ind Electron 2006;53(4).
[35] Ben Or Assaf, Appelbaum Joseph. Dependence of multi-junction solar cells parameters on concentration and temperature. Sol Energy Mater Sol Cells 2014;130:234–40.

PAPER 10: REFERENCE [232]

Numerical Parametric Study on the Performance of CPV-TEG Hybrid System

Sajjad Mahmoudi Nezhad, Alireza Rezania, Lasse Rosendahl

The paper was presented in
10th International Conference on Applied Energy (ICAE2018), 22-25 August 2018, Hong Kong, China

Available online at www.sciencedirect.com

ScienceDirect

Energy Procedia 00 (2018) 000–000

Energy Procedia

www.elsevier.com/locate/procedia

10th International Conference on Applied Energy (ICAE2018), 22-25 August 2018, Hong Kong, China

Numerical parametric study on the performance of CPV-TEG hybrid system

Sajjad Mahmoudinezhad[a], Alireza Rezaniakolaei[a,*], Lasse Aistrup Rosendahl[a]

[a]*Department of Energy Technology, Aalborg University, Pontoppidanstræde 101, Aalborg DK-9220, Denmark*

Abstract

The influence of the thermal contact resistance on a hybrid concentrated photovoltaic-thermoelectric generator (CPV-TEG) system has been investigated. A steady-state one-dimensional numerical model is developed. Governing equations are derived using the energy conversion law for each component in the CPV-TEG hybrid system. Power generation and efficiency of the CPV and TEG are obtained for different solar concentrations and heat transfer coefficients, provided by the heat sink, varying between 100 suns to 900 suns and 500 $W/(m^2K)$ to 5000 $W/(m^2K)$, respectively. Thermal contact resistance as a key parameter in real applications is considered in the simulation to check the sensitivity of the output power and efficiency of the system to the thermal resistance. The results show the substantial effect of the heat sink effectiveness, solar concentration and thermal contact resistance on the performance of the hybrid system.

Selection and peer-review under responsibility of the scientific committee of the 10th International Conference on Applied Energy (ICAE2018).

Keywords: Hybrid CPV-TEG System; Thermal Contact Resistance; Solar Concentration, Convective Heat Transfer Coefficient.

1. Introduction

Utilizing solar energy as a clean and unlimited source of energy is one of the promising ways to reduce using traditional fossil fuels that have many environmental and public risks like global warming. Concentrated photovoltaic cells can convert more than 40% of the solar energy to the electricity [1-2]. Even with using the CPV

* Corresponding author. Tel.: +4521370284; fax: +4598151411.
E-mail address: alr@et.aau.dk

Selection and peer-review under responsibility of the scientific committee of the 10th International Conference on Applied Energy (ICAE2018).

cells, more than half of the input energy is wasted. Harvesting this waste heat can be done by TEGs. TEGs have no moving parts and are highly reliable and also have a long lifetime and almost no maintenance cost. These special features make TEGs interesting and suitable for different applications [3-5]. The feasibility of using TEGs in hybrid PV-TEG systems has been investigated in many studies, but the CPV-TEG systems have been considered less in the literature. Urbiola et al. [6] considered the performance of different hybrid systems generating electricity with using the TEGs and under concentrated and non-concentrated solar radiations. They found that with the existing TEG elements some of the hybrid systems can be applicable, but some others can become practical if new TEG and PV materials are developed in future. Rezania et al. [7] developed a thermally coupled model of a PV-TEG hybrid system exposed under different real ambient conditions. The results showed that with the existing TEG materials, the contribution of the TEG in power generation by the hybrid system is not significant while it can be improved by using TEG materials with higher values of the figure of merit.

Sark [8] established a simple model to predict the efficiency of a hybrid PV-TEG system. The results indicate that with attaching a TEG behind a PV module, the efficiency can be enhanced 8-23%. This increment depends on the type of the module integration. Kwan and Wu [9] presented a theoretical analysis of the performance of a hybrid PV-TEG system working in outer space and then optimized the design of the TEG system. They found that in the space applications TEG has a substantial impact on the power generation by the hybrid system. Kossyvakis et al. [10] studied experimentally and theoretically the performance of a hybrid PV-TEG system using poly-Si and dye-sensitized solar cells. TEGs with different thermoelement geometries were used in their study. The results indicated that using shorter thermoelements increases the overall performance of the hybrid system.

The effect of the illumination level and the temperature as two key parameters in a hybrid PV-TEG system is examined by Cotfas et al. [11]. The results indicated that by using the TEG module, the temperature of the PV cell decreases and consequently, the output power by the PV enhances. Lamba and Kaushik [12] presented a numerical study including all primary and secondary effects of the TEG module. The influences of different parameters like concentration ratio, solar irradiance, and the number of thermoelements of the TEG, on the performance of the hybrid system, was investigated. The results showed that the efficiency of the hybrid PV-TEG system is 13.37% more that PV-only system for the concentration ratio 3 and number of thermoelements 127.

A hybrid system including multijunction PV cells, TEGs, and a flat plate solar collector was experimentally studied by Cotfas et al. [13]. The hybrid system was examined under different illumination levels. The results showed that the maximum output power by the TEG decreases significantly when it works under load resistance. A numerical model for the transient response of the CPV-TEG hybrid system was developed by Mahmoudinezhad et al. [14-15]. The results indicate that by increasing the solar radiation, the efficiency of the CPV decreases while the efficiency of the TEG enhances. It is also found that using TEG in such hybrid system leads to having more stable output power. Rezania and Rosendahl [16] presented a steady-state one-dimensional model without considering the thermal contact resistance effect. All the contacts were considered ideal, and the effects of other parameters were considered in this condition. They found that the TEG has a considerable contribution in power generation by the hybrid system, particularly at high solar concentrations.

In this study, a practical CPV-TEG hybrid model that is considering all primary and accessorial effects of the TEG has been developed. The impact of solar concentration and convective heat transfer coefficient in the heat sink as two main external parameters has been investigated. In the real industrial and research applications, thermal contact resistance has a huge effect on the performance of the systems. The efficiency and power generation by the TEG and CPV for the ideal system with no thermal contact resistance is compared with the system with thermal contact resistance varying in a realistic range.

2. Modeling and simulation analysis

Figure 1 shows the schematic of the one- dimensional heat transfer physical model. Energy conservation law is applied to each layer in the hybrid system to obtain the thermally coupled governing equations. The CPV and TEG are assumed to be thermally insulated except the radiative heat loss from the top surface of the CPV. For the top surface of the hybrid system with considering radiative heat loss, the corresponding equation is:

$$SC \times G \times A_{CPV} - Q_{rad} + KA\left(\frac{\partial T}{\partial x}\right) - P_{CPV} = 0 \quad (1)$$

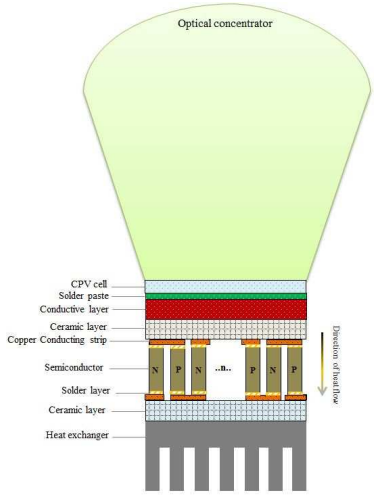

Figure. 1. One-dimensional physical model of the CPV-TEG system.

In this equation Q_{rad} is the radiative heat loss and P_{CPV} is the output power by the CPV and can be obtained as:

$$P_{CPV} = SC \times G \times A_{CPV} \times \eta_{CPV} \tag{2}$$

Where, η_{CPV} is the efficiency of the CPV that can be defined as a linear equation [17]:

$$\eta_{CPV} = \eta_{ref}\left[1 - \beta_{ref}\left(T_{CPV} - T_{ref}\right)\right] \tag{3}$$

η_{ref} and β_{ref} are the electrical conversion efficiency and temperature coefficient of the CPV at the reference temperature ($T_{ref} = 25℃$), respectively.

A Bi_2Te_3-based TEG is used in the simulation. All the TEG material properties are considered temperature dependent. For the equations through the TEG, all the primary and accessorial effects including Seebeck effect, Peltier effect, Thomson effect, Joule effect and Fourier effect have been considered in the equations. Owing to the phenomena of electron and phonon transportation in conductors and semiconductors, electrical current and heat flux are, generally, coupled and linear functions of the electric field and the gradient of temperature [18-19], i.e.:

$$\mathbf{J} = \sigma\mathbf{E} - \sigma\alpha\nabla T \quad \left(\frac{A}{m^2}\right) \tag{4}$$

$$\mathbf{q} = \pi\mathbf{J} - k\nabla T \quad \left(\frac{W}{m^2}\right) \tag{5}$$

Where, **E** and T are the electric field and temperature, respectively. α is the Seebeck Coefficient, π is the Peltier Coefficient, σ is the electrical conductivity and *k* is the thermal conductivity.

Applying the abovementioned equations for different layers of the TEG leads to having a set of non-linear thermally coupled equations the have to be discretized and solve together. Finite volume method [20] is used to solve these equations. In the heat sink, water is used as the working fluid, therefore, for the contact surface between heat exchanger base and the cooling fluid:

$$k_{hx}A_{hx}\left(\frac{\partial T}{\partial x}\right) + h_f A_f\left(T - T_f\right) = 0 \tag{6}$$

Solving all the obtained equations for different layers lead to having the temperature of different layers of the CPV-TEG hybrid system, and the efficiency and power of the TEG can be achieved as:

$$\eta_{TEG} = \left(\frac{T_H - T_C}{T_H}\right).\frac{\sqrt{1+ZT_m}-1}{\sqrt{1+ZT_m}+(T_C/T_H)} \tag{7}$$

$$P_{TEG} = \eta_{TEG} \times (SC \times G \times A - Q_{rad} - P_{CPV}) \tag{8}$$

Where η_{TEG} is the efficiency of the TEG, P_{TEG} is the power generation by the TEG, Z is the figure of merit, T_H, T_C and T_m are the hot side, cold side and average temperatures of the TEG, respectively.

3. Results and discussion

The offered numerical model can determine the effect of different parameters on the performance of the CPV-TEG hybrid system. In this study, solar concentration and convective heat transfer of the heat sink as two crucial external parameters along with the thermal contact resistance as a key parameter in industrial design and practical application are considered. Solar concentration is varied between 100 to 900 suns (1 sun= $1000\ W/m^2$) and convective heat transfer and thermal contact resistance are changed between 500 to 5000 W/m^2K and 5×10^{-6} and $5 \times 10^{-4}\ m^2.℃/W$, respectively.

Convective heat transfer in the heat sink plays a very crucial role in such hybrid system. Figures 2 and 3 show the power generation and efficiency of the CPV and TEG versus convective heat transfer and for the thermoelement length of $L = 1.5mm$ and constant solar concentration $SC = 300$ suns. As it mentioned before, in the real applications thermal contact resistance has a huge effect on the performance of the system. This substantial effect is displayed in the figures. Due to having higher cooling power, by increasing the convective heat transfer, power generation and efficiency of the CPV and TEG enhance as well. The reason is that by increasing the cooling power, the temperature of the CPV drops and consequently the power generation and efficiency increase. For the TEG, increasing the cooling power leads to have a higher temperature gradient across the TEG and therefore having more power and efficiency.

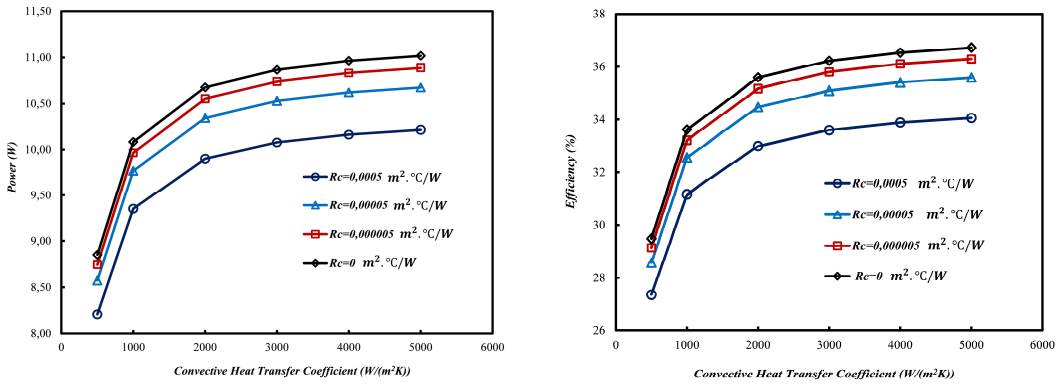

Figure. 2. Power generation and efficiency of the CPV versus convective heat transfer coefficient for different thermal contact resistances.

As can be seen in Figures 2 and 3, the rate of increasing the power and efficiency decrease by enhancing the convective heat transfer. Therefore, to reduce the costs in such this system, it would be better to use an optimum value for the convective heat transfer in the heat sink. Depends on the geometry and material properties and the design of the hybrid system this value can be changed.

Thermal contact resistance has a significant effect on the power generation and efficiency of the CPV and TEG. Comparing the values of the power of the CPV and TEG in Figures 2 and 3 shows that this effect in the TEG is more considerable.

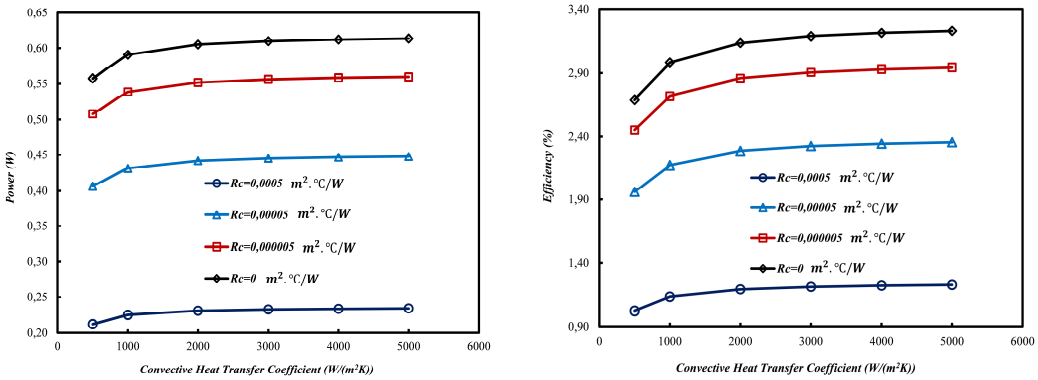

Figure. 3. Power generation and efficiency of the TEG versus convective heat transfer coefficient for different thermal contact resistances.

The impact of the solar concentration on the output power and efficiency of the CPV and TEG can be observed in Figures 4 and 5. In the simulation, the length of the semiconductors are considered $L = 1\ mm$ and convective heat transfer coefficient is $h = 2000\ W/(m^2K)$. Due to the increment of the input energy to the hybrid system, the both output power by the CPV and TEG increase by enhancing the solar concentration. As can be observed, by increasing the solar concentration, the efficiency of the CPV cell will drop dramatically because the temperature of the CPV increases significantly. The negative effect of the thermal contact resistance on the output power and efficiency of the CPV and TEG can be seen in all the figures.

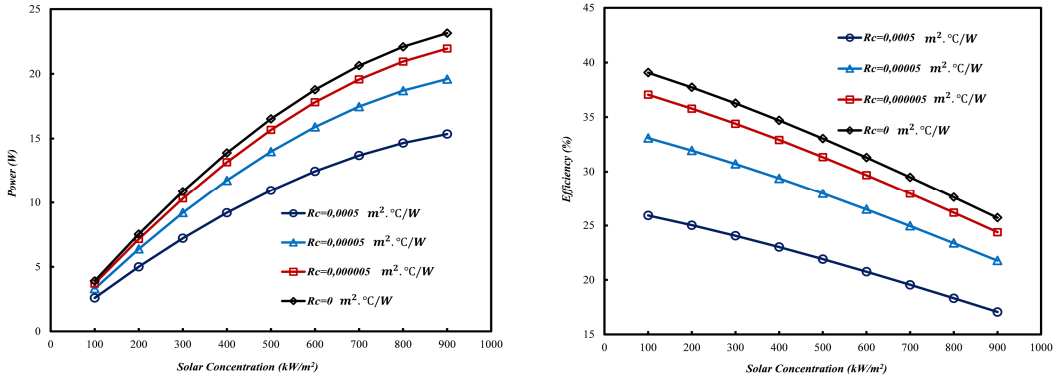

Figure. 4. Power generation and efficiency of the CPV versus solar concentration for different thermal contact resistances.

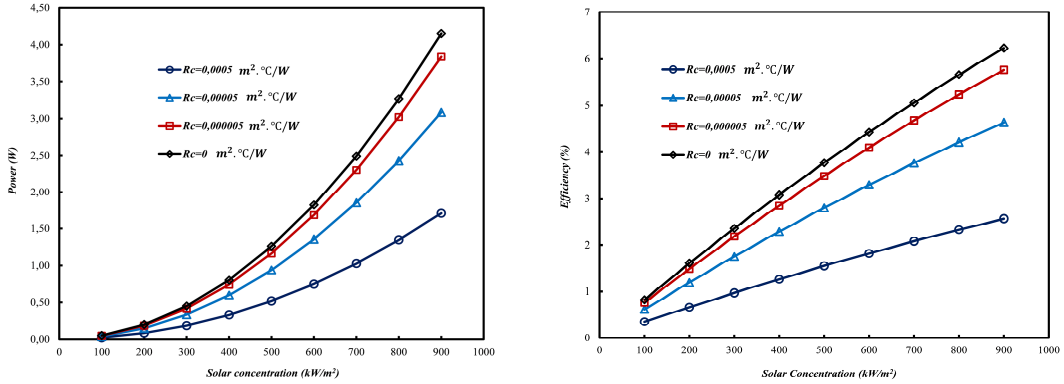

Figure. 5. Power generation and efficiency of the TEG versus solar concentration for different thermal contact resistances.

4. Conclusion

Performance of a hybrid CPV-TEG system is evaluated numerically. Energy conservation law is applied to obtain the governing equations for different components of the system, and the finite volume method is used to discretize and solve the thermally coupled equations. The impact of three vital parameters including convective heat transfer, solar concentration, and thermal contact resistance is examined. The results indicate that increasing the convective heat transfer leads to enhance in power generation and efficiency of the CPV and TEG. The rate of this increment drops in higher convective heat transfers, therefore to reduce the costs an optimum convective heat transfer has to be found. Increasing the solar concentration leads to having higher power for both CPV and TEG while the efficiency of the CPV drops at higher solar concentrations. The results show that the thermal contact resistance has a negative impact on the performance of both the CPV and TEG over studied convective heat transfer and solar concentration values.

References

[1] New world record for solar cell efficiency at 46% French-German cooperation confirms competitive advantage of European photovoltaic industry, in, Fraunhofer ISE report, Freiburg, 2014.
[2] M.A. Green, K. Emery, Y. Hishikawa, W. Warta, E.D. Dunlop, Solar cell efficiency tables (version 47), Prog. Photovolt. Res. Appl. 2016; 24: 3-11.
[3] Nader Rahbar, Amin Asadi, Solar intensity measurement using a thermoelectric module; experimental study and mathematical modeling, Energy Conversion and Management 2016; 129: 344–353.
[4] Sajjad Mahmoudi Nezhad, Alireza Rezaniakolaei, Lasse Aistrup Rosendahl, Experimental Study on Effect of Operating Conditions on Thermoelectric Power Generation, Energy Procedia 2017; 142: 558–563.
[5] Nader Rahbar, Javad Abolfazli Esfahani, Amin Asadi, An experimental investigation on productivity and performance of a new improved design portable asymmetrical solar still utilizing thermoelectric modules, Energy Conversion and Management 2016; 118: 55–62.
[6] Urbiola EAC, Vorobiev YV, Bulat LP. Solar hybrid systems with thermoelectric generators. Sol. Energy 2012; 86: 369–78.
[7] Rezania A, Sera D, Rosendahl LA. Coupled thermal model of photovoltaic-thermoelectric hybrid panel for sample cities in Europe. Renewable Energy 2016;99:127-135.
[8] W.G.J.H.M. van Sark, Feasibility of Photovoltaic – Thermoelectric hybrid modules, Applied Energy 2011; 88: 2785–2790.
[9] Trevor Hocksun Kwan, Xiaofeng Wu, Power and mass optimization of the hybrid solar panel and thermoelectric generators, Applied Energy 2016; 165: 297–307.
[10] Kossyvakis DN, Voutsinas GD, Hristoforou EV. Experimental analysis and performance evaluation of a tandem photovoltaic–thermoelectric hybrid system. Energy Convers Manage 2016; 117: 490–500.
[11] D. T. Cotfas, P. A. Cotfas, O. M. Machidon, D. Ciobanu, Investigation of the photovoltaic cell/ thermoelectric element hybrid system performance, Materials Science and Engineering 2016; 133: 012037.
[12] Ravita Lamba, S.C. Kaushik, Modeling and performance analysis of a concentrated photovoltaic– thermoelectric hybrid power generation system, Energy Conversion and Management 2016; 115: 288–298.
[13] Daniel T. Cotfas, Petru A. Cotfas, Laura Floroian, Dan I. Floroian, Study of combined photovoltaic cell/thermoelectric element/solar collector in medium concentrated light, Optimization of Electrical and Electronic Equipment (OPTIM) & 2017 Intl Aegean Conference on Electrical Machines and Power Electronics (ACEMP), 2017 International Conference on Date of Conference: 25-27 May 2017 Brasov, Romania, 978-1-5090-4489-4/17/$31.00 ©2017 IEEE.
[14] S. Mahmoudinezhad, A. Rezania, L.A. Rosendahl, Behavior of hybrid concentrated photovoltaic-thermoelectric generator under variable solar radiation, Energy Conversion and Management 2018;164:443–452.
[15] Sajjad Mahmoudinezhad, Shaowei Qing, Alireza Rezaniakolaei, Lasse Aistrup Rosendahl, Transient Model of Hybrid Concentrated Photovoltaic with Thermoelectric Generator, Energy Procedia 2017; 142: 564–569.
[16] Rezania A, Rosendahl LA. Feasibility and parametric evaluation of hybrid concentrated photovoltaic-thermoelectric system. Appl Energy 2017;187:380–9.
[17] Evans DL. Simplified method for predicting photovoltaic array output. Sol Energy 1981;27:555–60.
[18] J. M. Ziman. Thermoelectrics: Basic Principles and New Material Developments. Oxford: Oxford Clarendon Press, 1960.
[19] Gang Chen. Nanoscale Energy Transport and Conversion. Oxford: Oxford University Press, 2005.
[20] Patankar SV. Numerical heat transfer and fluid flow. USA: Taylor & Francis; 1980.

ISSN (online): 2446-1636
ISBN (online): 978-87-7210-365-5

AALBORG UNIVERSITY PRESS